VRIJE UNIVERSITEIT

Holocene climate variability in the Nordic Seas: numerical model simulations compared with proxy-based reconstructions

ACADEMISCH PROEFSCHRIFT

ter verkrijging van de graad Doctor aan
de Vrije Universiteit Amsterdam,
op gezag van de rector magnificus
prof.dr. F.A. van der Duyn Schouten,
in het openbaar te verdedigen
ten overstaan van de promotiecommissie
van de Faculteit der Aard- en Levenswetenschappen
op dinsdag 4 november 2014 om 11.45 uur
in het auditorium van de universiteit,
De Boelelaan 1105

door

Michael Blaschek

geboren te Wenen, Oostenrijk

promotor: prof.dr. H. Renssen

reading committee:

prof.dr. G. J. Brummer
prof.dr. M. Crucifix
prof.dr. H. Dolman
dr. J. Giraudeau
dr. E. Tuenter

This research was carried out at:
Vrije Universiteit Amsterdam

Faculteit der Aard- en Levenswetenschappen
Department of Earth Sciences
Earth and Climate Cluster
De Boelelaan 1105, 1081HV Amsterdam
The Netherlands

Copyright: Michael Blaschek

Cover: Daniel Sommergruber

This project was funded by the European Community's 7th Framework Programme FP7 2007/2013, Marie-Curie Actions, under Grant Agreement No. 238111 "CASE ITN". This support is gratefully acknowledged.

"Would one willingly fly on an untested airplane designed using an aeronautical code of "intermediate complexity" – even if it sat, impressively, on the runway?"

C. Wunsch, 2010, discussing simplifications of physics in numerical models

Abstract

This thesis deals with climate variability in the Nordic Seas during the Holocene derived from numerical model simulations, and compared to proxy-based reconstructions. The main focus of the research presented in this thesis aims at describing and understanding climate variability involving decaying ice sheets, in particular the effect of the Greenland ice sheet and its corresponding melt water during times of warmer than present-day climates. Another aspect of melting ice sheets is the effect of rising sea levels and the corresponding flooding of former land areas, such as the Siberian shelf in the Arctic Ocean. These two influences on the variability of the Nordic Seas climate have been studied in this thesis during the Holocene period, using numerical simulations performed with the LOVECLIM global climate model of intermediate complexity. The Holocene started about 11.700 yrs before present (BP, 1950 A.D.) and followed the preceding cold period, the last glacial. During the transition from a glacial to an interglacial state the climate system reorganises and large land-based ice sheets start to melt and release huge amounts of freshwater to the surrounding oceans. Initiated by the impact of increased orbital-based summer insolation on the Northern Hemisphere, the ice sheets decay and a thermal maximum is reached in the early Holocene. This thermal maximum is found in numerous proxy-based reconstructions of the Northern Hemisphere and it has been previously shown by Renssen et al. (2009) that the decaying ice sheets affected the spatial and temporal structure of the thermal maximum. Including such a factor improves the comparison to proxy-based reconstructions

around the North Atlantic. However, the Greenland ice sheet (GIS) has been mostly neglected in this context, leading to the following question, addressed in the second chapter.

What is the impact of GIS melting on the Holocene Thermal Maximum?

Our model results show that the effect of melt water on the surface ocean is a stratification and subsequent cooling (up to 2°C), as well as an increase of sea-ice cover. The cooling is stronger in the western Nordic Seas compared to the eastern, thus altering the spatial structure of the warmest temperatures and the timing of the Holocene thermal maximum in the Nordic Seas. The simulation results agree better with proxy-based reconstructions from this area and confirm that the Greenland ice sheet is important on a regional scale during its time of melting in the early Holocene.

Related to effects of melt water from ice sheets is the rise of global sea level. However, there are regional differences and lower sea level stands have been reconstructed for the Siberian shelf during the early Holocene. An extrapolation of regional sea level stands to the whole Arctic indicates that large shelf areas must have been land in the early Holocene. Thus, the question arises:

What impact does the flooding of an Arctic shelf introduce in the Nordic Seas?

The Arctic shelf areas are zones of sea-ice production and supply the Arctic ocean and it's main gateway, the Fram Strait, with sea ice. This major route of sea-ice export through Fram Strait and along the East Greenland current as far as the tip of Greenland posses a strong influence on the climate of the Nordic Seas. These cold and sea-ice covered waters on the western side are opposed by warm and salty Atlantic waters on the eastern side of the Nordic Seas. Our model results show that the flooding of the shelf increases the sea-ice production (15%), but decreases the

Fram Strait sea-ice export (-15%). Contrary to our hypothesis, changes to the Nordic Seas' climate are not caused by increased sea-ice export, but by local sea-ice production and forcing from the atmospheric winds. The conversion of land to ocean impacts the atmospheric circulation and enforces the Greenland winter High, yielding stronger winds. In response, the production and transport of sea-ice is increased, resulting in lower surface temperatures (up to 4°C) during the whole year in the Nordic Seas. Related to all feedbacks the transport of heat to the higher latitudes is reduced, thus showing the importance of this in reality dynamic feedback to an orbitally-induced warming and rising of sea level. In direct consequence of results from our previous questions, we found that melting of the Greenland ice sheet has impacted the Atlantic Meridional Overturning Circulation (AMOC). The AMOC transports heat and salt from the tropical Atlantic to the Northern high latitudes and thereby contributes to a warmer climate over Europe compared to similar latitudes such as for example in North America.

The recent efforts to measure the AMOC's strength allow better insights into the complex ocean circulation and proves to be valuable information for assessing future changes. Expanding the history of measurements is a much-needed effort to increase confidence into future projections. Employing proxy relations to reconstruct past ocean circulation properties is a valuable tool that allows giving qualitative estimates of changes and indicates long-term trends. However, given the nature of these reconstructions, trends differ by proxy and location. Therefore, using numerical model simulations to compare to proxy-based reconstructions, allows us to address the following question in Chapter 4.

What was the strength of the AMOC and its subcomponents during the Holocene?

The climate and the ocean circulation in the North Atlantic region changed over the course of the Holocene, partly because of disintegrating ice sheets and partly because of an orbitally-induced summer insolation

trend. In the early Holocene, the Laurentide ice sheet in North America, cooled large parts of the Northern Hemisphere by melt fluxes into the North Atlantic and by the cooling effect of the remnant ice sheet itself. In the Nordic Seas, this impact was accompanied by a rather small, but significant, amount of Greenland ice sheet melting that reduced local ocean surface temperatures even further. We compared transient simulations of the Holocene AMOC strength with proxy-based reconstructions. The modelled ocean circulation in the North Atlantic evolved from a melt water-impacted reduced state in the early Holocene to an evenly strong present-day state by 7,000 yrs BP. This evolution is partly confirmed by proxy-based reconstructions employing carbon isotopes, however showing a weaker response during the melting phase in the early Holocene compared to the model, whereas a comparison to proxy-based reconstructions focusing on the deep ocean currents is more problematic and only a few records agree with model results. The overall comparison shows that different trends in subcomponents of the AMOC can agree with each other and represent a long-term evolution of the AMOC similar to our model simulations. These results thus suggest that the evolution of the AMOC was mostly stable over the Holocene, with reduced values only in the early part.

Our results on the early Holocene are relevant in the context of present-day warming and its impact on the contemporary Greenland ice sheet. However, the early Holocene was not the only time period in the past, when the Greenland ice sheet was melting and in particular the Last Interglacial is often referred to as a period of extreme Greenland ice sheet melting. Given the fact that there is evidence of Greenland ice sheet melting in the past and a large likelihood in future projections, we address the fourth and final question in Chapter 5.

What is the impact of GIS melting beyond the Holocene and what can we learn for the future?

The climate system responds to, for example, a radiative forcing in every component of the climate system with certain positive or negative responses, called feedbacks. Thus, the sensitivity of the climate system to a forcing is determined by the response of the individual components. When comparing past and future warm climates, it is important to account for the forcing that makes the climate warm. In the case of the considered past climates, the orbitally-induced insolation is redistributed to cause for example warmer summers as well as cooler winters in the Northern Hemisphere. The response of the climate system, however is than seasonally dependent and not as straight forward as one might anticipate. In the case of the future climate, with the projected increases in greenhouse gas concentrations, the forcing is more globally uniform compared to the Holocene and the Last Interglacial. When we consider the impact of Greenland ice sheet melting in these past and future climates in our climate model, we find different responses in the melt-water-reduced AMOC strength for the past climates compared to the future projections. This indicates that the origin of this difference is likely to be related to the nature of the radiative forcing and melt water-related feedbacks in the different components of the climate system. The most likely candidate is the dynamic response of the sea ice to Greenland ice sheet melting in a set of differently warm climates. However, this highlights that a simplified extrapolation from past climates towards the future might be misleading, as this dynamic feedback is likely to be different in the future compared to the past.

This thesis provides a detailed introduction into the field of climate as well as individual introductions to the specific questions asked before and a final chapter summarising the major findings and future research suggestions.

Samenvatting

Holocene klimaatvariabiliteit in de Noord-Atlantische regio: numerieke simulaties in vergelijking tot reconstructies

Dit proefschrift gaat over klimaatschommelingen tijdens het Holoceen in de Noordelijke IJszee en het noordelijke deel van de Atlantische Oceaan, waaronder de Groenlandzee en Noorse Zee (hierna tezamen aangeduid met GNZ). Deze klimaatschommelingen zijn afgeleid uit numerieke modelsimulaties, en worden vergeleken met klimaatreconstructies welke zijn gebaseerd op geologische gegevens, de zogeheten proxies. De belangrijkste focus van dit proefschrift is op het beschrijven en begrijpen van de klimaatvariabiliteit onder invloed van smeltende ijskappen, met name het effect van de Groenlandse ijskap en het bijbehorende smeltwater in periodes met een warmer klimaat dan tegenwoordig. Een ander aspect van het smelten van ijskappen is het stijgen van de zeespiegel en de bijbehorende overstroming van kustgebieden, zoals het overstromen van het Siberisch continentaal plat in de Noordelijke IJszee na de laatste ijstijd. Deze twee invloeden op de Holocene klimaatvariabiliteit in de Noordelijke IJszee en het noordelijke deel van de Atlantische Oceaan

zijn onderzocht in dit proefschrift met behulp van numerieke modelsimulaties, uitgevoerd met het wereldomvattende LOVECLIM klimaatmodel. Het Holoceen is het huidige interglaciaal en begon ongeveer 11.700 jaar geleden en volgde op de laatste ijstijd. Tijdens de overgang van een ijstijd naar een interglaciaal reorganiseert het klimaatsysteem zich en beginnen de grote ijskappen in Europa en Noord-Amerika te smelten, waardoor een enorme hoeveelheid zoet smeltwater naar de omringende oceanen stroomt. Deze grootschalige smelt wordt genitieerd door de toegenomen zomerse instraling van de zon op het noordelijk halfrond, welke het gevolg is van een verandering in de baanparameters van de aarde, de zogeheten orbitale forcering. Deze zomerse instraling zorgt voor een periode met maximale zomertemperaturen in het vroege Holoceen. Dit Holocene thermische maximum is te vinden in tal van op proxies gebaseerde temperatuurreconstructies op het noordelijk halfrond en eerder werd door Renssen et al. (2009) aangetoond dat de smeltende ijskappen resulteerden in variaties in de expressie van dit thermische maximum in ruimte en tijd. Het in beschouwing nemen van deze processen verbetert de gelijkenis van modelresultaten met de op proxies gebaseerde klimaatreconstructies rond de Noord-Atlantische Oceaan. Echter, veranderingen in de Groenlandse ijskap (in het Engels 'Greenland Ice Sheet', of GIS) zijn tot op heden meestal niet meegenomen in deze context, wat leidt tot de volgende vraag, welke in het tweede hoofdstuk aan bod komt.

Wat was de impact van het smelten van de GIS op het Holocene thermische maximum?

Onze modelresultaten laten zien dat het toevoegen van smeltwater aan het oceaanoppervlak leidt tot een sterkere stratificatie, samengaand met afkoeling (tot 2°C) en tot een toename van de zee-ijsbedekking. De afkoeling is sterker in het westelijke dan in het oostelijke deel van de GNZ, waardoor de ruimtelijke structuur en het tijdstip van het Holocene thermische maximum in deze regio verandert. De modelresultaten komen beter overeen met de op proxies gebaseerde temperatuurreconstructies

uit dit gebied en bevestigen dat het gedeeltelijk smelten van de Groenlandse IJskap in het vroege Holoceen van groot belang is voor de regionale klimaatveranderingen.

Gedurende de ijstijd was de zeespiegel wereldwijd aanzienlijk lager dan de huidige (ongeveer 120 meter). Het smelten van de ijskappen aan het einde van de ijstijd en in het vroege Holoceen veroorzaakte een wereldwijde stijging van de zeespiegel en vele laaggelegen kustgebieden kwamen hierdoor onder water te staan. Echter, hierin zijn belangrijke regionale verschillen. Zo blijkt bijvoorbeeld uit gereconstrueerde zeespiegelstanden dat delen van het Siberisch continentaal plat tijdens het vroege Holoceen nog droog stonden. En een extrapolatie van de regionale zeespiegel voor het gehele Arctische gebied geeft aan dat grote delen van het continentale plat in deze regio droog hebben gestaan in het vroege Holoceen. Hieruit volgt de volgende vraag (hoofdstuk 3):

Welke impact had de Holocene overstroming van het Arctisch continentaal plat op het klimaat in het noordelijk deel van de Atlantische Oceaan?

Het Arctisch continentaal plat bestaat tegenwoordig uit gebieden waar veel zeeijs wordt gevormd. Dit zeeijs verlaat uiteindelijk de Noordelijke IJszee via de Fram Straat, en vervolgt zijn weg naar het zuiden langs de kust van Oost-Groenland tot aan de zuidelijkste puntje van Groenland. Dit zeeijs heeft een sterke invloed op het klimaat van de noordelijke Atlantische Oceaan, met name in de GNZ. De koude en met zeeijs bedekte wateren aan de oostkant van Groenland ontmoeten in de GNZ de warme en zoute Atlantische wateren welke langs de Noorse kust naar het noorden stromen. Onze modelresultaten tonen aan dat de overstroming van het Arctisch continentaal plat de zeeijsproductie verhoogt (15%), maar ook de zeeijsexport door Fram Straat verlaagt (-15%). In tegenstelling tot onze vooraf opgestelde hypothese, worden veranderingen in het klimaat tussen Noorwegen en Groenland niet veroorzaakt door een

verhoogde zeeijsexport, maar door de lokale zeeijsproductie en de invloed hiervan op de atmosferische stroming. De verandering van land naar oceaan benvloedt namelijk de atmosferische circulatie en versterkt het winterse hogedrukgebied over Groenland, wat weer leidt tot sterkere winden. In reactie daarop neemt de productie en het transport van zeeijs toe, wat resulteert in lagere oppervlaktetemperaturen (tot 4°C) gedurende het hele jaar in noordelijkste deel van de Atlantische Oceaan. Door terugkoppelingen in het klimaatsysteem wordt het transport van warm water naar de hogere breedtegraden verminderd, daarmee het belang aangevend van deze in werkelijkheid dynamische terugkoppeling, welke op gang wordt gebracht door opwarming als gevolg van orbitale forcering en het stijgen van de zeespiegel.

Eerder vonden we al dat het smelten van de Groenlandse IJskap de Atlantische meridionale oceaancirculatie (AMOC) heeft benvloed. De AMOC transporteert warmte en zout uit de tropische Atlantische Oceaan naar de noordelijke hoge breedtegraden en draagt daarmee bij aan een relatief warm klimaat in Europa in vergelijking met soortgelijke breedtegraden in bijvoorbeeld Noord-Amerika.

De recente inspanningen om de sterkte van de AMOC te meten, om zo een beter inzicht te krijgen in de complexiteit van oceaanstromingen, heeft veel waardevolle informatie opgeleverd die gebruikt kan worden om beter in te schatten wat er in de toekomst is te verwachten. Het verlengen van de meetreeksen tot ver in het verleden is een noodzakelijke inspanning om het vertrouwen in de toekomstprojecties te verhogen. Aan de hand van op proxies gebaseerde verbanden kunnen de eigenschappen van oceaanstromingen in het verleden gereconstrueerd worden. Dit geeft kwalitatieve informatie over veranderingen die plaats vinden op lange tijdschalen. Echter, gezien de aard van deze reconstructies, verschillen deze gereconstrueerde veranderingen per proxy en per locatie. Het vergelijken van modelsimulaties met op proxies gebaseerde reconstructies, stelt ons in staat om de volgende vraag in hoofdstuk 4 te beantwoorden.

Wat was de sterkte van de AMOC en zijn componenten tijdens het Holoceen?

Het klimaat en de oceaancirculatie in de Noord-Atlantische regio zijn veranderd in de loop van het Holoceen, deels ten gevolge van het uiteenvallen van ijskappen en deels ten gevolge van orbitale forcering van veranderingen in de zomerse instraling. In het vroege Holoceen hadden de restanten van de Noord-Amerikaanse IJskap nog steeds een afkoelend effect op grote delen van het noordelijk halfrond. Dit kwam door het temperende effect van smeltwaterstromen op de AMOC en door de koelende werking van de ijskap zelf. In noordelijk deel van de Atlantische Oceaan ging dit gepaard met een vrij kleine, maar significante hoeveelheid smeltwater van de Groenlandse IJskap dat lokaal de temperatuur van het oppervlaktewater nog verder reduceerde. We vergeleken tijdsafhankelijke simulaties van de AMOC-sterkte gedurende het Holoceen met op proxies gebaseerde reconstructies van de diepe oceaancirculatie. De gesimuleerde Atlantische Oceaancirculatie in het vroege Holoceen is gelijkmatig veranderd van een relatief zwakke toestand onder invloed van het smeltwater, tot een op de huidige toestand gelijkende relatief sterke circulatie rond 7000 jaar geleden. Deze evolutie komt deels overeen met op proxies gebaseerde reconstructies aan de hand van koolstofisotopen, zij het met een zwakkere respons in het vroege Holoceen ten opzichte van het model. Uit ons onderzoek is gebleken dat een vergelijking met op proxies gebaseerde reconstructies van diepe oceaancirculatie problematisch is, aangezien slechts enkele reconstructies overeenkomsten vertonen met de modelresultaten. Het blijkt wel dat verschillende trends in onderdelen van de AMOC overeenkomen. Ook de lange termijn trend in de AMOC is vergelijkbaar met onze modelsimulaties. Deze resultaten suggereren dat de evolutie van de AMOC overwegend stabiel was gedurende het Holoceen, met alleen een relatief zwakke fase in het vroege deel.

Onze resultaten voor het vroege Holoceen zijn relevant in de context van het huidige opwarming en de invloed hiervan op de huidige Groenlandse

IJskap. Echter, deze ijskap smolt niet alleen tijdens het vroege Holoceen, maar ook in eerdere warme perioden. In het bijzonder het laatste interglaciaal (het Eemien) wordt vaak aangeduid als een periode met aanzienlijke smelt in Groenland, resulterend in een substantieel kleinere ijskap dan tegenwoordig. Deze gegevens uit het geologisch verleden kunnen wellicht gebruikt worden om een beter inzicht te krijgen over de invloed van de GIS in een toekomstig warm klimaat. Dit komt aan bod in de vierde en laatste vraag in hoofdstuk 5:

Wat is de impact van GIS smelt in een warm klimaat voorafgaand aan het Holoceen en wat kunnen we hiervan leren voor de toekomst?

In het klimaatsysteem spelen allerlei positieve en negatieve terugkoppelingen een rol, waardoor het effect van een verandering in, bjivoorbeeld, een stralingsforcering versterkt of verzwakt kan worden in onderdelen van het klimaatsysteem (zoals oceaan en atmosfeer). De gevoeligheid van het klimaatsysteem voor een forcering wordt daarom bepaald door de reacties van deze individuele componenten. Voor onze vergelijking van warme klimaten uit het verleden (Eemien en Holoceen) en met die uit de toekomst, is het belangrijk om rekening te houden met de forcing die de opwarming genereert. In het geval van klimaten uit het Eemien en het Holoceen, werd de opwarming veroorzaakt door orbitale forcering, welke de seizoenaliteit op het noordelijk halfrond versterkte, met warmere zomers en koudere winters tot gevolg. Maar in deze gevallen is de reactie van het klimaatsysteem afhankelijk van de seizoenen en daardoor niet zo eenvoudig als men zou verwachten. In het geval van het toekomstige klimaat, met de verwachte toename van de concentratie van broeikasgassen, is de forcering wereldwijd uniform vergeleken met die van het Holoceen en Eemien, en niet seizoensafhankelijk. Onze modelanalyse van de invloed van het smelten van de GIS in warme klimaten uit het verleden en de toekomst laat zien dat de AMOC verschillend reageert. De oorsprong van dit verschil ligt in de aard van de stralingsforcering en van de reactie op het smeltwater in de verschillende

componenten van het klimaatsysteem. We concluderen dat met name de dynamische respons van het zeeijs op het smelten van de Groenlandse IJskap van belang is. Dit wijst erop dat een eenvoudige extrapolatie van een warm klimaat uit het verleden naar de toekomst misleidend zou kunnen zijn, want deze dynamische feedback reageert in de toekomst waarschijnlijk anders dan in het verleden.

Dit proefschrift begint met een gedetailleerde inleiding in de onderzoeksproblematiek, en geeft ook specifieke introducties op de eerder beschreven specifieke vragen. Het laatste hoofdstuk, tenslotte, geeft een samenvatting van de belangrijkste bevindingen en ook suggesties voor toekomstig onderzoek.

Acknowledgements

Many friends and colleagues provided input into the development of ideas and research questions that are to be found in this thesis and I would like to thank them again. Special thanks are due to Hans and Didier for trusting me to finish the job, when we first met in Vienna, April 2010. Thanks go to the great community of the CASE project that allowed me to travel to universities all over Europe and meet outstanding people. Very special thanks to Robert Spielhagen for alerting me to the topic of shelf flooding in the Arctic and to Jacques Giraudeau for being a true model critic (smile) and companion to all project adventures. Thanks to Johan for talking German to me and annoying everyone else by doing so. Very special thanks to Pepijn for everything. Thanks to Leo for being patient.

Very special thanks to Hans for being my supervisor and an anchor in the rough sea to be called the PhD endeavour. Whenever the journey arrived at something like a hurricane at sea, he always found a save course of action to navigate around it and still, make it, a not too terribly boring 'save' adventure. Thanks for a great ice-skating memory I can make everyone else jealous.

Thanks are due to the members of the reading committee for a strait forward evaluation of my thesis, even though it was during summer.

It has been a great pleasure to find so many friendly people in Amsterdam and share the experience of living abroad with them. Thanks for distracting me from work and making Amsterdam a greater experience. I will sure miss you in Vienna.

I am grateful for my family and friends in Vienna, who kept the connection at the distance. Thanks to Daniel for finishing the cover in so little time. An unspeakable amount of thanks are due to Mari, my faithful companion on this and many other journeys.

Table of Contents

Abstract **vii**

Samenvatting (Dutch Summary) **xiii**

Acknowledgements **xxi**

Table of Contents **xxi**

List of Figures **xxvii**

List of Tables **xxix**

Nomenclature **xxxi**

1 Introduction **1**
1.1 Climate, Climate Change and Climate Variability 1
1.2 This Thesis 11
1.3 Reconstructing Past Climates 12
1.4 LOVECLIM 15
1.5 Research Questions 18

2 The Holocene thermal maximum in the Nordic Seas: the impact of Greenland Ice Sheet melt and other forcings in a coupled atmosphere-sea ice-ocean model **27**
2.1 Introduction 28
2.2 Experimental design 33
2.2.1 The model 33
2.2.2 Experimental design 34
2.2.3 Snapshot experiments 34
2.2.4 Transient experiments 36
2.3 Results and discussion 38
2.3.1 Early Holocene response 38

2.3.2 Transient Holocene response 50
2.4 Conclusions 55

3 The impact of Early Holocene Arctic Shelf flooding on climate in an atmosphere-ocean-sea-ice model 59
3.1 Introduction 60
3.2 Methods 65
3.2.1 The LOVECLIM Model 65
3.2.2 Experimental Design 66
3.3 Results 69
3.3.1 Impact on Arctic sea-ice 69
3.3.2 Impacts on Nordic Seas 73
3.3.3 Impact on Northern Hemisphere climate 76
3.4 Discussion 84
3.5 Conclusions 87

4 Holocene North Atlantic Overturning in an atmosphere-ocean-sea-ice model compared to proxy-based reconstructions 91
4.1 Introduction 93
4.2 Methods 100
4.2.1 The Model 100
4.2.2 Experimental Setup 102
4.3 Results from transient model simulations 104
4.3.1 Atlantic Meridional Overturning Circulation . . . 104
4.3.2 Convection areas and contribution to the overall deep water production 107
4.3.3 The Subpolar North Atlantic 108
4.4 Discussion: Proxy 113
4.4.1 Proxy-based reconstructions over the Holocene . . 114
4.4.2 Discussion of model results and proxy-based reconstructions 124
4.5 Conclusions 129

5 The influence of Greenland Ice sheet melting on the Atlantic meridional overturning circulation during past and future warm periods: a model study 131
5.1 Introduction 132
5.2 Methods 136
5.2.1 The Model 136
5.2.2 Experiment Set-up 139

5.2.3 Periods - Background Climate 140
5.3 Results & Discussion 146
5.3.1 AMOC state in the background climates 147
5.3.2 Impact of freshwater forcing on the AMOC strength 149
5.3.3 Convective activity and sea-ice feedback 156
5.3.4 Discussion and Context 164
5.4 Conclusions 169

6 Synthesis and Perspective **173**
6.1 Synthesis 173
6.2 Perspective 179

Supplementary Information A Holocene AMOC **183**

Supplementary Information B Past and Future **187**

Bibliography **196**

List of Figures

1.1 The Climate System . . . 3
1.2 Climate Variability . . . 4
1.3 Response time of components . . . 4
1.4 Glacial Interglacial Cycles . . . 5
1.5 Orbital parameters . . . 6
1.6 Last Glacial Maximum Ice sheet Reconstructions . . . 8
1.7 The Global Ocean Circulation . . . 9
1.8 Summary of LOVECLIM components . . . 17

2.1 Equilibrium and transient forcings applied in simulations 37
2.2 Sea Surface Temperature Maps . . . 39
2.3 Sea Surface Salinity Maps . . . 40
2.4 Simulated east–west SST differences across the Nordic Seas . . . 43
2.5 March Mixed Layer Depth and sea-ice extent . . . 47
2.6 Transient August SST East-West Difference . . . 51
2.7 Timing of the Holocene Thermal Maximum . . . 54

3.1 Topographic Map of the Arctic ocean bathymetry . . . 62
3.2 Arctic sea-ice volume comparison . . . 70
3.3 Fram Strait sea-ice export . . . 74
3.4 Maximum winter sea-ice extent and March mixed layer depth . . . 75
3.5 Monthly means of western Nordic Seas . . . 77
3.6 Seasonal surface temperature anomalies . . . 78
3.7 Atmospheric circulation at 500 and 800 hPa . . . 80
3.8 Winter sea-ice production . . . 82
3.9 Schematic feedback loop . . . 83

4.1 Equilibrium and transient forcings applied in simulations 103
4.2 Simulated North and South Atlantic overturning . . . 105

4.3 Deep convection areas in the North Atlantic 107
4.4 Contribution of convection areas to the overall simulated deep convection 109
4.5 Simulated flow speeds and density differences South of Iceland 110
4.6 Simulated exchange between the Nordic Seas and the sub polar North Atlantic 111
4.7 Modelled flow across Straits 113
4.8 Export and Import of deep waters across 20° S 114
4.9 Map of proxy core locations 116
4.10 Holocene proxy records of δ^{13}C , Magnetic Susceptibility (κ) and Sortable Silt 120

5.1 Comparison of insolation anomalies and background climate states 141
5.2 Comparison of background climate states 147
5.3 Summary of AMOC changes due to GIS melt water . . . 150
5.4 AMOC response to GIS melting 152
5.5 Summary of sea-ice area response to GIS melting 155
5.6 Convection areas, SSS and sea-ice margin maps 158
5.7 Labrador Sea normalized convective volume 159
5.8 March Labrador Sea vertical profiles of density, temperature and salinity 161
5.9 AMOC reduction to GIS melting compared to relevant parameters 162

SI.A.1 Sortable Silt Records 184
SI.A.1 δ^{13}C Records 185
SI.A.1 Magnetic Susceptibility (κ) Records 186

SI.B.1 Schematic summary - impacts of parameter sets 189
SI.B.2 Relative AMOC Changes vs. GIS freshwater forcing. . . 191
SI.B.2 Absolute AMOC Changes vs. GIS freshwater forcing. . . 192
SI.B.3 Summary of convection areas and normalized convective volume. 193
SI.B.4 Summary of convection areas and sea surface density. . . 194

List of Tables

2.1 Summary of the experimental design 35
2.2 Summary of key variables from all snapshot simulations . 44

3.1 Summary of Experiments 67
3.2 Summary of sea-ice quantities of nine simulations 72

4.1 Summary of experiment setup 102
4.2 Summary of used proxy records 119

5.1 Summary of forcings 140

SI.B.1 Summary of model parameter sets 188

Nomenclature

AABW	AntArctic Bottom Water
AD	Anno Domini
AMOC	Atlantic Meridional Overturning Circulation
BP	Before present (i.e. 1950 AD)
CAA	Canadian Arctic Archipelago
DSOW	Denmark Strait Overflow Water
EGC	East Greenland Current
EMIC	Earth System Model of Intermediate Complexity
GIS	Greenland Ice Sheet
GSR	Greenland-Scotland Ridge
HTM	Holocene Thermal Maximum
IRD	Ice-rafted debris
ISOW	Iceland-Scotland Overflow Water
LDW	Lower Deep Water
LGM	Last Glacial Maximum (at 21 kyr BP)
LIS	Laurentide Ice Sheet
LSW	Labrador Sea Water
MLD	Mixed layer depth [m]
NAC	North Atlantic Current
NADW	North Atlantic deep water
PI	Pre-Industrial
RCP	Representative Concentration Pathways
SSS	Sea surface salinity [p.s.u.]
SST	Sea surface temperature [$^\circ$ C]
Sv	Sverdrups = 10^6 [m^3/s]

Dedicated to Mari ...

Chapter 1

Introduction

The discussion on climate, climate change and impacts from human emissions is a global topic, which has been recently addressed in the recent, 5th assessment report (AR5) by the Intergovernmental Panel of Climate Change (IPCC). The AR5 summary for policymakers clearly states that the warming of the climate system is unequivocal and that many of the observed changes are unprecedented over decades to millennia (IPCC, 2013). Further, it clearly says that human influence on the climate system is clear and that this human influence has been the dominant cause of observed warming since the mid-20th century (IPCC, 2013). It thus seems clear that recent events are only the beginning of what we are about to experience in the next 50 yrs or so. This thesis is a contribution to better understanding climate change and climate variability from past climates.

1.1 Climate, Climate Change and Climate Variability

In order to discuss climate, we have to define what climate means. Everyone knows about weather and its sudden changes (predicted or not)

from a perfectly sunny Sunday afternoon to a water pouring hell, but that is not climate. As Edward N. Lorenz (1995) expressed it in a single sentence: "*Climate is what you expect and weather is what you get*". In this sense, climate represents the long-term statistics of the short-term weather. Weather is concerned with the formation, movement and prediction of an individual storm, whereas climate addresses the question of how many storms will occur in the next years. Easily connected to near-future changes, we speak of climate change when the "weather statistics" over a longer timescale (decades to million of years) change and of climate variability when there are deviations from the long-term statistics. For example, a single decadal-scale extreme event is referred to as climate variability, but a series of such extreme events is called climate change. The terminology "climate" describes not only atmospheric conditions, but the conditions of the whole climate system. The climate system (Fig. 1.1) consists of the atmosphere, the hydrosphere (ocean, lakes, rivers), the cryosphere (ice sheets, glaciers), land surfaces (pedosphere and lithosphere) and the biosphere. All of these components are undergoing changes at different timescales.

It has been shown by Mitchell (1976) that climate varies on all timescales in response to random and periodic forcings (Fig. 1.2 Ghil, 2002). A forcing is a factor that affects the climate or a component of the climate system and can be either external or internal to the earth system. For instance, internal forcings are the winds' impact on the ocean surface or greenhouse gas concentrations. However, these are also dynamic processes and their strength co-evolves with the whole climate system. This is in contrast to an external forcing, which is not influenced by the climate system, and is usually considered a boundary condition in for instance climate model experiments. External forcings include volcanic eruptions, solar variability and orbital variations. A forcing can have an internal cycle originating from a certain mechanism, such periodic forcings are denoted by peaks in Fig. 1.2. Examples of periodic forcings include variations in the Earth's orbital parameters (ranging from 100 to

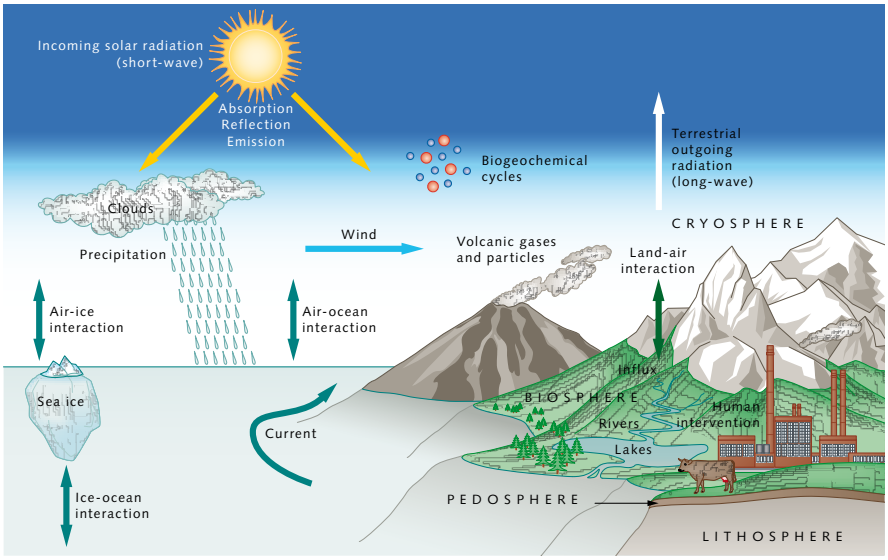

Figure 1.1: The climate system and its components. ©maribus, Bosch et al. (2010)

20 kyr, Milankovitch, 1941; Berger and Loutre, 1991) or the annual and daily cycle. The understanding of periodic forcings makes it possible to predict past and future climate change. However, the random forcings are caused by internal processes and associated feedbacks (Goodess et al., 1992). Thus, they arise from the complex and chaotic behaviour of the climate system in response to forcing (Lorenz, 1991; Palmer and Stoffer, 1989; Ghil, 2002; Rial et al., 2004). The overall response of the climate system to a forcing depends on the response time of the components of the climate system (Fig. 1.3). Within the climate system, the atmosphere, for example, has a response time in the range of minutes to days and might respond relatively quickly to a given forcing, whereas the deep ocean responds over hundreds of years and will smooth the overall response at longer timescales. A change in one component will naturally cascade through the coupled components and the effect will be transferred and modified in character or scale. In some cases the effect will be amplified (positive feedback) and in others it will be weakened (negative feedback). Feedbacks can be considered internal forcings, which

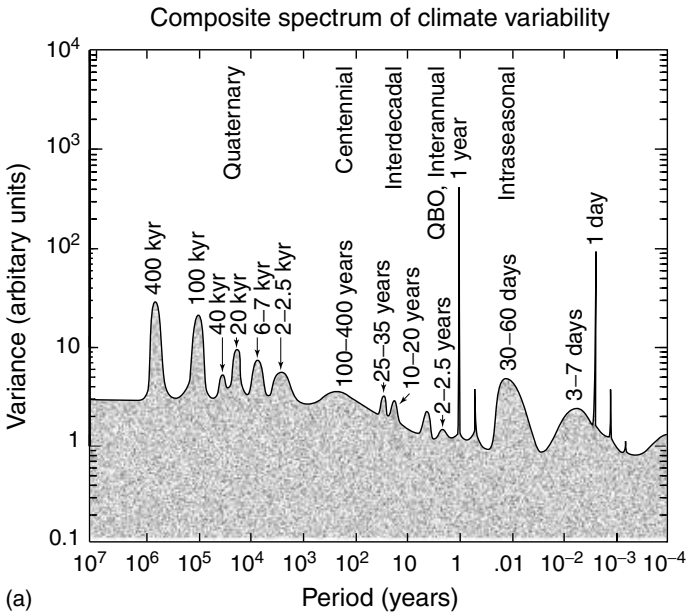

Figure 1.2: Climate Variability on different timescales. Mitchell (1976)

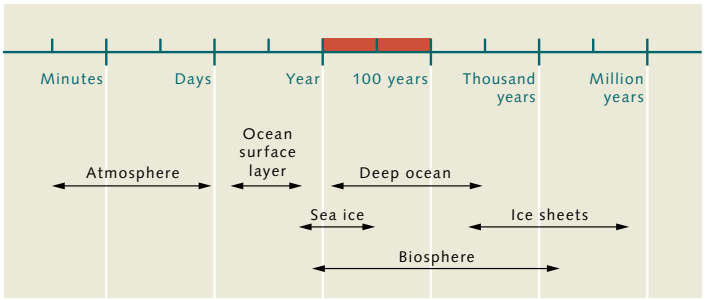

Figure 1.3: The response time of components of the climate system to a forcing. Red bar denotes the life span of a human being. ©maribus, (Bosch et al., 2010)

depend on the dynamics of the climate system and are the most likely processes behind most nonlinearities in climate (Rial et al., 2004), which lead to a threshold behaviour and abrupt climate change. Specifically, positive feedback mechanisms, which amplify the climate response to a forcing, lead the climate away from its natural balance. Therefore, positive feedbacks cause the climate system to adapt and modify the states

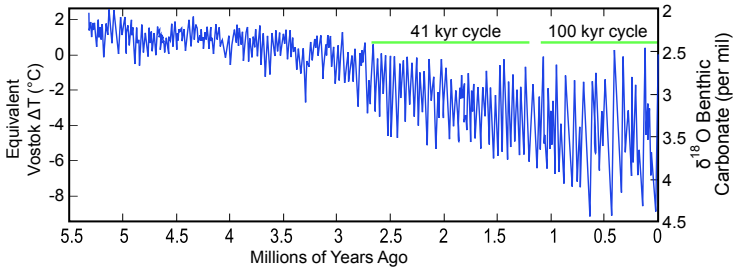

Figure 1.4: Glacial Interglacial Cycles over the past 5 million years from the oxygen isotopic stack LR1 (Lisiecki and Raymo, 2005). Source: `www.wikipedia.com`

of its components to restore the balance, whereas a negative feedback mechanism makes the system less responsive to a forcing, thus stabilising its balance. An example of a positive feedback is the ice-albedo feedback. Consider an increased radiative forcing, inducing warming, that will decrease the surface ice cover by melting snow cover, glaciers and sea-ice. This in turn decreases the surface albedo and allows absorbing more shortwave radiation, which accelerates the initial warming and closes the positive feedback loop. When we speak of the climate system, we have to remember the complexity of the climate system and that climate change is also a natural process, which happens at different timescales in all components of the climate system.

During the Earth's history, the climate has experienced cold glacial and warm interglacial states over the past 2.58 million years (Fig. 1.4, Gradstein et al., 2005) and since the Mid-Quaternary (800 ka before present, BP), glacial-interglacial cycles show a periodicity of about 100,000 yrs. In 1920, M. Milankovitch proposed that the variations in the Earth's orbital parameters modify the distribution of solar radiation that is seasonally received by the Earth and that these variations are the main source of glacial-interglacial climate change. The periodicities in the Earth's orbit, described by the main orbital parameters, eccentricity (100,000 yrs), obliquity (41,000 yrs) and precession (23,000yrs) are sometimes called the "pacemakers" of the glacial-interglacial cycles (Fig. 1.5, Hays et al., 1976). At present it seems clear that these external forcings have

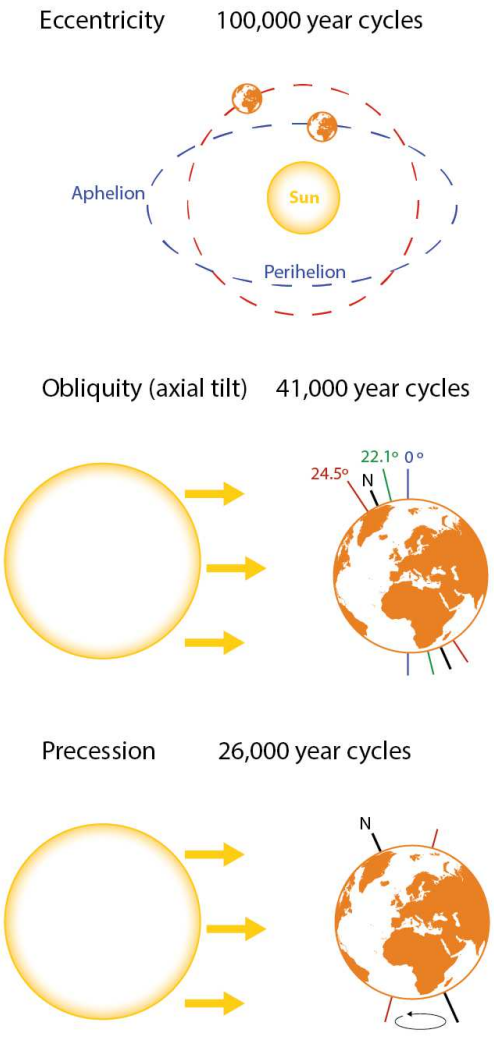

Figure 1.5: Orbital parameters, eccentricity, obliquity and precession. Source: ©2014 Climatica.org.uk

influenced the climate system, but large transitions from glacials to interglacials require the interaction between the components of the climate system.

The recent direction of explaining glacial-interglacial cycles involves the non-linear interaction between the climate system's components, in particular the ice sheets and the ocean, and external forcings (Kukla and Gavin, 2004; Wunsch, 2004; Crucifix, 2013). However, climate variability happens as well at time scales much shorter than glacial-interglacial

time scales. For example, the present interglacial period started about 11,700 years BP, when the last glacial period was terminated by a strong Northern Hemisphere summer insolation maximum (Berger and Loutre, 1991). Increased summer temperatures caused the melt down of Northern Hemisphere ice sheets (Fig. 1.6, North America and Scandinavia) and a subsequent warming of the climate into the interglacial state. The present interglacial is called the Holocene and it is one of the most studied geological periods of time, simply because it is recent, and therefore easily accessible in the billions of years the Earth existed and the climate changed. The climate system is in constant transition, however during terminations, when the climate system moves from a glacial to an interglacial period, then the whole climate system has to adapt and its components align in a new balance. Hence, this time of reorganisation is the time of large and abrupt shifts in the climate system (Ganopolski and Rahmstorf, 2001; Roche et al., 2012).

For the present interglacial (the Holocene) and the last deglaciation, there have been at least three events that are interesting in the sense that they exhibit abrupt changes and are related to the interactions of the components of the climate system. We will outline two of them here, the Bølling-Allerød and the 8.2 ka cooling event.

Coming from cold glacial times, the start of the Bølling-Allerød (14.7 ka BP) warm phase around 14.7 ka BP is recorded in the Greenland ice core as a 15 K warming (Liu et al., 2009), indicating a fast rise in Northern Hemisphere temperatures to almost interglacial levels. This transition occurs within a few hundred years and has been found to relate to an abrupt ending of melt water supply to the North Atlantic (Liu et al., 2009). The basic concept behind this abrupt warming is a combination of the general warming trend from glacial to interglacial state and the recovery of the ocean circulation, which was perturbed by the melting of the land-based ice sheets on the North American continent. The melt water inhibits convection in the ocean, where it freshens the ocean surface enough to reduce its density and prevent surface waters

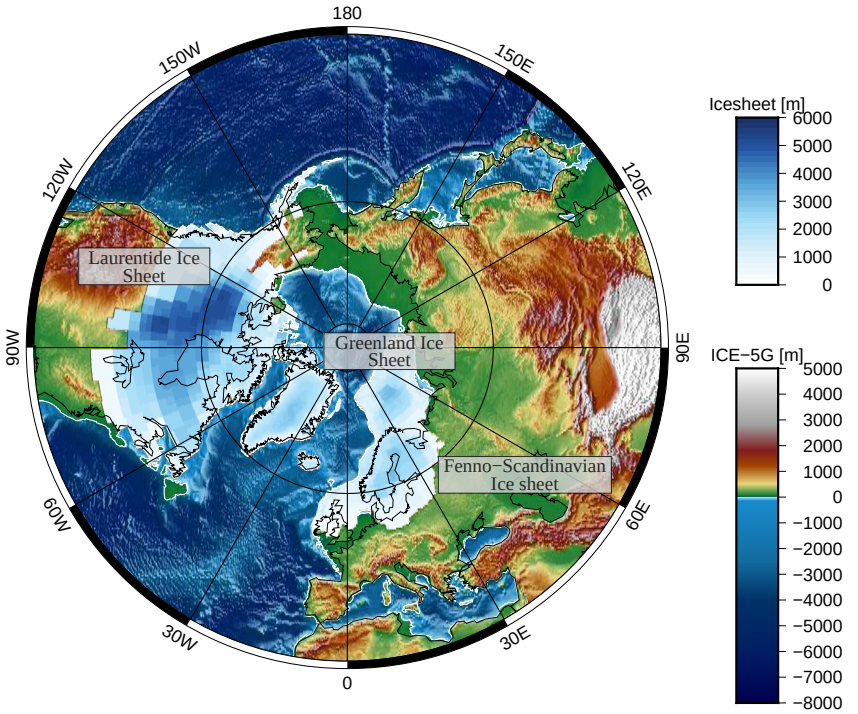

Figure 1.6: Icesheet Reconstruction at the Last Glacial Maximum (21 kyr BP) , showing the Northern Hemisphere glaciation over North America and Scandinavia and corresponding lower sea level (-120 m relative sea level) and coastline regression. Sources: Peltier (2004), Siddall et al. (2003)

from sinking into the deep ocean. This process is critical for the ocean circulation and a major process in the transport of heat from the tropics to the poles. In the Atlantic basin this is called the Atlantic Meridional Overturning circulation (AMOC, Fig. 1.7). The AMOC is part of the global transport system of water masses and heat. At present the AMOC transports about 25 % of the total meridional heat flux (Trenberth and Caron, 2001; Ganachaud and Wunsch, 2003; Johns et al., 2011) from both ocean and atmosphere at 26°N. This heat release results in relatively warm conditions, over the greater North Atlantic region compared to similar latitudes of the North Pacific, with an air temperature increase of up to 10°C relative to the zonal mean climatology (Rahmstorf and Ganopolski, 1999; Vellinga and Wood, 2002), demonstrating the climatic

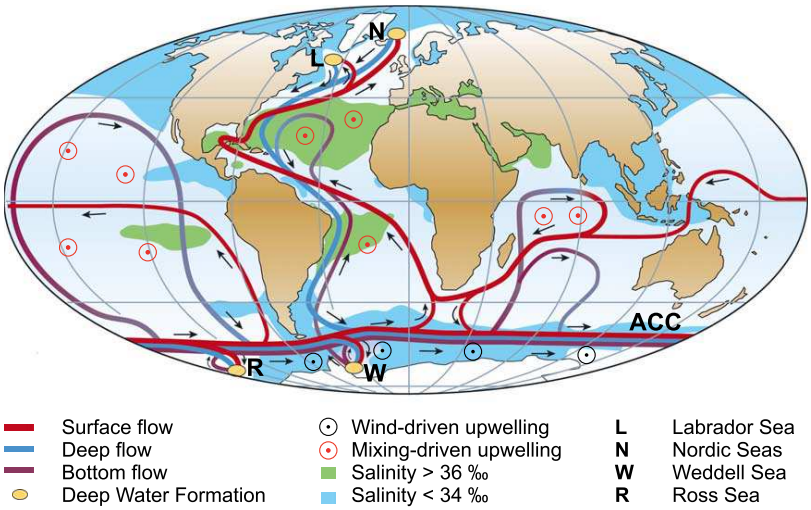

Figure 1.7: The Global Ocean Circulation. Atlantic Meridonal Overturning Circulation (AMOC) after Kuhlbrodt et al. (2007)

importance of the AMOC. There are two distinct driving mechanisms of the AMOC: the thermohaline circulation and wind-driven upwelling (Kuhlbrodt et al., 2007). The first describes the conversion of surface waters to deep waters by increasing their density through cooling and/or increasing salinity and is essential for the deep-water formation (Huang, 2004; Kuhlbrodt et al., 2007). If the density of a surface water mass becomes significantly higher than the density of the surrounding water masses, then a threshold density can be crossed and deep convection can occur. The deep mixing associated with this process leads to the formation of relatively dense, deep waters, which flow southward and sum up to form the North Atlantic Deep Water (NADW, Kuhlbrodt et al., 2007). In the present North Atlantic basin, deep convection occurs preferentially in the Labrador, the Irminger and the Nordic Seas (e.g. Marshall and Schott, 1999; Pickart et al., 2003). A disruption of convection in these areas by, for example, melt water from ice sheets will slow down the AMOC, hence the transport of heat to the Northern Hemisphere.

Episodic melt water discharges into the North Atlantic provide a mechanism that can explain the observed climate variability during these times of climate change from glacial to interglacial (Clark et al., 2001). Another example of a rapid event, depicting climate variability, is linked to a melt water injection into the North Atlantic from a catastrophic lake drainage event at about 8.2 ka BP (Alley et al., 1997). During this relatively late phase of the deglaciation, large amounts of freshwater were stored in a lake that was dammed by the ice, which drained within a short interval (∼160 yrs, Alley et al. (1997)) into the North Atlantic (Hillaire-Marcel et al., 2007) and caused a cool event recorded in numerous Northern Hemisphere reconstructions (e.g. Alley et al., 1997; Kleiven et al., 2008; Thornalley et al., 2009). However, a recent study, Carlson and Clark (2012), rejects the simple hypothesis of a drainage event and indicates the complex nature of interactions between ice sheets and ocean circulation that is not yet fully revealed to the scientific community. Further research of these vital processes is needed to better understand past reconstructions and apply lessons learnt to future projections.

We can summarise from these examples of the recent geological past that at least interactions of land-based ice sheets and ocean circulation can have a significant impact on the climate and affect climate variability. In a more general sense, all components of the climate system will be involved in these changes and interactions, and will respond in positive or negative feedbacks to the external forcings such as the orbital insolation forcing.

The Holocene climate exhibits a large variety of climatic factors, which makes it a perfect time period to study climate variability in more detail. In this thesis we will investigate the Holocene climate and its variability.

1.2 This Thesis

This thesis is part of the European Commission's 7th Framework Project "*Changing Arctic and Subarctic Environment*" (CASE) that started in April 2010 and was set up as an Initial Training Network (ITN) with 6 partner institutes/universities. The project allowed all 12 early career researchers (ESR) to visit the partner institutes and to get to know their way of working. The partners are

- Université Bordeaux (EPOC)
- Norges Geologiske Undersøkelse (NGU)
- Helmholtz Zentrum für Ozeanforschung Kiel (GEOMAR)
- University of Plymouth
- Universitetet i Tromsø
- Vrije Universiteit Amsterdam

The project emphasises the need for further research in the Arctic and the Nordic Seas region, because of the vulnerability of these regions to future climate change. One important reason is the polar amplification of future greenhouse-gas driven warming that will warm the Polar Regions more intensely than the rest of the globe. Because of this amplification changes in Arctic climate are already visible. The Arctic has warmed twice the global rate (1-2°C, McBean et al., 2005) in the last 50 yrs, Arctic sea-ice area has considerably retreated (7.4 %, Johannessen et al., 2004) and the melting of the Greenland ice sheet has accelerated since 1992. Thus, ice sheet melting will be a major contributor to global sea level rise in the 21st century (Rignot et al., 2011). The goal of the CASE project was to employ a multi-disciplinary approach to investigate these aspects of Arctic and Nordic Seas climate change in past climates and provide a wider view of changes that happened and are predicted to happen in the future.

1.3 Reconstructing Past Climates – Proxies and Modelling

The modern perspective of climate relies on direct observations of for example temperature and as direct observations are not available earlier than the 17th century (1659 AD, Manley, 1974), an indirect observation of for example temperature is needed. This is called a proxy, an indirect indicator of climate that is recorded in proxy-archives like tree rings, pollen, stalagmites in caves, ice cores (Greenland and Antarctica), corals, lake- and ocean-sediments. For example, the actual proxy that links with temperature, in ice cores is the ratio of heavy (^{18}O) vs. light (^{16}O) oxygen isotopes, called δ^{18}O. This isotopic ratio is a function of the temperature at which condensation occurs (Dansgaard, 1964), which indicates climate conditions at that time. Sampling the ice core at certain intervals results in a time series.

Another method that is commonly used is to analyse ocean sediments, which contain skeletons of millions of marine organisms. The most commonly used ones in palaeoceanography are foraminifera (calcareous zooplankton), coccoliths (calcareous algae), radiolarians and silicoflagellates (siliceous zooplankton), and diatoms (siliceous algae). Using these microfossils, there are many methods that can be applied to obtain palaeoclimatic information from marine sediments. We briefly discuss here two of these methods that are commonly used: Oxygen isotope composition of calcium carbonate (e.g. Emiliani, 1977, 1978; Shackleton, 1977) and relative abundance of warm- and cold-water species (e.g. Williams and Johnson, 1975). The reconstruction of past climate conditions from oxygen isotopes is a lot more complex than from ice cores, because of numerous effects that act on the recorded signal, such as the vital effect of the organisms (Urey, 1948) or changes of the isotopic composition of the ocean reservoirs (Fontugne and Duplessy, 1978). Despite these uncertainties, oxygen isotope records have proven to be a reliable source of

information and given us an indication of million of years of Earth history (as in Fig. 1.4, Emiliani, 1955; Shackleton, 1967; Hays et al., 1976; Lisiecki and Raymo, 2005). The second method aims at understanding the abundance of a certain species, which can tell you a lot more than just climate conditions, such as environmental conditions (e.g. food supply or acidity of the ocean). Despite this additional information on the ocean environment, a transfer function is often applied to these abundances, which allows transferring past species compositions to present-day and corresponding to certain temperatures (Imbrie et al., 1973) of, for example, the sea surface. This method is often applied in sub polar regions, where different species depend on different water masses and can therefore indicate changes in the ocean surface conditions.

All these proxy reconstruction methods are extremely useful to go back in time as far as million of years. However, there are several uncertainties associated with these reconstructions that limit their quantitative use. First of all, the relationship that connects to the physical climate parameter (e.g. temperature (air, sea surface) or precipitation) and secondly, the timing of these reconstructions as expressed in the age model. Every reconstruction depends on the quality of its age-depth model (Telford et al., 2004; Huybers and Wunsch, 2010). Proxy-based reconstructions are a good way to gain information on past climates and apply our knowledge of physical relations to past times, but of course they do not allow making useful predictions of future climate change. Fortunately our physical understanding can be described by mathematical equations and with the capabilities of modern computers, it is possible to create a physical approximation of our understanding, a numerical model.

These numerical climate models have come from a long history of atmospheric models used to predict weather and evolved into fully coupled models covering all components of the climate system in all kind of complexities. Hence, it is fair to say that these models are among the most complicated machineries that have ever been assembled and

consist of millions of lines of code, the equivalent of moving parts (Wunsch, 2010). But every model is a simplification of the real world and although potentially seen as a disability, it is the model's great power to simplify and make things understandable, as a completely realistic machinery would be as complex as the real climate system itself. The challenge is to find a balance between physical completeness and costs in terms of computing power. Therefore, a large variety of models have emerged from these limitations that sufficiently comply with different applications. Claussen et al. (2002) distinguishes three classes of models, comprehensive models (Coupled Global Climate Models, CGCMs), Earth system Models of Intermediate Complexity (EMICs) and conceptual models (mostly energy balance models). The above order indicates their integration of processes or complexity. Thus, the most complex models are at present CGCMs, including at least a physically and spatially detailed, 3-dimensional description of the coupled ocean and atmosphere system. These models are extensively used in future climate projections (IPCC, 2013). However, their application to longer timescales is rather limited, as an integration of several thousand years would simply take too long to be feasible, even on the fastest computer systems. Therefore, to make multi-millennial scale experiments it is necessary to reduce the complexity and use EMICs. Simulations on even longer time-scales require a further reduction in complexity (as in energy balance models) to calculate millions of years into the past or the future. Hence, all these models have a comfort zone, where they are useful to apply.

The development of climate models involves several principal steps: Simplification of the mathematical expressions describing physical laws, implementing these mathematical expressions in a computer requiring numerical algorithms, and finally building and implementing conceptual models (parameterizations) for processes that cannot be represented because of their complexity or because of their spatial and temporal scales (Flato et al., 2013). For example, atmospheric convection or clouds

would require unrealistically high (∼1km) horizontal, vertical and temporal (seconds) resolutions and thus, cloud physics are commonly parameterized in global climate models. Trade-offs in the model parameterizations are guided by the intended model application and lead to the mentioned several classes of models of different complexity. Every model development includes a verification step, which compares the model results with direct observations. This is usually done for each component of the coupled climate model individually and when assembled to a comprehensive model it is done even more so. At this stage it is not uncommon to tune the coupled model to better represent the large-scale observational constrains and correct for un-natural drifts (Flato et al., 2013).

Originating from this problem of representativeness, studies focusing on longer time-scales are limited to the use of simplified models, thereby accepting certain trade-offs. In this thesis, the focus is on centennial-millennial time-scales and only simulations with the EMIC LOVECLIM are used and analysed.

1.4 LOVECLIM

LOch-Vecode-Ecbilt-CLio-agIsm Model (LOVECLIM, Fig. 1.8) is an Earth System Model (ESM) of intermediate complexity including a 3-dimensional, global representation of the atmosphere, the ocean and sea ice and the vegetation that is simplified compared to CGCMs (Goosse et al., 2010). There are additional dynamical components available that have not been used in this thesis, such as the carbon cycle, ice sheets and icebergs. The atmospheric component of the model is called EcBilt a 3-layer quasi-geostrophic, spectral model truncated at wavenumber 21 (T21), translating to a horizontal resolution of about 5.6° in latitude and in longitude (Opsteegh et al., 1998). Due to the low resolution of the model, convection has to be parameterized (Held and Suarez, 1978) and cloud cover is prescribed from climatology, and is thus not

treated dynamically (Rossow, 1996). Precipitation in the Arctic and North Atlantic is systematically overestimated and, to keep the ocean circulation from being sluggish, this precipitation surplus is artificially removed and redistributed over the North Pacific, where precipitation is systematically underestimated (a so-called flux correction, Goosse et al., 2010). EcBilt includes a land-surface model calculating snow cover and handling the runoff of excess precipitation to the adjacent ocean. The ocean-sea ice component of LOVECLIM is called CLIO and consists of a free-surface ocean general circulation model with a horizontal resolution of 3° in latitude and longitude (Goosse and Fichefet, 1999; Goosse et al., 2010) and a vertical resolution of 20 levels. The effects of small-scale processes such as isopycnal[1] mixing, vertical mixing and convection are parameterized (Goosse et al., 2010). To improve the representation of dense water flow a downslope parameterization has been included (Campin and Goosse, 1999). The sea-ice component of CLIO is a three-layer thermodynamic model with an elaborate scheme to determine the sea-ice edge more precisely in a coarse resolution grid (Fichefet and Maqueda, 1997, 1999). The free surface of the model requires the sea-ice component to exchange freshwater as positive or negative virtual salt fluxes. The vegetation component of LOVECLIM is called VE-CODE and simulates the dynamics of two plant functional types, trees and grasses, as well as desert (Brovkin et al., 2002), under influence of changes in temperature and precipitation that are obtained from EcBilt.

In principle LOVECLIM includes a dynamic ice sheet (Huybrechts, 2002) that is coupled to the other components and it has been applied in numerous studies of the past and future climate (Ridley et al., 2005; Simpson et al., 2009; Huybrechts et al., 2011). The advantage of including an ice sheet model in simulations of past climates is the completeness of the dynamic climate system components in respect to a fixed pre-industrial ice sheet extent and interaction. However, including dynamical ice sheets is a lot more complex, because of the slow response

[1] Isopycnal is a surface of constant potential density of water.

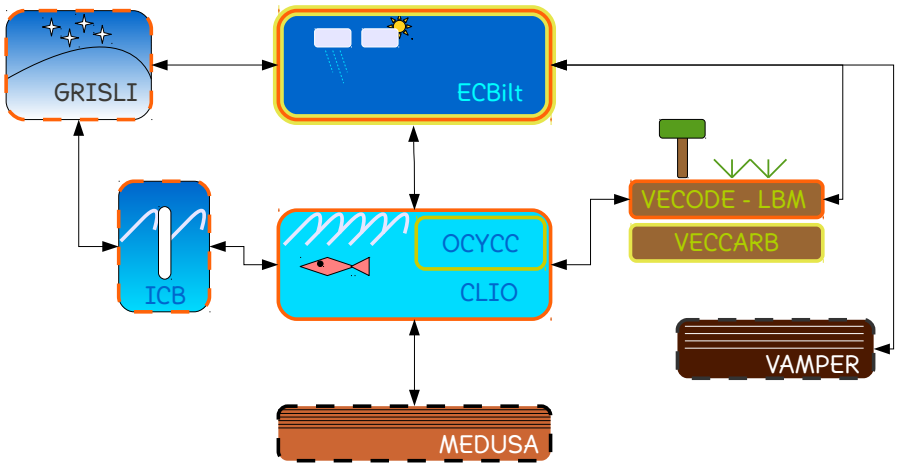

Figure 1.8: Summary of the coupled components in LOVECLIM. ECBilt is the atmospheric model. CLIO is the ocean and sea-ice model. VECODE is the vegetation model. GRISLI is the dynamical ice-sheet model. ICB is the iceberg model. VAMPER is the permafrost and MEDUSA the sedimention model. ©Roche (2013) additional information in Goosse et al. (2010)

time of this component (Fig. 1.3) and the additional degrees of freedom of the coupled system. Thus, the problem would be to make the ice sheet and therefore the whole coupled climate model behave according to known reconstructions of past ice sheet extent and volume (Peltier, 2004; Zweck and Huybrechts, 2005; Charbit et al., 2007). This can be considered to be still an open challenge. Therefore, we have chosen to prescribe the ice sheets from reconstructions rather than dynamically modelling them throughout this thesis. This bears the advantage of being able to control the influence of the ice sheet on climate and in our simulations and regard it as a forcing, rather than a dynamic component of the climate system. Of course this methodology can only be applied when reconstructions of ice sheets from geological data are available, which is the case for the past 21.000 years (Peltier, 2004).

Despite its low resolution, LOVECLIM reproduces the major characteristics of the observed climate both for present-day and past conditions, such as the Last Glacial Maximum (LGM, Roche et al., 2007) or the

Mid-Holocene (Braconnot et al., 2007). LOVECLIM has been applied in numerous paleoclimatic studies, for instance investigating the 8.2 ka BP event (Wiersma and Renssen, 2006), the Holocene (Renssen et al., 2009; Blaschek and Renssen, 2013a) and the Last Interglacial (Bakker et al., 2013b).

However, there are some serious biases still present in the model (Goosse et al., 2010): most prominently an overestimation of temperature in the tropics, a too symmetric distribution of precipitation between the two hemispheres and an overestimation of precipitation and vegetation cover in the subtropics (Goosse et al., 2010). Overall the atmospheric circulation is too weak and the model tends to underestimate surface temperature changes, mainly in the tropics, and to overestimate oceanic heat uptake compared to observations of the last decades.

The ocean circulation in LOVECLIM performs reasonably well with slightly higher values of the absolute AMOC strength and a weaker response to future warming scenarios, in a comparison of 25 Atmosphere-Ocean Global Circulation Models (AOGCM) and 5 EMICs in the Coupled Model Intercomparison Project (CMIP5, Weaver et al., 2012). However, Huybers and Wunsch (2010) emphasise that the exact value of the AMOC is unknown and that the ability to represent a good estimate of the recently observed AMOC strength (Kanzow et al., 2010) of 18.7 $\pm$2.1 Sv inside a model does not necessarily proof to be a reliable estimate of the real ocean and its circulation. Anyhow, an application on longer timescales considering large-scale changes is regarded a valuable purpose of LOVECLIM and its dynamic subcomponents.

1.5 Research Questions

The ITN-CASE project defined in its goals that the Arctic and the Subpolar Regions are important in the context of understanding the climate

system and its response to natural and human induced changes. Therefore, the overall topic of this thesis is set to investigate Holocene climate change and variability by employing a climate model and compare results to proxy based reconstructions. The advantage of employing a climate model compared to proxy-based reconstructions is the ability to make predictions. However, to make predictions it is necessary to understand how well the model is able to reproduce past climates and events that can be constrained by proxy-based reconstructions.

The recent past seems to be a good starting point for investigating climate variability in the Arctic and sub-Arctic environment. In simulations of for example the mid-Holocene (6,000 yrs BP) the Arctic sea-ice extent has been found to be very different between 25 climate models (Berger et al., 2013), showing both decreases and increases due to slightly warmer summers as well as cooler winters. These experiments have been performed within the framework of the Paleoclimate Modelling Intercomparison Project (PMIP) Phase 2 and 3 (Braconnot et al., 2007; Braconnot et al., 2012), which aims to test climate models employed for future projections under palaeo situations. The results highlight the Arctic as a key region among others (e.g. Asian Monsoon) of climate variability and therefore of dynamical processes relevant for understanding and predicting climate change in past and future climates.

Previous Holocene modelling studies such as Crucifix et al. (2002) for example showed employing the EMIC MoBidiC over the past 9.000 yrs a long-term cooling trend in line with orbitally-induced insolation changes over the Northern Hemisphere. Their results indicated that vegetation changes increase Arctic sea-ice extent due to cooling and highlight the relevance of this dynamic vegetation feedback on longer timescales. Building on these results Renssen et al. (2005b) showed employing a previous version of LOVECLIM (ECBilt-CLIO-VECODE) similar cooling trends over the past 9.000 yrs, which showed spatial differences compared to proxy-based reconstructions. Results indicate that the interaction of sea-ice and convective activity in the Nordic Seas and Labrador

Sea enhances inter annual variability following the cooling trend. They further considered topography and albedo changes from the Laurentide Ice Sheet (LIS) before 7 kyr BP, which resulted in extended cooling and contributed to the later work of Renssen et al. (2009), who showed that the early Holocene was significantly influenced by the remnant Laurentide Ice Sheet (LIS). The LIS covered large parts of North America and released huge amounts of melt water (up to 0.09 Sv, 1 Sv = 10^6 m^3/s) to the surface ocean. This large land-based ice sheet affected the large-scale atmospheric circulation by cooling due to higher surface albedo and by redirecting the atmospheric flow due to the large topographic barrier the ice sheet constitutes. Hence it has been shown by Renssen et al. (2009) that the LIS had a significant impact on the timing and the spatial distribution of the Holocene Thermal Maximum (HTM). The warmest period during an interglacial period is usually referred to as the Thermal Maximum. It was shown by Renssen et al. (2009) that the HTM was delayed due to melt water and downwind cooling from the ice sheet and that simulations including these feedbacks corresponded better to proxy-based reconstructions (Kaufman et al., 2004). The early Holocene differs due to the melting of ice sheets from the rest of the Holocene, but the LIS was not the only ice sheet that was melting at that time. The Greenland ice sheet (GIS) was also considerably larger during the LGM (65% larger than at present-day, Funder et al., 2011a) and contributed to the sea level rise. Although the estimated melt water flux from the GIS is at least a magnitude smaller compared to the LIS, the location of the GIS is closer to convection areas in the Labrador, the Irminger and the Nordic Sea. Therefore, it is important to estimate the impact of GIS melting in the early Holocene and on the HTM. Additionally, related to the HTM, Andersen et al. (2004b) reconstructed Nordic Seas' sea surface temperatures, which show an early HTM in the eastern part of the Nordic Seas and no or relatively late in the western part. This zonal difference is not well explained and it seems likely that the GIS melt water might be a key witness to this unexplained spatial discontinuity. Hence we formulate the following more general question,

but will focus in our analysis on the Nordic Seas:

1st Research Question – *What is the impact of GIS melting on the Holocene Thermal Maximum?*

During the deglaciation, the melting of the ice sheets does not only affect the ocean circulation, but it also affects the sea level stand. The LGM had a 120 m lower sea level stand (Siddall et al., 2003) with considerable impacts on global coastlines. The Arctic Ocean for example was reduced by 53% of its present-day area (Jakobsson, 2002; Darby et al., 2006, cf. Fig. 1.6) and large shelf areas that are presently flooded, became land and partly glaciated (e.g. Barent Sea Ice Sheet, Svendsen et al., 2004). Few reconstructions of Arctic coastline transgression exist (e.g. Bauch et al., 2001; Taldenkova et al., 2010) and few modeling studies have taken these changes of bathymetry into considerations and then mostly during the LGM (Roche et al., 2007; Friedrich et al., 2010; Roche et al., 2012) when the changes have been most dramatic. However, considering a record from the Laptev Sea (Bauch et al., 2001) and extrapolating its lower sea level stand to the whole Arctic Ocean bathymetry indicates a large area, the East Siberian Sea, to become dry land in the early Holocene. Here, the sea level rose from 8.9 ka BP to 7.5 ka BP by 24 m (Bauch et al., 2001; Taldenkova et al., 2010), resulting in the flooding of the East Siberian shelf area. At present-day the Arctic shelves, and the Laptev Sea, are important as sea-ice production areas and relate to the export of Arctic sea ice into the Nordic Seas (Dethleff and Kuhlmann, 2010). The relation of Arctic shelf flooding, Fram Strait sea-ice export and climate variability in the Nordic Seas remains unknown and leads to the following question:

2nd Research Question – *What impact does the flooding of an Arctic shelf introduce in the Nordic Seas?*

When we investigate the Holocene and its climatic changes due to melt water and ice sheet decay, and introduce GIS melting as a new forcing, then we have to investigate changes in the AMOC. The impact of

melting ice sheets has been considered in numerous modelling studies (e.g. Rahmstorf, 1996; Renssen et al., 2009) and can be found in numerous proxy-based reconstructions (McManus et al., 2004; Alley and Ágústsdóttir, 2005; Thornalley et al., 2013), thus allow insights into the highly variable nature of the AMOC and its mode of operation on short (decadal) and long (millenial) time scales (Srokosz et al., 2012). Unfortunately, the period of direct observations is rather short (∼4yrs, Kanzow et al., 2010) and the long-term evolution of the AMOC is uncertain, both its past and future. It has been once said (F.P. Shepard, 1948) that mankind knows more about the moon's surface than about the deep ocean floor. The statement is of course an exaggeration of the complex problem of observing an ever-changing system, but a short summary of the present-day challenge to explain the driving mechanisms of the AMOC in detail (Kuhlbrodt et al., 2007). Nevertheless, there exists a large number of reconstructions using different kind of proxy relationships to investigate past AMOC changes. Past proxy-based reconstructions focus on deep water transport and mostly on subcomponents of the lower limb of the AMOC, such as the overflow waters across the Greenland-Scotland Ridge, via the Denmark Strait or the Iceland-Scotland Ridge. Changes in flow speeds (Bianchi and McCave, 1999) for example can be recorded in ocean sediments and qualitatively reconstructed to estimate large-scale or small-scale changes. However, the information available from proxy-based reconstructions and previous model results do not provide a consistent view on the history of the AMOC and its variability. Hence, we propose the following question:

3rd Research Question – *What was the strength of the AMOC and its subcomponents during the Holocene?*

Of course the investigation of past changes in the climate system can be seen as an academic endeavour to acquire knowledge, but it certainly is also an elaborate way to improve projections of climate change. A greater understanding of past climates allows saying what is probable and what is improbable, thus increasing the confidence one puts into

future climate model projections. It has been often said that the future will be in many ways different from the past and for the climate system this is certainly true, considering future anthropogenic greenhouse gas emissions. The amount of greenhouse gases pumped into the earth system by various industries and transportation means is already exceeding the 800 kyr record from Antarctica (Masson-Delmotte et al., 2013). Given the implications to all components of the climate system at different timescales, the following question emerges: How different will the future be? Certainly this is not a question that can be easily answered or answered at all, but we have to assume that the past and the future climate are connected and knowing about the past will help to answer this question. However, given the complexity of this problem and our previous investigations, we focus on a more detailed question that relates to changes of the AMOC in future climates and melt water from the Greenland ice sheet. Today, the increasing temperatures in Greenland cause the ice sheet to lose mass and release relatively large volumes of melt water and ice bergs to the surrounding ocean (Rignot et al., 2011). Given present-day melt rates (18 mSv, Dickson et al., 2007) and future increases, the fate of the Greenland ice sheet is uncertain and the implications of its melt water to the North Atlantic and the global ocean circulation as well. Thus, to understand in what ways the future will be different from the past we propose to investigate the sensitivity of the AMOC to GIS melt water in the early Holocene, the last interglacial period and in future emission scenarios. The last interglacial period is particularly interesting as recent studies indicated a sea level rise from Greenland melting of up to 2 m compared to present-day (Dahl-Jensen et al., 2013). Thus, leading to the following question:

4th Research Question – *What is the impact of GIS melting beyond the Holocene and what can we learn for the future?*

Our research questions make clear that our focus lies on the Nordic Seas and impacts in the Nordic Seas from various ice sheets (LIS, GIS) and Arctic impacts related to sea level rise due to ice sheet melting.

The interaction of atmosphere, ocean and ice sheets is one of the most complicated and nonlinear interplays that determined changes in the climate system since the beginning of land-based glaciations 35 million years ago.

Chapter 2

The Holocene thermal maximum in the Nordic Seas: the impact of Greenland Ice Sheet melt and other forcings in a coupled atmosphere-sea ice-ocean model

Based on: Blaschek, M. and Renssen, H.: The Holocene thermal maximum in the Nordic Seas: the impact of Greenland Ice Sheet melt and other forcings in a coupled atmosphere–sea-ice–ocean model, Climate of the Past, 9, 1629–1643, doi: 10.5194/cp-9-1629-2013, 2013a

The relatively warm early Holocene climate in the Nordic Seas, known as the HTM, is often associated with an orbitally forced summer insolation maximum at 10 ka BP. The spatial and temporal response recorded in proxy data in the North Atlantic and the Nordic Seas reveals a complex interaction of mechanisms active in the HTM. Previous studies have investigated the impact of the Laurentide Ice Sheet (LIS), as a remnant from the previous glacial period, altering climate conditions with a continuous supply of melt water to the

Labrador Sea and adjacent seas and with a downwind cooling effect from the remnant LIS. In our present work we extend this approach by investigating the impact of the Greenland Ice Sheet (GIS) on the early Holocene climate and the HTM. Reconstructions suggest melt rates of 13 mSv for 9 ka BP, which result in our model in an ocean surface cooling of up to 2 K near Greenland. Reconstructed summer SST gradients agree best with our simulation including GIS melt, confirming that the impact of the early Holocene GIS is crucial for understanding the HTM characteristics in the Nordic Seas area. This implies that modern and near-future GIS melt can be expected to play an active role in the climate system in the centuries to come.

2.1 Introduction

In the early Holocene a period of relatively warm climate, the Holocene Thermal Maximum (HTM), has been associated with the orbitally-forced Northern Hemisphere summer insolation maximum at approximately 10 ka BP (Jansen et al., 2008). Indeed, detailed analyses of proxy data and model results have confirmed that orbital forcing is the dominant long-term forcing considering temperature response at the scale of the Arctic (Renssen et al., 2009). Compared to this impact of orbital forcing, the effect of variations in atmospheric greenhouse gases on the temperature response is relatively small (Renssen et al., 2009). Although the HTM is mainly orbitally forced, the spatial and temporal response of the climate system is diverse. Maximum temperatures were often delayed by several thousand years compared to the summer insolation maximum, as evidenced by numerous terrestrial and marine proxy records (e.g. Jansen et al., 2007). The causes of this spatial and temporal complexity of the HTM have not been resolved for all regions, for instance the Nordic Seas. This region is the transition zone of two major ocean currents: the North Atlantic Current (NAC) to the East, transporting warm and saline waters to the North and the EGC to the

West, transporting cool and less saline waters to the South. In this paper we evaluate the characteristics of the HTM in this important region by analysing the impact of potential forcing factors in numerical climate model simulations and by comparisons with available proxy evidence.

In a previous study, Renssen et al. (2009) have shown in transient climate model simulations, combined with summer temperature reconstructions based on terrestrial proxies, that the Laurentide Ice Sheet (LIS) delayed the HTM over the North Atlantic and down-wind continents (Europe and Asia) by up to 3000 yr. This ice sheet persisted until around 6 ka BP and caused regional cooling by inducing melt water discharges and by altering the surface albedo and topography. An important effect of the LIS melt flux was that it suppressed deep convection in the Labrador Sea, causing expanded sea ice cover and cooler surface conditions compared to today. An important part of this spatio-temporal complexity can be explained by the impact of the remnant LIS in North America (Kaufman et al., 2004; Kaplan and Wolfe, 2006). However, the simulated characteristics of the HTM of Renssen et al. (2009) were not specifically compared to reconstructions of sea surface conditions so that it remained unclear what the impact of the LIS was on modelled Holocene sea surface temperatures (SSTs) in the North Atlantic Ocean and the Nordic Seas, and if the model results were consistent with marine proxies from this region.

The characteristics of the HTM (timing and magnitude) in the Nordic Seas are rather unclear, as different marine proxies suggest different SST evolutions during the Holocene. Sea surface reconstructions based on diatoms show a non-uniform response of SSTs in the eastern and western parts of the Nordic Seas over the last 10 000 yr (Andersen et al., 2004a). These diatom-based reconstructions indicate that over the Vøring Plateau (in the east), maximum warming occurred between 10 and 9 ka BP, with summer SSTs being 4–5 K above the pre-industrial mean, while on the western side the thermal maximum was later (between 8.5 and 6.5 ka BP) and less expressed (1 K above the pre-industrial mean). Consequently,

SSTs based on diatoms show an earlier (by 1.5–2.5 ka) and warmer HTM (3–4 K difference) on the eastern than on the western side. This east-west contrast has been explained by a stronger cooling impact by post-glacial sea ice and melt water in the West before 8.5 ka BP, leading to a clearer expression of the early Holocene warming influence by insolation in the East (Andersen et al., 2004a). However, it has been argued by Koç et al. (1993) and other studies (Kaufman et al., 2004; Jansen et al., 2008; Risebrobakken et al., 2011) that these warmer temperatures cannot be due to insolation alone. Eastern SSTs reconstructed from alkenones (Calvo et al., 2002) show a behaviour similar to the orbital trend, but are considerably lower at the thermal maximum (by 2–3 K) and yield a later HTM (i.e. between 8.5 and 5.5 ka BP) at the Vøring Plateau. Moreover, at the same site SST reconstructions based on foraminifera and radiolarians also lack this early HTM suggested by diatoms (Risebrobakken et al., 2003, 2011; Cortese et al., 2005; Dolven et al., 2002). Jansen et al. (2008) suggest that the SST maximum recorded in proxy data above the seasonal thermocline (diatoms, alkenones) is forced by the summer insolation maximum and that deeper dwelling species (foraminifera and radiolarians) are not influenced. Andersson et al. (2010) support this hypothesis in a comparison with climate model simulations of the 6 ka BP climate performed with the CCSM3 model. These model results suggest that seasonal summer warming, related to the orbitally-forced summer insolation maximum, is restricted to the upper 30 m in the Nordic Seas during the early Holocene. Recently, Risebrobakken et al. (2011) separated the impact of orbitally-forced summer insolation and early Holocene warm surface waters associated with increased advection of Atlantic waters (Kaufman et al., 2004; Koç et al., 1993) and emphasized the effect of both horizontal heat advection and radiative forcing on overall conditions in the Nordic Seas. The non-uniform response across the Nordic Seas as reconstructed by Andersen et al. (2004a) seems to be a robust feature in palaeoceanographic reconstructions, thus raising the question of the origin of this zonal difference. Consequently, the expression of the HTM in the Nordic Seas and the impact of possible

feedbacks like increased heat advection by the NAC or Greenland melt water are still unclear.

In principle, climate model simulations could shed light on the role of different forcings and the SST response during the Holocene in the Nordic Seas. The model results of Renssen et al. (2009) suggest an earlier (8–7 ka BP) and warmer (more than 2 K above pre-industrial level) thermal maximum in the western part of the Nordic Seas than in the eastern part (7–6 ka BP and up to 1 K above pre-industrial level). Hence, these simulations did not capture the timing of the HTM and the gradient in the Nordic Seas as indicated by the diatom-based SST reconstructions. However, in the experiments of Renssen et al. (2009), the impact of the Greenland Ice Sheet (GIS) was not included, while potentially sea surface conditions in the Western Nordic Seas were strongly influenced by GIS melt. Geological records (as reviewed in Funder et al., 2011a) and modelling studies (Simpson et al., 2009) agree that the GIS was bigger in the early Holocene compared to present-day and may have reached its Holocene minimum at 6 ka BP, followed by a regrowth. Estimates from Peltier's (2004) ICE5G model suggest a 25 % larger GIS at 9 ka BP that loses mass until 7 ka BP and expands again before returning to its present-day extension at $\sim$5 ka BP. Reconstructed GIS borehole site elevations from Vinther et al. (2009) indicate that these sites were 100–300 m higher for 9 ka BP compared to today. Lower elevation sites like Camp Century and Dye3 show a fast decrease in elevation in the early Holocene, whereas NGRIP and GRIP give a steady decrease from the early to the late Holocene. Consequently, both these estimates support the idea that in the early Holocene the GIS melt flux was larger than today. No quantified estimates of this early Holocene melt flux have yet been published, but based on Peltier (2004) we could infer a best guess additional flux of 13 mSv ($1\,\mathrm{Sv} = 1 \times 10^6\,\mathrm{m^3\,s^{-1}}$) for 9 ka BP.

How does this early Holocene GIS melt flux compare to projections of GIS melt for the present and the near future? Dickson et al. (2007) give a modern day estimate of GIS melt of 18 mSv including melt and

ice berg calving. For the past two decades Rignot et al. (2011) find an acceleration of Greenland mass loss of 21.9 ± 1 Gt yr^{-2}, converting into 12.5 mSv additional melt water during that period. Schrama and Wouters (2011) derive a similar estimate of mass loss acceleration (22 ± 4 Gt yr^{-2}), which converts into 4.9 mSv between 2003 and 2010. A simple extrapolation of these estimates yields 35 ± 1.5 cm of sea level rise by 2100, resulting from a steady increase of melt water flux of up to 80 mSv at 2100. Using a climate model coupled to a dynamical GIS model, Driesschaert et al. (2007) simulate a future retreat of the GIS within 3000 yr under an extreme warming scenario, peaking with a relatively large melt rate of 0.1 Sv after 1000 yr, which has a noticeable weakening effect on the Atlantic Meridional Overturning Circulation (AMOC) in the model. However, when extrapolating the estimates from Rignot et al. (2011), such high melt rates would be reached soon after 2100 AD. Although these estimates assume a fixed acceleration rate, the impact on the AMOC highlights the importance of the GIS in future and in warmer past climates.

It is our objective in this paper to quantify the effect of GIS melt on the early Holocene climate in the Nordic Seas and to compare this impact with that of other important forcings by extending the modelling approach of Renssen et al. (2009). We present several transient simulations and force our model with a transient LIS deglaciation and a GIS melt water flux derived from Peltier (2004). We use an updated version of the model (ECBilt-CLIO-VECODE) previously employed by Renssen et al. (2009). This model has now been renamed to LOVECLIM (Goosse et al., 2010). We focus on the expression of the HTM in the Nordic Seas and aim to distinguish the impact of different forcings on SSTs. We will also evaluate which expression of SSTs in the Nordic Seas, as reconstructed using the different marine proxies, appears most consistent with our model results. In other words, does our model reproduce the clear east–west gradient and early timing of the HTM suggested by the diatom-based SST reconstructions, or rather a more uniform response

across the Nordic Seas?

2.2 Experimental design

2.2.1 The model

We performed our experiments with the Earth system model of intermediate complexity (EMIC) LOVECLIM (version 1.2; Goosse et al., 2010), which includes a representation of the atmosphere, the ocean and sea ice, the land surface and its vegetation. We have not activated the components for dynamical ice sheets and the carbon cycle that are also included in LOVECLIM. We present here a brief summary of its key components, and more details can be found in Goosse et al. (2010). The sea-ice–ocean component is CLIO3 (Goosse and Fichefet, 1999), consisting of a free-surface ocean general circulation model with a horizontal resolution of $3^\circ \times 3^\circ$ latitude–longitude and 20 vertical levels, coupled to a sea ice component (Fichefet and Maqueda, 1997, 1999) employing a three-layer dynamic–thermodynamic model that simulates reasonably well the present-day Arctic sea ice distribution (Goosse et al., 2007). The atmospheric component is ECBILT (Opsteegh et al., 1998), a spectral T21, three-level quasi-geostrophic model including a bucket-type hydrological model for soil moisture and runoff. Cloud cover is climatologically prescribed. The vegetation is handled by VECODE (Brovkin et al., 2002) a dynamical vegetation model simulating two plant types, trees and grasses and desert as a dummy type. We prescribed the ice sheets manually. The climate sensitivity of LOVECLIM (version 1.2) to a doubling of the atmospheric CO_2 concentration is at the lower end of the range found in global climate models (1.9 K after 1000 yr; Goosse et al., 2010). The simulated deep-ocean circulation in LOVECLIM1.2 compares reasonably well with other model results (Schmittner et al., 2005), with deep convection taking place in both the Nordic Seas and

the Labrador Sea (Goosse et al., 2010). The model has been applied successfully in different palaeoclimatological modelling studies for settings like the 8.2 ka BP event (Wiersma and Renssen, 2006) and the Holocene (Renssen et al., 2009).

2.2.2 Experimental design

In this study we discuss the results of four transient experiments that cover the last 9000 yr and eight quasi-equilibrium snapshot experiments, seven with forcings fixed at 9 ka BP and one with forcings for the pre-industrial era (Summary in Tab. 2.1). Except for the experiment with pre-industrial forcings, the simulations were started at 9 ka BP because before that time the influence of the Younger Dryas cold period may still have an important influence on the climate through the long-term memory of the deep ocean. We forced all simulations with orbital and greenhouse-gas concentrations in line with the PMIP3 protocol (`http://pmip3.lsce.ipsl.fr`). An overview of the forcings is provided in Fig. 2.1.

2.2.3 Snapshot experiments

We performed one control snapshot experiment for background conditions at 9 ka BP with orbital and greenhouse gas forcing (9kOG). This experiment was spun up for 1000 model years to ensure quasi-equilibrium conditions in all components of the model to the forcings (cf. Renssen et al., 2006), implying that the mean global ocean temperature is stabilised. The final results of 9kOG have been used as initial conditions for all other 9k BP snapshot simulations which have a duration of 500 model years during which forcings were kept fixed. In PI and 9kOG, the land-sea-mask, GIS topography, albedo, solar constant and aerosol content were fixed at PI configuration. The fixed land-sea mask will not likely impact the results as the difference in sea level between the

Experiment name	Initial conditions	GIS Melt flux (Sv)	LIS Melt flux (Sv)
9kOG	Orbital (9000 BP), greenhouse gases (9000 BP)	0	0
PI	Orbital (1950 AD), greenhouse gases (1750 AD)	0	0
9kOGx1	9kOG + Greenland ice sheet melt	0.013	0
9kOGx2	9kOG + Greenland ice sheet melt	0.026	0
9kOGx4	9kOG + Greenland ice sheet melt	0.052	0
9kOGMELT	9kOG + Laurentide Ice Sheet melt water	0	0.09
9kOGMELTICE	9kOGMELT + ice sheet (albedo + topography)	0	0.09
9kOGGIS	9kOGMELTICE + GIS melt water	0.013	0.09
OG	Transient orbital and greenhouse gases (9–0 ka BP) from PMIP3 transient simulation setup	0	0
OGMELT	OG + Laurentide Ice Sheet melt water	0	0.09 – 0
OGMELTICE	OGMELT + ice sheet (albedo + topography)	0	0.09 – 0
OGGIS	OGMELTICE + GIS melt water	0.026 – 0	0.09 – 0

Table 2.1: Summary of the experimental design. Transient forcings are shown in Fig. 2.1. Orbital parameters and Greenhouse Gases are in line with the PMIP3 protocol (`http://pmip3.lsce.ipsl.fr/`) for transient simulations. Laurentide Ice Sheet melt water fluxes are from Licciardi et al. (1999). Greenland Ice Sheet melt water fluxes are calculated from Peltier (2004) ice thickness changes.

two periods is only 19.71 m (9 ka BP; Siddall et al., 2003), implying that only a few grid cells are affected at the relatively low resolution of our model (i.e. T21 or about 560 km × 560 km in the horizontal grid space for the atmosphere and 3° by 3° latitude-longitude in the ocean). We neglect changes to bathymetry in our simulations. Our analysis is based on averages that are calculated over the last 100 yr of the simulations.

We performed three 9 ka BP snapshot experiments to assess the sensitivity to the early Holocene GIS melt water flux (Tab. 2.1, 9kOGx1,

9kOGx2, 9kOGx4). In these experiments, we prescribed multiples of a best-guess estimate of the early Holocene GIS melt flux of 13 mSv. This melt flux is derived from ice thickness changes provided at 500-yr time steps by the Peltier (2004) ICE-5G model. We add the additional melt water to the normally calculated surface runoff (i.e., sum of excess precipitation and snow melt), which is then evenly distributed over 10 major runoff points (c.f. Bakker et al., 2012) for locations of river outflow points).

In two additional snapshot experiments (9kOGMELT, 9kOGMELTICE) we added the LIS forcing to the impact of 9ka BP orbital and greenhouse forcing, identical to Renssen et al. (2009). In these experiments, we separately investigate the effect of an additional freshwater flux (0.09 Sv, denoted by MELT), representing the background melting of the LIS introduced at the St. Lawrence River outlet and Hudson Bay outlet, and the total effect of the remnant LIS (i.e. additional freshwater, albedo and topography changes) indicated by the name MELTICE. In agreement with palaeoceanographic evidence (Hillaire-Marcel et al., 2001, 2007) Labrador Sea convection was suppressed by the LIS background melt flux.

Finally, we performed an equilibrium experiment (9kOGGIS) in which we combined all forcings of the previous one (9kOGMELTICE), and in addition included the best-guess GIS melt flux of 13 mSv.

2.2.4 Transient experiments

We performed one transient control simulation (OG) including only transient orbital and greenhouse gases and two transient simulations including additionally either LIS melt water (OGMELT) or the full LIS forcing (OGMELTICE). Following the setup of Renssen et al. (2009), the additional freshwater flux was set to 0.09 Sv between 9 to 8.4 ka BP, decreasing slightly to 0.08 Sv between 8.4 and 7.8 ka BP, and dropping to 0.01 Sv between 7.8 and 6.8 ka BP (Fig. 2.1). These freshwater rates are

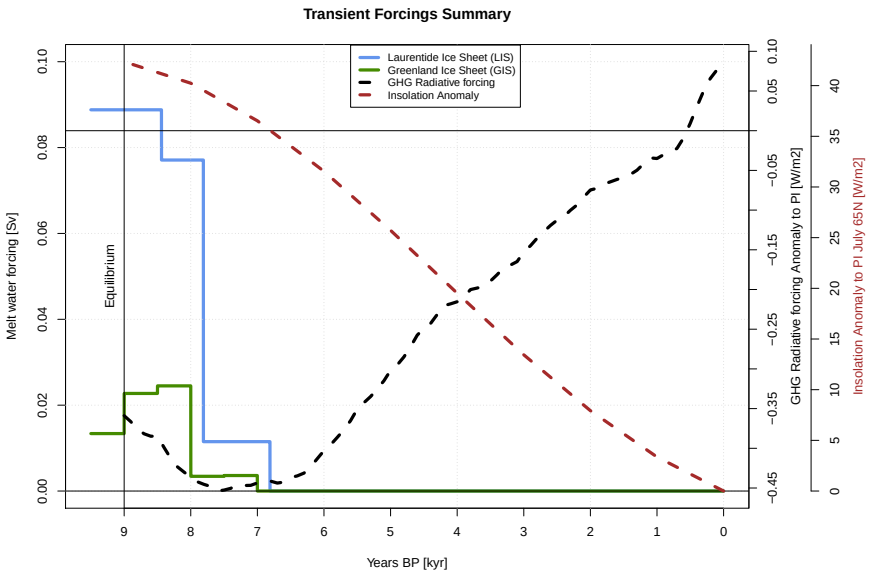

Figure 2.1: Equilibrium and transient forcings applied in simulations. Shown are melt water forcings and orbital and greenhouse gas changes compared to pre-industrial. Topography changes of the LIS are not shown. Blue is the total LIS melt water flux applied in simulation OGMELT, OGMELTICE and OGGIS (left axis). The Green curve denotes the calculated GIS melt water from Peltier (2004) prescribed in OGGIS (left axis). Black gives the radiative forcing due to greenhouse gas concentrations as anomaly to pre-industrial and the red curve gives the July 65° N insolation anomaly after Berger and Loutre (1991) (right axis). Greenhouse gas radiative forcing is calculated using IPCC (2001) formulation.

based on adapted estimates of Licciardi et al. (1999) and do not include short-term freshwater drainage events like the 8.2 ka BP event because the focus of our study is on multi-centennial to millennial timescales. In OGMELTICE the effect of the disintegrating LIS was accounted for by changing the surface albedo and topography at 50-yr time steps, interpolated from reconstructions provided by Peltier (2004), during the period 9 to 7 ka BP.

Finally, we performed a transient experiment (OGGIS) that included

the GIS melt water flux, in addition to all forcings prescribed in OGMELTICE. As shown in Fig. 2.1, the additional melt water was set to 13 mSv for 9 ka BP and increases to 23 mSv from 9 to 8 ka BP and then rapidly decreases to 3 mSv before vanishing completely at 7 ka BP (estimates derived from Peltier, 2004). Considering the coarse model grid resolution (T21), early Holocene GIS topography changes in the model are relatively small and are therefore neglected in this study.

2.3 Results and discussion

We separate our results into two sections. Section 2.3.1 presents the results of the equilibrium experiments on the early Holocene and discusses the impact of different forcings, and Section 2.3.2 presents the results for the transient simulations and the timing of the HTM together with some proxy estimates of the timing.

2.3.1 Early Holocene response

2.3.1.1 Simulated Sea Surface Temperature and Salinity

Simulations including GIS melt (9kOGx1,2,4) show a clear August SST response near the southern part of Greenland although the GIS melt is evenly distributed around Greenland. Compared to experiment 9kOG, in 9kOGx1 (Fig. 2.2a, 2.3a) 13 mSv of melt water reduces SSTs and SSSs around the southern tip of Greenland, especially the region near Denmark Strait is affected, with lowest values at about -3 K and -2 psu, respectively. For a doubling of GIS melt (26 mSv) in experiment 9kOGx2 (Fig. 2.2b, 2.3b) the geographical pattern is quite similar to 9kOGx1, but with a more pronounced cooling of up to 3 K near Denmark Strait and a SSS reduction of up to -3 psu. Noticeable is also the development of a cold tongue across the Nordic Seas to the eastern side accompanied by a decrease in salinity as well. Changes in 9kOGx4 (52 mSv, Fig. 2.2c,

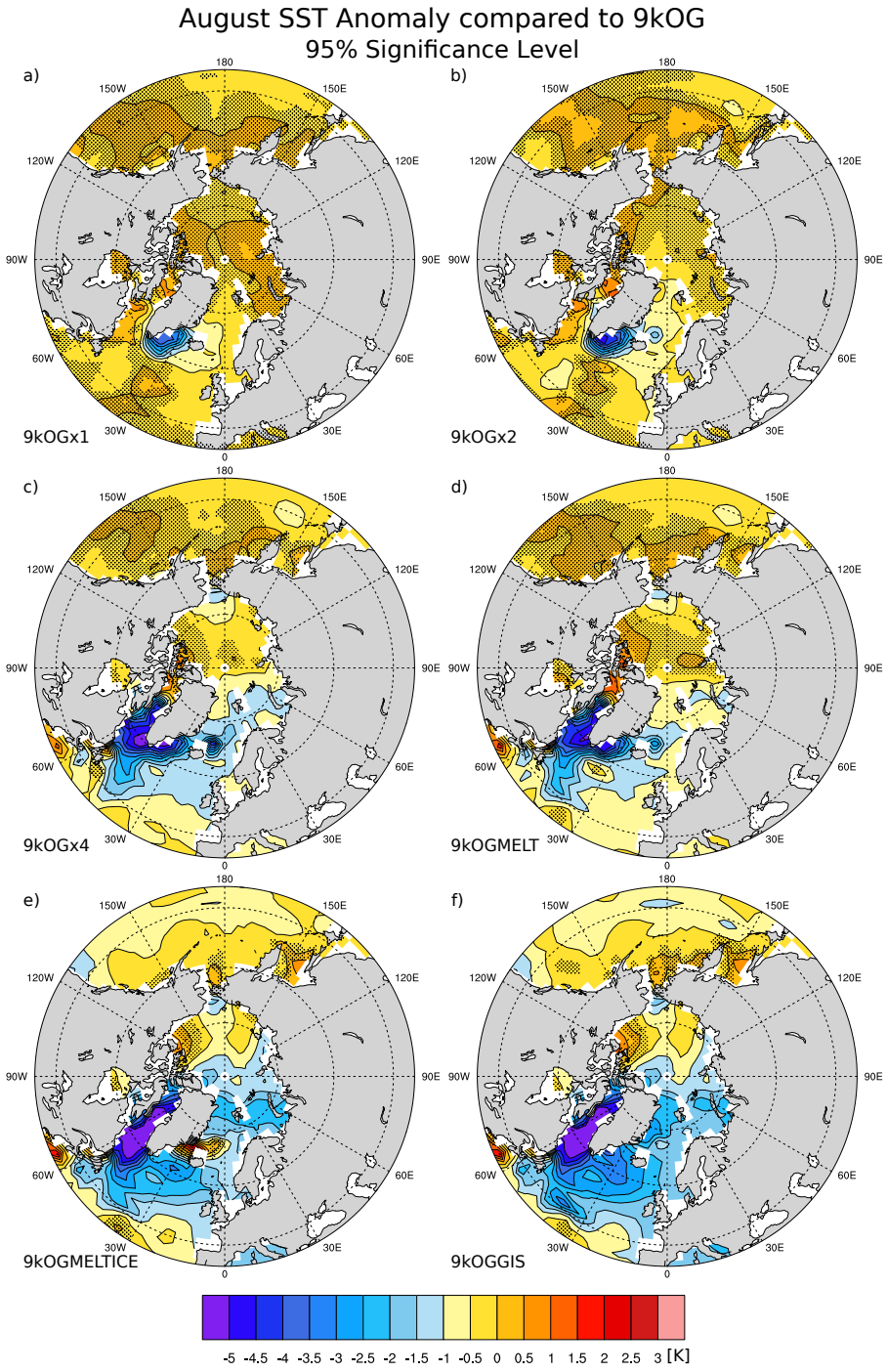

Figure 2.2: Sea Surface Temperature Maps (Caption on Page 41.)

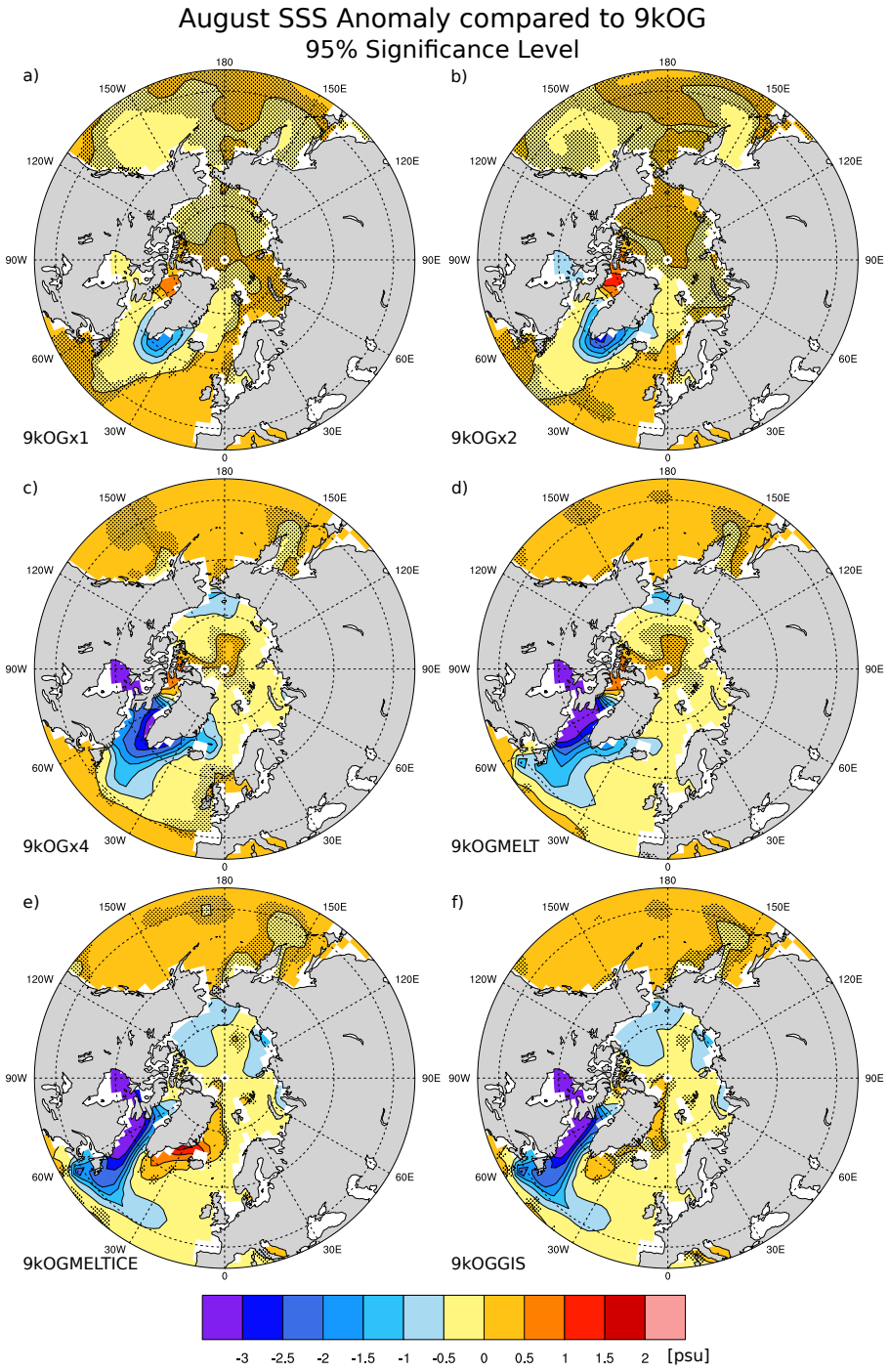

Figure 2.3: Sea Surface Salinity Maps (Caption on Page 41.)

Figure 2.2: (Continuing from Page 39) Sea Surface Temperature (SST, scale in K) anomaly compared to 9kOG for 9 ka BP snapshot simulations. Values are calculated from the last 100 yr of each experiment. Shaded area denotes **insignificant** changes compared to 9kOG according to a student-t test. **(a)** 9kOGx1 SST anomaly for GIS melt (13 mSv). **(b)** 9kOGx2 SST anomaly for GIS melt (26 mSv). **(c)** 9kOGx4 SST anomaly for GIS melt (52 mSv). **(d)** 9kOGMELT SST anomaly for LIS melt (0.09 Sv). **(e)** 9kOGMELTICE SST anomaly for LIS melt (0.09 Sv) + remnant ice sheet (albedo + topography). **(f)** 9kOGGIS SST anomaly for LIS melt + remnant ice sheet + additional GIS melt (13 mSv).

Figure 2.3: (Continuing from Page 40) Sea Surface Salinity (SSS, scale in p.s.u.) anomaly compared to OG for 9 ka BP snapshot simulations. Values are calculated from the last 100 yr of each experiment. Shaded area denotes **insignificant** changes compared to 9kOG according to a student-t test. **(a)** 9kOGx1 SSS anomaly for GIS melt (13 mSv). **(b)** 9kOGx2 SSS anomaly for GIS melt (26 mSv). **(c)** 9kOGx4 SSS anomaly for GIS melt (52 mSv). **(d)** 9kOGMELT SSS anomaly for LIS melt (0.09 Sv). **(e)** 9kOGMELTICE SSS anomaly for LIS melt (0.09 Sv) + remnant ice sheet (albedo + topography). **(f)** 9kOGGIS SSS anomaly for LIS melt + remnant ice sheet + additional GIS melt (13 mSv).

2.3c) are hugely different from previous experiments. The core area of cooling is now in the Labrador Sea with more than 5 K cooling as the deep convection is locally shut down here. The reduction of SSSs is strongest inside Hudson Bay and to the south–east of Greenland. This affects most of the North Atlantic as well as the northern Nordic Seas.

In the early Holocene the Laurentide ice sheet puts great amounts (50 mSv in Hudson Strait and 40 mSv in the St. Laurence outlet) of freshwater into the adjacent ocean. In experiment 9kOGMELT (Fig. 2.2d, 2.3d) cooling due to this LIS melt water is affecting primarily the Labrador Sea with a cooling of up to 5 K and a freshening of more than 3 psu. This cooling is due to the local shutdown of deep convection in the Labrador Sea (as expressed by Mixed Layer Depth (MLD) changes in Fig. 2.5c in the Labrador Sea), similar to what is seen here in 9kOGx4. However,

compared to the latter experiment, there is less cooling impact on the rest of the North Atlantic and the Nordic Seas in 9kOGMELT. Including the remnant LIS into experiment 9kOGMELTICE (Fig. 2.2e) further reduces SSTs (by more than 6 K) in the Labrador Sea and enhances cooling down-wind of the ice sheet. Additional cooling affects the northern Nordic Seas, whereas a more than 2 K warming appears in a small area in the western Nordic Seas, near Denmark Strait. The comparison with Fig. 2.3e shows that SSSs are increased near Denmark Strait resulting from an increase of convective activity there as previously discussed in Renssen et al. (2010). This can be seen as well in Fig. 2.5c by an increase in MLD compared to Fig. 2.5a. Ultimately combining the LIS forcing with one time GIS melt (13 mSv) in experiment 9kOGGIS (Fig. 2.2f, 2.3f) further reduces western Nordic Seas SSTs. Compared to 9kOGMELTICE, the warming near Denmark Strait is reversed into a cooling that now expands across the Nordic Seas. SSS values near Denmark Strait are very similar in 9kOGGIS and 9kOG.

2.3.1.2 Comparison with proxy-based SSTs

Based on diatoms, Andersen et al. (2004a) find a positive east–west August SST difference of 6 to 7 K for the early Holocene, whereas using alkenone based summer SSTs (Calvo et al., 2002) for the eastern side yields a difference of 3 to 4 K. We find in our experiment 9kOG an annual difference of $\sim$6 K and $\sim$4 K for August SSTs (Fig. 2.4). Modelling suggests zonal differences are greatest in winter when the contrast between eastern and western water masses is greatest, as can be seen in Fig. 2.4 by February east–west differences of 7 to 8 K. Including GIS melt in 9kOGx1 increases August and annual SST differences by 0.5 K as compared to 9kOG. Experiment 9kOGx2 and 9kOGx4 reveal that a larger GIS melt leads to a slightly smaller east–west difference, caused by an eastward spreading of the cold anomaly (compare with Fig. 2.4). In experiment 9kOGMELT the difference is almost not affected as compared

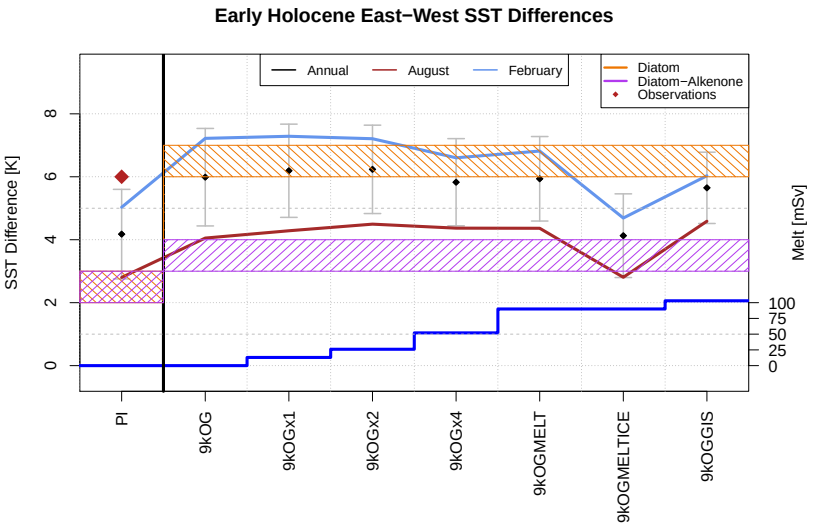

Figure 2.4: Simulated east–west SST differences across the Nordic Seas for 9 ka BP snapshot simulations and an additional present day (PI) simulation for comparison. Corresponding eastern model area 47.5–10° W, 68.75–81.25° N and western 2.5–20° E, 66.25–78.75° N. Points mark the annual mean difference, grey bars give associated standard deviation, red line gives August value, light blue line gives February value. Values are calculated from the last 100 yr of each experiment. Dark blue line at the bottom gives the total amount of freshwater added to the simulations in mSv. Orange bar indicates diatom based SST differences. The value shown in purple is constructed from Andersen et al. (2004a) by combining the diatom-based SST-estimate in the western Nordic Seas and the alkenone-based value (Calvo et al., 2002) in the eastern Nordic Seas. Red square indicates modern day value from Smith et al. (2008) in the period of 1854 to 1950 AD.

to 9kOG, but in 9kOGMELTICE a clear reduction of the difference is evident, with annual mean values around ~ 4 K compared to 6 K in 9kOG. Along with this smaller difference, a decrease in variability can be noted by smaller standard deviations. Finally, in 9kOGGIS the east–west SST difference increases again to similar values as in 9kOGx1. However note that all simulations are significantly different from 9kOG according to a student t-test (c.f. Tab. 2.2) and that the mentioned reduced variability

	Overturning Stream function				Sea Ice			
	Nordic Seas [Sv]		North Atlantic [Sv]		Area [10^6 km^2]		Volume [10^3 km^3]	
9kOG	2.78	± 0.15	13.93	± 2.31	8.80	± 0.24	8.86	± 0.62
9kOGx1	**2.80**	± 0.15	**12.83**	± 2.35	8.94	± 0.22	9.00	± 0.52
9kOGx2	**2.88**	± 0.16	**12.47**	± 2.33	**9.00**	± 0.26	**9.16**	± 0.60
9kOGx4	**2.72**	± 0.28	**9.78**	± 2.45	**9.72**	± 0.41	**10.06**	± 0.88
9kOGMELT	**2.75**	± 0.17	**9.27**	± 2.40	**9.58**	± 0.30	**9.87**	± 0.79
9kOGMELTICE	**2.53**	± 0.21	**10.10**	± 2.50	**10.26**	± 0.29	**11.29**	± 0.80
9kOGGIS	**2.65**	± 0.19	**9.47**	± 2.50	**10.37**	± 0.26	**11.36**	± 0.71

	NADW Export [Sv]		Oceanic Meridional Heat Flux 0° N [PW]		East–West August SST Difference [K]	
9kOG	9.78	± 0.50	0.447	± 1.001	3.82	± 0.60
9kOGx1	**9.81**	± 0.47	**0.423**	± 0.994	**4.39**	± 0.57
9kOGx2	**9.55**	± 0.42	**0.414**	± 1.018	**4.25**	± 0.53
9kOGx4	**9.66**	± 0.63	**0.338**	± 1.041	**4.08**	± 0.87
9kOGMELT	**9.41**	± 0.67	**0.331**	± 1.037	**4.07**	± 0.81
9kOGMELTICE	**9.60**	± 0.74	**0.347**	± 1.059	**2.80**	± 0.88
9kOGGIS	**9.52**	± 0.56	**0.334**	± 1.052	**4.51**	± 1.05

Table 2.2: Summary of key variables from all snapshot simulations. Mean and standard deviation of the (1) Maximum meridional overturning stream function in the Nordic Seas and the North Atlantic at 27° N, (2) Sea ice area and volume in the Northern Hemisphere, (3) North Atlantic Deep Water exported south at 20° S, (4) Meridional heat flux in the Atlantic ocean at the equator and (5) Nordic Seas east–west August SST difference. Values are calculated from the last 100 yr of each experiment. Bold numbers are significant changes as compared to 9kOG according to a student-t test.

is insignificant.

We find that GIS melt increases the east–west difference and generates a model climate closer to the proxy-based reconstructions. Our simulations have not been able to fully reproduce the diatom-based east-west difference, because in our model it was not possible to increase summer SSTs to values as high as reconstructed based on diatoms in the eastern Nordic Seas. However, if we take the alkenone-based SSTs in the east and combine this with diatom-based SSTs in the west, there is good agreement with the simulated August SST differences. One could argue that it is preferable to compare model results to reconstructions based on a single proxy, but on the other hand a particular proxy could also be more suited for SST reconstructions at one location than another

proxy. MARGO Project Members et al. (2009) have shown for the Last Glacial Maximum that in the Nordic Seas large discrepancies exist in paleotemperature reconstructions based on mircofossil proxies and that it is unclear how to reconcile. We thus propose that this may also be true for the Early Holocene. In any case, a lower east-west difference compares better to our model results. The difference is strongest in winter. In conclusion, the better model-data fit in the experiments with the GIS melt indicates that it is important to include the GIS melt in simulations of Holocene climate in the Nordic Seas. In other words, we propose that the impact of GIS melt has been registered in the proxies, producing the observed SST difference across the Nordic Seas in the early Holocene. Simulation 9kOGGIS includes all presented forcings and still agrees to some extent to the proxy reconstructions, meaning that the results are more complete as compared to the other simulations. Regarding the foraminifera-based SSTs, our model shows that seasonal summer warming in the early Holocene is mainly active in the upper $\sim$100 m (not shown), in line with findings of Andersson et al. (2010) for the Mid-Holocene. Our model further shows that GIS melt affects only the uppermost 50 m of the water column (not shown). Therefore, it is likely that deeper dwelling foraminifera species were less affected by orbitally-forced summer warming and GIS melt as compared to surface dwellers. According to Risebrobakken et al. (2011), this was likely the case, implying that these deeper species record an early Holocene increase of horizontal heat advection that weakens towards the present. However, in our experiments an increase of horizontal heat advection cannot be found.

2.3.1.3 Mechanisms behind SST patterns

As discussed in Section 2.3.1.1, we have simulated clear cooling patterns in the Labrador Sea, the Irminger Sea and the Nordic Seas. What has caused these cooling patterns?

In our simulations we find the impacts of the following forcings on August SSTs: **F1** GIS melt near Greenland, **F2** LIS melt water in the Labrador Sea, **F3** the topography and surface albedo of the remnant LIS and **F4** the combination of all forcings.

We would like to give a brief summary of the mechanisms connected to these forcings. We find that forcings **F1** and **F2** freshen the upper ocean and reduce oceanic vertical heat transfer by limiting downward summer heat transfer. Connected to this freshening of the ocean surface we find increased sea ice growth accompanied by stratification of the upper water column and inhibiting convection in winter. This is clearly related to forcing **F2** and in a smaller scale also to **F1**, near the Denmark Strait. We find an amplification of the sea ice expansion and associated stratification by the downwind atmospheric cooling from a large ice-sheet, which is mainly related to forcing **F3**. These three effects (i.e. 1) upper ocean freshening, 2) sea-ice expansion, 3) downwind cooling from the LIS) will be discussed in more detail in the following paragraphs and are mostly active in combination with each other.

The pattern found in SSTs from Greenland melt water (Fig. 2.2a, b, 9kOGx1, 2) is a result of freshening and stratifying the upper ocean column. Surface waters become more buoyant and the density difference with the subsurface increases (up to 0.18 $\mathrm{kg\,m^{-3}}$ from 5 to 100 m depth for 9kOGx1), thus reducing vertical heat transfer and causing surface cooling (note that we do not show this directly, but it can be inferred from Fig. 2.5a,b as changes in MLD near the southern tip of Greenland). In general, the southern tip of Greenland is where the freshwater (runoff, sea ice) from the Arctic and Greenland results in the largest cooling in 9kOGx1 and 9kOGx2. In the Arctic Ocean, however, surface waters are already quite fresh (c.f. Fig. 2.3a,b) and stratified, minimising the effect of additional melt water. As a consequence of cooler and fresher surface waters, sea ice growth is facilitated at the southern tip of Greenland and local convection in winter is reduced (9kOGx1) by up to -200 m of

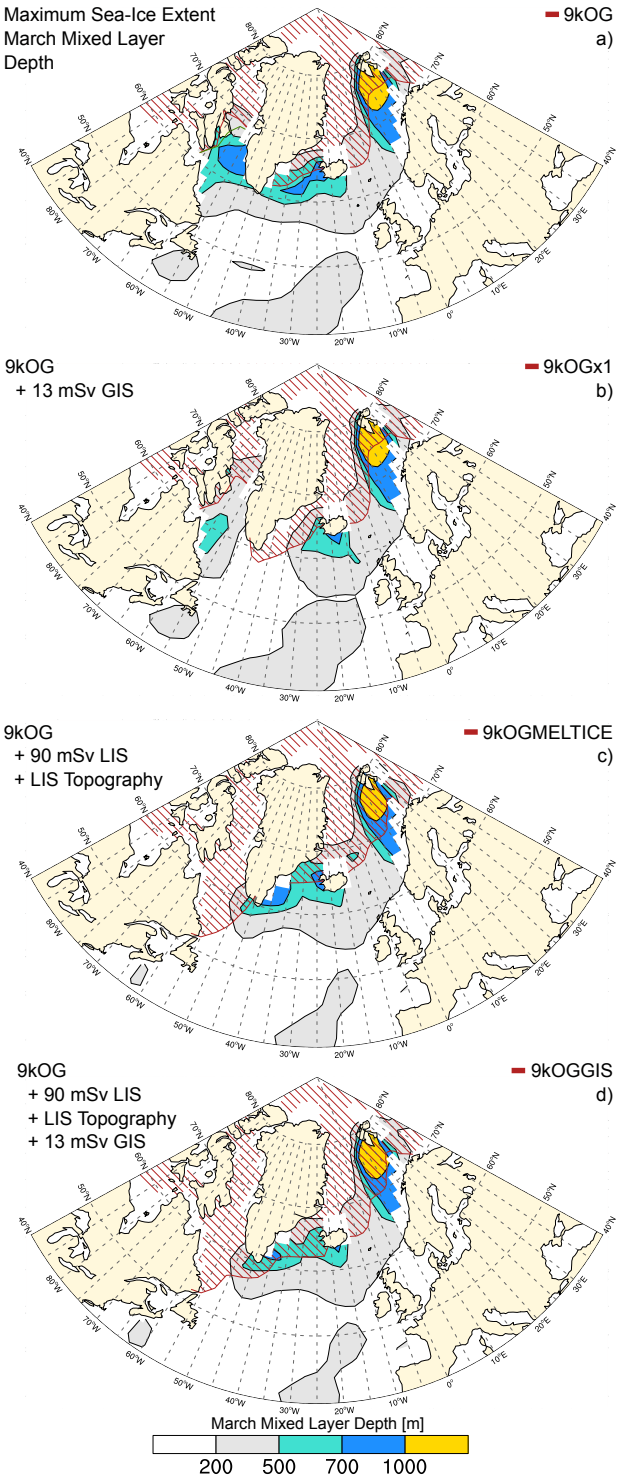

Figure 2.5: March Mixed Layer Depth and sea-ice extent (Caption on Page 48)

Figure 2.5: March Mixed Layer Depth (MMLD, in meters) and winter maximum Sea-Ice Concentration (SIC) over 15%, denoting sea-ice extent. Values are calculated from the last 100 yr of each experiment. **(a)** Shows MMLDs for simulation 9kOG and SIC for simulation 9kOG. **(b)** Shows MMLDs for simulation 9kOGx1 and SIC. **(c)** Shows MMLDs for simulation 9kOGMELTICE and SIC. **(d)** Shows MMLDs for simulation 9kOGGIS and SIC.

maximum convection depth relative to 9kOG (not shown, but note the reduction in MLD Fig. 2.5b), assisting in an overall cooling effect.

Considering the combined effect of all mentioned forcings (by comparing 9kOGGIS to 9kOG), the Northern Hemisphere sea ice area and volume increase by up to 18 % and 28 % (Tab. 2.2), respectively, with the biggest changes in the Labrador Sea area (c.f. Fig. 2.5a,d sea ice extent), while the increases are minor in the Nordic Seas. The strong cooling in the Labrador Sea is linked to a local collapse of deep convection and expansion of sea ice cover as a result of strong surface freshening here. In 9kOGGIS this freshening is primarily resulting from LIS melt (c.f. Renssen et al., 2005b, 2009), but the same effect is seen when GIS melt is increased, as in 9kOGx4 (Fig. 2.3c). The absence of deep convection in the Labrador Sea results in a reduction of meridional overturning strength in the North Atlantic (Fig. 2.5c,d). The simulated deep ocean circulation for 9kOG has a maximum overturning stream function at 27° N of 13.9 ± 2.3 Sv (AMOC, Tab. 2.2) and an export of North Atlantic Deep Water (NADW) towards the Southern Ocean of 9.8 ± 0.5 Sv. Observed values for the AMOC strength at 26.5° N for 2004–2008 by Kanzow et al. (2010) are somewhat higher (18.7 Sv) but variable alike (±2.1 Sv). In LOVECLIM, deep convection takes place in both the Nordic Seas and the Labrador Sea, similar to the conditions in a simulation with pre-industrial forcings (Goosse et al., 2010). In our experiments the GIS melt has a discernible impact on convection depth near Denmark Strait which is contributing to the North Atlantic overturning. In 9kOGx1 a reduction of ∼ 8 % (12.8 Sv vs 13.9 Sv, Tab. 2.2) of

the maximum meridional overturning strength is simulated as compared to 9kOG. As expected, the AMOC weakens further when also LIS melt is included, resulting in similarly reduced values of the maximum meridional overturning strength in 9kOGMELTICE (10.1 Sv) and in 9kOGGIS (9.5 Sv). This weakening corresponds to a reduced annual northward heat transport in the ocean at the equator in the Atlantic basin of 25 % for 9kOGGIS (0.334 PW) as compared to 9kOG (0.447 PW), contributing to the cooling of the Northern Hemisphere. This is best expressed in 9kOGx4 ($\sim$ 24 % reduction) and 9kOGMELT ($\sim$ 26 % reduction), as in these experiments the impact on meridional overturning strength is the largest.

Another superimposed effect contributes to cooler North Atlantic SSTs in 9kOGMELTICE and 9kOGGIS, which is the enhanced cooling (by 2 K in 9kOGMELTICE vs 0.5 K in 9kOGMELT, Fig. 2.2e, f) downwind of the remnant LIS as discussed in detail in Renssen et al. (2009). Meridional overturning in the Nordic Seas and therefore NwAC (Norwegian Atlantic Current) strength are weakly affected (c.f. Tab. 2.2) by overall cooling and freshening (2.65 Sv in 9kOGGIS vs 2.78 Sv in 9kOG), because of their competing effects on surface density and therefore convective activity. In the Nordic Seas at the main deep convection site south-west of Svalbard, the freshening is relatively modest (as compared to the Labrador Sea, Fig. 2.3). The reduction in surface density resulting from this freshening is almost compensated by the increase in density caused by the surface cooling (not shown, c.f. Fig. 2.2, 2.3). As a consequence, maximum winter convection depth is reduced by 200 m in 9kOGGIS as compared to 9kOG at the convection site (not shown). These findings are accompanied by a slight (5%) reduction of the northward heat flux into the Nordic Seas (at 60° N) in simulation 9kOGGIS as compared to 9kOG. Therefore, our model experiments do not support the idea that higher summer SSTs were caused by increased inflow of warm Atlantic waters as proposed by Risebrobakken et al. (2011). However, in other modelling studies, for instance Swingedouw et al. (2012),

Kleinen et al. (2009) and Stouffer et al. (2006), such increase in warm inflow is simulated in response to surface ocean freshening.

2.3.2 Transient Holocene response

From our snapshot simulations we could derive a discernible response to GIS melt that seems to be visible also in the proxy-based reconstructions and is denoted by an increased August SST gradient across the Nordic Seas in the early Holocene. Therefore we want to investigate the temporal evolution of this impact on the HTM.

2.3.2.1 Simulated SST trends

The modelled Nordic Seas' SST difference responds stronger to GIS melt water than to effects inflicted by the remnant Laurentide ice sheet. The Eastern Nordic Seas SSTs in OG show a clear early HTM (before 8 ka BP) and a subsequent decline towards pre-industrial temperatures. LIS melt water in OGMELT has a minor effect on the Nordic Seas (less than 0.5 K difference). In contrast, in OGMELTICE the additional remnant ice sheet reduces SSTs by 1.5 K in the early Holocene (Fig. 2.6a) relative to OG. With the ice sheet vanishing at around 7 ka BP, temperatures return to the general orbitally forced trend during the remainder of the Holocene, depicted by simulation OG. The GIS melt affects previously mentioned results only in the first 500 yr, when GIS melt is at its peak, causing warmer conditions by 0.5 K. In contrast, SSTs in the western Nordic Seas (Fig. 2.6b) are more strongly reduced by GIS melt (by ~ 3 K) in OGGIS than by the influence of the LIS in OGMELTICE (~ 2 K). This impact wears off at 7.5 ka BP, when temperatures return to the general cooling trend displayed by OG.

The noted different effects in the western and eastern Nordic Seas clearly indicate that the difference across the Nordic Seas is more influenced by GIS melt and less by the remnant LIS. Simulated SSTs for the East

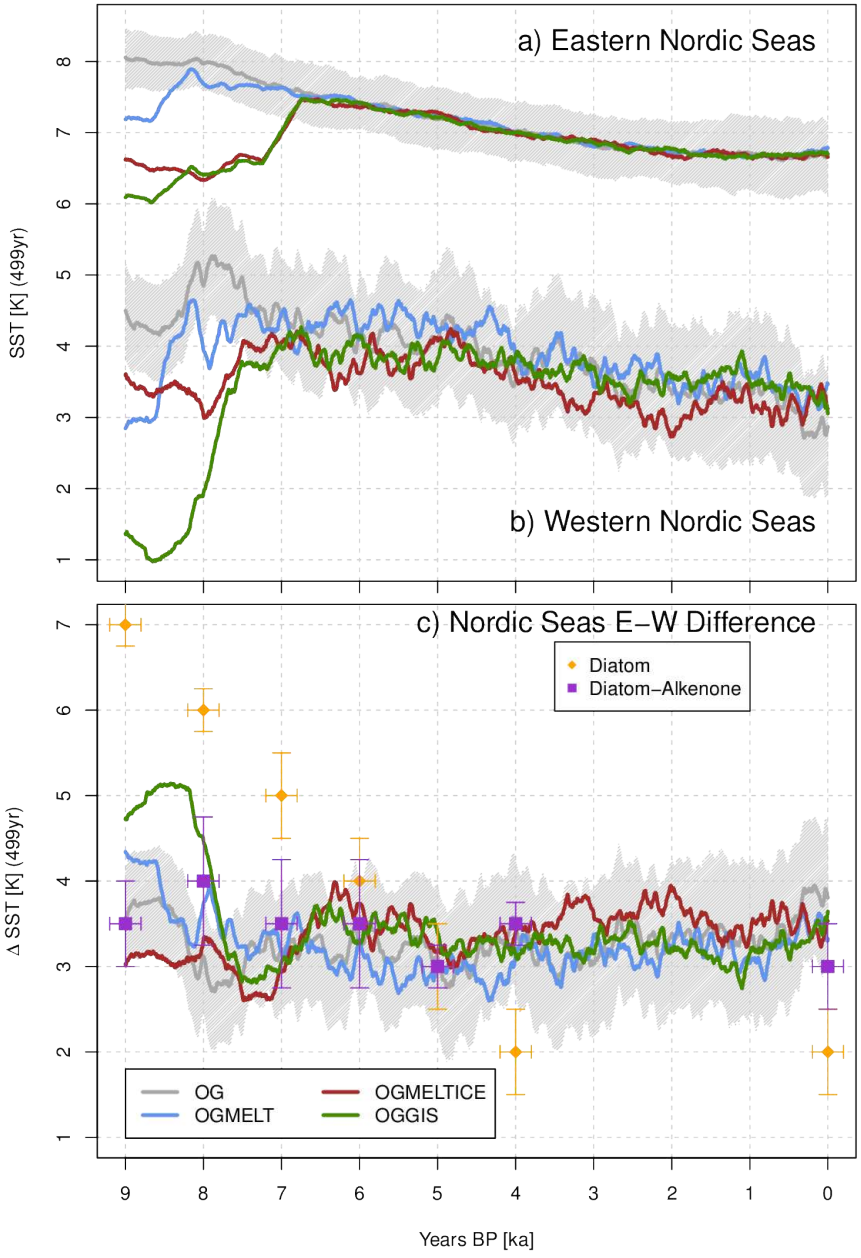

Figure 2.6: (Caption on next Page)

Figure 2.6: Transient area weighted August SSTs for Eastern and Western Nordic Seas and the difference from four transient simulations. **(a)** August SST in the Eastern Nordic Seas (2.5–20° E, 66.25–78.75° N) from 9 to 0 ka BP. **(b)** August SST in the Western Nordic Seas (47.5–10° W, 68.75–81.25° N) from 9 to 0 ka BP. **(c)** August east–west SST difference across the Nordic Seas from 9 to 0 ka BP. Grey OG, Blue OGMELT, Red OGMELTICE and Green OGGIS. The grey area denotes the standard deviation of simulation OG. Orange dots represent approximate values from Andersen et al. (2004a) for diatom based SST gradient. The values shown in purple are constructed from Andersen et al. (2004a) by combining the diatom-based SST-estimate in the western Nordic Seas and the alkenone-based values (Calvo et al., 2002) in the eastern Nordic Seas. Error bars denote approximate errors of mean values in time (default 200 yrs) and magnitude.

(Fig. 2.6a) and West (Fig. 2.6b) decrease over time, whereas in Fig. 2.6c the difference is mostly constant over the Holocene, except for the early and late Holocene. The east-west difference is clearly stronger in OGGIS than in OGMELTICE, because of the strong impact of GIS melt water. As soon as GIS melt vanishes, the difference in OGGIS returns to the same level as the other experiments. A more gradual decrease, as seen in proxy reconstructions (Andersen et al., 2004a), would only have been simulated with continued additional GIS melt water fluxes after 7 ka BP. We could thus speculate that we underestimated GIS melt and/or increase of sea ice cover over the western side in our experiments.

2.3.2.2 Impact on the HTM

The spatial pattern of the HTM timing is mainly influenced by the remnant LIS and secondly, but fundamentally in the Nordic Seas, by GIS melt (Fig. 2.7). Our main interest here is in the millennial-scale trend. To filter out decadal to centennial variability, we used a 1000 yr running mean and calculated the timing (in yr BP) of the maximum for August SSTs. Relative to OG, peak warmth is delayed by up to 3500 yr in the

Nordic Seas and is highly variable between the four transient simulations. In OGMELT, the LIS delays the timing of the HTM over the whole North Atlantic by ~ 1000 yr (Fig. 2.7a, b). The Denmark Strait and the region south of it show HTM timings ~ 2000 yr later than in OG. A major step happens by including the remnant ice sheet in OGMELTICE, which further increases the timing delay to 2000–2500 yr for large parts of the North Atlantic. The eastern Nordic Seas are delayed by 2000 yr, whereas the delay on the western side ranges between 500 to 2500 yrs, suggesting a west-east spatial timing difference, rather than an east–west difference. Including the GIS melt in OGGIS uniformly delays the HTM on the western side, resulting in a spatial timing difference of 2000 yr across the Nordic Seas. It should be noted that the HTM timing in our transient experiment depends strongly on the time-scale of the applied forcings. Therefore, it is preferable to consider the relative timings (i.e. timing delays compared to orbital and freshwater forcing) when comparing with proxy data, as explained in Section 2.3.2.3.

2.3.2.3 Proxy trends and timings

Despite uncertainties in model and proxy results, the combination of LIS and GIS forcings link reconstructed and modelled estimates of SST trends and the timing of the HTM. The zonal Nordic Seas SST difference in Andersen et al. (2004a) decreases less abruptly than our associated modelled SST difference. However, given the step-like nature of our prescribed melt fluxes an abrupt termination is inevitable. We calculate SST trends from the early Holocene maximum to the pre-industrial minimum for both proxy and model results. Therefore the time interval of the trends vary. Reconstructed proxy SST trends from Andersen et al. (2004a) are 5 K/8ka (eastern) as compared to 1–2 K/7ka for the model and 1–2 K/8ka (western) as compared to 1 K/7ka for the model. SST trends from Calvo et al. (2002) with 2–3 K/8ka compare better to 1–2 K/7ka for the model. Marine sites from Kaufman et al. (2004) in the Nordic Seas give SST trends between 2.5 and 6.6 K/8 − 10ka, based

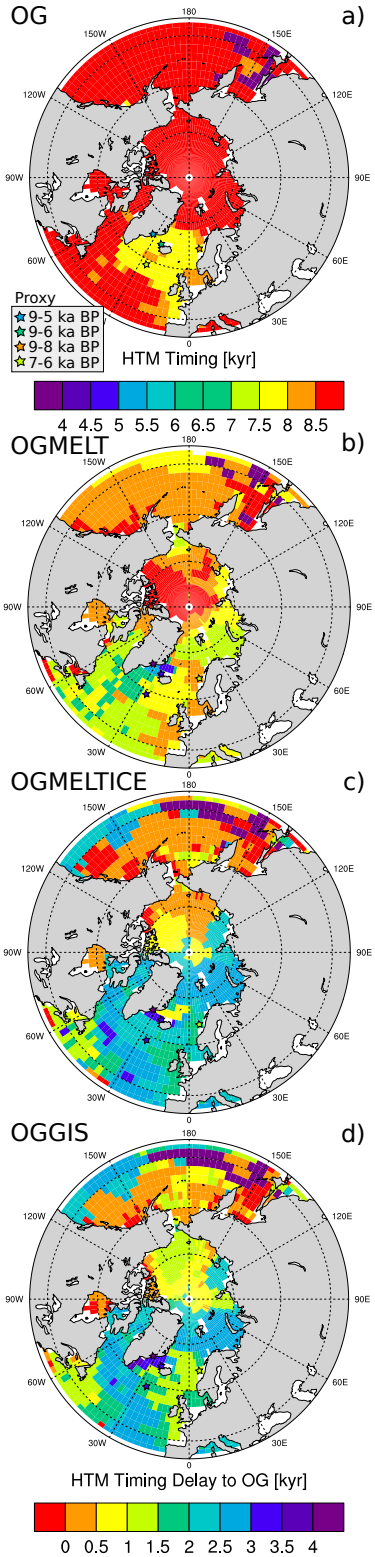

Figure 2.7: Timing of the Holocene Thermal Maximum (in yr BP) based on simulated August SSTs in the Northern Hemisphere. The timing is taken to be the maximum of a 1000 yr running mean filtered August SST time series. Proxy core locations are indicated by stars: BS-88-06-5A (near Greenland); MD99-2269 (North Iceland); MD95-2011 (near Norway); MD95-2015 (Gardar Drift). The colours of the stars represent the minimum of the HTM timing (a) and the maximum of the HTM delay (b,c,d). Estimates of HTM timing are shown in the top figure. **(a)** Shows simulation OG in absolute timing; **(b)** Shows simulation OGMELT as delays compared to OG; **(c)** Shows simulation OGMELTICE as delays compared to OG; **(d)** Shows simulation OGGIS as delays compared to OG.

mostly on diatom proxies and also coccoliths (1 core). Despite this weak consistency in absolute temperatures, the proxies give east–west differences that vary more (between ~ 2 K for present-day and ~ 6–8 K for the early Holocene (Calvo et al., 2002; Andersen et al., 2004a) as compared to the model (2.5–4.5 for present-day and ~ 5 K for the early Holocene). It is hard to determine the cause of this mismatch, as it can be partly attributed to our model having a too low sensitivity to applied forcings and partly to uncertainties in proxy reconstructions.

The spatial complexity of the HTM is best expressed by estimating delays and spatial timing differences (c.f. Fig. 2.7, stars indicate core locations of Kaufman et al., 2004). According to Kaufman et al. (2004) the timing of the HTM at the eastern Greenland shelf ranges between 9 and 5 ka BP, translating into a 0 to 4 ka delay relative to 9 ka BP. We take 9 ka BP as a reference because our simulations start at this time, enabling us to compare these proxy estimates to our model. At the South Iceland shelf the timing is between 7 and 6 ka BP according to Kaufman et al. (2004), whereas the reconstructed timing on the North Iceland shelf is between 9 and 6 ka BP, resulting in delays between 0 and 3 ka and a spatial timing-difference of 0 to 2 ka from south to north. Similar results can be obtained from Andersen et al. (2004a) for Greenland and Iceland sites, however for the eastern side the timing delay is ~ 1 ka.

Our model results for OGGIS seem to be in the range of most of these timing differences, except for the spatial difference between the areas north and south of Iceland that is unmatched. We find it reversed.

2.4 Conclusions

We have applied a fully coupled atmosphere-ocean-sea-ice-vegetation model to study the impact of early Holocene GIS melt on the climate of the Nordic Seas. Our results suggest the following.

1. From our sensitivity experiments we find that GIS melt has a discernible impact on the AMOC strength and facilitates sea-ice growth along the EGC and the Denmark Strait. August SSTs are up to 3 K lower near the Denmark Strait, overturning is reduced by 2–3 Sv and the winter sea-ice margin expands south of Denmark Strait in a simulation with 13 mSv GIS melt as compared to a simulation forced by changes in orbital parameters and greenhouse gas concentrations.

2. GIS melt can explain some of the spatial differences across the Nordic Seas as reconstructed in several proxy records for the early Holocene. Absolute model temperatures do not compare well with absolute reconstructed temperatures at core locations because of the coarse resolution of our model, but the model seems to catch well the spatial difference across the Nordic Seas. Our model was not able to reproduce the warmth in the early Holocene as suggested by diatom reconstructions near the Norwegian Shelf and agrees better with alkenone-derived SSTs.

3. The spatial distribution of the timing of the HTM in the Nordic Seas is better reproduced in a simulation with GIS melt as compared to a simulation without additional GIS influence. We find delays between the eastern and western sides of ~ 2000 yr.

4. We find in our experiments that GIS melt plays an active role in the Nordic Seas environment. The GIS evolution therefore has to be considered in the evolution of the early Holocene climate and future melting scenarios.

In the context of future climate change this study underlines the importance of GIS melt water and its active role in the climate system. Compared to today, in the early Holocene the annual and summer insolation forcing at 65° N (i.e. in South Greenland) was 2.4 and 42 W m^{-2}, respectively (Berger and Loutre, 1991). This value of 2.4 W m^{-2} is close to the lower range of the annual radiative forcing of proposed future

anthropogenic emission scenarios, that varies between 3 and 8.5 $\mathrm{W\,m^{-2}}$ (Meinshausen et al., 2011). Therefore it is not surprising that recently Rignot et al. (2011) reported an acceleration of GIS melt rates that could soon exceed those of the early Holocene, thereby stressing the importance of GIS melt for Nordic Seas future climate evolution.

Chapter 3

The impact of Early Holocene Arctic Shelf flooding on climate in an atmosphere-ocean-sea-ice model

Based on: Blaschek, M. and Renssen, H.: The impact of early Holocene Arctic shelf flooding on climate in an atmosphere-ocean-sea-ice model, Climate of the Past, 9, 2651–2667, doi: 10.5194/cp-9-2651-2013, 2013b

Glacial terminations are characterized by a strong rise in sea level related to melting ice sheets. This rise in sea level is not uniform all over the world, because regional effects (uplift and subsidence of coastal zones) are superimposed on global trends. During the early Holocene the Siberian Shelf became flooded before 7.5 ka BP and the coastline reached modern-day high stands at 5 ka BP. This area is currently known as a sea-ice production area and contributes significantly to the sea ice exported from the Arctic through the Fram Strait. This leads to the following hypothesis: during times of

rising sea levels, shelves become flooded, increasing sea-ice production on these shelves, increasing sea-ice volume and export through Fram Strait and causing the sea-ice extent to advance in the Nordic Seas, yielding cooler and fresher sea surface conditions. We have tested this hypothesis in an ocean-sea ice-atmosphere coupled model of intermediate complexity (LOVECLIM). Our experiment on early Holocene Siberian Shelf flooding shows that in our model the Northern Hemisphere sea-ice production is increased (15%) and that the Northern Hemisphere sea-ice extent increases (14%) but sea-ice export decreases (-15%) contrary to our hypothesis. The reason of this unexpected behaviour has its origin in a weakened polar vortex, induced by the land-ocean changes due to the shelf flooding, and a resulting decrease of zonality in the Nordic Seas pressure regime. Hence the winter Greenland High and the Icelandic Low strengthen, yielding stronger winds on both sides of the Nordic Seas. Increased winds along the East Greenland Current support local sea-ice production and transport towards the South, resulting in a wider sea-ice cover and a southward shift of convection areas. The overall strength of the Atlantic Meridional Overturning Circulation is reduced by 4% and the heat transport in the Atlantic basin by 7%, resulting in an annual cooling pattern over the Nordic Seas by up to -4° C. We find that the flooding of the Siberian shelf resulting from an orbitally-induced warming and related glacioeustatic sea level rise causes a Nordic Seas cooling feedback opposed to this warming.

3.1 Introduction

The melting of land-based ice sheets during the last deglaciation (approximately 21 to 7 ka BP) caused a prominent rise in global sea level of about 120 m (Siddall et al., 2003), with about half of this rise ($\sim$60 m) taking place during the early Holocene (11.5 to 7 ka BP). This rise in global sea level caused flooding of many exposed shelves around the

world, although considerable regional differences in the timing of this shelf flooding existed due to the local uplift and subsidence of coastal zones (Lambeck and Chappell, 2001; Carlson and Clark, 2012), especially due to isostatic effects of the main ice sheets. This is especially important for the Arctic Ocean, where major shelves existed near these ice sheets, with some shelves actually being ice covered (e.g. Barents Shelf). Estimates for the Laptev Sea (i.e. a shelf not covered by ice sheets during the last glacial), illustrate the rapid rise in the sea level in the Arctic, from 31 m to 7 m below the present level between 8.9 ka BP and 7.5 ka BP (Bauch et al., 2001; Taldenkova et al., 2010), leading to a completely flooded shelf at 5 ka BP. A tentative extrapolation of these sea level stands to other shallow seas in the Arctic suggests that large areas were affected by similar flooding during the early Holocene, such as the large shelf areas in the East Siberian Sea, the Kara Sea and parts of the Bering Sea (Fig. 3.1). This raises the question what the impact of such large scale flooding of shelves was on the climate during the early Holocene.

At present-day Arctic shelves are zones for numerous processes in the ocean, like ocean–atmosphere heat exchange, upper ocean stratification, deep-water formation and freshening of the upper ocean from river input. And most importantly, Arctic shelves are zones of sea-ice production. Sea-ice processes and feedbacks dominate the Arctic Ocean, the only polar ocean. Sea ice is formed all over the Arctic Ocean and sea-ice production rates are highly variable and location dependent (Tamura and Ohshima, 2011). Most literature divides sea-ice production into total and polynya-based sea-ice production. In a current study by Tamura and Ohshima (2011), 10 zones of considerable polynya-based sea-ice production are listed in the Arctic for present day. They find high ice production rates in the Canadian Archipelago ($842 \pm 243\,\mathrm{km^3\,yr^{-1}}$), the Northern Baffin Bay ($353 \pm 69\,\mathrm{km^3\,yr^{-1}}$, NBB) and the Kara Sea ($342 \pm 71\,\mathrm{km^3\,yr^{-1}}$). The rates for the East Siberian Sea ($195 \pm 46\,\mathrm{km^3\,yr^{-1}}$)

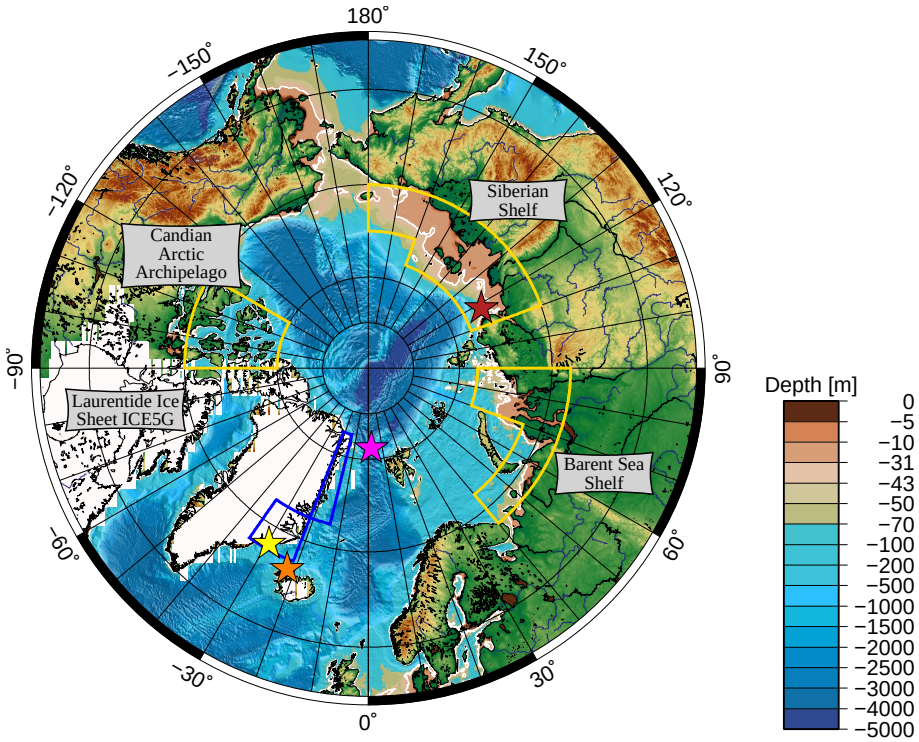

Figure 3.1: Topographic map showing modern day bathymetry (National Geophysical Data Center, 2001) in the Arctic and 9 ka BP ICE5G ice mask from Peltier (2004). Contour level −31 (white) is chosen to reflect lower sea-level stand for the Laptev Sea as reconstructed by Bauch et al. (2001) (their study area is indicated by a red star). Other stars show study locations referred to in the discussion: the orange star is the study area from Andrews et al. (2009), the purple star near the Fram Strait is from Müller et al. (2009) and the yellow star denotes the core location from Jennings et al. (2002). Yellow boxes indicate shelf areas and blue boxes indicate regions used in Fig. 3.5, north-western and south-western Nordic Seas.

and the Laptev Sea ($152 \pm 43\,\mathrm{km^3\,yr^{-1}}$) are ranked 7th and 9th individually, but taken together they are similar to the rate for the Kara Sea. However, estimates for ice production rates vary substantially between different studies. For instance, estimates of the polynya-based sea-ice production in the Laptev Sea range from $55\,\mathrm{km^3\,yr^{-1}}$ (Willmes et al., 2011) to $258\,\mathrm{km^3\,yr^{-1}}$ (Dethleff et al., 1998). In a similar way total

sea-ice production in the Laptev Sea varies between $845\,\mathrm{km^3\,yr^{-1}}$ (Zakharov, 1966) and $950 \pm 350\,\mathrm{km^3\,yr^{-1}}$ (Dmitrenko et al., 2009). Despite the uncertainty in these estimates and therefore relative importance, a striking feature of most of these polynya-based production zones is that they are shelf regions. Polyak et al. (2010) summarize that for the present day most first-year ice is formed over continental shelves. Another study by Dethleff and Kuhlmann (2010) connects deposited sea-ice rafted sediments near the Fram Strait to shelves in the Kara and Laptev Sea, indicating these regions as a major origin of Fram Strait sea-ice export. Just like Rigor and Colony (1997), who have identified that 20 % of the sea ice leaving the Fram Strait originates in the Laptev Sea. The Transpolar Drift transports sea ice across the pole into the Nordic Seas passing through the Fram Strait. Transported along the East Greenland Current (EGC) southward, melting of the sea ice is subsequently expected to release relatively cool freshwater, cooling the upper ocean and reducing surface salinities in the Nordic Seas. To summarize, a dynamic link between Arctic shelves and sea-ice production is evident and its implications on Arctic sea-ice volume and extent are probably closely related to the climate in the Nordic Seas.

Bauch et al. (2001) have suggested that, in the early Holocene, the flooding of the Arctic shelves increased sea-ice production, impacting the transport and export of sea ice to the Nordic Seas. Recently Werner et al. (2013) suggested such a stepwise response of Fram Strait sea-ice conditions due to postglacial Siberian shelf flooding before 5 ka BP. This leads to the following hypothesis: the flooding of the Arctic shelves resulted in a major increase in sea-ice production, leading to enhanced ice volume and export through the Fram Strait. Following this hypothesis, we expect that during times of lower sea levels (e.g. before the flooding at 7.5 ka BP), the lower sea-ice cover was associated with relatively high sea surface temperatures (SSTs) and sea surface salinities (SSSs) along the EGC, compared to the case when the shelves are flooded (e.g. later in the Holocene). Thus, the shelf flooding is expected to have had

a cooling influence in the Nordic Seas, implying that flooding of the Arctic shelves could have acted as a negative feedback, during a warming climate. This feedback might have been active during terminations when global climate is responding to an orbital-induced warming, leading to melting of land-based ice sheets and rising sea level. The shallow Arctic shelves facilitate sea-ice production compared to the deep Arctic Ocean and counteract high latitude warming, possibly reversing the long-term warming trend and resulting in a cold reversal. Important for the severity of the impact on climate seems to be the speed of this transgression.

The dynamic relationship between sea-ice production and dry shelves can be tested with an ocean–atmosphere coupled climate model to evaluate the significance of such changes on past climates. Previous modelling studies focusing on the last deglaciation have either kept the land-sea mask fixed (e.g. Roche et al., 2007; Friedrich et al., 2010; Roche et al., 2012) or have not specifically analysed the impact of the changes in land-sea distribution (Singarayer and Valdes, 2010). Thus, to our knowledge the impact of shelf flooding has not yet been addressed in modelling studies.

Our aim in this study is to address changes induced by Arctic shelf flooding with the help of LOVECLIM, a fully coupled climate model of intermediate complexity (Goosse et al., 2010). We designed simulations for the early Holocene with and without dry shelves. From previous studies of the early Holocene, the Laurentide ice sheet (LIS, e.g. Renssen et al., 2009) and the Greenland ice sheet (GIS, e.g. Blaschek and Renssen, 2013a) have been recognized as important factors in the Nordic Seas climate. Together with the downwind cooling effect of the LIS and its melt water and additional melt water from the GIS, sea-ice conditions are considerably altered and sea-ice production is facilitated by atmospheric cooling and shutdown of local convection. Therefore, we extend on the study of Blaschek and Renssen (2013a) and include an

analysis of simulations for the early Holocene including both LIS and GIS forcings together with and without flooded Arctic shelves.

3.2 Methods

3.2.1 The LOVECLIM Model

We extend the modelling approach applied by Blaschek and Renssen (2013a), using the same Earth system Model of Intermediate Complexity (EMIC) LOVECLIM (version 1.2; Goosse et al., 2010) for our experiments. The model includes a representation of the atmosphere, the ocean and sea ice, the land-surface and its vegetation. The components not activated in our LOVECLIM version are the dynamical ice sheet model and the carbon cycle model. As a detailed description of the model can be found in Goosse et al. (2010), we only provide a brief summary and highlight relevant features. The ocean-sea ice component is CLIO3 (Goosse and Fichefet, 1999), a ocean general circulation model with a horizontal resolution of 3°x3°latitude-longitude and 20 vertical levels, coupled to a three-layer dynamic-thermodynamic sea ice model (Fichefet and Maqueda, 1997, 1999) with an advanced scheme to determine the sea-ice edge more precisely in a coarse resolution model as explained by Goosse et al. (2010). For present-day it simulates a reasonably well Arctic sea-ice distribution, although the magnitude of the seasonal cycle is too weak (Goosse et al., 2010; Goosse et al., 2007). Mass exchanges between the ocean and sea ice are treated as negative and positive salt fluxes, implying that ice-related freshwater fluxes are virtual salt fluxes. As detailed by Goosse et al. (2010), this is a simplification that originates in CLIO's free-surface. The ocean bathymetry and the land-sea mask are derived from modern observations and reduced to the lower resolution of our model. To mimic dry shelves in the model, we converted ocean cells in selected shelf areas from vertical level 4 (-38 to -45 m depth) upwards to land cells, consistent with

sea level estimates of Bauch et al. (2001) for 8.9 ka BP of -31 m. As the coupling between ocean and atmosphere depends thoroughly on the land-sea mask, we had to recalculate coupling parameters to account for the changes in the prescribed land-sea distribution.

The atmospheric model is called ECBILT (Opsteegh et al., 1998) a spectral T21 three-level quasi-geostrophic model with a built-in bucket-type hydrological model for soil moisture and runoff. Cloud cover is climatologically prescribed. The vegetation is handled by VECODE (Brovkin et al., 2002), a dynamical vegetation model simulating two plant functional types (trees and grasses), and desert as a dummy type. As in Blaschek and Renssen (2013a), the extent and elevation of ice sheets are manually prescribed and consistent with sea level as in Peltier's (2004) ICE-5G model. The climate sensitivity of LOVECLIM (version 1.2) to a doubling of the atmospheric CO2 concentration is at the lower end of the range found in global climate models (1.9 K after 1000 yr; Goosse et al. (2010)). Deep convection takes place in both the Nordic Seas and the Labrador Sea (Goosse et al., 2010) and the simulated characteristics of the deep ocean circulation compare reasonably well with other model results (e.g. Weaver et al. (2012)). The model has been used successfully in numerous palaeoclimatological modelling studies for example in Wiersma and Renssen (2006) investigating the 8.2 ka BP event or by Renssen et al. (2009, 2010, 2012) in studies of the Holocene Thermal Maximum.

3.2.2 Experimental Design

In this study we use the experiments 9kOG and 9kOGGIS from Blaschek and Renssen (2013a) and an additional five quasi-equilibrium snapshot experiments with fixed forcings at 9 ka BP and one with fixed pre-industrial forcings. In all experiments, orbital parameters and greenhouse-gas concentrations are taken from the PMIP3 protocol (`http://pmip3.lsce.ipsl.fr/`). Our snapshot experiments have been run for 500

Table 3.1: Summary of experiments. Shelf areas according to Fig. 3.1.

Experiment name		Initial conditions	Changes
0kOG		Orbital (0 BP), Greenhouse Gases (1750 AD)	no
9kOG		Orbital (9 ka BP), Greenhouse Gases (9 ka BP)	no
9kOGBAR	9kOG +	Dry Barent Sea Shelf	Land-Sea mask + Bathymetry
9kOGCAN	9kOG +	Dry Canadian Arctic Archipelago Shelf	Land-Sea mask + Bathymetry
9kOGSIB	9kOG +	Dry Siberian Shelf	Land-Sea mask + Bathymetry
9kOGSHELF	9kOG +	Dry Arctic Shelves	Land-Sea mask + Bathymetry
		Additional experiments	
9kOGGIS	9kOG +	Laurentide ice sheet (LIS, remnant ice sheet + Melt water (0.09 Sv)) + Greenland ice sheet (GIS) melt water (13 mSv)	Topography, Melt water
9kOGSIBGIS	9kOGGIS +	Dry Siberian Shelf	Land-Sea mask + Bathymetry, Topography, Melt water
PRE2005	Transient simulation including orbital and greenhouse gases from 1765 to 2005		no

model years, and the analysis is based on the last 100 yrs of each simulation. Key features about our experimental setup are summarized in Tab. 3.1.

We use the same control snapshot experiment for 9 ka BP background conditions with orbital and greenhouse-gas forcing (9kOG) and an experiment that includes the impacts of LIS and GIS (9kOGGIS) as in Blaschek and Renssen (2013a). In order to test our hypothesis, we designed five experiments to affect sea-ice production zones relevant in our model, mimicking dry shelf areas. In all our simulations the Bering Strait remains open, consistent with palaeoceanographic evidence indicating that this strait already became active again at 11.1 ka BP when sea level was 50 m below the current level (Elias et al., 1996). The "new" land cells at the shelves are set to behave like adjacent land cells with seasonal changes in albedo and vegetation.

In the five additional experiments, we prescribed different combinations of land-sea masks in the Arctic region, which correspond in each experiment to a different land area added, to represent a specific dry shelf area. These simulations are named 9kOGBAR, 9kOGCAN, 9kOGSIB, 9kOGSHELF and 9kOGSIBGIS. In 9kOGBAR changes in the land-sea mask in the bigger Kara and Barents sea area (cf. Fig. 3.1, Barents Sea Shelf) result in five ocean cells becoming land and four being lowered. In 9kOGCAN the existing shelf region in the Canadian Arctic Archipelago

(CAA) is removed and four ocean cells are converted to land (cf. Fig. 3.1, CAA). In 9kOGSIB the new land-sea mask for the East Siberian Shelf (cf. Fig. 3.1) converts 10 coastal ocean cells to land and lowers two surrounding ocean cells. Simulation 9kOGSHELF combines the impact of the three shelf areas (9kOGBAR, 9kOGCAN, 9kOGSIB). Coming from the glacial, shelf areas in the Barents Sea and the CAA are likely to be subject to subsidence from the Barents and Laurentide ice sheets, respectively (Bauch et al., 2001; Svendsen et al., 2004), lowering the relevance of our 9kOGBAR, 9kOGCAN and 9kOGSHELF simulation. From surface altitude differences between 9 and 0 ka BP derived from Peltier's (2004) ICE-5G model, it can be inferred that the Barents Sea and the CAA were already flooded at 9 ka BP. Therefore simulations 9kOGBAR and 9kOGCAN should be considered as sensitivity experiments, and are only used for evaluating the impact on sea-ice production in our model. Likewise, experiment 9kOGSHELF overestimates the total exposed Arctic shelf area at 9 ka BP, and should thus be interpreted as a maximum impact simulation. For the early Holocene it has been shown that during the Holocene Thermal Maximum (HTM) the Laurentide ice sheet (LIS) (cf. Fig. 3.1, Renssen et al., 2009) and the Greenland ice sheet (GIS) (Blaschek and Renssen, 2013a) had a significant impact on the climate, especially on sea ice and convection depth in the Nordic Seas. These important climate features are relevant for the early Holocene climate but not necessarily for our hypothesis to test, but in order to have a complete overview of the response to the combination of all forcings, we also simulated the impact of the Siberian shelf on the early Holocene background climate affected by the LIS (melt flux to the St. Lawrence outlet (50 mSv) and Hudson Bay (40 mSv), as well as the remnant ice sheet as in Renssen et al., 2009) and melt water from the GIS (13 mSv) (Blaschek and Renssen, 2013a) in simulation 9kOGSIBGIS. A comparison between 9kOGGIS (Blaschek and Renssen, 2013a) and 9kOGSIBGIS therefore provides an idea of the relative importance of shelf flooding compared to all other forcings, including additional ice sheet topography, albedo and background melt fluxes, whereas a comparison of 9kOG

and 9kOGSIB shows the effects of shelf flooding without this influence of the ice sheets.

To compare observed sea-ice volumes (Fig. 3.2), we also performed a transient simulation (PRE2005) that follows the Representative Concentration Pathways (RCP) (Meinshausen et al., 2011) greenhouse-gas concentrations from 1765 to 2005 AD.

3.3 Results

In order to test our hypothesis, we conducted experiments with different dry shelves to estimate the impact of these changes to the climate and the sea-ice conditions. We will first discuss the performance of our model for the present climate (Section 3.3.1.1), then analyse the impacts of the flooding of these shelf areas on sea-ice production and volume (Section 3.3.1.2) and proceed with impacts on the Nordic Seas (Section 3.3.2) and Northern Hemisphere (Section 3.3.3).

3.3.1 Impact on Arctic sea-ice

3.3.1.1 Modern climate

Our model simulates the modern seasonal cycle of Arctic sea-ice volume reasonably well, as is shown by a direct comparison with observations (Zhang and Rothrock, 2003, Fig. 3.2). The simulated seasonal cycle in sea-ice volume in our pre-industrial experiment 0kOG is very close to the observed mean for 1979–2010. However, our recent-past simulation (PRE2005) underestimates sea-ice volumes compared to these mean observations by $7.12 \times 10^3 \mathrm{km}^3$ ($\sim 34\,\%$), with values that are closer to recent sea-ice minima observed in 2011 and 2012. A major difference between PRE2005 and 0kOG is the radiative forcing (approx. $2\,\mathrm{W\,m^{-2}}$

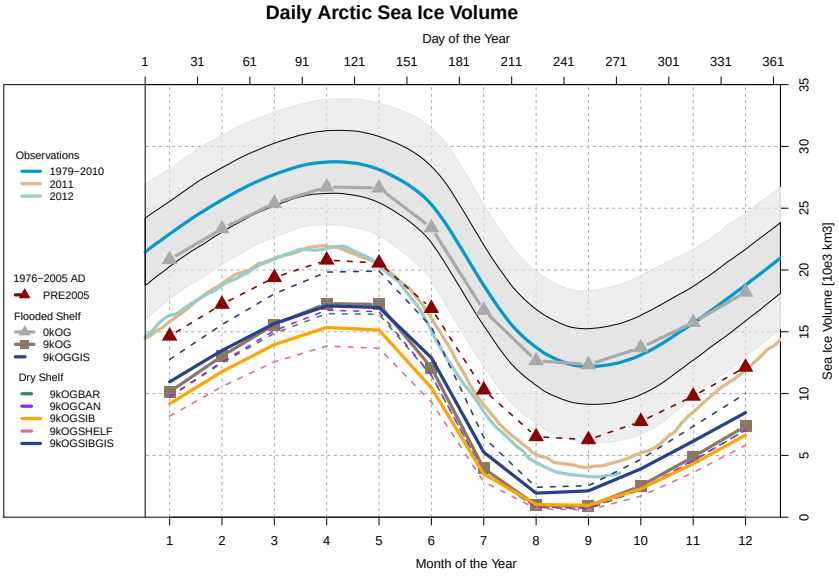

Figure 3.2: Daily Arctic sea-ice volume from PIOMAS (Zhang and Rothrock, 2003) and monthly means for model experiments at 9 ka BP and 0 ka BP. Separated lines for most recent years 2011 and 2012. Grey areas denote one (two) standard deviations from 1979 to 2010 climatological mean. Please notice that LOVECLIM uses a fixed calendar with 360 days and the data embodies leap years. Model values are monthly means of the last 100 yr of each simulation, except for simulation PRE2005 giving monthly means of the period 1976 to 2005 AD.

globally higher for 1976 to 2005 as compared to 1750) due to greenhouse-gas concentrations. Goosse et al. (2007) found for LOVECLIM that the simulated sea-ice area fits reasonably well with modern-day observations. Our results confirm this, as we find that the simulated annual sea-ice area in our PRE2005 and 0kOG simulations (9.6×10^{12} km^2 and 10.6×10^{12} km^2, respectively) agree well with observations (10.6×10^{12} km^2, cf. Tab. 3.2).

However observed Fram Strait sea-ice export shows considerable lower (2.6×10^3 km^3, Spreen et al., 2009) volumes compared to 10.6×10^3 km^3 of annual cumulative sea-ice export in our model. Consequently, the

export of sea ice through the Fram Strait is likely to be too large in our model. The distribution of sea-ice production in the model is different from observations, because in our model the transpolar drift transports sea-ice from the western to the eastern side of the Arctic (Goosse et al., 2001; cf. Fig. 3.8, 9kOG, distribution is similar to present-day). This model bias results from the low resolution of the atmospheric component (Goosse et al., 2003; Goosse and Renssen, 2001), although Goosse et al. (2001) found that the atmospheric circulation in the Arctic and the position of Icelandic and Aleutian low is relatively close to observed ones under present-day conditions. The opposite wind direction is a result of an overestimation of the Aleutian low. Despite this deficiency we conclude that our model is able to produce sea-ice quantities at larger scale in a reasonable range at pre-industrial, suggesting that our model is suitable for a study of the impact of early Holocene shelf flooding on sea ice (cf. Fig. 3.2).

3.3.1.2 Early Holocene

Comparison of our orbital and greenhouse-gas simulations for 9k and 0k BP (9kOG and 0kOG, respectively), reveals that annual cumulative Arctic sea-ice production was higher (+24 %) in the experiment with early Holocene forcings (Tab. 3.2), while the values for both sea-ice area and volume are reduced for 9 ka BP. This counter-intuitive result can be explained by insolation differences of the early Holocene compared to present day. Associated with orbitally forced insolation anomalies ($-15\,\mathrm{W\,m^{-2}}$ in October), the early Holocene had a bigger seasonal contrast than today, allowing more sea ice to grow during the winter half year, but decay faster in summer. Thus, the reduced annual mean sea-ice area and volume reflect the response to summer conditions, while the enhanced annual sea-ice production reflects the impact of reduced insolation in the winter half year.

Table 3.2: Summary of annual mean and standard deviation of sea-ice parameters in nine different model simulations. Northern Hemisphere sea-ice volume in km^3. Northern Hemisphere and Arctic annual cumulative sea-ice production (0–360° E and 40–90° N, 20–280° E and 65–90° N) in km^3. Northern Hemisphere annual mean sea-ice area in $10^{12}km^2$. Annual cumulative Fram Strait sea-ice export in km^3. Meridional overturning strength in the North Atlantic (AMOC) at 27° N in Sv. All values are calculated from the last 100 yr of the simulations except for PRE2005 over 1976 to 2005 as Fig. 3.2. The corresponding data source for Northern Hemisphere sea-ice volume is the PIOMAS data from Zhang and Rothrock (2003). For Northern Hemisphere annual cumulative sea-ice production there are two estimates, the first one derived from Zhang and Rothrock (2003) and the second one from Tamura and Ohshima (2011), the latter denoting only polynya-based sea-ice production. Northern Hemisphere sea-ice area is taken from HadISST data (Rayner et al., 2003). Fram Strait sea-ice export estimates are taken from Spreen et al. (2009) (1st) and Kwok et al. (2004) (2nd). Recent estimates of the AMOC strength have been published by Kanzow et al. (2010).

		Sea ice [10^3km^3]		
		Annual volume	Annual cumulative production	
	Experiments	Northern Hemisphere		Arctic
	Observations	20.66 ± 6.72	16.08 ± 6.18	–
	(mul. Sources)	–	2.94 ± 0.37	–
Flooded shelves	PRE2005	13.54 ± 5.40	13.89 ± 5.19	11.76 ± 4.27
	0kOG	19.65 ± 5.49	13.54 ± 5.11	11.16 ± 4.07
	9kOG	8.83 ± 5.99	16.09 ± 6.10	13.81 ± 5.08
Dry shelves	9kOGBAR	8.36 ± 5.77	15.48 ± 5.88	13.29 ± 4.88
	9kOGCAN	8.44 ± 5.84	15.73 ± 5.97	13.46 ± 4.94
	9kOGSIB	7.88 ± 5.29	13.99 ± 5.33	11.90 ± 4.41
	9kOGSHELF	6.95 ± 4.88	12.89 ± 4.93	10.99 ± 4.08
Flooded Dry	9kOGGIS	11.37 ± 6.32	17.25 ± 6.41	14.23 ± 5.12
	9kOGSIBGIS	9.58 ± 5.48	14.88 ± 5.55	12.35 ± 4.46
		Annual sea-ice area [$10^{12}km^2$]	Annual cumul. Fram Strait sea-ice export [10^3km^3]	Atlantic Meridional Overturning Streamfunction [Sv]
	Observations	10.58 ± 3.16	1.54 ± 0.18	18.70 ± 2.10
	(mul. Sources)		2.22 ± 0.50	
Flooded shelves	PRE2005	9.64 ± 3.67	7.07 ± 1.88	14.32 ± 2.28
	0kOG	10.65 ± 3.08	10.64 ± 3.33	15.27 ± 2.18
	9kOG	8.82 ± 4.65	6.36 ± 1.89	13.93 ± 2.31
Dry shelves	9kOGBAR	8.44 ± 4.50	6.30 ± 2.07	13.68 ± 2.42
	9kOGCAN	8.51 ± 4.60	6.58 ± 1.95	13.26 ± 2.37
	9kOGSIB	7.74 ± 4.15	7.49 ± 1.92	14.54 ± 2.39
	9kOGSHELF	7.00 ± 3.90	6.55 ± 1.77	14.54 ± 2.40
Flooded Dry	9kOGGIS	10.40 ± 4.44	7.06 ± 2.14	9.47 ± 2.50
	9kOGSIBGIS	9.02 ± 4.12	7.56 ± 2.23	10.59 ± 2.43

As expected, flooding of the Arctic shelves results in an increase in simulated Arctic sea-ice production, as is clearly shown by the comparison of 9kOG with the experiments with dry shelves. For the Siberian shelf this increase due to flooding is 16 % (i.e. 9kOG $13.8 \times 10^3\,\mathrm{km}^3$ compared to 9kOGSIB $11.9 \times 10^3\,\mathrm{km}^3$), accompanied by an increase of 12 % in sea-ice volume over the whole Northern Hemisphere (Tab. 3.2). However, this difference in volume is mainly related to changes in winter, as in summer (August–September) our model simulates an almost ice-free Arctic Ocean for 9kOG and any other shelf experiment (cf. Fig. 3.2). Impacts of shelf flooding on sea-ice production, sea-ice volume and sea-ice area are in the range of 2 to 5 % for simulations 9kOGBAR and 9kOGCAN compared to 9kOG. This is quite surprising as the associated shelves are categorized as high production areas by Tamura and Ohshima (2011) and one would expect a greater impact from these shelf areas, meaning that sea-ice production is obviously very robust there. The potential total impact of Arctic shelf flooding, as indicated by the difference between 9kOG and 9kOGSHELF, is a strong increase in sea-ice production (+25 %), and sea-ice volume (+27 %). When the impact of the remnant ice sheets is taken into account (i.e. by comparing 9kOGGIS and 9kOGSIBGIS), the impact of the flooding of the Siberian shelf on sea-ice production (+15 %) is similar to the results without this ice sheet effect (+16 %).

3.3.2 Impacts on Nordic Seas

The flooding of the Arctic shelves and the combined increase in sea-ice production have an indirect impact on the Nordic Seas via the export of sea ice through the Fram Strait. Despite the increase in sea-ice volume and area due to shelf flooding, the export of Arctic sea ice through the Fram Strait into the Nordic Seas (Fig. 3.3) decreased in simulation 9kOG from January to May relative to 9kOGSIB and shows a maximum of 41 mSv ($1293\ \mathrm{km}^3\,\mathrm{yr}^{-1}$) in April compared to 52 mSv in 9kOGSIB. However, the reduced mean values are not significantly different for those

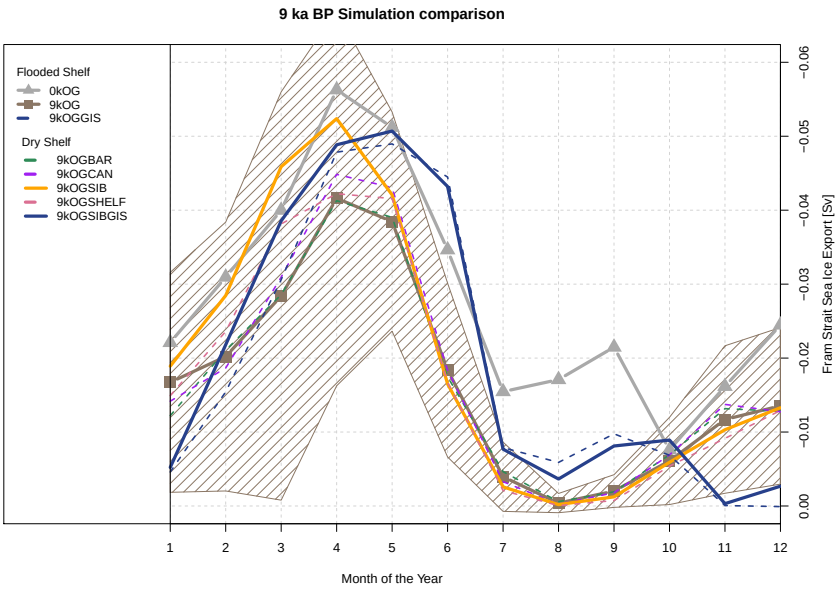

Figure 3.3: Monthly mean Fram Strait sea-ice export for different simulations in Sv of the last 100 yr. The more negative the values are the more southward transport occurs. In the literature values are normally given as yearly exports, resulting from a sum of monthly values (cf. Tab. 3.2). Shaded area gives an estimation of the standard deviation of the monthly means for simulation 9kOG.

months given the large inter-annual variability in these exports. This seasonal response is much weaker in the results showing the impact of flooding of the shelves in CAA and the Barents Sea on the Fram Strait sea-ice export. This indicates that the discussed response in sea-ice export, with a reduction from January to May, is mainly connected to flooding of the Siberian shelf. This reduction in Fram Strait sea-ice export due to shelf flooding is in contradiction with our hypothesis and counter-intuitive, raising the following question: what caused this response? The first step in explaining this response is to take a closer look at the changes induced in the Nordic Seas, followed by an analysis of polar atmospheric circulation changes and finally Arctic sea-ice transport.

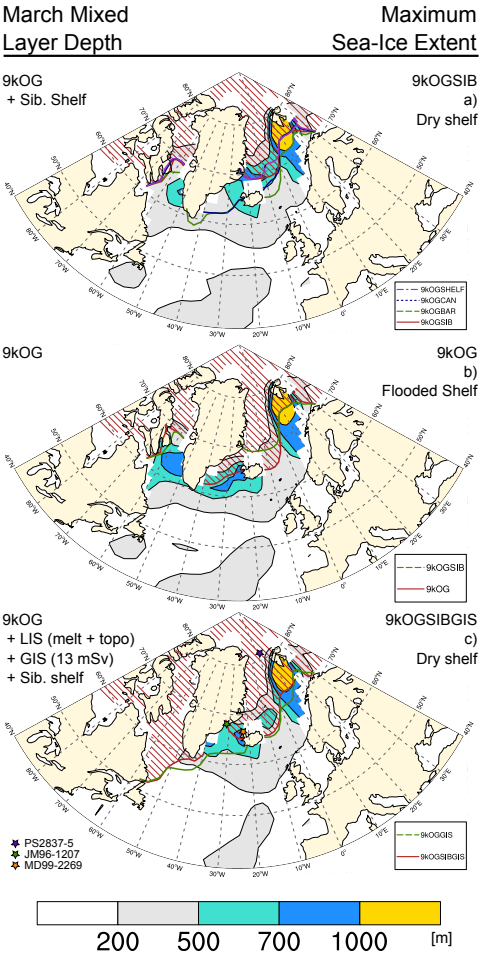

Figure 3.4: Maximum winter sea-ice extent and March mixed layer depth for different simulations. **(a)** Simulation 9kOGSIB, and sea-ice extent contours for additional simulations 9kOGSHELF (purple), 9kOGBAR (green) and 9kOGCAN (blue). **(b)** simulation 9kOG and contours for simulation 9kOGSIB. **(c)** Simulation 9kOGSIBGIS and sea-ice extent contour for simulation 9kOGGIS (Blaschek and Renssen, 2013a).

The discussed expansion of Northern Hemisphere sea-ice cover in 9kOG causes the sea-ice edge along the EGC to advance, leading to a southward shift of local deep convection from 70° N in 9kOGSIB (Fig. 3.4b) to the southern tip of Greenland at 63° N (Fig. 3.4a). These changes in deep convection also affect the overall Atlantic meridional overturning circulation (AMOC), decreasing its strength by 4 %, from 14.5 Sv in 9kOGSIB to 13.9 Sv in 9kOG.

The southward shift of convection results in cooler and fresher surface waters near the Denmark Strait (Fig. 3.5d–f) and along the east coast of Greenland as far north as the Fram Strait (Fig. 3.5a–c). The southward expansion of sea ice along the EGC increases sea-ice cover and sea-ice

melting in the western Nordic Seas. Although less sea ice is transported out of the Arctic Ocean (15 %), the sea-ice thickness on the northern part of the EGC is higher in 9kOG compared to 9kOGSIB (Fig. 3.5a), implying that more sea ice is produced there. In our simulation with a dry shelf (9kOGSIB) sea-ice production in the Arctic is reduced, but also the area of ocean covered with sea ice, with the net effect that more sea ice is available for export rather than piling up in the Arctic Ocean. Annual Arctic sea-ice volume increases due to shelf flooding ($+933\,km^3$), as a result of both an increase in annual cumulative ice production and a decrease in annual cumulative ice export through the Fram Strait (Tab. 3.2). However, it should be noted that this surplus of ice is divided over a larger area in 9kOG, since the available ocean area increases by 12 % due to the shelf flooding. This shows that a dry Siberian shelf has a clear impact on sea-ice production and on the export to the Nordic Seas. However, given the fact that we find a reduction in ice export through the Fram Strait, the increase of sea-ice cover and related cooling and freshening of the ocean surface in the Nordic Seas is only indirectly caused by the flooding of the shelf rather than a direct consequence of an increase in sea-ice export as was suggested in the original hypothesis. Thus, an additional mechanism is required to explain the changes in the Nordic Seas. This additional mechanism is associated with an atmospheric feedback that is incorporated in the response to the flooding.

3.3.3 Impact on Northern Hemisphere climate

3.3.3.1 Atmospheric changes

The flooding of the shelf decreases the pole-to-equator temperature gradient in the winter atmosphere resulting in a weakened polar vortex and increased mid-latitude North Atlantic pressure system, amplifying zonal pressure differences across the Nordic Seas and increasing the surface winds in this area. The winter warming in the Arctic (2 to 8 °C,

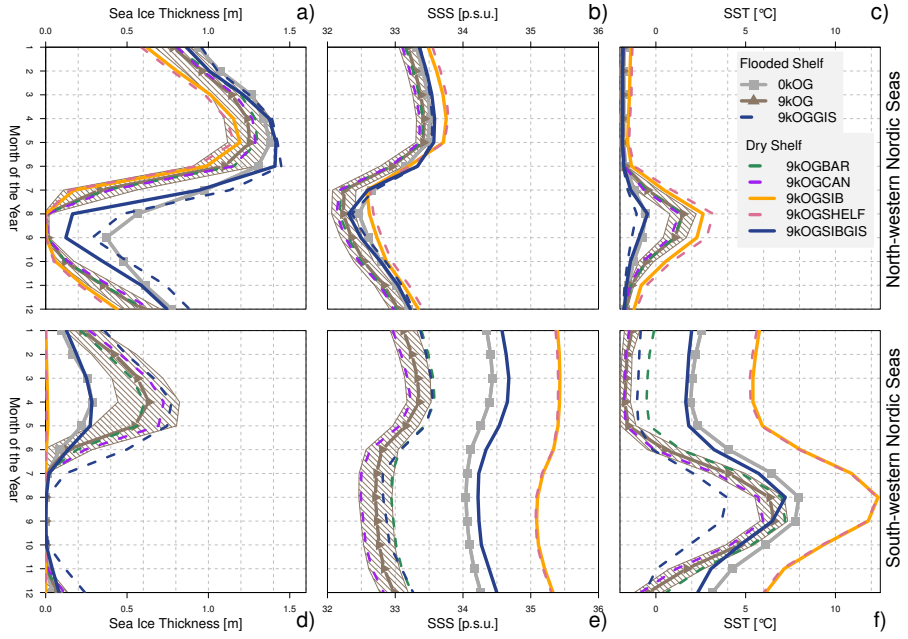

Figure 3.5: Monthly means of the last 100 yr of each simulation for the north-western Nordic Seas (20–15° W, 73.75–81.25° N) in the upper panel and for the south-western Nordic Seas (47.5–22.5° W, 68.75–71.25° N) as denoted in Fig. 3.1 blue boxes. (**a/d**) sea-ice thickness in metres, (**b/e**) sea surface salinities (SSS) in p.s.u., (**c/f**) sea surface temperatures in degree Celsius. Shaded areas give an estimation of the standard deviation of the monthly means for simulation 9kOG.

Fig. 3.6a) by the shelf flooding in 9kOG as compared to 9kOGSIB is directly related to changes in the land-sea mask. In summer, a cooling of 2 to 8 °C is noted over Siberia (Fig. 3.6b). On an annual basis the flooding results in a cooling only over the Nordic Seas (up to −4 ° C) as contrasting seasonal changes (Fig. 3.6 a, b) balance each other out over the Siberian shelf. In summer the cooling in Siberia influences a strong summer Siberian low pressure system, but results in hardly any feedback on sea ice. In winter the flooded shelf is only relatively warmer, as it is still far below zero there, but the meridional temperature gradient is somewhat reduced (by −1.4 °C). The polar vortex is strongest in winter when the pole-to-equator temperature gradient is strongest. A weakening of the polar vortex and a strengthening of a mid-latitude

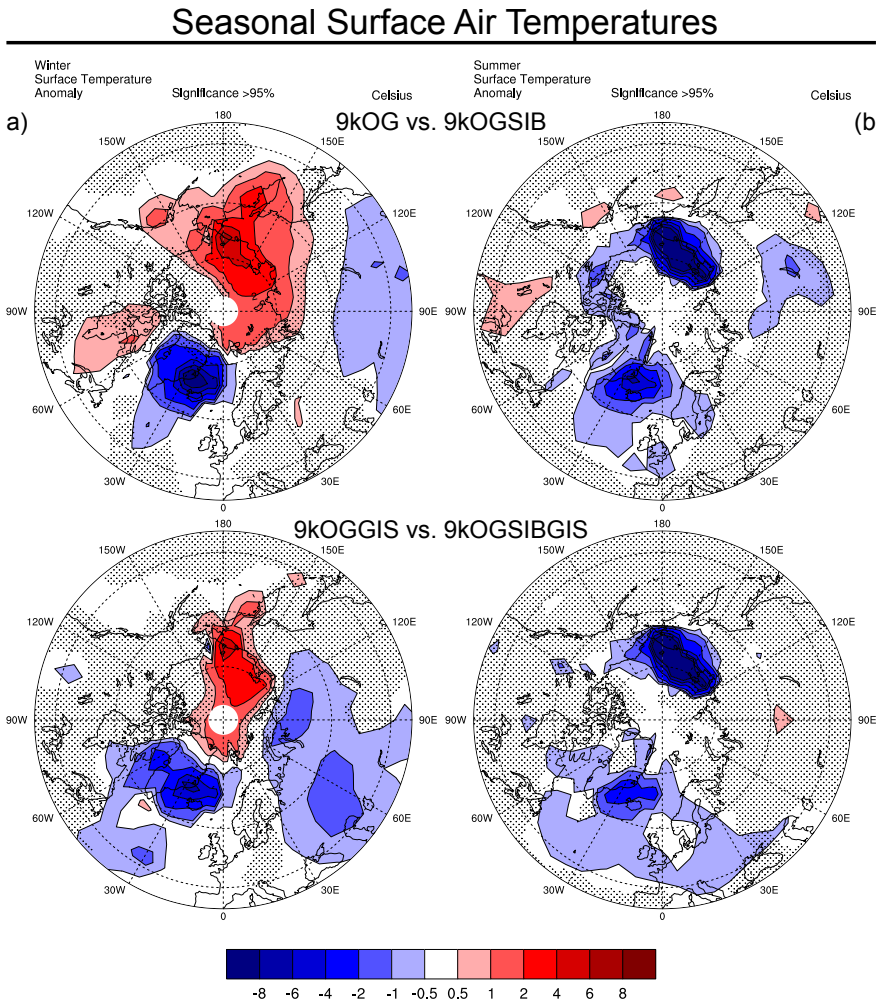

Figure 3.6: Seasonal surface temperature anomalies of simulation 9kOG as compared to 9kOGSIB (upper panel) and simulation 9kOGGIS as compared to 9kOGSIBGIS (lower panel). Winter is DJF (**a**), Summer is JJA (**b**). Shaded area denotes insignificant changes compared to 9kOGSIB or 9kOGSIBGIS according to a Student t test.

North Atlantic high (Fig. 3.7a), increase the zonal pressure difference across the Nordic Seas by strengthening both the Greenland high and the Icelandic low (Fig. 3.7b). As a result, the associated surface winds are also strengthened, both the southward winds in the western part of the Nordic Seas and the northward winds in the eastern part (Fig. 3.7c). Despite the substantial difference in mean climate between 9kOG and 9kOGGIS (−0.5 K globally cooler) the impact of the shelf flooding remains clearly present as an atmospheric pattern in Fig. 3.7, indicating that the impact is robust. The previously mentioned bias in the Arctic atmospheric circulation in our model is affecting the transport of sea-ice in the Arctic due to changed winds, whereas one can argue that the meridional thermodynamic structure of the atmosphere is likely to be less affected by this bias, because the polar atmospheric circulation is mainly governed by its meridional component.

3.3.3.2 Arctic sea-ice transport

The flooding of the Siberian shelf alters the sea-ice transport in the Arctic (compare 9kOG with 9kOGSIB, Fig. 3.8) in a way that more sea ice is transported away from the production centres on the western side towards the eastern Arctic (Fig. 3.8) and leading to reduced export through the Fram Strait (Fig. 3.3). These changes in Arctic sea-ice transport are mainly associated with the new sea-ice production area over the flooded shelf. Lower export rates at the Fram Strait are mainly caused by redirection of sea ice towards the eastern side of the Arctic (Fig. 3.8). The impact of the shelf flooding on the ice export can be seen in the ratio of Fram Strait sea-ice export and Arctic sea-ice production, which is a measure of the Arctic sea-ice balance (e.g. for simulation 0kOG this ratio is 95 %, meaning that 95 % of the volume that has been produced until spring was also exported). This ratio decreases by 17 % for simulation 9kOG (46 %) as compared to 9kOGSIB (63 %) and by 11 % for 9kOGGIS (50 %) as compared to 9kOGSIBGIS (61 %). The response to the flooding of the Barents or the CAA shelf do not show

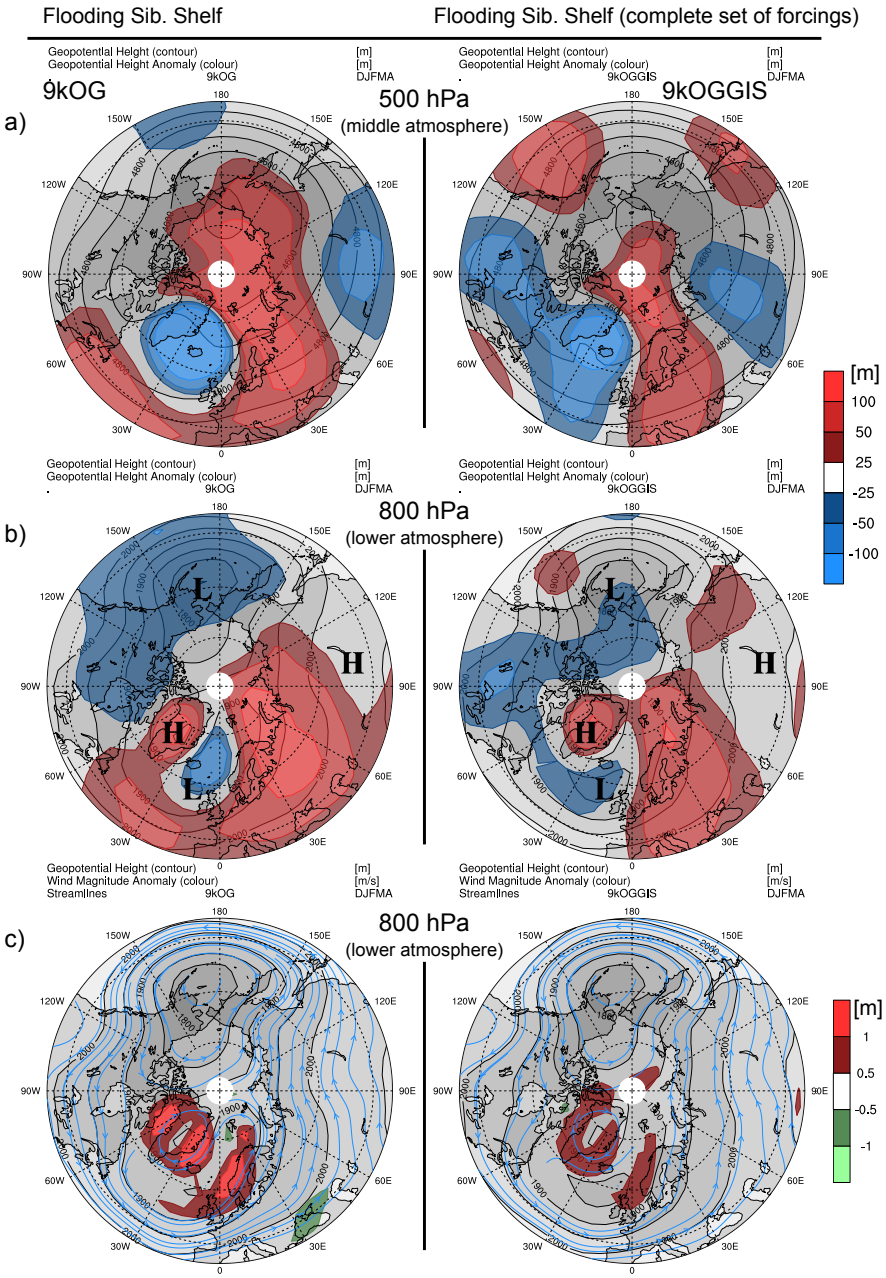

Figure 3.7: Atmospheric circulation at 500 and 800 hPa (Caption on Page 81.)

Figure 3.7: (Continuing from Page 80) Atmospheric circulation shown as heights of the 500 hPa and 800 hPa level. Left column represents results from simulation 9kOG and anomalies to 9kOGSIB, indicating the impact of shelf flooding. Right column shows results from simulation 9kOGGIS and anomalies to 9kOGSIBGIS, indicating again the impact of shelf flooding but with a complete set of forcings (LIS topography and melt water and GIS melt water). **(a)** upper panel shows middle atmosphere, 500 hPa geopotential heights (gray filled contours) and anomalies (coloured contours) of geopotential height. **(b)** middle panel shows lower atmosphere, 800 hPa geopotential heights (gray filled contours) and anomalies (coloured contours) of geopotential height. **(c)** lower panel shows 800 hPa geopotential heights (same as middle panel) and wind magnitude anomalies (coloured contour) as well as streamlines.

such decreases. An increase of Arctic sea-ice production and a decrease of Fram Strait export represents a unique combination of cause and effect in our model that is connected to the flooding of Siberian shelf. In the northern EGC, higher values of sea-ice thickness are related to a local increase in sea-ice production that is mainly caused by increased southward winds (see Sect. 3.3.3.1) bringing cold polar air to the area. Subsequently, this locally produced ice is then transported further South to regions close to the Denmark Strait.

3.3.3.3 Summary

Feedbacks from the Siberian shelf flooding as revealed in our model are illustrated in Fig. 3.9 and relate our findings to the bigger picture. We find a 10-step way to arrive from an orbital induced summer warming to a cooling over the Nordic Seas. The summer warming causes Northern Hemisphere ice sheets to melt (1) and raise global sea level (2). This results in flooding of the Arctic shelves (3) and thus changes land into ocean (4), which impacts both ocean and atmosphere. In the Arctic Ocean, sea-ice production is increased and Arctic sea-ice transport is

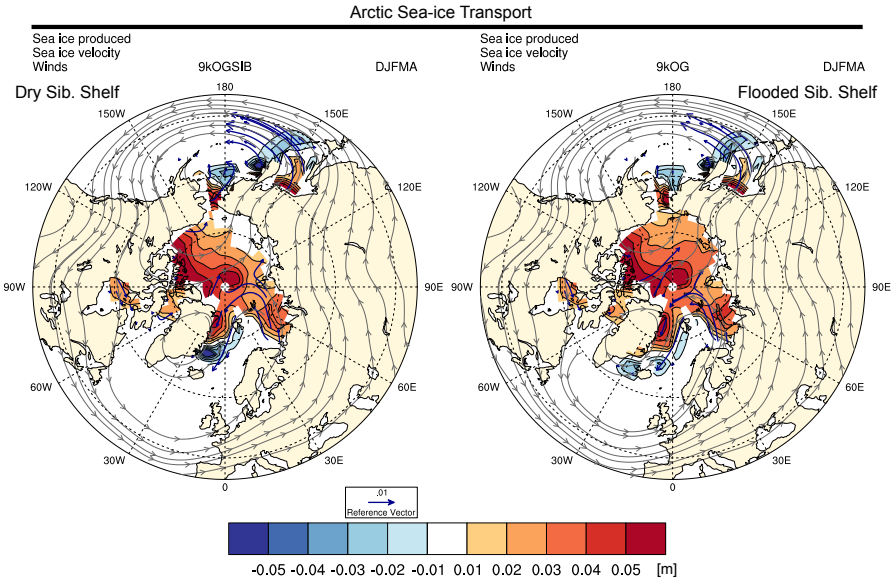

Figure 3.8: Winter (December to April) cumulative sea-ice production (in m, colour shaded), sea-ice velocity (in $\mathrm{m\,s^{-1}}$) as curly vectors (blue) and atmospheric winds (in $\mathrm{m\,s^{-1}}$) as streamlines (grey). Left panel shows the dry Siberian shelf simulation 9kOGSIB. Right panel shows the flooded Siberian shelf simulation 9kOG.

changed resulting in decreased Fram Strait export. This reduced export was not expected in our original hypothesis (as indicated in red in Fig. 3.9), implying that the direct impact of the shelf flooding on the Nordic Seas through sea-ice export is not present in our simulations. However, it should be noted that our model has a low spatial resolution potentially leading to a biased atmospheric circulation over the Arctic (Goosse et al., 2003; Goosse and Renssen, 2001). In the atmosphere, the polar vortex is weakened (5) and increased pressure difference across the Nordic Seas yield stronger winds bringing relatively cold air to the area that increase the Nordic Seas sea-ice production and transport of sea ice along the EGC (6). As a result, the sea-ice margin expands further south (7), resulting in a southward shift of deep convection (8) in the western Nordic Seas. Convection and sea-ice margin are closely bound to each other and migrate north and south together. Nonetheless these changes to convection in the western Nordic Seas reduces the Atlantic meridional

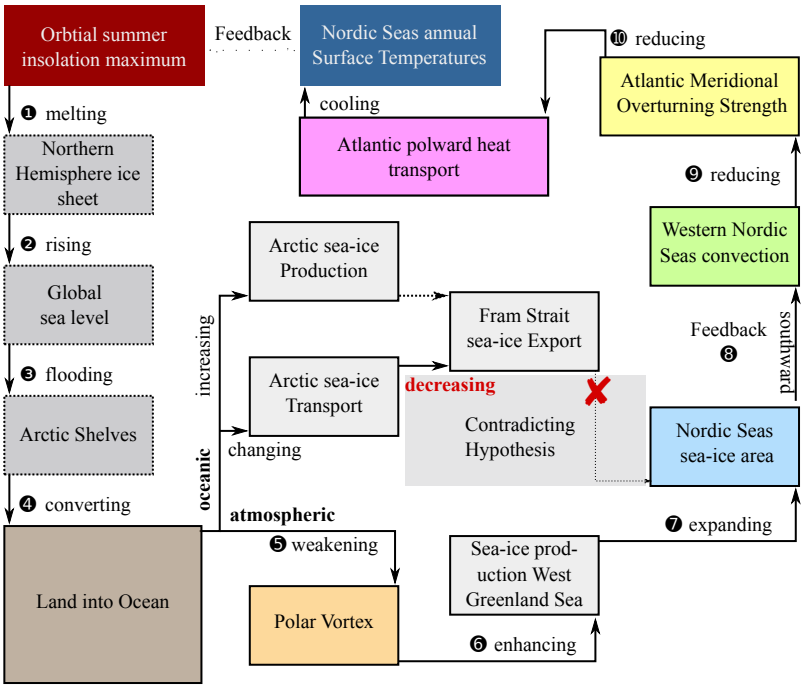

Figure 3.9: Schematic 10 step way showing the connections between found feedbacks due to Arctic shelf flooding. In red is indicated where our results do not match our original hypothesis (we proposed increased Fram Strait sea-ice export and therefore an increase of Nordic Seas sea-ice area).

overturning strength (9) at 27° N by 4 % (3.2) and the Atlantic oceanic heat transport at the equator by 7 % (not shown), but produce no significant change in atmospheric heat transport (not shown). This chain of processes due to a flooding of the Siberian shelf is also active in our simulations including LIS and GIS background forcings and give a 11 % reduction of the overturning strength and a 12 % decrease of Atlantic oceanic heat transport. Finally, the flooding leads to a significant annual cooling over the Nordic Seas connected to sea-ice expansion south along the EGC (Fig. 3.4) as opposed to an orbitally induced warming that is usually associated with the early Holocene.

3.4 Discussion

An important result from our early Holocene simulations is that the impact of the flooding of the Siberian shelf on the Arctic sea-ice production cycle remains even with major forcings as the LIS and the GIS being included in 9kOGGIS as compared to 9kOGSIBGIS. Given that the flooding of the Siberian shelf proved to have important effects on the climate in the Arctic, and in particular in the Nordic Seas, we want to compare our results in the following section with proxy estimates of sea-ice conditions and try to relate our found feedbacks of the Siberian shelf flooding to the reconstructed transgression of Bauch et al. (2001) and Taldenkova et al. (2010), which gives our simulated impacts a time frame from 9 ka, a dry shelf as in 9kOGSIB / 9kOGSIBGIS, to 7.5 ka BP, a flooded shelf as in 9kOG / 9kOGGIS.

The early Holocene is a period that is still strongly influenced by deglaciation, with pronounced melting of the Laurentide and Greenland ice sheets, resulting in relatively cold conditions in large parts of the Northern Hemisphere (Renssen et al., 2009; Blaschek and Renssen, 2013a) and a rise in sea level across the globe. As these impacts begin to fade out, the orbitally induced changes in summer insolation become the main driver of Northern Hemisphere climate, leading first to a thermal maximum, followed by a long-term cooling. Connected to our results a direct impact can be seen in the Nordic Seas sea-ice extent which can be inferred by sea-ice proxies near the Denmark Strait. Andrews et al. (2009) present a drift ice record from North Iceland (Fig. 3.1, 3.4, orange star) showing a decrease from 12 to 10 ka BP, followed by an increase with a maximum around 8.2 ka BP, a slight reduction thereafter and a continuous increase from 6 ka BP until pre-industrial. The increase between 10 and 7 ka BP seems odd, as this period is also known as the Holocene Thermal Maximum (HTM) and reduced drift ice would be expected. Following the reconstructions by Bauch et al. (2001), the Siberian shelf

must have been dry before 7 ka BP, followed by flooding. From our simulations with a dry Siberian shelf (9kOGSIB, 9kOGSIBGIS) the sea-ice expansion should have been relatively small until 7 ka BP, followed by an increase, assuming that this was related to the shelf flooding. As reconstructed drift ice values by Andrews et al. (2009) between 10 and 7 ka cannot be explained by orbital forcing or Siberian shelf flooding, another mechanism should be responsible, and it seems likely that the early Holocene LIS and the GIS have played a role. This is consistent with Blaschek and Renssen (2013a), who have investigated the impact of both ice sheets on the early Holocene climate and found an advance of the sea-ice margin southward past the Denmark Strait, as can be seen in our simulation 9kOGGIS (Fig. 3.4c) as well. Another record from the Nansen Trough (Fig. 3.1, 3.4, green star) from Jennings et al. (2002) shows an increase in ice-rafted debris (IRD) from around 5 ka BP after relatively low values for the early Holocene. This low IRD content indicates either that ice margins must have retreated or that the icebergs melted in the fjords (Jennings et al., 2002). In simulation 9kOG the sea-ice margin reaches beyond the Nansen Fjord and including LIS and GIS into the simulations (9kOGGIS) increases the likelihood of a sea-ice margin in that region (Fig. 3.4c). Thus, including a dry Siberian shelf in simulation 9kOGSIBGIS (Fig. 3.4c) forces the sea-ice margin in that particular area to retreat and could potentially explain these lower IRD reconstructions in the early Holocene.

Another way of retrieving information on past sea-ice conditions are biomarkers produced by sea-ice diatoms, such as IP25 (isoprenoid lipid) and sterol brassicasterol derived from phytoplankton (Müller et al., 2009). In combination with brassicasterol, IP25 can be used to estimate sea-ice cover for spring and its seasonal behaviour. Müller et al. (2009) used these proxies to reconstruct sea-ice conditions at the Fram Strait over the last 30 ka (Fig. 3.1, 3.4, purple star). They find that IP25 was higher from 11.5 to 8.4 ka BP and strong fluctuations in the IP25 flux occurred from 8.4 to 8.2 ka BP, followed by a period of relatively low

IP25 from 8 to 5 ka BP. Higher IP25 values indicate less persistent sea-ice cover in spring, while lower values refer to more persistent sea-ice cover in spring. Although it is difficult to find a model variable that is comparable to these reconstructed values, we find an increase in the seasonal sea-ice cover over the north-western Nordic Seas (Fig. 3.5a) in response to the Siberian shelf flooding in simulation 9kOGGIS as compared to 9kOGSIBGIS. This equilibrium response of sea-ice cover near the Fram Strait and the northern EGC can be seen as a temporal evolution of sea-ice cover from 9 to 7.5 ka BP from reduced (9kOGSIBGIS) to increased sea-ice cover after the flooding (9kOGGIS). The flooding of the Siberian shelf from 9 to 7.5 ka BP increased the sea-ice cover at the Fram Strait, especially during summer. From our early Holocene simulations, we can see that the Northern Hemisphere becomes almost sea-ice free (Fig. 3.2, 3.5a, d), allowing insolation to warm surface waters, thus delaying the subsequent winter cooling and sea-ice production. This is also important because it means that in the early Holocene Arctic sea-ice cover had to build up each winter and that in comparison to present day the Arctic Ocean was not a reservoir for sea ice, which could then affect reconstructed sea-ice quantities. Nevertheless one has to keep in mind that LOVECLIM underestimates present-day sea-ice volume and that early Holocene sea-ice loss is likely to be less severe.

Additional reconstructions of past sea-ice conditions would be required to shed more light on the sequence of events in the early Holocene and in particular on the impact of shelf flooding. This relates also to times of rising sea levels during terminations, when Arctic shelves became flooded and cooled Nordic Seas surface temperatures, possibly impacting moisture transport to adjacent ice sheets and altering Northern Hemisphere climate response to orbital-induced insolation maxima. The opposite response could be proposed during times of relatively low sea levels when a warming of the Nordic Seas could increase moisture transport to adjacent ice sheets.

3.5 Conclusions

In this paper we tested the following hypothesis in simulations with early Holocene forcings, performed with the LOVECLIM model: the flooding of Arctic shelves results in a major increase in sea-ice production, leading to enhanced sea-ice volume and export through the Fram Strait. Following this hypothesis, we expected to find in the early Holocene (before the flooding at 8.9 ka BP) a reduction of sea-ice production and lower sea-ice cover along the EGC together with increased SSTs and SSSs. Our model results indicate the following:

- There is 15 % (3100 km^3) more sea-ice produced in a simulation with flooded Siberian shelf (9kOG) relative to an experiment with a dry Siberian shelf (9kOGSIB), accompanied by an increase of 12 % (943 km^3) in Northern Hemisphere mean sea-ice volume and 14 % (1.08×10^{12} km^2) area.

- In contrast to the hypothesis, sea-ice export through the Fram Strait is reduced by 15 % (1138 km^3, annual sum) in a simulation with a flooded shelf (9kOG) compared to an experiment with a dry shelf (9kOGSIB). This annual decrease is statistically significant and originates from changes in the Arctic sea-ice transport.

- The reduction of high latitude land surface area in a simulation with a flooded shelf reduces the seasonal temperature contrast by 2–10 °C at the shelf and reduces the winter pole-to-equator temperature gradient by 1.4 °C.

- A weakening of the polar vortex due to the noted weaker meridional temperature gradient, results in a strengthening of the Greenland winter high and Icelandic winter low. Increased zonal pressure differences in the Nordic Seas yield stronger southward winds along the EGC, bringing relatively cold air, and stronger northward winds along the Norwegian Atlantic Current.

- Stronger, relatively cold, southward winds along the EGC enhance local sea-ice production and push the sea-ice extent in the Nordic Seas further south, thereby shifting convective activity, to a site closer to the new ice edge near the Denmark Strait (63° N), and reducing local SSTs and SSSs along the EGC.

- In a simulation with only a flooded shelf, the Nordic Seas region is cooled up to −4 °C. In a simulation with a more complete set of forcings (i.e. also including Laurentide ice sheet topography and melt water and Greenland ice sheet melt water) in the early Holocene, the flooding of the shelf results in a similar cooling.

We find that our hypothesis can be mostly confirmed from our model sensitivity study, despite the unforeseen decrease of Fram Strait sea-ice export. The atmosphere–ocean interaction shows clearly that changes in land-sea distribution are able to force changes in sea-ice production and affect sea surface conditions in the Nordic Seas, which is the major pathway of Arctic sea-ice export. Changes in Nordic Seas sea-ice extent affect local convection and alter ocean–atmosphere heat exchange, modifying seasonal atmospheric circulation. This finding underlines the importance of the Nordic Seas for the global climate and its influences originating from Arctic shores. It is likely that during previous terminations of glacial periods, a rising sea level must have also triggered Arctic shelf flooding events, temporarily pausing the progress of a termination by an external forcing, possibly even causing a reversal event. Therefore, global sea level and in particular regional sea level rise is of high significance for all terminations and must be considered in modelling of terminations.

Chapter 4

Holocene North Atlantic Overturning in an atmosphere-ocean-sea-ice model compared to proxy-based reconstructions

Based on: Blaschek, M., C. Kissel, D. Thornalley and H. Renssen. Holocene North Atlantic Overturning in an atmosphere-ocean-sea ice model compared to proxy-based reconstructions. In preparation for Climate of the Past.

Climate and ocean circulation in the North Atlantic region changed over the course of the Holocene, partly because of disintegrating ice sheets and partly because of an orbitally-induced summer insolation trend. In the early Holocene, the Laurentide ice sheet cooled large parts of the Northern Hemisphere through melt fluxes into the North Atlantic and by the cooling effect of the remnant ice sheet itself. In the Nordic Seas, this impact was accompanied by a rather small, but significant, amount of Greenland ice sheet melting that reduced local ocean surface temperatures even further. After about 7 ka BP, these ice-sheet impacts vanished, marking the start of a relatively warm

period (known as the Holocene Thermal Maximum period) under influence of the orbitally-forced, relatively high summer insolation. This was the warmest period in the Northern Hemisphere in the Holocene before the climate continued to follow the orbital induced cooling trend towards present-day. We have compared our model simulations with proxy-based reconstructions using $\delta^{13}\mathrm{C}$, sortable silt (SS) and magnetic susceptibility (κ) allowing to infer changes of past ocean circulation over the last 9000 years. The various reconstructions exhibit different long-term evolutions suggesting changes of either the overturning in the Atlantic in total or of subcomponents of the ocean circulation, such as the overflow waters across the Greenland-Scotland ridge (GSR). Thus, the question arises whether these reconstructions are consistent with each other or not? A comparison with model results indicates that $\delta^{13}\mathrm{C}$, employed as an indicator of overturning, agrees well with the long-term evolution of the modelled Atlantic meridional overturning circulation (AMOC). Regional differences in the reconstructions are most likely originating from influences of $^{13}\mathrm{C}$ depleted water masses, such as Antarctic Bottom Water. The modelled AMOC evolution corresponds well to a $\delta^{13}\mathrm{C}$ record in the Norwegian Sea, but the recorded magnitude is much smaller than suggested by the model. In a further step to trace Nordic Seas deep water across the GSR, we compared our model results to reconstructions employing SS and κ to infer changes in the Iceland-Scotland Overflow Waters (ISOW). Reconstructions at the Gardar Drift correspond well with modelled Nordic Seas normalised convective volume, representing overflow source waters. However, a direct comparison of modelled flow speed at the location and reconstructed deep water flow strength from SS do not agree on the long-term evolution from 7 kyr BP towards present. In summary, the model results including early Holocene ice sheet impacts suggest that different long-term trends in subcomponents of the AMOC, such as ISOW, are consistent with proxy-based reconstructions and allow

reconciling some of the reconstructions with each other. The modelled and reconstructed (from δ^{13}C) AMOC strength over the past 9000 years, showed an early Holocene weakening and a fast recovery until about 7 kyr BP and a weak increasing trend of 12 mSv/kyr towards present, with relatively low variability on centennial to millennial time scales.

4.1 Introduction

The Atlantic meridional overturning circulation (AMOC) is critical to the global climate system. This circulation transports important amounts of heat (1.33 ±0.4 PW at 26°N, Johns et al., 2011) in the near-surface layer from the tropical Atlantic northwards to the mid- and high-latitudes of the Northern Hemisphere. In winter, part of this heat is released to the relatively cold atmosphere in the sub-polar North Atlantic. This heat release results in relatively warm conditions over the greater North Atlantic region compared to similar latitudes of the North Pacific, with an air temperature increase of up to 10°C relative to the zonal mean climatology (Rahmstorf and Ganopolski, 1999), demonstrating the climatic importance of the AMOC.

There are two distinct driving mechanisms of the AMOC: the traditional thermohaline circulation and wind-driven upwelling (Kuhlbrodt et al., 2007). On smaller scales a larger variety of processes including horizontal gyre circulation, local atmospheric cooling and Greenland ice sheet melting play a role in driving its strength (Kuhlbrodt et al., 2007). However, from Sandström (1908) theorem it is clear that surface buoyancy fluxes alone cannot supply the energy needed to sustain the AMOC (Kuhlbrodt et al., 2007). Nonetheless, these surface fluxes are essential for deep-water formation (Huang, 2004) and thus the lower limb of the AMOC, hence the conversion of surface waters to deep waters by increasing their density by cooling and/or increasing salinity. If the density of a surface water mass becomes significantly higher than the density of

surrounding water masses, then a threshold density can be crossed and deep convection can occur. The deep mixing associated with this process leads to the formation of relatively dense, deep waters, which flow southward and sum up to form the North Atlantic Deep Water (NADW). In the present North Atlantic basin, deep convection occurs preferentially in the Labrador Sea, the Irminger Sea and the Nordic Seas. The deep waters that form in the Nordic Seas flow southwards at depth and have to cross a major sill, the Greenland-Scotland Ridge (GSR), to enter the North Atlantic Ocean as overflow waters. These waters are known as Denmark Strait overflow water (DSOW) and Iceland-Scotland overflow water (ISOW), and are named after the two main locations of the overflow. The modern rates for DSOW and ISOW have been estimated at 2-3.5 Sv (1 Sv = $1x10^6 m^3 s^{-1}$) and 3-5.7 Sv, respectively (Dickson and Brown, 1994; Hansen and Østerhus, 2000; Macrander et al., 2005; Smethie et al., 2013). In addition, deep water formed in the Labrador Sea (so called Labrador Sea Water, LSW) contributes 11.7±1.6 Sv to NADW (LeBel et al., 2008; Smethie et al., 2013). Although deep convection has been observed in the Irminger Sea, quantified estimates of the contribution to the NADW are not yet available (Kuhlbrodt et al., 2007). Together with some entrainment of intermediate waters (about one third of the NADW flux, Hansen and Østerhus, 2000), this adds up to a total southward NADW flux of 15-19 ±2Sv (Ganachaud and Wunsch, 2003; Kanzow et al., 2010; Smethie et al., 2013). From this summary, it is clear that changes in the rates of overflow waters or LSW formation will affect the strength of the NADW flow. A recent review by Lozier (2012) points out that from modern observations it is not clear whether the overturning strength in the North Atlantic can be directly linked to the intensity of deep-water formation. The biggest problem in this respect is undersampling. For example, the measurement period of the strength of the AMOC from a moored array near the Florida Strait is relatively short (∼4 yrs, Kanzow et al., 2010), making its long-term evolution uncertain. However, modelling studies (e.g. Straneo, 2006; Rhein et al., 2011) have

shown the impact of deep-water formation on the overturning circulation, such as Jungclaus et al. (2008), who found in a modelling study that 30% of the entire AMOC volume is directly coming from the Nordic Seas and that these waters together with considerable entrainment (approximately the same volume) form the backbone of the overturning. This discrepancy between modelled and observed results has not been resolved so far (Lozier, 2012). However, considering longer times scales, numerous proxy-based reconstruction studies have attempted to extend these short present-day observations of AMOC strength into the past, and to expand the knowledge of this so important climatic indicator.

Basically, there are two categories of reconstructions of past North Atlantic Ocean circulation: for the surface and the deep ocean. We will focus in this paper on deep ocean circulation reconstructions, which are based on a number of proxies: ratios of carbon and oxygen isotopes (δ^{13}C and δ^{18}O) measured in shells of benthic foraminifera (Oppo et al., 2003; Kleiven et al., 2008; Hoogakker et al., 2011), deep ocean sediment characteristics, such as the sortable silt (SS) content (Bianchi and McCave, 1999; Hoogakker et al., 2011; Thornalley et al., 2013; Kissel et al., 2013), magnetic properties of grains (abbreviated as "κ",Kleiven et al., 2008; Kissel et al., 2009, 2013), geochemical data such as the Pa/Th ratio (McManus et al., 2004; Gherardi et al., 2009) and bulk mineralogy and isotopic composition of sediments (such as Nd, Sm, Pb; Fagel and Mattielli, 2011). The deep-ocean-circulation reconstructions are mainly influenced by the region, the water depth and the assumptions contained in the reconstruction of the proxy itself. The proxies for deep ocean circulation can be separated into proxies representing a local property of the deep water, such as its water speed, or representing the larger scale of a water-mass property, that will link the recorded signal to the production of the deep water. SS and the magnetic properties of grains belong to the first category, while δ^{13}C , δ^{18}O, Pa/Th ratio and the geochemical data belong to the second category. Three of these proxies have been most widely applied: SS, κ and δ^{13}C .

The SS proxy is based on the grain size of silt, which can be used to reconstruct bottom-current strength on the basis of depositional sorting associated with variable flow speeds (Praetorius et al., 2008). Coarser grain sizes would indicate faster near-bottom flow speeds. The physical connection is based on Stokes's settling principle, implying that the grain size distribution of the sediment reflects the mean kinetic energy of the flow (McCave et al., 1995, 2006; Praetorius et al., 2008), and that the strength of a certain bottom current is proportional to the amount of sortable silt at a certain location. Uncertainty in the SS proxy is connected to source effects, spatial variability of the flow, downslope supply at continental margins and the influence of ice-rafted detritus (McCave and Hall, 2006; Thornalley et al., 2013). This method has, for instance, been successfully applied to drift deposits, involving high sedimentation rates, from South of Iceland to reconstruct past rates of ISOW during the last glacial and present interglacial (McCave et al., 1995; Thornalley et al., 2013; Kissel et al., 2013).

The second proxy κ is the volume-normalized magnetic susceptibility measured on sediments in which titanomagnetites are the main magnetic carrier with uniform grain size. The transport of magnetic minerals from an identified source to the core location allows to deduce the flow strength of bottom currents and its deposition along the flow path (Kissel et al., 2009). This has been especially fruitful in determining the ISOW strength given a source of magnetic minerals at the Greenland-Scotland Ridge. The measurement of κ is therefore an additional source of information complementary to SS. Uncertainties in κ are connected to the supply of magnetic source material and spatial variability of the flow (Kissel et al., 2013).

The third proxy δ^{13}C is the ratio of stable isotopes ^{13}C and ^{12}C and is measured in the carbonate of benthic foraminifera shells (mostly *Cibicidoides wuellerstorfi*) and indicates the strength of ventilation including convection. During times of convection, surface waters that are enriched in carbon-13 compared to the deep ocean, sink and supply

carbon-13 to the deep ocean and its fauna. Hence, higher δ^{13}C values in benthic foraminifera are usually interpreted to indicate more downward transport and subsequent mixing, and are therefore indicative of the ventilation strength. The second most important process that acts on the δ^{13}C values of deep ocean waters is re-mineralization of organic carbon and is seen as a source of error (0.1-0.3‰ present ocean, Curry et al., 1988). In the North Atlantic, deep waters have a different isotopic composition depending on the source region of the water masses. For example, Antarctic bottom water (AABW) is more depleted than NADW.

The long-term evolution of the AMOC is uncertain and mostly only the evolution of its subcomponents, upper and lower limb or further subcomponents, such as the Florida Strait flow or the Greenland-Scotland Ridge overflow, is estimated by proxy-based reconstructions. For example, (Thornalley et al., 2013) measured SS in drift deposits along a depth transect South of Iceland to reconstruct the ISOW strength over the past 9,000 yrs. Their results show an early Holocene minimum followed by a maximum of ISOW at 7,000 yrs before present (7 ka BP) and a subsequent decrease towards present-day. (Thornalley et al., 2013) subsequently compared these reconstructions to our modelling results discussed in Blaschek and Renssen (2013a), and found a good match between the reconstructed trend in ISOW strength and the simulated Nordic Seas winter convection layer depth (CLD). However, convection or deep water mixing in the Nordic Seas can also be reconstructed from δ^{13}C. For instance, a reconstruction of Sarnthein et al. (2003) from a site near the western Barents Sea, shows a continuous supply of carbon-13 to the deep ocean over the Holocene,indicating a steady long-term trend in convection without long-term changes. This steady supply of deep waters,indicated by δ^{13}C, towards the Iceland-Scotland Ridge seems to be in conflict with an unsteady flow strength South of Iceland, indicated by SS. Consequently, at first sight, different proxy-based reconstructions suggest different trends in Holocene deep

ocean flow. This raises the question if they are really in conflict or if they can be reconciled? Further investigation is thus required to better understand what these proxies represent, and to analyse how the proxy-based reconstructions relate to model results. A first step, however, is to discuss previous, similar modelling studies on Holocene deep ocean circulation to see if these are consistent with the results of Blaschek and Renssen (2013a).

Previous modelling studies have shown different trends in the simulated Holocene ocean circulation. Renssen et al. (2005a) found a decreasing trend of deep convection in the Nordic Seas over the last 9,000 yrs and an increasing trend in the Labrador Sea, hence stabilizing the strength of the AMOC by compensation. The deep convection decrease in the Nordic Seas was attributed to the expansion of Arctic sea ice as the climate was cooling towards present-day and more sea ice interfered with convective activity there. Renssen et al. (2005a) explained the Labrador Sea increasing convection trend by a response to the orbitally-forced surface cooling that enhanced surface density, and as a compensation of the decrease in the Nordic Seas. However, they have not considered the impact of early Holocene ice sheet melting. A more recent study by Ritz et al. (2013), who used a hind cast modelling approach allowing to estimate the AMOC strength from surface proxy-based reconstructions and to compare to $^{231}Pa/^{230}Th$ ratios (McManus et al., 2004), indicative of deep water circulation strength, found a weak decrease of the AMOC strength over the past 10,000 yrs in agreement with the $^{231}Pa/^{230}Th$ ratios. Incompatible to the previously presented results are simulations from Lunt et al. (2006) employing an EMIC (GENIE-1) forced with transient ice sheet topography (Peltier, 1994; ICE-4G) showing an increasing AMOC strength over the last 10,000 yrs, only interrupted by an abrupt event at about 9 ka BP. These results are relatively similar to an accelerated transient simulation over the past 120 kyr employing the FAMOUS GCM (Smith and Gregory, 2012), with the model being forced with different ice sheet topographies (Peltier, 2004; Zweck and

Huybrechts, 2005) showing for the past 10 kyr an increasing trend in AMOC strength. Results indicated that the model and the subsequent AMOC strength responded strongly to the different ice sheet configurations. However, the impact of melt water was not included in the study of Smith and Gregory (2012). In summary, different modelling studies that included different forcings (orbital parameters, Greenhouse gases, ice sheet topographies, melt water) indicate that the AMOC depends strongly on these forcings and on the model employed, mainly due to differences in model sensitivity. Hence, no consistent view on Holocene deep ocean circulation emerges from different proxy-based and model-based studies. Therefore we think it is useful to study this in more detail. We focus on the following questions: What are the contributions of different convection areas to overflow waters and to the simulated AMOC strength? To what extent are these model results for the AMOC consistent with proxy-based reconstructions? And finally, can we explain differences between proxies and model results, and uncover potential biases?

To answer these questions, we provide here a more detailed analysis of the simulated AMOC dynamics and compare these simulations with selected proxy-based reconstructions.

In our present study, we will focus on SS, κ and δ^{13}C , because the first two proxies focus on the speed of bottom-water masses, whereas the third one focuses on the activity of ventilation, therefore supply of deep water. Thus, these three proxies describe two characteristics of the overturning in the North Atlantic, the density of deep water and the overall transport or circulation of water. We compare SS, κ and δ^{13}C reconstructions and their long-term evolution to our model simulations that cover the past 9kyr. These simulations were performed with a fully coupled atmosphere-ocean sea-ice-model of intermediate complexity by Blaschek and Renssen (2013a). The Holocene started about 11.7 kyr BP and was dominated in its early phase by the decaying ice sheet remnants from the last glacial period until about 7 kyr BP (Blaschek and

Renssen, 2013a). During the past 7 kyrs, the Northern Hemisphere climate followed more or less the orbitally-forced summer insolation trends (e.g. Kaufman et al., 2004; Kaplan and Wolfe, 2006; Lorenz et al., 2006), and were only slightly affected by trends in atmospheric greenhouse gas levels. Therefore, it is important to account for changes in ice sheets, orbital parameters and greenhouse gases in our simulations. We designed four simulations including remnant ice sheet decay of the Laurentide ice sheet (LIS), described by melt water and ice sheet topography on land, as well as melting of the Greenland ice sheet (GIS). The LIS is known to have released huge amounts of melt water into the Labrador Sea and surroundings, preventing deep convection in the Labrador Sea until about 7 kyr BP (Hillaire-Marcel et al., 2001).

In the following we highlight important features of our model (Section 4.2.1) and give detailed information on the experimental setup (Section 4.2.2). In Section 4.3 we introduce the results of our numerical simulations. In Section 4.4.1 we present the proxy-based reconstructions and discuss the reconstructions in the light of our modelling results in Section 4.4.2.

4.2 Methods

4.2.1 The Model

We performed our experiments with the Earth system model of intermediate complexity LOVECLIM (version 1.2; Goosse et al., 2010). We employed a version of this model that includes dynamical representations of atmosphere, ocean and sea ice, land surfaces and vegetation. Additional components, such as a dynamical ice sheet, the carbon cycle or ice bergs have not been activated in the present study. We present here a brief summary of the key components and refer to Goosse et al. (2010) for more details.

The ocean-sea-ice component is CLIO3 (Goosse and Fichefet, 1999), consisting of a free-surface ocean general circulation model with a horizontal resolution of 3°x3° latitude-longitude and 20 vertical levels. Smaller scale processes not explicitly resolved by the model are parameterized. Vertical mixing and convection are parameterized via an approximation of the turbulent kinetic energy, calculating viscosity and diffusivity, and an additional convective adjustment scheme, which increases vertical diffusivity in a statically unstable water column. To further improve the representation of dense water flows, Campin and Goosse (1999) included a parameterization of downslope currents within the grid-box resolution. These approximations for sub grid ocean processes require numerous parameters of which the isopycnal mixing is one of the most crucial (Stone, 2004). The resolution of the model has implications on the amount of details being resolved by the bathymetry in the model compared to the real ocean. For example the Greenland-Scotland Ridge is uniformly about 1200 m deep compared to 400-800 m in the real ocean with canyons and trenches changing on scales far below what the model resolution does permit. The ocean model is coupled to a sea-ice component (Fichefet and Maqueda, 1997, 1999) employing a three-layer dynamic-thermodynamic model. The atmospheric component is ECBILT (Opsteegh et al., 1998), a spectral T21, three-level quasi-geostrophic model coupled to a land-surface model that contains a bucket-type hydrological model for soil moisture and runoff. Cloud cover is prescribed according to observed present-day climatology (Rossow, 1996). The dynamical vegetation model, VECODE (Brovkin et al., 2002), simulates two plant types (trees and grasses) and desert as a dummy type. In our simulations we prescribed the ice sheets manually.

LOVECLIM has been shown to have a climate sensitivity to a doubling of CO_2 concentrations just outside the lower end (1.9K after 1000yr; Goosse et al., 2010) as found in global climate models (2.1 to 4.5 K, Meehl et al., 2007). Deep convection takes place in both the Nordic Seas and the Labrador Sea (Goosse et al., 2010) and the simulated deep

Name	Forcings
OG	Orbitals and Greenhouse Gases
OGMELT	OG + Laurentide Ice sheet melt water (0.09 - 0 Sv)
OGMELTICE	OGMELT + Laurentide Ice sheet topography + albedo
OGGIS	OGMELTICE + Greenland Ice sheet melt water (0.025 - 0 Sv)

Table 4.1: Summary of experimental setup

ocean circulation is in good agreement with other model results (Weaver et al., 2012). The model has been used successfully in numerous palaeoclimatological modelling studies, for example by Wiersma and Renssen (2006) to investigate the 8.2 kyr BP event and by Renssen et al. (2009, 2010, 2012) and Blaschek and Renssen (2013a) in studies of the Holocene Thermal Maximum.

4.2.2 Experimental Setup

In this study we use the results of four transient experiments OG, OGMELT, OGMELTICE and OGGIS that cover the last 9 kyr and have been discussed in detail by Blaschek and Renssen (2013a) and Thornalley et al. (2013). All simulations have been forced with orbital parameters and atmospheric greenhouse gas concentrations in line with the PMIP3 protocol (`http://pmip3.lsce.ipsl.fr`). An overview of the forcings is provided in Fig. 4.1.

We have performed one control simulation (OG) including only transient orbital and greenhouse gases and two simulations including additionally either LIS melt water (OGMELT) or the full LIS forcing (OGMELTICE). Following the setup of Renssen et al. (2009), the additional freshwater flux was set to 0.09 Sv between 9 to 8.4 kyr BP, decreasing slightly to 0.08 Sv between 8.4 and 7.8 kyr BP, and dropping to 0.01 Sv between 7.8 and 6.8 kyr BP (Fig. 4.1). These freshwater rates are based on adapted estimates of Licciardi et al. (1999) and do not include short-term drainage events like the one centred at 8.2 kyr BP (Alley and Ágústsdóttir, 2005), because the focus of our study is on

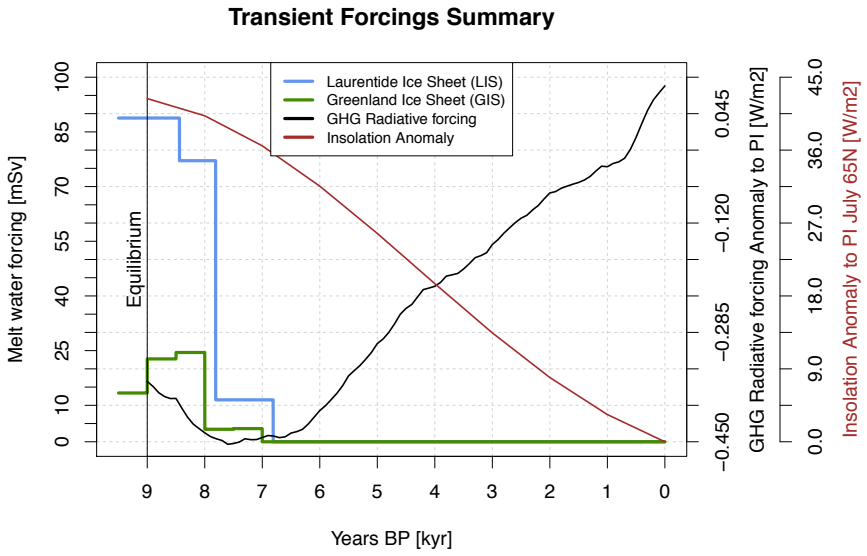

Figure 4.1: Summary of forcings applied in different simulations. Shown are melt water forcings and orbital and greenhouse gas changes compared to pre-industrial. Topography changes of the LIS are not shown. Blue is the total LIS melt water flux applied in simulation OGMELT, OGMELTICE and OGGIS (left axis). The Green curve denotes the calculated GIS melt water from Peltier (2004) prescribed in OGGIS (left axis). Black gives the radiative forcing due to greenhouse gas concentrations as anomaly to pre-industrial and the red curve gives the July 65° N insolation anomaly after Berger and Loutre (1991) (right axis). Greenhouse gas radiative forcing is calculated using IPCC (2001) formulation.

multi-centennial to millennial time scales. In OGMELTICE the effect of the disintegrating LIS was accounted for by changing the surface albedo and topography at 50-yr time steps, interpolated from reconstructions provided by Peltier (2004), during the period 9 to 7 kyr BP. Finally, we have performed a experiment (OGGIS) that included the GIS melt water flux, in addition to all forcings prescribed in OGMELTICE. As shown in Fig. 4.1, this additional GIS melt water was set to 13 mSv for 9 kyr BP and increases to 23 mSv from 9 to 8 kyr BP and then rapidly decreases to 3 mSv before vanishing completely at 7 kyr BP (estimates derived

from Peltier, 2004). Considering the coarse model grid resolution (T21), early Holocene GIS topography changes in the model are relatively small (Blaschek and Renssen, 2013a) and are therefore neglected in this study.

4.3 Results from transient model simulations

We propose to structure our results from the larger to the smaller scales in the following way: First we will look at the Atlantic overturning strength in our simulations (Section 4.3.1), which should compare well with δ^{13}C in Section 4.4.1.1, because both represent the overturning of water and are likely to be in good agreement with each other (c.f. Section 4.4.2). Secondly, we will investigate the contribution of different convection areas to the overturning circulation (Section 4.3.2), which will allow us to estimate the importance of these convection areas and make connections to the overflow waters as reconstructed by SS and κ at the Gardar Drift. Finally, we will investigate the exchange between the Nordic Seas and the Subpolar North Atlantic as well as the balance between NADW and AABW (Section 4.3.3), which will be compared to SS-based reconstructions at the Orphan Knoll site and δ^{13}C reconstructions in the eastern North Atlantic.

4.3.1 Atlantic Meridional Overturning Circulation

In our simulations, long-term changes of the AMOC strength are mainly driven by variations in the prescribed melt water flux. Our experimental set-up with a considerable additional freshwater input related to the LIS and GIS melt from 9 to7 kyr, implies already that there is a difference between the early Holocene and the last 7,000 yrs. We have to distinguish between simulations including only orbital parameters and greenhouse gases (OG), additional melt water from the LIS (OGMELT), additional effects (albedo and topography changes on land) of the remnant LIS (OGMELTICE) and additional GIS melt (OGGIS), as summarised

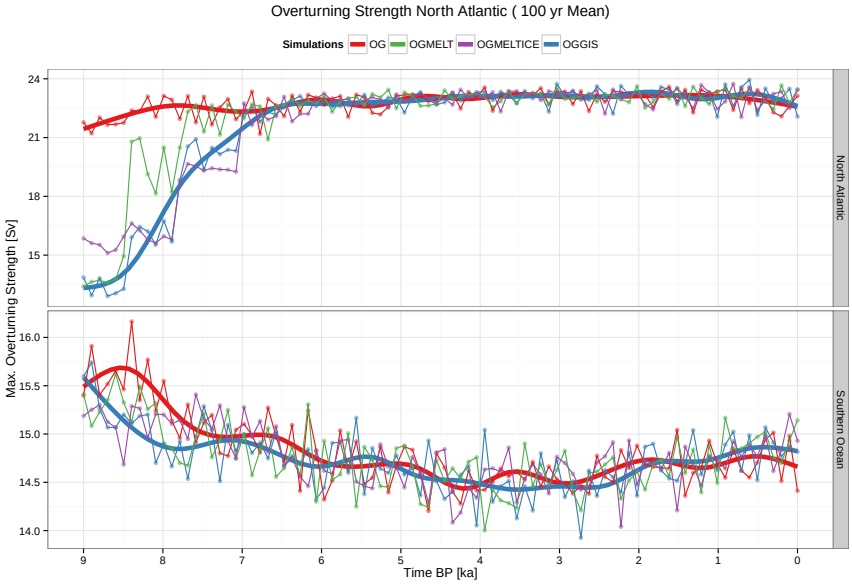

Figure 4.2: Simulated Overturning in the North Atlantic and the Southern Ocean in Sv. Shown are 100 yr averages of the maximum meridional stream function in the North Atlantic and Southern Ocean for 4 transient simulations. Thick lines indicate smoothed long-term trends for OG and OGGIS (n=9).

in Tab. 4.1. The simulated AMOC strength depends therefore on these choices and allows us to separate our analysis into an early Holocene (9 to 7 kyr), influenced by melting ice sheets and a later part (past 7 kyr), representing the transient climate change towards present-day.

We present in Fig. 4.2 the maximum overturning strength in the North Atlantic and the Southern Ocean, with the latter acting as a reference for inter-hemispherical changes. The strength in the North Atlantic follows the prescribed melt forcing in timing very precisely, indicating the rapid response due to melt water from both the LIS and the GIS. However, we can see different reductions in OGMELT and OGMELTICE from 8.5 to 7 kyr BP originating from changes in the topography and albedo of the LIS, which modify the atmospheric circulation and the interaction with the ocean. It has been previously reported (Renssen et al., 2009; Smith

and Gregory, 2012), that the remnant ice sheet produced a downwind cooling effect on the North Atlantic, therefore cooling the surface ocean and allowing sea ice to expand in the whole Northern Hemisphere and especially in the Labrador Sea (as depicted for OGGIS compared to OG in Fig. 4.3). In the Labrador Sea at 9 kyr BP, the sea-ice area increases by 100 ±10 % in OGMELT, OGMELTICE and OGGIS compared to OG (sea-ice area $3.6x10^{11}$ m^2) and decreases for OGMELT already at 8.7 kyr BP. Some of the differences in AMOC strength (8.5-7 kyr BP, Fig. 4.2) between OGMELT and OGMELTICE are related to this change in sea-ice extent. However, this effect is not always constant and evolves with the melt water forcing and the decay of the land-based ice sheet. For example in the beginning (i.e. at 9 kyr BP), simulation OGMELT shows a weaker AMOC strength (by -3 Sv) compared to OGMELTICE, because of the positive feedback the cooling effect of the remnant ice sheet in OGMELTICE has on the AMOC (i.e. strengthening, due to enhanced surface density). This has been attributed to a shift of convection from the Labrador Sea to the Irminger Sea by Renssen et al. (2009). Likewise, as melt water from the LIS decreases at 8.4 kyr BP, the AMOC strength increases in OGMELT (+6.2 Sv), but remains lower in OGMELTICE (+0.6 Sv), because of the expansion of sea ice in the Labrador and the Nordic Seas. Hence, we find that the combined forcing of melt water and land-based ice sheet changes (topography and albedo) produce a stronger and less melt water-dependent AMOC compared to melt-only forcing. However, including GIS melt in OGGIS reduces the AMOC between 9 and 8.5 kyr BP again, because of the relative closeness of the GIS melt water to the convection area in the Irminger Sea. The additional GIS melt water (13 mSv at 9kyr BP, Fig. 4.1) suppresses convection there. Therefore, we can see in the early Holocene a stepwise increase of the AMOC strength (OGGIS, 13.3 ±0.5 (>8.5 kyr BP), 16.1 ±0.5 (8.5 - 7.8 kyr BP), 20.1 ±0.8 (7 kyr BP - present)) related to the ice sheet forcing until it reaches present-day values at about 7 kyr BP (22.9 ±0.6 Sv). The latter part shows a statistically significant increasing long-term trend (consistent with the long-term orbitally-forced surface

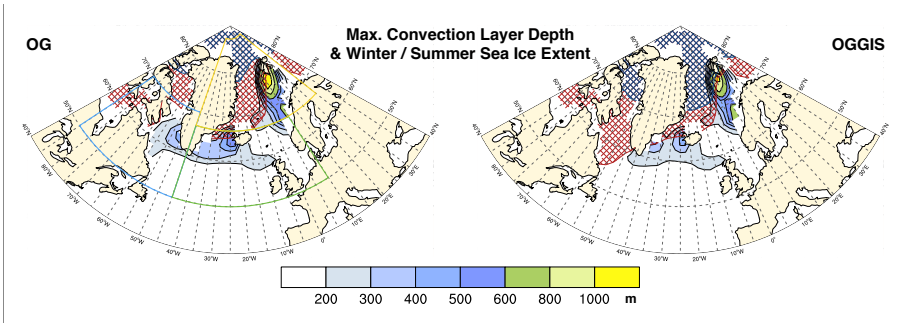

Figure 4.3: Deep convection areas in the North Atlantic in our model. Shown are 50yr averages of winter maximum convection depth in meters and maximum (red) and minimum (blue) sea-ice extent for simulations OG and OGGIS.

cooling, +7.8 mSv/kyr), which is relatively weak compared to the much larger changes in the early Holocene. Consequently, we conclude that the early Holocene shows reduced AMOC strength, which comes to its full strength at about 7 kyr BP, followed by relatively weak increase towards present. In the Southern Hemisphere the overturning circulation is hardly affected by the Northern Hemisphere melt water and remnant ice sheet decay.

4.3.2 Convection areas and contribution to the overall deep water production

The strength of the overturning circulation (Section 4.3.1) is associated with the intensity of deep convection at the different convection areas in the North Atlantic (Kuhlbrodt et al., 2007; Jungclaus et al., 2008). Therefore, it is important to investigate convection areas and their contribution to the overall deep water circulation in the North Atlantic Ocean. We have three main deep convection areas in our model: the Labrador Sea, the Irminger Sea and the Nordic Seas, as shown in Fig. 4.3a for simulation OG. In the early Holocene, the melt water from the LIS and GIS (simulation OGGIS, Fig. 4.3b) reduces convective activity in these areas, especially convection in the Labrador Sea. Due

to the drainage of ice sheet melt water from both the LIS and GIS, convection in the Labrador Sea, the Irminger Sea and the Nordic Seas are reduced in the early Holocene (Fig. 4.4). In order to investigate this transient behaviour, we calculated a first-order estimate of the normalised convective volume (NCV), using the convection layer depth and grid box area for the three convection areas normalised against their sum (Fig. 4.4), which should give an estimation of deep water production. Although not directly related, we find that the changes in the overturning strength (Fig. 4.2) agree well with the changes in NCV for the whole North Atlantic in the early part (Fig. 4.4d, until 7ka BP), giving lower values and a fast recovery. However, the long-term evolution in the second phase towards present-day is reversed compared to overturning strength. The results show a substantial decrease of convection (and NCV as well), in the Nordic Seas (Fig. 4.4c) in the early Holocene, thus potentially reducing the Greenland-Scotland overflow waters as well. It has been previously indicated by Thornalley et al. (2013) that reduced winter convection in the Nordic Seas (here represented by NCV in the Nordic Seas, Fig. 4.4c) resembles flow speed changes of the ISOW, resulting in less intense overflow before the major drop in ice sheet melt at 7 kyr BP. The results support the idea that the strength of the overflow is linked to water-mass properties, such as the density difference between the convected water and the surrounding waters. The question is if this link is also visible in flow speeds South of Iceland as recorded by SS.

4.3.3 The Subpolar North Atlantic

The subpolar North Atlantic is strongly affected by ice sheet melting during the early Holocene, resulting in a larger density difference with the Nordic Seas. We present the meridional velocities (negative is southwards) from two of our simulations (OG, OGGIS) at different depths (Fig. 4.5). From the direction of the flow we can easily distinguish between what is flowing out of the Nordic Seas (below 1225 m) and what is

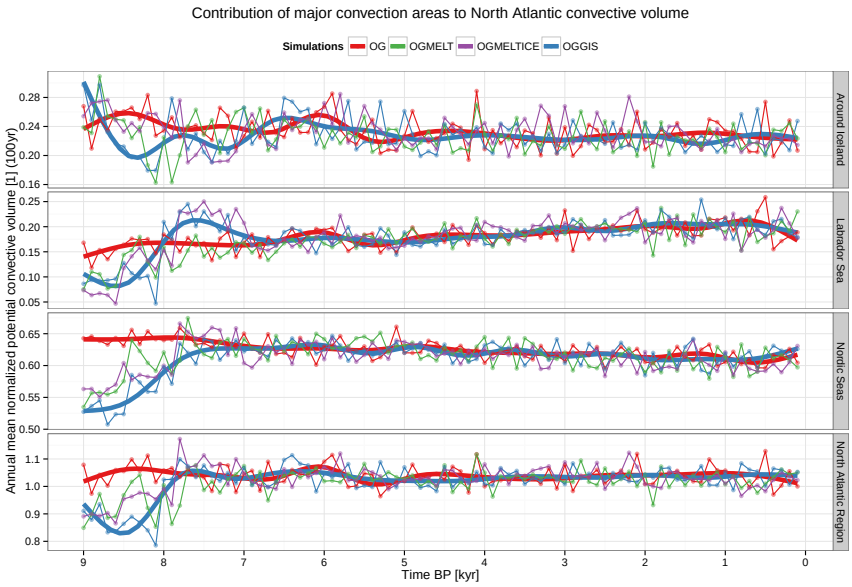

Figure 4.4: Estimated convection site contribution to the overall simulated deep convection in the North Atlantic for three convection areas (Labrador Sea, Around Iceland and Norwegian Sea) and the sum of the three areas. Shown are 100yr averages of the maximum of the convective volume, which is calculated from convection layer depth (m) multiplied by the grid-area (m^2) and normalized by the sum of all convection areas. Boxes in Fig. 4.3a indicate the areas.

flowing into it (above 850m). These results are accompanied by density differences between the Nordic Seas and the subpolar North Atlantic at different depths. Before 7 kyr BP we find a higher inflow of lighter waters into the Nordic Seas, and a weaker outflow of denser waters from the Nordic Seas at greater depth (1225-1705 m) in our simulation including all ice sheet impacts (OGGIS) compared to OG. After 7 kyr BP there is hardly any difference between the simulations and long-term trends do not significantly exist in both density-difference and flow speeds. The Nordic Seas are always denser (not explicitly shown, but indicated by the map in Fig. 4.6) below 850 m in our model than the subpolar North Atlantic and during the early Holocene the subpolar NorthAtlantic was more affected by the freshening than the Nordic Seas.

Figure 4.5: Comparison of simulated flow speeds South of Iceland and density differences between the Nordic Seas and the Subpolar North Atlantic from the 4 dimensional model output of our simulations OG and OGGIS. Shown are 50yr averages of the density difference (kgm^{-3}) and the meridional velocity (mm/s), as well as smoothed lines (n=9) to represent the long-term trends.

The density (Fig. 4.6) of the 1225 m level in our model between OG and OGGIS shows that at this level the Arctic Ocean and the Nordic Seas are denser compared to the subpolar North Atlantic. The comparison shows us that in OGGIS reduced convection, forced by melting ice sheets (melt water and topography), affect the density field at this depth in the North Atlantic considerably, especially in the Labrador Sea and in the subpolar North Atlantic. In addition, speed and direction of the flow are changed in OGGIS compared to OG, most noticeably South of the Denmark Strait, where overflow waters are directed towards the West. As expected, the density difference between the Nordic Seas and the Subpolar North Atlantic results in stronger flow, but only across the Denmark Strait, and clearly not across the Iceland Scotland Ridge (ISR), otherwise we would have found this in Fig. 4.5b. To investigate

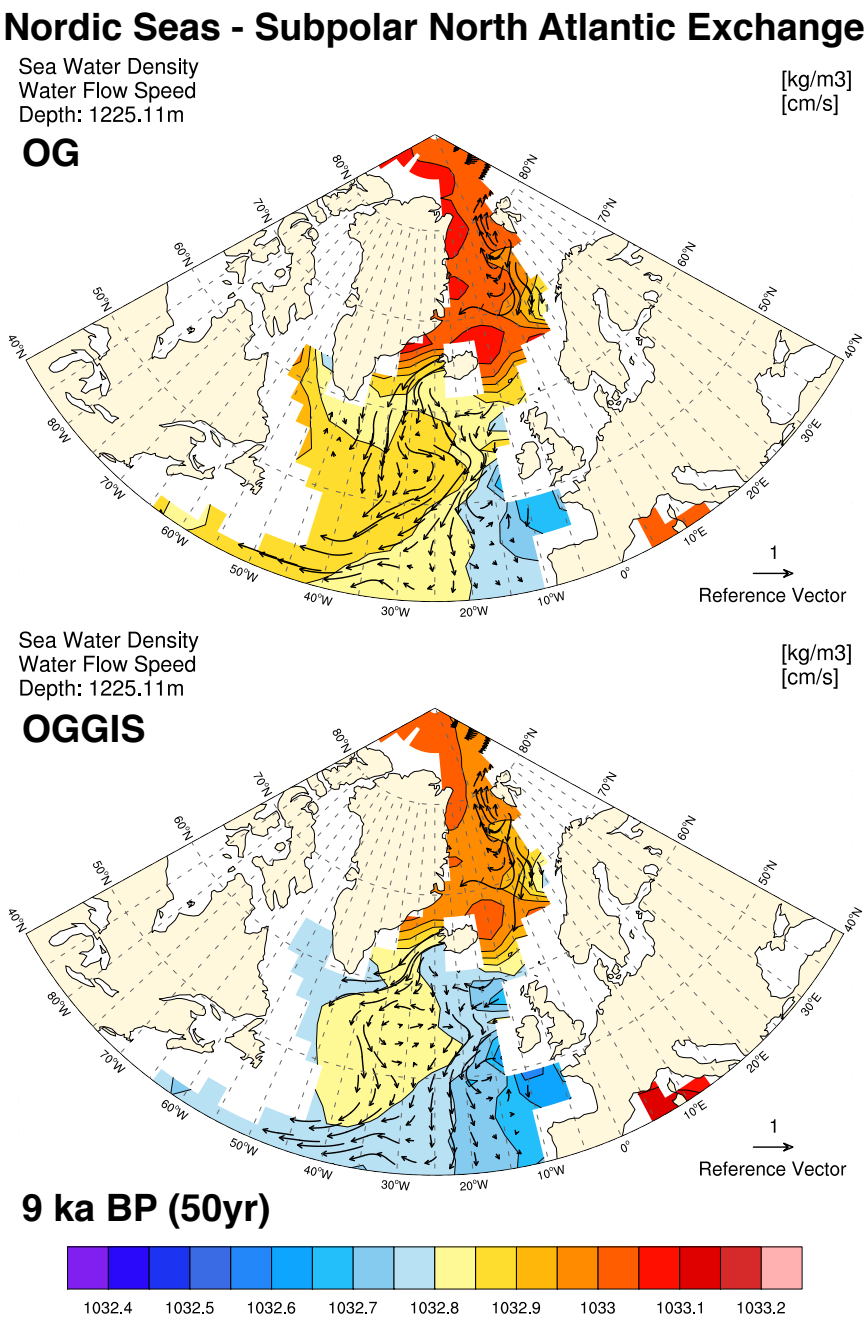

Figure 4.6: Simulated exchange between the Nordic Seas and the Subpolar North Atlantic at 1225 m depth at 9k BP. Shown are 50 yr averages of sea water density (kgm^{-3}, filled contours) and water flow speeds (vectors) in the North Atlantic at the 1225 m depth level of our model for simulations OG and OGGIS.

this further we show in Fig. 4.7 the deep water flow across the Fram Strait, the Denmark Strait and ISR. First, we find only small changes in OGGIS compared to OG of deep water exchange between the Arctic and Nordic Seas, confirming that the Arctic Ocean is not a source or a sink of NS deep water. Second, we find a stronger overflow in OGGIS compared to OG before 7 kyr BP in the Denmark Strait. ISOW flow is slightly reduced before 7 kyr BP, followed by an increasing long-term trend towards present-day. Contrary to present-day observations, ISOW is weaker than DSOW in our model. This difference arises from the simplification of the bathymetry in our model and from the fact that a flux increases further away from the sill as more water is entrained. Nevertheless, the results indicate that in the early Holocene, the deep water flow is redirected and increased towards the Denmark Strait. The early Holocene increase is potentially linked to lower densities in the western North Atlantic (Fig. 4.6) compared to the eastern North Atlantic, therefore reinforcing the flow by a steeper density gradient.

The combined deep water production of the North Atlantic results into an export of deep waters towards the Southern Hemisphere. At present the observed overflow waters across the GSR contribute about 40 % (7.9 Sv, Smethie et al., 2013) of the deep waters to the total NADW (19.6±2 Sv, Smethie et al., 2013). In Fig. 4.8 we show the strength of the bottom cell in the Atlantic at 20°S over the Holocene, representing either the northward AABW or the southward NADW. The export of NADW follows closely the maximum strength of the AMOC, which follows closely the prescribed melt water forcing and gives a weak but steady increase towards present-day. The AABW flow strength shows in general much less variations, and during the enhanced melting phase of the Northern Hemisphere ice sheets, a decreased northward flow (up to -0.9 Sv in OGGIS compared to OG), in agreement with reduced export of NADW. However the long-term trend of AABW in OGGIS seems to suggest a maximum at about 6 kyr BP with a continuous decrease

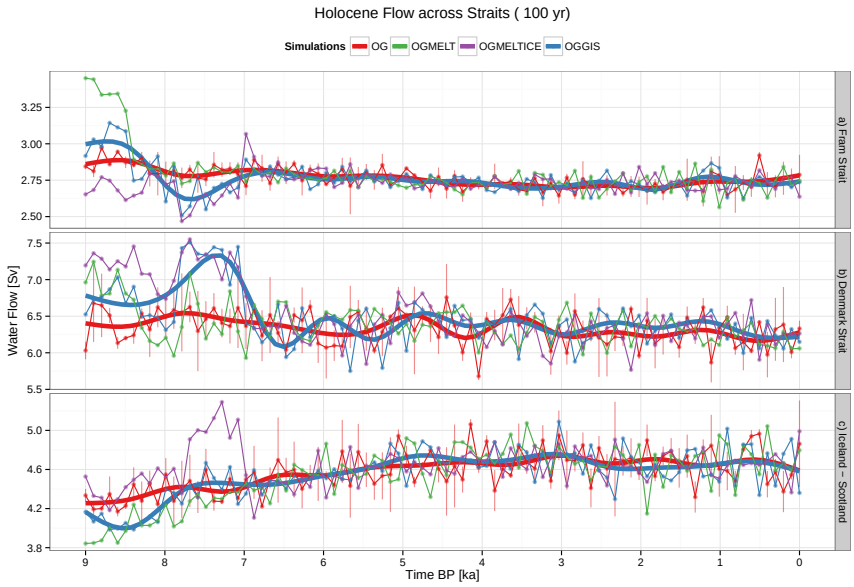

Figure 4.7: Modelled flow across the major pathways in the North Atlantic, the Fram Strait, the Denmark Strait and the Iceland-Scotland Ridge. Shown are 100 yr averages of bottom current strength in Sv for four simulations (OG, OGMELT, OGMELTICE and OGGIS). Thick lines represent smoothed values (n=9) and red bars indicate the standard deviation of simulation OG.

towards present-day (-5.2 mSv/kyr) as opposed to the long-term increasing trend in NADW (+10.9 mSv/kyr). However, it should be noted that the changes in AABW strength are relatively small (within 1 Sv).

4.4 Discussion: comparison to proxy-based reconstructions

We would like to introduce the proxy-based reconstructions used in this study first and describe in short what the corresponding authors have found, and then continue with a discussion of our model results in context of these proxy-based reconstructions to answer our questions from the introduction: What are the contributions of different convection

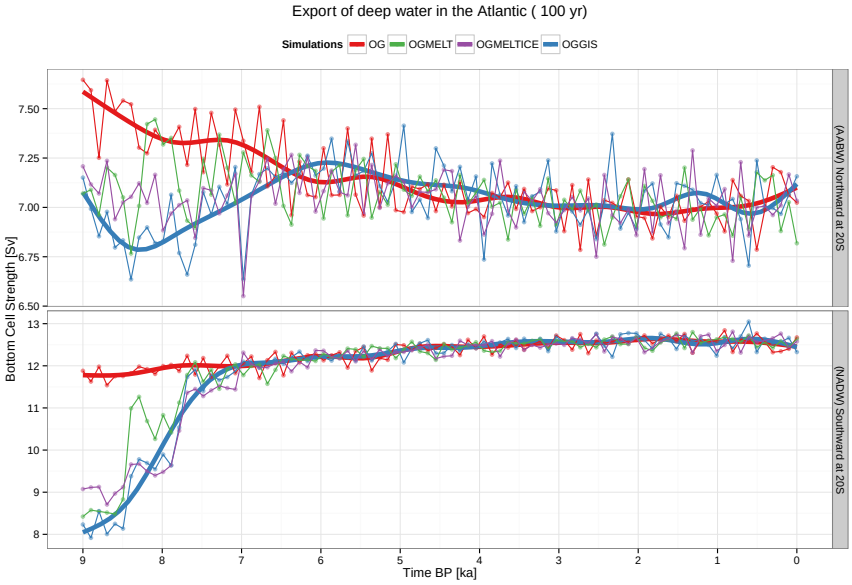

Figure 4.8: Export and Import of deep waters in the North Atlantic in our model. Shown are 100 yr averages of the maximum (minimum) of the meridional stream function of the bottom cell at 20°S in Sv indicating the northward flow of AABW (max) and the southward flow of NADW (min). Thick lines show the smoothed long-term trends (n=9) for simulations OG and OGGIS.

areas to overflow waters and to the simulated AMOC strength? And to what extent are these model results for the AMOC consistent with proxy-based reconstructions available? Can we explain differences between proxies and model results and potentially uncover biases?

4.4.1 Proxy-based reconstructions over the Holocene

The large number of reconstruction studies that have been published over the past few years, have improved our understanding of deep water circulation in the North Atlantic (Hoogakker et al., 2011; Kissel et al., 2013; Thornalley et al., 2013). The combined interest is to extend the limited time-period covered by observations of a major part of the climate system, the AMOC. In our study we focus on a set of SS-based

reconstructions from Praetorius et al. (2008), Hoogakker et al. (2011), Kissel et al. (2013) and Thornalley et al. (2013), reconstructions based on magnetic properties from Kissel et al. (2013) as well as δ^{13}C from Sarnthein et al. (2003), Oppo et al. (2003), Praetorius et al. (2008) and Kissel et al. (2013) to compare to our model results over the past 9000 yrs. The locations are shown in Fig. 4.9 and additional information on the exact locations is presented in Tab. 4.2, as well as information on the mean temporal resolution of the data. The time series are presented in Fig. 4.10, grouped together by type (δ^{13}C , SS, κ). For individual time series and other details we refer to the corresponding original papers and the supplementary Fig. SI.A.1 on page 184.

In the following we summarize key aspects of each reconstruction, as each location has some oceanographic factors that are relevant to its interpretation.

Shackleton et al. (2000) - Iberian Margin
The authors present a δ^{13}C record measured in benthic foraminifera derived from a core from the Iberian margin (Fig. 4.9, MD95-2042, 3146m). Unfortunately the Holocene part of this record was not studied in much detail in the presented study, because the focus of that study was on phase relation between Northern and Southern Hemisphere climate change. Their results show for the Holocene an early increase of δ^{13}C values until 7 kyr BP, followed by a strong decrease until 5 kyr BP, a subsequent recovery by 4.5 kyr BP and a weak decrease towards present-day. The interpretation of these variations during the Holocene are likely to be similar to results from Oppo et al. (2003) (see below), that show a similar decrease at about 5 kyr BP.

Sarnthein et al. (2003) - Western continental margin of the Barents Sea
Sarnthein et al. (2003) present a δ^{13}C record from benthic foraminifera from the Western continental margin of the Barents Sea (GIK23258-2 at 1768m depth), near the present-day Nordic Seas convection area. The interpretation of their results indicate that the AMOC during the

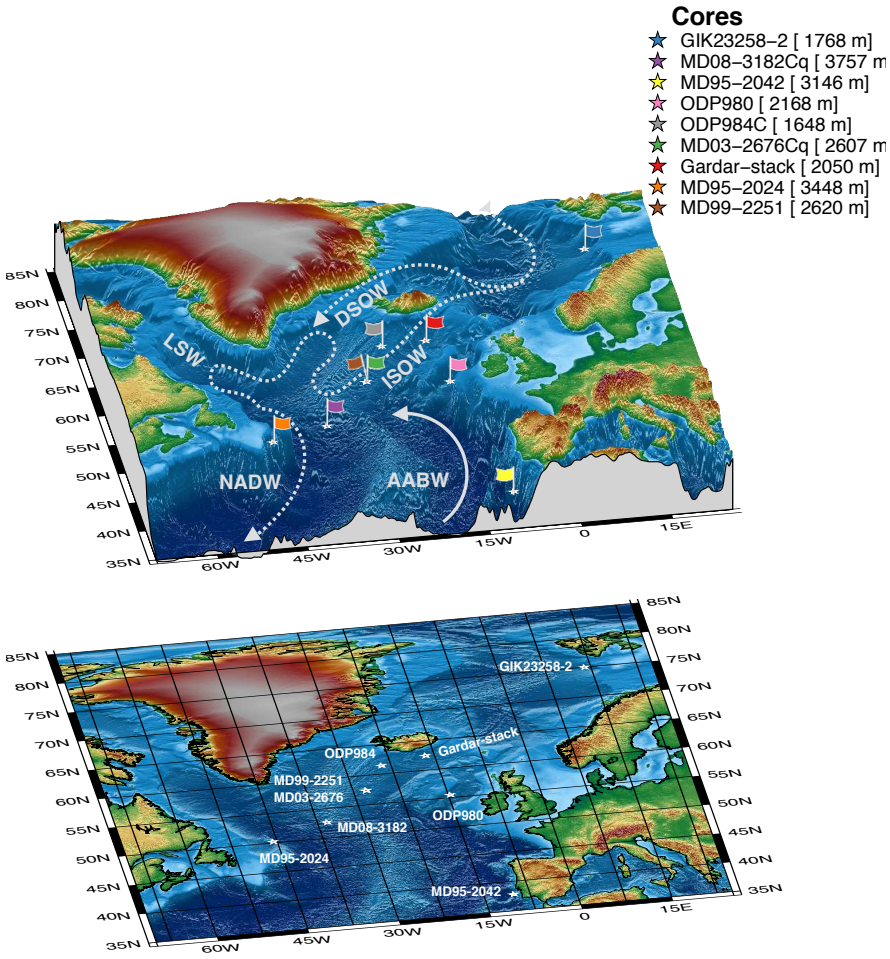

Figure 4.9: Map of proxy core locations and schematic depiction of the bottom-current locations, relevant for this area.

Holocene was much more stable compared to glacial times, hence the relatively stable δ^{13}C values of 1.21 $\pm$0.09 ‰

Oppo et al. (2003) - Feni Drift

Oppo et al. (2003) published a δ^{13}C record from benthic foraminifera from the ODP Site 980 at Feni Drift (Fig. 4.9, ODP980, 2179m). The record shows increasing values (1.2‰) until 7 kyr BP, followed by long-term fluctuations with two minima at about 5 kyr and 2.8 kyr BP. The location of this core allows to monitor the influence of NADW versus Southern originating waters, such as Lower Deep Water (LDW) or

Antarctic Bottom Water (AABW), therefore showing times of enhanced or reduced NADW production. The authors conclude that strong variations (mostly a decrease) of NADW (at about 5 kyr BP) can occur without the interference of large ice sheets, therefore NADW seems to be more sensitive to larger changes than has been previously anticipated in interglacials.

Praetorius et al. (2008) - Gardar Drift

The authors present the core of the Ocean Drilling Program Site 984 (Fig. 4.9, ODP984, 1648m), with reconstructions based on both δ^{13}C and sortable silt. The location allows reconstructing ISOW at a certain depth. The authors find that during the Holocene variations in the current strength (SS) are observed without corresponding variations in the source water (δ^{13}C). For example the record shows a rise of δ^{13}C from 10 to 5 kyr BP, a subsequent drop until 3 kyr BP followed by higher values again by 1 kyr BP. The corresponding SS record shows hardly any variations but a weak long-term increasing trend. This indicates that δ^{13}C values are not always associated with changes in the current strength, thus according to these authors it is important to pair both proxies for an integrated view of the dynamics of the overturning circulation (Praetorius et al., 2008).

Hoogakker et al. (2011) - Orphan Knoll and Gardar Drift

Hoogakker et al. (2011) present two high-resolution sortable silt records from the Gardar Drift (2620m) and the Orphan Knoll (3448m; Fig. 4.9, named MD99-2251 and MD95-2024) sites. The flow speeds near the Gardar Drift site are likely to represent changes in the ISOW at a certain depth and give a long-term decreasing trend towards the present. Kissel et al. (2013) have raised some doubts about the reliability of the results from MD99-2251, due to influences from the coring process. However, flow speeds at the Orphan Knoll represent the deepest North Atlantic water-mass and describe the characteristics of a kind of final NADW mass, after ISOW, DSOW and LSW have been incorporated. Still, there are potentially more water masses that can influence flow speeds at that

location such as the Lower Deep Water (LDW), Antarctic Bottom Water (AABW) and Subpolar Mode Water (SPMW). The long-term trend at the Orphan Knoll is weak, but increasing over the past 10,000 yrs.

Kissel et al. (2013) - Charlie-Gibbs Fracture Zone (CGFZ) and Gardar Drift

This study introduces a new and updated (compared to Kissel et al., 2009) reconstruction based on magnetic property records at the Gardar Drift (2607m) and at the CGFZ (3757m), where the ISOW flow westwards. The core at the Gardar Drift is in close proximity of Hoogakker et al. (2011)'s core MD99-2251, allowing a close comparison between SS and the reconstructed κ. The second core lies further south at the CGFZ, providing sortable silt, κ and δ^{13}C. The combination of all three proxies from one core is a good anchor in the comparison towards each other. The record at the Gardar Drift, representing ISOW current strength, shows higher values in the early Holocene, with a minimum at 8.2 kyr BP, followed by a new maximum at 6.5 kyr BP and a subsequent decrease towards present. The second core further south shows similar trends in magnetic properties, but reconstructed values of SS differ especially in the earliest part of the Holocene. The δ^{13}C values are lower in the early Holocene and remain relatively constant after 7 kyr BP. The core near the CGFZ is likely to show not only ISOW influences, but some impacts from other water masses such as LDW as well (McCartney, 1992; LeBel et al., 2008; Kissel et al., 2013). The polynomial fit is different between the original paper (n=5) and the data presented here (n=13).

Thornalley et al. (2013) - Gardar Drift

Thornalley et al. (2013) introduce a new reconstruction based on sortable silt from multiple cores at different depth along the main axis of the ISOW over the past 9,000 yrs (Fig. 4.9, named by us as Gardar-stack). In total 13 cores (in a depth range of 1200-2400m, including the Praetorius et al., 2008 data) have been used to reconstruct the strength of the ISOW. The multi-core setup allows the reconstruction to account for

Core	Investigator	Parameter	Location	Depth	Temporal Res.
Gardar-Stack	Thornalley et al. (2013)	Mean SS	Gardar Drift	1200 - 2400m	1000 yr (bins)
MD99-2251	Hoogakker et al. (2011)	SS	Gardar Drift	2620m	13 ± 5 yr
MD95-2024	Hoogakker et al. (2011)	SS	Orphan Knoll	3448m	50 ±15 yr
ODP984	Praetorius et al. (2008)	SS, δ^{13}C	Gardar Drift	1648m	770 ±680 yr 380 ±440 yr
MD08-3182Cq	Kissel et al. (2013)	SS, κ δ^{13}C	CGFZ	3757m	50 ±90 yr 40 ±70 yr 40 ±25 yr
MD03-2767Cq	Kissel et al. (2013)	Mag. Sus.	Gardar Drift	2607m	25 ±10 yr
GIK23258-2	Sarnthein et al. (2003)	δ^{13}C	W. Barent Shelf	1768m	60 ±60 yr
ODP980	Oppo et al. (2003)	δ^{13}C	Feni Drift	2179m	80 ±50 yr
MD95-2042	Shackleton et al. (2000)	δ^{13}C	Iberian Margin	3146m	710 ±300 yr

Table 4.2: Summary of proxy-based reconstruction studies and their core information as displayed in Fig. 4.9. The temporal resolution is given as means and standard deviation from the spacing between points.

the vertical migration of the main axis of the ISOW. The authors have shown that their reconstructed overflow strength from SS corresponds well with winter convection layer depth in the Nordic Seas modelled by Blaschek and Renssen (2013a), employing the very same model as this study. The concept behind is that denser waters, as indicated by a deeper mixed layer depth, will overflow faster across the ISR and will be recorded by SS after the sill. The SS-based reconstruction reveals a maximum ISOW strength at 7 kyr BP with a subsequent decrease towards present-day.

We conclude that in all records some impacts have been found that relate to their specific location and can influence the reconstructed values on different time-scales. However, what these impacts are and how these have evolved over time, is uncertain. Our interest in the present study is on long-term trends, such as millennial changes in the AMOC strength. When we compare δ^{13}C and SS records in Fig. 4.10, we can see that some long-term trends agree with our simulation results and some disagree. We propose to look at the three proxies separately first,before we continue with the combined discussion in Section 4.4.2.

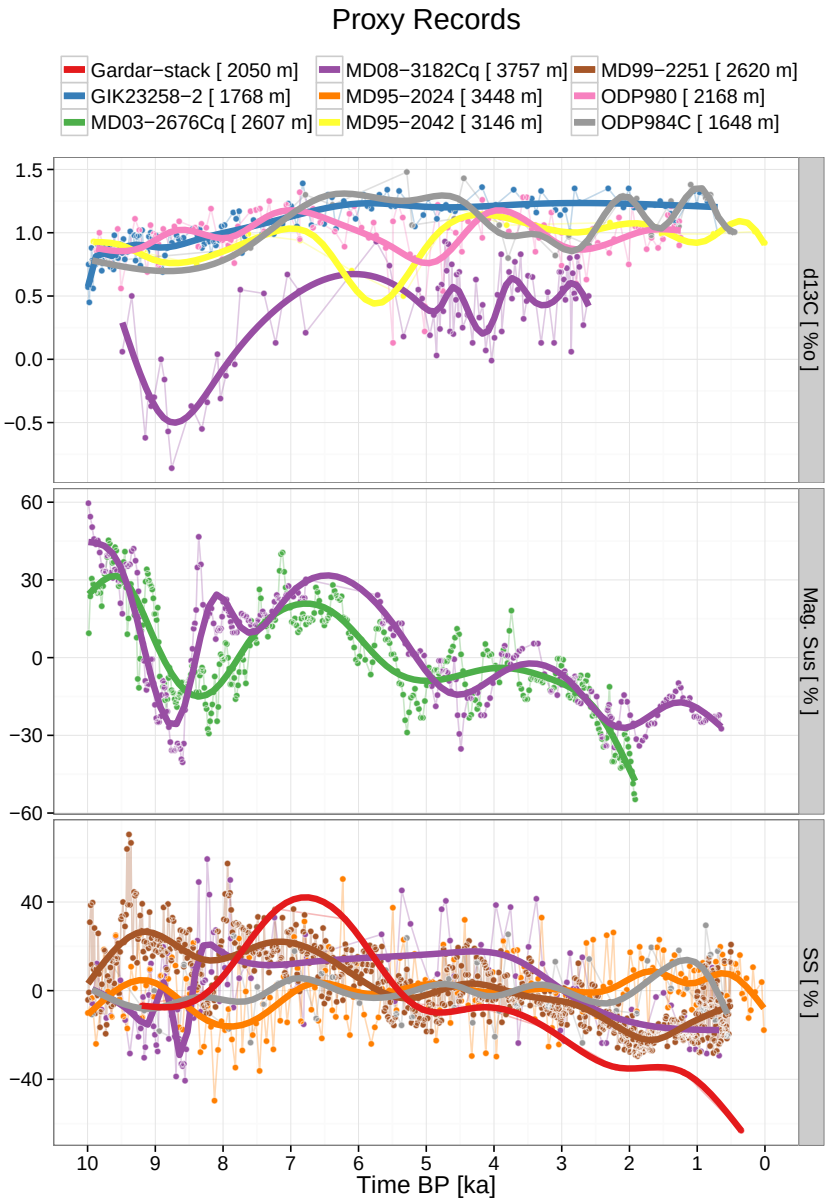

Figure 4.10: Proxy Records (Caption on next Page)

Figure 4.10: Holocene proxy-records δ^{13}C , Magnetic Susceptibility (κ) and Sortable Silt (SS) from the 9 different locations shown in Fig. 4.9. The upper panel shows δ^{13}C values for GIK23258-2 (Sarnthein et al., 2003), MD95-2042 (Shackleton et al., 2000), ODP980 (Oppo et al., 2003) and ODP984 (Praetorius et al., 2008). The middle panel shows normalized κ records for MD03-2676Cq and MD08-3182Cq (Kissel et al., 2013). The lower panel shows normalized SS records for Gardar-stack (Thornalley et al., 2013), MD95-2024 and MD99-2251 (Hoogakker et al., 2011) and ODP984 (Oppo et al., 2003). Thick lines denote smoothed splines (n=9 or n=13) to give longer term trends. The normalized values are divided by their corresponding range. For absolute values we refer to the supplementary information A on page 183.

4.4.1.1 Reconstructions based on Carbon 13

From 10 to 7 kyr BP the δ^{13}C records of the various locations share a relatively similar upward trend that originates from numerous feedbacks such as less vegetation, a cooler and saltier ocean, ocean circulation and changes in the calcification budget of the ocean on glacial to interglacial time scales (Broecker and Peng, 1986; Köhler et al., 2005; Jansen et al., 2007). Lower values are in general found during glacial times, rising to higher values during interglacials. At about 7 kyr BP the cores to the eastern North Atlantic (MD95-2042, ODP980) show lower values and higher variability compared to the one core near the western Barent Sea margin, in the Norwegian Sea. This difference has been discussed by Hoogakker et al. (2011) and they propose that this difference emerges due to an increase of LDW volume (low δ^{13}C values originating from AABW) and the onset of deep eastward advection of LSW, as the Labrador Sea convection started at about 7 kyr BP (Hillaire-Marcel et al., 2001). Oppo et al. (2003) interpreted δ^{13}C fluctuations on millennial timescales in core ODP980 as an indicator of northern vs. southern deep water influence, arguing as well that a strong reduction in δ^{13}C must be the result of mixing with a depleted δ^{13}C water mass such as LDW originating from AABW. Oppo et al. (2003) have argued that

it is likely that these variations in δ^{13}C are originating from a Southern source rather than a Northern source. In the Norwegian Sea (GIK23258-2) the reconstructed δ^{13}C values are relative constant for the rest of the Holocene, with minor variations, thus indicating that a continuous supply of deep water must have reached the site. The core MD08-3183Cq near the CGFZ shows overall lower values in the early Holocene, particularly at about 8.8 kyr BP, followed by relative constant values from 7 kyr BP towards present. The offset compared to the other reconstructions can potentially indicate the mixing of LDW and ISOW.

In summary, the δ^{13}C records from different locations in the North Atlantic show an early Holocene increase and from 7 kyr BP onwards higher variability in the sub-polar North Atlantic compared to the Nordic Seas. This indicates weaker vertical mixing or convective activity in the early phase and evenly strong activity towards the present with influences from AABW at the core locations South of Iceland impacting the recorded signal there. The early Holocene phase is, however, potentially impacted by the glacial to interglacial differences and not only by changes in the ocean circulation.

4.4.1.2 Reconstructions based on Sortable Silt

The long-term trends in the SS-based reconstructions from different sites do not exhibit a common trend, but some of the reconstructions agree with each other. Therefore we have to make a distinction based on their location. In our comparison, four out of five sites are from the area South of Iceland at the Gardar Drift (MD99-2251, ODP984, Gardar-stack) and at CGFZ (MD03-3182Cq) and one is from the Orphan Knoll site near the Labrador Sea (MD95-2024). The latter one is thus representing a "down-stream" water mass, including ISOW, DSOW, LDW and LSW. Four of the SS-based reconstructions are created from a single core and one uses multiple cores at different depth (Gardar-stack). The advantage of a multi-core reconstruction is that a potential migration of the

main flow can be considered and an overall strength can be calculated by weighting normalised sortable silt by its depth (Thornalley et al., 2013). Thornalley et al. (2013) have reported that the core of the ISOW was shallower (∼1400m) in the early Holocene, deepest at about 5 kyr BP (∼2200m) and again becoming shallower (∼1800m) towards the present-day. This suggests that the interpretation of long-term trends in a single core should consider its depth and position. In Fig. 4.10 we present normalised SS records (divided by their range) that are comparable to each other. Regardless of their actual position, we find that there are different long-term trends in all reconstructions. The Gardar-stack shows weaker values in the early Holocene followed by a maximum around 7 kyr BP and a decrease towards present-day. The Labrador Sea core (MD95-2024) gives a weak but variable increase towards present-day. MD99-2251 gives a steady but variable decrease towards present-day, similar to the decrease in MD08-3182Cq from 8 kyr BP towards present and ODP984 exhibits hardly any long-term trend. Despite the relatively coarse temporal resolution (∼1000 yr) of the Gardar-stack, the long-term decrease after 7 kyr BP agrees with a decrease in MD99-2251 and MD08-3182Cq, but before 7 kyr BP only MD08-3182Cq and the Gardar-stack agree.

4.4.1.3 Reconstructions based on Magnetic Susceptibility

The two reconstructions from a core at the Gardar Drift (MD03-2676Cq) and a core near the CGFZ (MD08-3182Cq) show remarkably similar long-term evolutions (Fig. 4.10). Both records show an early Holocene decrease with a local minimum at about 8.5 kyr BP followed by an intermediate maximum between 7 and 6 kyr BP and a subsequent decrease towards present-day. The core at the Gardar Drift is in close proximity to the SS record of core MD99-2251 and indicates similar variability and long-term trends. The Gardar-stack SS record agrees even closer to the κ from MD03-2676Cq from 8.5 kyr BP towards present. Thus,

supporting the reconstruction of deep water flow from both proxies, SS and κ.

In summary, the strength of the deep ocean circulation during the Holocene is not clear from all the reconstructions we looked at. Most of the δ^{13}C records seem to agree to some extent that the overturning strength increased from the early Holocene to present-day, whereas the sortable silt records South of Iceland seem to show that the ISOW strength decreased over the Holocene and the strength of deep water flow increased in the Labrador Sea over the Holocene. The κ-based reconstruction agrees relatively well with some of the SS-based reconstructions, supporting the early Holocene decrease, a maximum at about 7-6 kyr BP and the long-term decrease in ISOW strength. The question is if and how these results can be actually reconciled. Our model results might be helpful to answer this question.

4.4.2 Discussion of model results and proxy-based reconstructions

The goal of this study is to get a better understanding of Holocene changes of the North Atlantic ocean circulation and compare model results to reconstructions from proxies. We have introduced reconstructions based on δ^{13}C, SS and κ records from the subpolar North Atlantic and the Nordic Seas in Section 4.4.1 (Fig. 4.10) and have shown results from four transient model simulations in Section 4.3. In this section we discuss modelled and reconstructed deep water circulation.

Carbon Isotopes

From the δ^{13}C-based reconstructions we might conclude that there is an early part, where all records presented give increasing values until about 7 kyr BP, when different signals start to emerge. In our first attempt we compare these reconstructions with the stream function of the AMOC to represent the volume transport on a large scale. Indeed there are some similarities, a relatively weak early part followed by a relatively

stable part, with higher values until present. However cores MD95-2042 (Iberian Margin) and ODP980 (Feni Drift), which are located in the eastern North Atlantic, seem to show much higher variability within the last 7,000 yrs than the core in the Norwegian Sea (GIK23258-2). It has been argued by the authors of these reconstruction studies that the δ^{13}C values are likely to have been affected by the supply of LDW, originating from AABW, which is particularly low in carbon isotopes. This is potentially also visible in the overall lower δ^{13}C values from core MD08-3182Cq (3757m), which shows a strong minimum at 8.8 kyr BP and some variations 6 and 4 kyr BP, similar to cores in the eastern North Atlantic. Thus, strong variations in δ^{13}C could indicate the balance between LDW and ISOW and as we showed in Fig. 4.8 the strength of the simulated AABW flux shows some small changes (0.9 Sv) and gives a maximum at around 6 kyr BP. Therefore our model results seem consistent with the δ^{13}C records, with variability induced by the supply of deep waters from the Southern Hemisphere. Therefore, a site that is not influenced by these impacts from the Southern Hemisphere could correspond better to the strength of the AMOC in our model. For this, we could use core GIK23258-8 from the shelf of the Western Barent Sea. Indeed there seems to be a better correspondence between simulated AMOC strength (as in Fig. 4.2a) and δ^{13}C of the benthic foraminifera from this core. The question remains, however, why the magnitude of the early decrease in AMOC strength is not that well recorded at this site, as changes in the modelled AMOC strength are stronger and would suggest stronger impacts in δ^{13}C as well. However, from our analysis of the convection areas (Fig. 4.3), it has become clear that the NS site is not shutdown, but its ventilation depth is reduced in the early Holocene (Fig. 4.4c), which is potentially still sufficient to supply enough ^{13}C to the bottom. Therefore, changes that are to be recorded in δ^{13}C have to affect the supply of deep waters, or the magnitude of changes to the overall AMOC strength is underestimated. However, the long-term downward trend in convective volume from NS is as well not recorded in GIK23258-8, because the signal is probably too weak to show up in this

ventilation proxy. Thus, it can be concluded that the site is a good indicator of NS convection, but changes in the strength of the AMOC are only represented when the NS convection area is affected, showing potentially strong variations when it is shut down or restarted. Variations in δ^{13}C in the subpolar NA are likely to be influenced by AABW supply, but it cannot be said with certainty from a comparison to our model results. Changes in the total solar irradiance (TSI) or volcanic eruptions or other potentially unknown changes are not included in our simulations, which might be responsible for stronger variations in these proxies (Oppo et al., 2003; Praetorius et al., 2008) or the AMOC strength.

Sortable Silt

The SS-based reconstructions at different core locations in the subpolar North Atlantic, give different long-term trends that are influenced by their location and their depth. For the reconstructions near the Gardar Drift (MD99-2251, ODP984, Gardar-stack) we find that the long-term trends vary substantially between the reconstructions. It has been noted by Thornalley et al. (2013) that single core reconstructions have a potential weakness, as the position of the main flow axis can migrate with depth, potentially creating a signal that is not necessarily related to changes in flow speed. However, long-term trends in SS hardly compare to the evolution of the AMOC strength in our model (Fig. 4.2). A closer match was found between, on the one hand, simulated changes in mixed layer depth or convective volume in the NS (Fig. 4.4c), and on the other hand the reconstructed SS-based overflow evolution at the Gardar Drift from the Gardar-stack. This suggests that a link between deep water production, its water mass properties and the recorded SS South of Iceland exists. Therefore, when convection is shallower, less dense waters are produced and exported via the ISR and result in less deep water flow, leading to a maximum of SS that is recorded in a shallower core. The ISOW is influenced by the actual depth of convection in the NS, but also by the density structure of the subpolar North Atlantic (Thornalley et al., 2013), which will influence how deep overflowing waters will

sink and mix. Thus, it is important to know what the density difference between the subpolar North Atlantic and the Nordic Seas was during theHolocene. Our analysis shows that the density difference (Fig. 4.5) increased before 7 kyr BP in a simulation including remnant ice sheet melt waters (OGGIS) compared to a simulation including only orbital and greenhouse gases (OG). From Fig. 4.6 it is clear that the density in OGGIS decreased compared to OG all over the North Atlantic at that depth and most likely in the whole water column as well due to ice sheet melting. During this early phase, the potential for overflow waters was actually increased and in Fig. 4.7, we find that the modelled DSOW strength is increased, whereas the ISOW strength is decreased. Our model shows higher DSOW strength at present-day compared to recent observations (Smethie et al., 2013), which might indicate an unsuited comparison of reconstructed and modelled deep water flow strength at a site influenced by either DSOW or ISOW. A potential source of this bias could be the simplified bathymetry in the model. However, the origin of these waters is undeniably the NS convection site and changes will be exported either via the Denmark Strait or the ISR. Thornalley et al. (2013) used this argumentation already and more information from the same model does not help to explain these reconstructions better. The relatively low resolution of our model does not allow looking at depth changes along the main axis of the ISOW. Nevertheless, we find that simulated lower flow speeds at the Gardar Drift site (Fig. 4.5b) agree with lower SS-based flow estimates in the early part before 7kyr BP, but modelled long-term trends do not correspond to trends seen in either mean SS or modelled NS convection depth.

Considering all our results presented in this study, we cannot find a consistent explanation for the long-term decreasing trend of SS in MD99-2251 at the Gardar Drift, especially as values at about 9.4 kyr BP are highest. It has been noted by Kissel et al. (2013) that this core might have some perturbation due to the coring process itself, implying that the results may be less reliable. Some of the SS-based reconstructions

have a higher variability compared to the δ^{13}C-based records as well as some other SS records, partly because of a higher temporal resolution (Tab. 4.2). However, the long-term increasing trend in MD95-2024 in the Labrador Sea is consistent with the simulated trend in Labrador Sea convective volume (Fig. 4.4b). The location of the core and its depth (3448 m) would also suggest that there might be a link to the NADW flow (Fig. 4.8b) and its strength over the Holocene. Indeed weak long-term increasing trends can be found in both simulated NADW strength and SS-based flow speed in the second phase (after 7 kyr BP), in contrast to the early phase. Nevertheless this similarity is rather small.

Magnetic Susceptibility
Reconstructions from the Gardar Drift and the CGFZ indicate similar long-term trends and correspond well with SS-based reconstructions from the Gardar Drift, indicating a close relationship to ISOW. Given this similarity, κ values correspond as well with NS convection depth (Fig. 4.5b), showing an early Holocene low (8.8-8 kyr BP), followed by a maximum (7-6 kyr BP) and a subsequent decrease towards present.

At this point it is unclear whether the mismatch between modelled AMOC strength and reconstructed deep water flow can be attributed to localised effects that are important for the proxy signals, but cannot be resolved by the model, or to a more fundamental problem in the model and its deep water production, flow and overturning. Considering that we employed this model, we think it is appropriate to conclude with a discussion of our model's performance and emphasise the need for higher resolution models to conduct long-term experiments including several different forcings. In a present-day comparison of CMIP5 and EMIC models (Weaver et al., 2012), LOVECLIM produces a maximum of the AMOC flow (23.2 Sv) that is somewhat higher than the majority of the models, while the decrease of the AMOC strength to future warming is comparable to most models used in that study. Unfortunately, there are hardly any comparisons of deep water flow including multiple models, as well as palaeo-modelling studies discussing past deep water

circulation changes in details (besides Thornalley et al., 2013). From present-day observations (Smethie et al., 2013) we know that our model shows weaker ISOW and stronger DSOW and that a comparison to reconstructions depending only on one of these components alone might be impacted by this specific bias. However, we have to emphasise that the agreement between the ISOW strength recorded from SS in the Gardarstack and the convective volume in the NS is still valid, as the source signal is likely to be transported to the location of the reconstruction.

4.5 Conclusions

We have compared four transient simulations over the past 9,000 yrs including early Holocene remnant ice sheet decay to proxy-based reconstructions using δ^{13}C , κ and SS in the North Atlantic. We have in detail tried to reconcile the different long-term trends in the reconstructions with the help of our model results, to gain a better understanding of the AMOC changes of the past 9,000 yrs. In summary our results indicate the following:

- δ^{13}C in the Norwegian Sea allows reconstructing convective activity in the Norwegian Sea. The record shows an increasing trend from the glacial until about 7 kyr BP, followed by relatively stable values towards present-day. However, the actual strength of the deep ocean flow is not recorded, and only stronger changes that affect the supply of deep water can alter the recorded δ^{13}C signal.
- δ^{13}C in the subpolar North Atlantic is influenced by ^{13}C-depleted waters originating from AABW, leading to low values at North Atlantic sites. Our investigation partly supports the idea that long-term variations seen in δ^{13}C -values are likely to be caused by the influence of AABW in the deep North Atlantic. However, the corresponding variations in AABW advances and retreats are

weak in the model and give therefore only an indication of these dynamics.

- We find a good agreement between depth-weighted SS and κ at the Gardar Drift with simulated Nordic Seas normalized convective volume, suggesting a direct link between ISOW and NS convection activity. The combined results suggest weaker ISOW at 9 kyr BP, followed by a maximum at about 7-6 kyr BP and a subsequent decrease towards present-day.

We can conclude from this comparison that localized changes recorded in proxy-based reconstructions are difficult to assess in a relatively low-resolution model like LOVECLIM, because most local features that might be important are likely to be missing. It is uncertain if using higher spatial resolutions would resolve this discrepancy, because local impacts can be defined from narrow changes in bathymetry in the real ocean that will be under represented in even the highest resolved model. However, in terms of the origin of deep water and dynamical water mass properties, the model showed promising results in agreement with highly complex SS reconstructions at the Gardar Drift. Considering the long-term evolution of the AMOC, we have shown that despite the early Holocene melt water-induced reduction, the long-term trend is relatively stable, contrary to trends from reconstructed subcomponents, thus suggesting either a balancing mechanism or a localization of reconstructed values.

Chapter 5

The influence of Greenland Ice sheet melting on the Atlantic meridional overturning circulation during past and future warm periods: a model study

Based on: Blaschek, M., Bakker, P., and Renssen, H.: The influence of Greenland ice sheet melting on the Atlantic meridional overturning circulation during past and future warm periods: a model study, Climate Dynamics, pp. 1–21, doi: 10.1007/s00382-014-2279-1, 2014

The sensitivity of the climate system to changes in radiative forcing is crucial for our understanding of past and future climates. Especially important are feedbacks related to melting of ice sheets like the Greenland Ice Sheet (GIS) and its potential impact on the Atlantic meridional overturning circulation (AMOC). These effects are likely to delay and dampen predicted long-term warming trends. Estimates of climate sensitivity may be deduced from palaeoclimate-reconstructions, but this raises the question whether past climate sensitivity is

applicable to the future. Therefore we have analysed the impact of GIS melt water on the AMOC strength in two past warm climates (Last Interglacial and early Present Interglacial) and three future scenarios with three different model parameter sets. These model parameter sets represent three different model sensitivities to freshwater perturbation: low, moderate and high. In both the moderate and high sensitivity versions, we find for lower GIS melt rates (below 54 mSv, Sv = 10^6 m^3/s) a clear difference between past and future warm climates in the sensitivity of the AMOC to GIS melt. This difference is connected to the convective activity in the Labrador Sea and the amount of additional surface freshening by sea ice melting. In contrast, for higher GIS melt rates (over 54 mSv) we find similar reductions of the AMOC strength in all cases. Considering the low sensitivity version of our model, we find that for all GIS melt rates the influence of freshwater forcing on the AMOC is independent of the background climate. Our results and implications are thus strongly determined by the parameter set considered in our model. Nonetheless, our results from two out of three model versions suggest that proxy-based reconstructions of past AMOC sensitivity to GIS melt are likely to be misleading if interpreted for future applications.

5.1 Introduction

It is fundamental to know the climate system response to changes in radiative forcing in order to understand future climate change. This response involves different feedbacks and recent studies (Roe, 2009; Köhler et al., 2010; Lunt et al., 2010; Palaeosens Project Members et al., 2012; Zeebe, 2013) emphasize the importance of so-called slow feedbacks, involving changes in ice sheets, vegetation, ocean circulation and biogeochemical cycles, to have a considerable effect on long-term climate sensitivity and result in a prolonged warming in simulations forced by future emission scenarios. One such feedback is related to the melting of

the Greenland Ice Sheet (GIS) and its potential to weaken the Atlantic Ocean circulation strength. However, the impact of this slow feedback has until now hardly been taken into account in the IPCC AR4 ensemble projections of future climate change, with the exception of IPSLCM4 (Swingedouw et al., 2006, 2007; Schneider et al., 2007). Therefore, in this paper we study the impact of GIS melt on the behaviour of the Atlantic Meridional Overturning Circulation (AMOC) under warm past and future climate conditions.

The AMOC is part of the global ocean circulation and transports heat in the near-surface layer from the Tropics to the Northern Hemisphere mid- and high-latitudes. Today the northward heat transport of 1.33±0.4 PW at 26°N (Johns et al., 2011) in this current system contributes to a relatively warm Northern Hemisphere climate, in particular over Europe. This oceanic heat transport is dominated by the AMOC (88% or 1.18 PW, Johns et al., 2011), that transforms northward moving relatively saline waters into North Atlantic Deep Water (NADW) and returns these waters southward in the deep ocean. Convection of waters from the surface to the deep ocean is largely determined by the heat exchange between ocean and atmosphere that is in turn sensitive to a stratification of the ocean surface and to the insulation effect of sea ice (Ganopolski and Rahmstorf, 2001; Kuhlbrodt et al., 2007). In the North Atlantic basin there are at present three main regions where deep water formation occurs, in the Nordic Seas, Labrador Seas (e.g. Marshall and Schott, 1999) and the Irminger Sea (Pickart et al., 2003).

Climate model simulations indicate that a projected temperature rise of up to 4.4 K by 2100 AD outlined by the IPCC AR4 (scenario A1B) is accompanied by more precipitation (globally 1 to 6% more, Meehl et al., 2007) over the North Atlantic, higher river inflow as well as increased melt water discharge from the GIS (3 to 24 mSv until 2100 AD, Meehl et al., 2007). The expected increases in sea surface temperatures and precipitation over convection areas will lower sea surface density, and is expected to weaken deep convection, and thereby potentially decreasing

the AMOC strength by 25% at the end of this century (Schmittner et al., 2005; Meehl et al., 2007). The northward meridional heat transport is likely to follow this trend, unless it is compensated by a strengthened baroclinic gyre circulation as found by Drijfhout and Hazeleger (2006) in ensemble predictions of the near future. In simulations of the next century, the impact of enhanced melting of the GIS has mostly been neglected in IPCC AR4-type models (Meehl et al., 2007; Srokosz et al., 2012) as well as in the recent update AR5 (CMIP5, Weaver et al., 2012). There are a few exceptions, such as the studies by Fichefet et al. (2003), Swingedouw et al. (2007) or Hu et al. (2011). The latter found that only high GIS melt rates (a total of $\sim$0.3 Sv over 100 yrs) will cause a significant weakening of the AMOC and indicate that AMOC-induced cooling is not likely to overcome greenhouse-induced warming. This confirms a previous result from Ridley et al. (2005), who found a complete retreat of the GIS within 3,000 yrs, but only small long-term effects on the global climate employing a GCM coupled to a dynamical ice sheet model.

All climate model predictions crucially depend on the Earth system's sensitivity of the model under consideration. In climate models, Earth system's sensitivity is not a single tuneable parameter, but the net effect of all included processes and their parameterizations, as well as all internal feedbacks. The AMOC's sensitivity to GIS melt is one part of the Earth system sensitivity and thus relevant for evaluation of future projections. However, large uncertainty remains concerning the AMOC's sensitivity (Stouffer et al., 2006), its stability (Hofmann et al., 2009) and its long-term impact on the Earth system's sensitivity (Meehl et al., 2007; Zeebe, 2013). Studying the relation between the AMOC and GIS melt in the past can help constrain the impact of GIS melt on the climate sensitivity to freshwater perturbations. In a model study of past, present and future AMOC strength and its sensitivity to GIS melting, Swingedouw et al. (2009) reported that the background climate state is important for the AMOC's sensitivity and that the response is

not linear with the freshwater forcing. This has been previously investigated by Ganopolski and Rahmstorf (2001), who found the cooler glacial climate to be more sensitive to freshwater input than the warmer interglacial climate, partly because of the ice-albedo feedback involving sea ice and the position of deep convection sites. Indeed, palaeoclimatological reconstructions provide strong evidence for higher sensitivity of the AMOC under glacial conditions, instabilities (e.g., Bianchi and McCave, 1999; Elliot et al., 2002; Rahmstorf, 2002; Alley, 2007; Srokosz et al., 2012) and abrupt shifts between different modes of operation (Rahmstorf, 2002). An important question is whether climate models are sensitive enough to reproduce such abrupt behaviour (Valdes, 2011). However, abrupt changes in the strength of the AMOC appear largely absent during interglacial periods, with the exception of a number of events during the early deglaciation phases of the interglacials (Alley et al., 1997; Lang et al., 2010; Irval et al., 2012). All the above gives rise to the question whether we can relate past changes in GIS melt and AMOC strength to evaluate future scenarios.

We present a systematic investigation of changes in the AMOC's response in simulations covering different warmer than present-day background climates (Last Interglacial, Present Interglacial, Future) and different GIS melt scenarios (ranging between 0 and 100% GIS mass loss), performed with a coupled global climate model. Indeed, estimates of GIS melt rates during the LIG and PIG (respectively 12.7 mSv at 125 kiloyear before present, hereafter ka BP; van de Berg et al. (2011); up to 26 mSv at 9 ka BP, Peltier, 2004; Blaschek and Renssen, 2013a) suggest that these were within the middle to upper range of what is expected for the future (3 to 24 mSv by 2100 AD, scenario A1B, Meehl et al., 2007). We argue that, with the time dependence of Earth systems sensitivity in mind, our approach enables us to estimate to what extent future AMOC changes are going to be similar to past changes. To take into consideration the importance of the model-dependent AMOC sensitivity to freshwater forcing, we include three different model versions

with different AMOC sensitivities (low, medium and high). In short, our objective is to quantify three different aspects of the AMOC response to GIS melt: 1) characteristics of the warm background climate, related to the corresponding radiative forcing, 2) different magnitudes of GIS melt, and 3) different model sensitivities of the AMOC's response to a melt water perturbation. Investigating these aspects will enable us to assess the underlying question to what extent we can use past warm climates to infer the AMOC's response to future climate warming.

In the following we review the important features of our model (Section 5.2.1) and outline the experimental set-up in Section 5.2.2. In Section 5.2.3 we provide a description of the considered three time periods and the main characteristics of the simulated background climates. Section 5.3 presents the simulated AMOC characteristics, the role of sea-ice feedbacks and the discussion of the results and the context.

5.2 Methods

5.2.1 The Model

We performed experiments with the Earth system model of intermediate complexity (EMIC) LOVECLIM (version 1.2; Goosse et al., 2010). We included the interactive atmospheric, oceanic, sea ice and land surface components, but disabled the dynamical ice sheet model. In our approach GIS melt rates are prescribed and therefore allows a systematic analysis of its impacts as well as a precise control of the forcing, which is harder or even impossible to achieve when using a dynamical ice sheet component in a coupled model set-up. The elevation and extent of the GIS are fixed at present-day conditions, therefore snow and liquid precipitation accumulated on the ice sheet will be drained back to the ocean. Consequently, we do not take into account the negative impact of AMOC weakening on the GIS melt rate or atmospheric

changes due to a diminished ice sheet. It has been previously shown that feedbacks involve changes in sea-ice cover, precipitation patterns and atmospheric circulation (Lunt et al., 2004; Junge et al., 2005; Stone and Lunt, 2013), which affect the GIS itself, but also its surroundings. Lunt et al. (2004) argue that due to the decreased orography and change in albedo, temperatures rise in Greenland and reduce the meridional temperature gradient resulting in a reduced meridional heat transport. Arguably this is not to be neglected. However, Junge et al. (2005) find the atmospheric resolution of a model to be an important criteria of the potential impacts of a lowered GIS. Therefore, it is uncertain whether these effects are competing on the sensitivity of the AMOC to GIS melt or not. Future research including interactive ice sheets could address these uncertainties and their impact on AMOC stability. Here we introduce only key-aspects of the model and refer for more details and a discussion of the performance of LOVECLIM under present-day, past and future forcings to Goosse et al. (2010).

The sea-ice-ocean component of LOVECLIM (CLIO3; Goosse and Fichefet, 1999) is a free-surface ocean general circulation model with a horizontal resolution of 3 x 3 degrees latitude-longitude and 20 vertical levels, coupled to a sea-ice component (Fichefet and Maqueda, 1997, 1999). The atmospheric component (ECBILT; Opsteegh et al., 1998) is a spectral T21, three-level quasi-geostrophic model coupled to a land-surface module that employs a bucket-type hydrological model for soil moisture and runoff. Global cloud cover is prescribed from climatological seasonal means at present-day (Rossow, 1996). As a result of an overestimation of precipitation over the North Atlantic and the Arctic, a fixed precipitation correction (8.5% and 25%) is applied that removes part of this freshwater and repositions it to the North Pacific, where precipitation is underestimated. The dynamical vegetation model is called VECODE (Brovkin et al., 2002) and simulates two plant-functional types, trees and grasses and desert as a dummy type. The climate sensitivity to a doubling of the atmospheric CO_2 concentration is 1.9 K after 1000 yr

(Goosse et al., 2010) in the default version of LOVECLIM (version 1.2; using its standard parameter set). This is just outside the lower end of the range found in global climate models (2.1 to 4.4 K, Meehl et al., 2007). The simulated deep ocean circulation in LOVECLIM compares reasonably well with other model results (Schmittner et al., 2005), with deep convection taking place in both the Nordic Seas and the Labrador Sea (Goosse et al., 2010) and a maximum of the overturning stream function in the North Atlantic at 27°N of 15.6 ±2.2 Sv (compared to observations at similar latitude of 18.7 ±2.1 Sv in Kanzow et al., 2010).

Like any other climate model, LOVECLIM has numerous parameters that can be tuned to represent parameterized processes. Loutre et al. (2011) present different parameter sets for the LOVECLIM model, producing different model versions that span the full range of CO_2 sensitivities as well as cover a broad range of sensitivities of the AMOC to freshwater forcing. Yet, all these model versions produce results for present-day climate that are consistent and within the uncertainty of observations (global mean temperature, AMOC strength, sea-ice extent as in the supplementary of Loutre et al., 2011). In a comparison of model results with recent sea-ice extent decreases, the low sensitivity version was rejected by Goosse et al. (2007), because the sea-ice response was too slow. In this study we consider it as the lower range sensitivity. We use two of their alternative parameter sets that correspond to model versions that are more (high) or less sensitive (low) to freshwater forcing compared to the standard version (medium), but have almost the same CO_2 sensitivity. The corresponding naming in Loutre et al. (2011) is 112 for the less sensitive version and 222 for the more sensitive version. The differences in parameter values compared with the standard parameter set are shown in Table SI.1 and are summarised as follows. There are common differences of the low and the high parameter set compared to the medium, such as a higher sensitivity to greenhouse gases (up to +0.42 K) and a reduced Gent-McWilliams thickness diffusion coefficient,

but also individual differences of each version that mark its characteristics. In the low version a major change is the lower diffusivity of the ocean compared to the medium and the high version, whereas in the high version an important change is a lower precipitation correction in the North Atlantic, resulting in a fresher surface ocean there. A simplified overview of the differences of the parameter sets and the impact on the sensitivity to greenhouse gas changes and sensitivity to freshwater forcing can be found in Fig. SI.B.1 (on page 189) and more information is provided by Loutre et al. (2011).

5.2.2 Experiment Set-up

With the three versions of our model (low, medium and high) we performed quasi-equilibrium simulations for two past warm periods (Last and early Present Interglacial) and three future cases that are based on the 2100 AD values of the so-called Representative Concentration Pathways (RCP3, RCP6 and RCP85 as in Meinshausen et al., 2011), with 9 different GIS melt fluxes for each of these periods. The total number of simulations is thus 135 (3x5x9), with 27 for the Last Interglacial (LIG), 27 for the early Present Interglacial (PIG) and 81 for three future cases. Initial conditions for the snapshot experiments were spun up for 2000 model years to reach quasi-equilibrium conditions in all components of our model to applied forcings (cf. Renssen et al., 2006). The individual simulations have a duration of 500 model years with constant forcings. Although the duration of the simulations should ideally be about 1000 yrs to ensure quasi-equilibrium in all model components, this was not feasible given the computational expense this large number of simulations would require. However, we argue that 500 years of simulation are sufficient to provide a reasonable estimate of equilibrium climate sensitivity. We forced all palaeoclimate simulations with orbital and greenhouse-gas concentrations in line with the PMIP3 protocol (`http://pmip3.lsce.ipsl.fr`). An overview of the simulations and their forcings is presented in Tab. 5.1.

Period	Name	Initial Conditions	Radiative Forcing Anomaly (W/m^{-2})		
			Global Annual	65°N Max	GHG
	PI	Orbital (0 BP), PRE2005 1850 to 1950 AD	0	0,51	0,51
Future	RCP85	PI + RCP85 (2100 AD)	0	0	8,09
	RCP6	PI + RCP6 (2100 AD)	0	0	5,57
	RCP3	PI + RCP3 (2100 AD)	0	0	2,74
Present Interglacial	PIG	Orbital (7 ka BP), Greenhouse Gases from PMIP	0,22	31,98	-0,44
Last Interglacial	LIG	Orbital (128 ka BP), Greenhouse Gases from PMIP	0,8	75,19	-0,06

Table 5.1: Summary of forcings in control and freshwater experiments. Insolation values (Wm^{-2}) are global annual weighted mean radiative forcings and 65°N maxima, calculated from Huybers (2006) daily insolation data. GHG radiative forcing is calculated after IPCC (2001) formulation (reference values for 1750 AD).

The nine GIS melt scenarios consist of one control simulation with fixed orbital and greenhouse gases and eight GIS melt water scenarios that represent the melting of different percentages of the present-day GIS volume (2.911.080 km^3) over a period of 500 yrs. These percentages are: 5, 10, 20, 30, 40, 50, 75 and 100 %. These ice volumes are converted to a melt flux as they are equally distributed over 500 yrs of model simulation, e.g. 5% (145.554 km^3) per 500 yrs $\sim$ 9 mSv. The melt water is added as additional runoff to the existing runoff from Greenland (precipitation and snow melt) that is distributed to the oceans around Greenland as is illustrated in Bakker et al. (2012).

5.2.3 Periods - Background Climate

We chose our different time periods because they all resemble warm periods in the past or potentially in the future and in order to compare them with one another, we focus on the radiative forcing as a measure of how warm a certain climate was or is going to be. Past periods are forced by orbitally-induced insolation changes, but in near-future warm

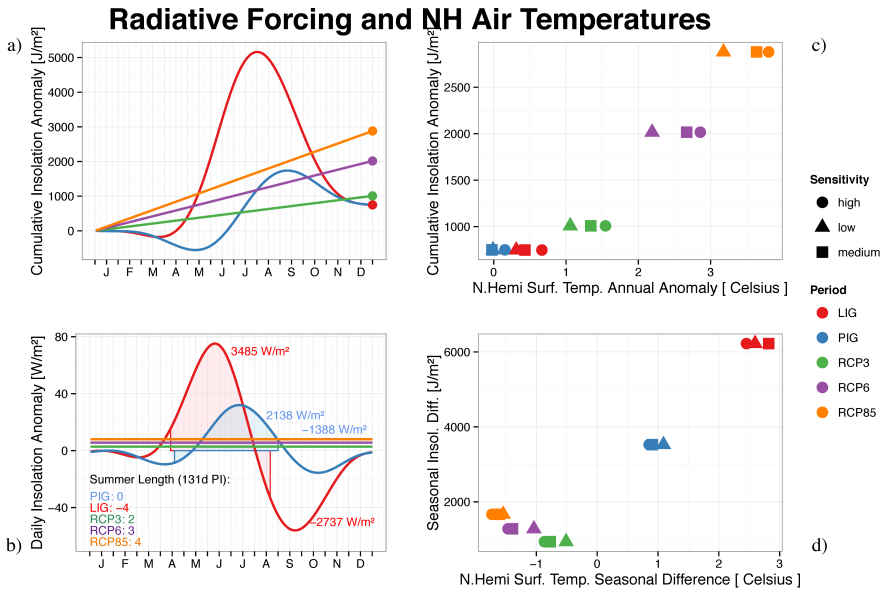

Figure 5.1: Comparison of insolation anomalies and background climate states. a) cumulative insolation anomalies over the year (Jm^{-2}), representing the annual radiative forcing input at 65°N. b) cumulative insolation anomalies (Jm^{-2}) and Northern Hemisphere (0-90°N) annual surface temperature anomalies. c) the daily insolation anomaly and season length anomaly in days for 65°N, defined as the days of the year with more than 300 Wm^{-2} insolation, representing the equilibrium temperature of a black body at 0°C (as in Huybers, 2006). Shaded area is the summer season radiative forcing for the LIG and PIG. d) the seasonal insolation difference (SID) compared to the seasonal difference in Northern Hemisphere surface air temperature anomalies.

climates these are negligible compared to the radiative forcing induced by greenhouse gas emissions. Thus, a first obvious distinction can be made between future and past climates on the basis of the radiative forcing. Here we introduce the three periods and provide the first results concerning the background climate state.

The Last Interglacial

The last interglacial lasted from about 130 to 115 ka BP. Its thermal maximum is recorded as one of the warmest periods during the last

250,000 years (Members, 2006). We have chosen 128 ka BP as our time slice because it corresponds to the timing of the maximum orbitally-forced insolation anomaly during summer in the Northern Hemisphere (+75 W/m^2 at 65°N compared to present-day, Fig. 5.1c; Huybers, 2006), potentially leading to highest melting of the GIS. van de Berg et al. (2011) showed that in a regional climate model coupled to an ice sheet model 45% of the GIS melt is directly related to insolation and 55% to the ambient temperature change. The contribution of GIS mass loss to the sea-level peak (6.6-8.4 m, Kopp et al., 2009; 2-4 m Dutton and Lambeck, 2012) in the last interglacial has been recently confined to about 2 m (Dahl-Jensen et al., 2013), which represents approximately 30% volume loss compared to the present-day ice volume (Tarasov and Peltier, 2003; Overpeck et al., 2006). However, the exact value remains uncertain and is within the range of 1.4 to 4.3 m (Robinson et al., 2011; Helsen et al., 2013; Stone and Lunt, 2013). Last interglacial reconstructions of GIS melt and ice-berg discharge yield about 12.7 ±0.1 mSv (∼400 Gt/yr at 125 ka BP, van de Berg et al., 2011) and are likely to have increased as the ice sheet lowered. In our last interglacial equilibrium control simulations (LIG, low to high) the Northern Hemisphere annual surface air temperatures are 0.3 to 0.7 K higher than at present-day (Fig. 5.1b) and the seasonal temperature difference, as defined by the annual range of monthly means, is 2.4 to 2.8 K higher than at present day (Fig. 5.1d). The increase in seasonality is mostly due to an increase in summer temperatures (1.8 to 2.1 K), whereas Fig. 5.1c shows as well lower insolation during early winter (-56 Wm^{-2}) and a 4 day shorter summer season. We define the summer season by the period during which daily insolation is above 300 Wm^{-2}, which corresponds to an equilibrium temperature of 0°C at 65°N as in Huybers (2006). This allows a dynamical definition of summer and winter half year as the length and starting point of the seasons are allowed to change over time.

The Present Interglacial - The Holocene Thermal Maximum

The present interglacial started at 11.7 ka BP and experienced an orbitally-induced summer insolation maximum at about 10 ka BP (Berger and Loutre, 1991). However, the timing of the warmest part of the present interglacial, the so-called Holocene Thermal Maximum, was delayed relative to the insolation maximum over large parts of the Northern Hemisphere to 7 to 5 ka BP. This delay was caused by the impact of remnants of the Laurentide Ice Sheet (LIS, Renssen et al., 2009) and related melt fluxes into the Atlantic Ocean. To circumvent such complexities we decided not to include remnant ice sheets and use 7 ka BP conditions, a period with a positive orbitally-induced insolation anomaly of + 32 Wm^{-2} at 65°N (Fig. 5.1c; Huybers, 2006) and still considerable GIS melt. Early Present Interglacial GIS melt fluxes can be inferred from ice thickness changes from Peltier's 2004 ICE5G model that is constrained by sea-level reconstructions and glacioeustatic adjustment, resulting in values ranging between 3 and 26 mSv (in the period of 9 to 7ka BP; Peltier, 2004; Blaschek and Renssen, 2013a). Other modelled estimates have been summarised in Funder et al. (2011b)(cf. Fleming and Lambeck, 2004; Simpson et al., 2009) and indicate a clear early Holocene retreat of the GIS, with contributions of up to 1.8 m of relative sea level from 10 to 7 ka BP. The minimum extent of the GIS was probably reached around 5 ka BP at the latest (Funder et al., 2011b). In our present interglacial equilibrium control simulations (PIG, low to high) the Northern Hemisphere annual surface air temperatures are 0 to 0.15 K warmer than at present-day (Fig. 5.1b), and the seasonal temperature ranges are 0.8 to 1.1 K larger than at present-day (Fig. 5.1d). The increase in seasonality is mostly due to increased summer temperatures (∼0.7 K), since Fig. 5.1c shows a small spring (-10 Wm^{-2}) and autumn (-16 Wm^{-2}) insolation anomaly minimum.

The Future Representative Concentration Pathways

The Future scenarios are based on the Representative Concentration Pathways (RCP) from Meinshausen et al. (2011) and represent fixed greenhouse-gas concentrations at 2100 AD from RCP3, RCP6 and RCP85.

To keep our approach simple and straightforward, we applied only changes of anthropogenic induced radiative forcing from greenhouse-gas concentrations. This forcing accounts for the majority of future anthropogenic induced changes (cf. Tab. 5.1) and represent a slightly reduced anthropogenic radiative forcing compared to the full emission scenarios presented by Meinshausen et al. (2011). The corresponding radiative forcing at 2100 AD is 2.7 Wm^{-2} for RCP3, 5.6 Wm^{-2} for RCP6 and 8 Wm^{-2} for RCP85. Note that, in our simulations we investigate the equilibrium response rather than the transient response, which is lagging the forcing. In our future equilibrium control simulations (RCP3, RCP6, RCP8, low to high) the Northern Hemisphere annual surface air temperatures are 1.1 to 3.8 K warmer than at present-day (Fig. 5.1b). We find that the seasonal temperature range decreases by 0.5 to 1.7 K (Fig. 5.1d), because winter temperatures rise stronger (1.2-4.4 K) than summer temperatures (0.7-2.6 K). Consequently, the summer season becomes longer as well (2-4 days, Fig. 5.1c). Connected to the temperature rise is the predicted contribution of future GIS melt to sea-level rise in the range of 0.03 to 0.21 m per century, translating to a melt flux of about 3 to 24 mSv (Meehl et al., 2007) in addition to a present-day flux of 22.2 $\pm$0.1 mSv (van de Berg et al., 2011; 18 mSv in Dickson et al., 2007 for pre-industrial). These predictions can be considered conservative, as recent increases in GIS melt rate (Rignot et al., 2011; Bamber et al., 2012) suggest that this continuing trend will lead to near-future GIS melt rates that are likely to exceed previous projections (Meehl et al., 2007). Previous studies, such as Ridley et al. (2005), suggested a peak rate of 60 mSv in the early phase of a 3000 yr long complete retreat of the GIS under increasing greenhouse-gas forcing. Overall the GIS will become a major contributor to future sea level rise (Rignot et al., 2011) and is likely an important source of freshwater in the North Atlantic region.

Comparison of past and future climates

In order to compare the three periods (LIG, PIG, future) we show in

Fig. 5.1 the radiative forcing from daily insolation data (Huybers, 2006) at 65°N and radiative forcing from greenhouse-gas emissions for the future cases (Tab. 5.1). The cumulative insolation anomaly (defined as the integrated insolation from January to December) in Fig. 5.1a shows that the LIG and the PIG have strong positive summer insolation anomalies compared to present day (cf. Fig. 5.1c), but also negative anomalies in spring and autumn. Therefore, accumulated over a whole year, LIG and PIG insolation anomalies add up to about 750 Jm^{-2} (here we neglect PIG and LIG greenhouse-gas changes), but for the future cases, greenhouse-gases induced radiative forcing anomalies add up to much higher yearly sums (1008 Jm^{-2} for RCP3, 2016 Jm^{-2} for RCP6 and 2880 Jm^{-2} for RCP85). When we compare the annual insolation accumulation with annual mean Northern Hemisphere surface air temperatures, we find a consistent pattern (Fig. 5.1b), indicating that more annual cumulative radiation forcing leads to higher annual Northern Hemisphere temperatures in our model. One has to keep in mind that this is particularly true for higher Northern latitudes, as past orbital insolation values varied substantially per latitude. On the one hand, it is possible that the annually warmer climates are less freshwater sensitive climates in line with previous findings of Ganopolski and Rahmstorf (2001). On the other hand, we have shown that the past climates are characterised by larger seasonal ranges in both insolation (Fig. 5.1c) and temperature (Fig. 5.1d), whereas for future climates we find reduced seasonal ranges. Arguably, seasonality is relevant to the strength of the AMOC because cooler winter temperatures result in more suitable conditions for both convection in deep water formation areas and more sea-ice formation. Relevant in this context are both the severity of winter cooling and the duration of the period with cold temperatures that are closely linked to orbital insolation for the past climates (Fig. 5.1c). On the one hand, cooler winter temperatures allow sea ice to grow faster and foster convection by brine rejection, while on the other hand, expanded sea ice might be shielding the ocean from the atmosphere and thus reducing convective activity. However, despite these local effects of sea ice and convection,

transport of freshwater from outside the vicinity of the convection area by increased sea-ice expansion would result in more surface freshening and stratification in the convection area, thus reducing convection and bringing that convection site closer to a collapse. This transport of freshwater would result from the sea ice melting during summer and winter transport of sea ice. This may indicate, therefore, that in climates with a larger seasonal contrast, such as the LIG and PIG, the AMOC could be more sensitive to freshwater forcing. Both interpretations, the annual and the seasonal, as well as the two mechanisms, the sea ice shielding convection and more freshwater being transported into convection areas, are valid at this point and it is in the next section, that we shall discuss this together with results of the AMOC strength.

Note that in the LOVECLIM model, the spring equinox is fixed to the 21st of March, which impacts the definition of monthly means used in our comparison to daily insolation data (Fig. 5.1d, e.g. further information in Joussaume and Braconnot, 1997). Our monthly model output includes this bias whereas our dynamic definition of the seasons based on daily insolation, allowing them to shift inside the year, does not. Note that we apply GIS melt water throughout the year without seasonal differences. Recently Hu et al. (2011) described a minor difference in AMOC strength between simulations with annual and summer only GIS melt forcing. However, in a study using the same LOVECLIM model, Bakker et al. (2013a) did not find any notable impact of seasonality.

5.3 Results & Discussion

We will first discuss our results in terms of impact of the background climate state on the unperturbed AMOC strength (Section 5.3.1), and continue with the impact of GIS melt on the AMOC strength and the importance of model parameter sets (Section 5.3.2), then we take a more detailed look at the mechanisms involved in Section 5.3.3 and finally we discuss our results in context of climate sensitivity in Section 5.3.4.

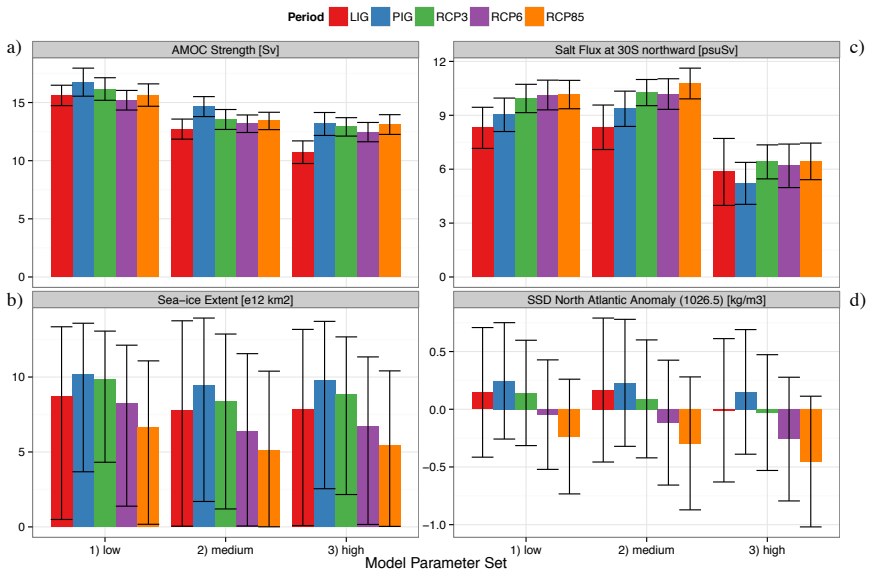

Figure 5.2: Comparison of the background climate state showing the mean unperturbed AMOC strength (a) in Sv, as well as the standard deviation, and the mean sea-ice extent of the Northern Hemisphere in km^2 (b), as well as the minimum and maximum of the sea-ice extent. (c) shows the salt inflow at 30°S in the North Atlantic northward in psuSv and the standard deviation. (d) shows the sea surface density in the North Atlantic (90-30°W, 35-90°N) as anomaly to 1026.5 kgm^{-3} to show the changes more clearly.

5.3.1 AMOC state in the background climates

The AMOC strength in the unperturbed background climates is relevant for our estimation of its sensitivity to GIS melt water. We find that the mean AMOC strength (14 ±1.6 Sv) at 27°N differs more by parameter set (1.4 to 2.5 Sv differences within one climate) than by time period (0.6 to 1 Sv differences per parameter set), with the strongest circulation in the low parameter set (15.9 Sv) and the weakest in the high parameter set (12.5 Sv, Fig. 5.2a). The early PIG is mostly the strongest within the range of simulations (∼14.8 Sv) and the LIG the weakest (∼13 Sv). The latter shows a particular minimum in our high

parameter set, which is potentially linked to the strong decrease in summer sea-ice extent in the Arctic (Fig. 5.2b). However, it is uncertain whether the unperturbed strength of the AMOC was stronger or weaker during the early LIG (Born et al., 2011; Bakker et al., 2013b). The mean AMOC strength is dependent on the parameter set showing a decrease with higher freshwater sensitivity, however the variability within each parameter set remains similar. Convection from the surface to the deep ocean depends mainly on the buoyancy of the surface waters and the stability of the water column itself. Impacts from salt fluxes, precipitation, evaporation, temperature and sea ice affect convection at these convection areas and are thus relevant for the AMOC in total. Seasonal changes in sea-ice extent (error bars in Fig. 5.2b) are large for all simulations, however the largest for the LIG ($\sim$13.2x10^{12} km^2). The salt flux at 30°S northward in the Atlantic Ocean (Fig. 5.1c) indicates that in the future scenarios the salt import is higher compared to PIG and LIG and that a large difference exists between the high sensitivity version and the other parameter sets. The combined impacts are visible in the sea surface densities (SSD) in the North Atlantic (90-30°W, 35-90°N, Fig. 5.1d). In the future scenarios SSDs are mostly lower compared to LIG and PIG. The highest densities are found in the PIG, and the lowest in RCP85. The lower SSDs in the future scenarios show that, despite higher salt import into the North Atlantic, SSDs are decreasing due to lower sea-ice area, higher temperatures and a more negative E-P balance (not shown). Despite these differences, the presence of convection (reaching more than 200m depth) at the three major convection sites (Nordic Seas, Labrador Sea and around Iceland; Fig. SI.B.3 on page 193) and the relatively similar AMOC strength in all unperturbed background climates suggests, that the AMOC state in the background climate is of minor importance for the sensitivity of the AMOC to GIS melt water.

5.3.2 Impact of freshwater forcing on the AMOC strength

In Section 5.2.3 we have summarized forcings and temperatures of our control experiments for each period and found that there is a difference between past and future climates that originates from their forcings. Therefore, we have decided to look more into the differences of past and future climates, rather than at each simulation separately. Individual results are available as supplementary information (Fig. SI.B.2 on page 191).

The results show (Fig. 5.3a) that the relative AMOC sensitivity (size of anomaly relative to control) to freshwater forcing depends strongly on the used model parameter set. As expected, our three model versions diverge into a more (medium, high) and a less (low) sensitive configuration that is consistent over all time periods and suggests that parameter changes are very relevant to the results and implications deduced. We will discuss this result in more detail in Section 5.3.4 and focus now on the differences of past and future climates per model parameter set. From Fig. 5.3b-c it is apparent that the difference in AMOC sensitivity to GIS melt between past and future is not constant, but changes as a function of the imposed GIS melt. This difference arrives at a maximum at 54 mSv GIS melt in the medium and high sensitivity parameter sets, before the difference decreases again with higher melt rates (Fig. 5.4a). The slopes of past AMOC changes for the medium and the high sensitivity parameter sets are steeper than their future counterparts before 54 mSv (Fig. 5.4b), weaker between 72 and 90 mSv and relatively similar at higher GIS melt rates. The difference between past and future, and the change of slope are both relevant for the interpretation, but do not provide a single melt rate value. Therefore, we define a transition zone from 36 to 72 mSv. This zone marks the transition in the AMOC response in past and future climates: with GIS melt rates lower than 36 mSv, the past and future climates respond very differently, while above 72 mSv they respond rather similarly. This transition zone is not valid for the

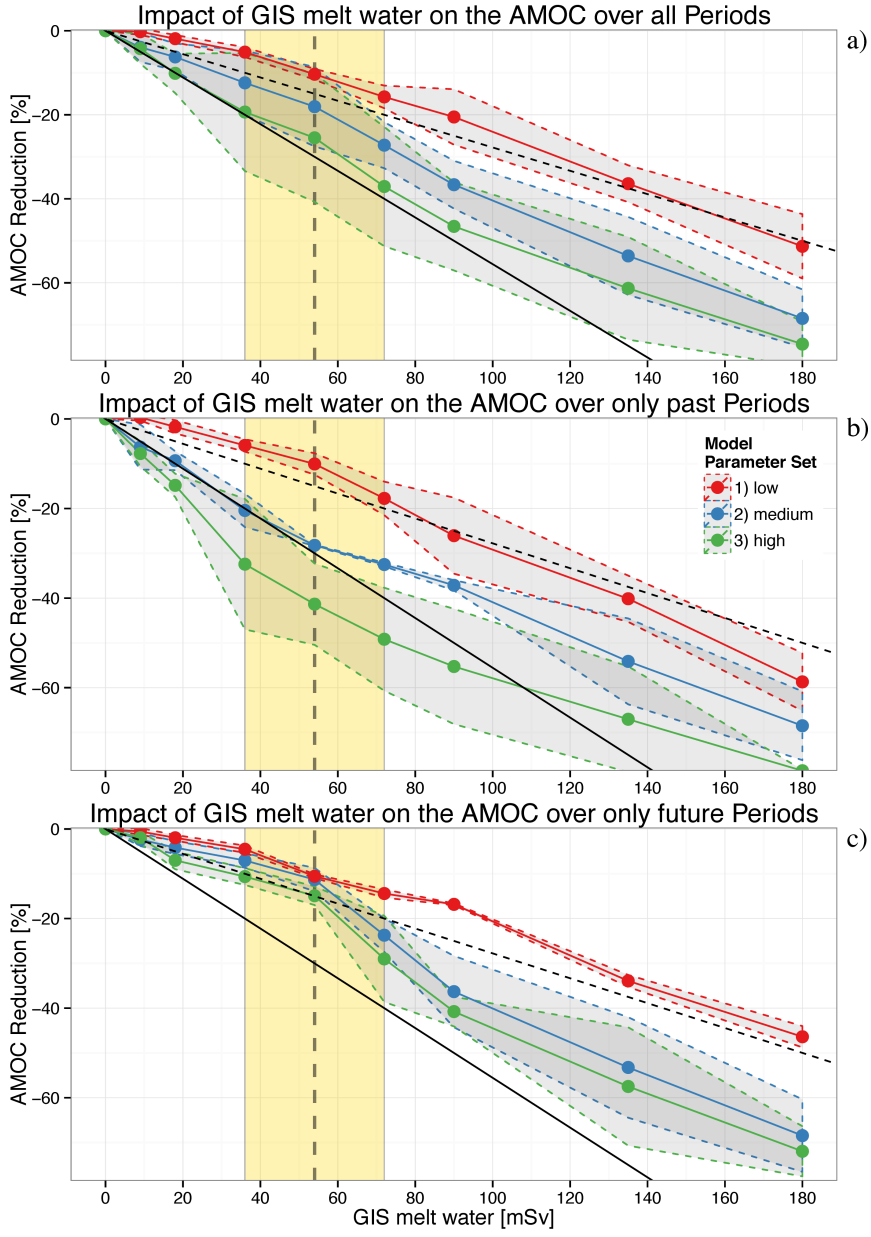

Figure 5.3: (Caption on next Page)

low-sensitivity version of our model that hardly shows these differences between past and future climates, as well as slope changes (Fig. 5.4b). The changes in response of the AMOC to GIS melt water is not unlike a separation that has been reported by Bakker et al. (2012) with the same model in different LIG GIS melting scenarios. They made a separation into three regimes (0-39 mSv, 52-130 mSv, 143-300 mSv) of AMOC response to GIS melt water. However, the distinction between regimes was based on the shutdown of convection areas and sea-ice extent using a finer GIS melt stepping to distinguish between regimes, which are potentially hidden as we have less simulations with high melt rates. Nevertheless a difference is visible in the lower GIS melt ranges in Fig. 5.3b-c or Fig. 5.4a between the future scenarios and the past climates, suggesting that the future climates change within the transition zone from being less sensitive to more sensitive with higher melt rates and come closer to the past climates. When we look at the absolute values of AMOC strength then the picture shifts a bit, because the periods and especially the model parameter sets have different mean values (Fig. 5.2,

Figure 5.3: Summary of the AMOC changes due to GIS freshwater forcing per model realization. All panels show percentages of AMOC reduction and GIS melt water flux in mSv. a) all simulations, past and future ones. b) only past simulations, LIG and PIG. c) only future simulations, RCP3, RCP6 and RCP85. Values are taken from 27°N and have been calculated over the last 100 yrs of each simulation and the percentages are presented as anomalies compared to the control simulation for each parameter set and period. The changes depicted by the percentages represent the AMOC's sensitivity to freshwater forcing. For individual simulations and absolute values of AMOC strength we refer to the SI. The shaded bands represent one standard deviation around the corresponding means. The area between 36 and 72 mSv is denoted as the transition zone and the black dashed line (at 54 mSv) indicates the maximum difference of past and future AMOC changes, as shown in Fig. 5.4. Solid black line (10% AMOC reduction vs. 18 mSv GIS melt) and dashed black line (5% AMOC reduction vs. 18 mSv GIS melt) give lines of constant AMOC sensitivity for reference.

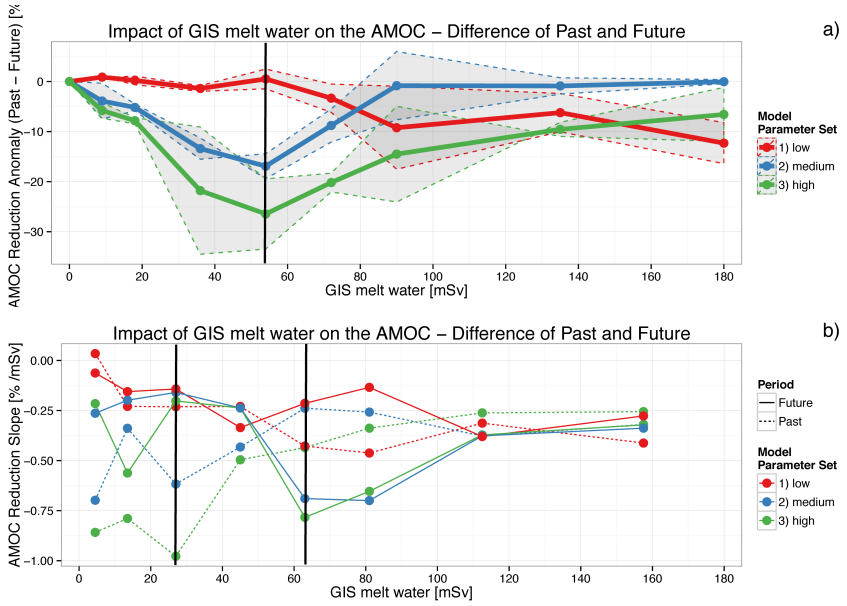

Figure 5.4: AMOC response to GIS melting per model parameter set, shown as difference between past and future scenarios (a) and slopes of AMOC changes for past and future climates (b). Black lines indicate the transition zone as in Fig. 5.3. Values used for the calculation of slopes and differences are shown in Fig. 5.3.

low: 15.9 Sv, medium: 13.5 Sv, high: 12.5 Sv, all time periods) and impacts differ especially for the past periods (Fig. SI.B.2 on page 191). Nonetheless, the similarity between the medium and the high version remains. Differences in the absolute values of AMOC strength indicate primarily differences in the parameter sets, such as the initial value of AMOC strength or how large the differences are between the different periods. We find that the high parameter set produces absolute values that are much lower for LIG and PIG compared to the future scenarios. In the medium set this is not the case. When using the high sensitive version, the LIG simulation remains below all other simulations, independent of melt rates. In accordance with Swingedouw et al. (2009) this shows already the importance of the background climate on the AMOC state and its sensitivity to GIS melt. When we consider for a moment that the low parameter set produces the same sensitivity to freshwater

forcing in all climates investigated (Fig. 5.3), then the absolute values (Fig. SI.B.2 on page 191) tell us that this is even possible with different mean values of AMOC strength. For the high version we find that the most sensitive time periods (LIG, PIG) are also the time periods with the weakest initial AMOC strength before perturbation with freshwater (Fig. 5.2a). As expected the medium version gives us an intermediate picture that shows weaker reductions compared to the high version, but still distinguishes between past and future climates.

The change in response to freshwater forcing within the transition zone seems to be linked to the actual setting and the background climate state of the different time periods. We can see in Fig. 5.4b that in the lower GIS melt range the past climates (PIG and LIG) are more sensitive compared to the future scenarios for both the medium and the high parameter sets. We have previously shown that Northern Hemisphere annual mean surface air temperatures align well with annual cumulative insolation forcing (Fig. 5.1b) and that applying these results to the sensitivity of the AMOC to GIS melt water suggests that the AMOC is more sensitive in climates with less annual mean insolation, such as the LIG and PIG. This interpretation is in general agreement with Swingedouw et al. (2009), however they also found that the response of the convection sites to freshwater forcing is critical in combination with the sea-ice cover. Therefore, it is not unlikely that both the seasonal (Fig. 5.1c) and annual mean insolation forcing are relevant for the AMOC sensitivity to freshwater forcing. A potential explanation for a connection to mean annual forcing could be the energy distribution in the climate system, making transport processes relatively more important, thus the climate system more sensitive to disruption, such as to GIS melt water slowing down the AMOC. Applied to, for example the LGM, a cooler climate with a higher meridional temperature gradient (e.g. Shakun and Carlson, 2010), depends more on the transport of heat from the tropics to the poles, thus resulting in a more sensitive AMOC to freshwater forcing (Swingedouw et al., 2009). However, this relationship between AMOC

sensitivity and annual mean forcing does not explain why the warmer future climates become more sensitive with higher GIS melt rates compared to past climates (cf. Fig. 5.3b-c), suggesting a dynamic response. We have reported on the seasonality of the forcing for LIG and PIG (Section 5.2.3), which implies cooler (-0.1 to -0.8 K) and longer winters (in LIG 4 days). In the model, these conditions lead to an increase in sea-ice cover (Fig. 5.2b). In a comparison between Northern Hemisphere seasonal surface air temperature differences and seasonal insolation difference (SID, Fig. 5.1d), we find that the future cases show the opposite response relative to the past climates. LIG and PIG show larger seasonal temperature differences, whereas in the future cases the difference decreases as the result of higher winter temperatures. The results suggest that not only the Northern Hemisphere annual mean temperatures are important, but that the seasonality of the background state is relevant for the strength of the AMOC, as climates with higher seasonality seem to be more sensitive to freshwater forcing as can be seen in Fig. 5.3b, lower GIS melt range. However, from seasonal temperatures or insolation forcing alone, it is not possible to explain why future cases become more sensitive above 54 mSv GIS melt (Fig. 5.3c). Therefore, we will analyse in the following section the impact of changes in seasonality on winter convection and sea-ice cover in the convection areas and its dependency on the amount of GIS melt water.

Figure 5.5: Summary of the sea-ice area response to GIS melting per model parameter set. All panels show percentages of sea-ice cover change and GIS melt water flux in mSv. a) all simulations, past and future ones. b) only past simulations, LIG and PIG. c) only future simulations, RCP3, RCP6 and RCP85. Values give Northern Hemisphere sea-ice cover over the last 100 yrs of each simulation and the percentages are presented as anomalies compared to the control simulation for each parameter set and period. Solid black line (5% sea-ice cover change vs. 18 mSv GIS melt) and dashed black line (5% sea-ice cover change vs. 9 mSv GIS melt) give lines of constant sea-ice cover change for reference.

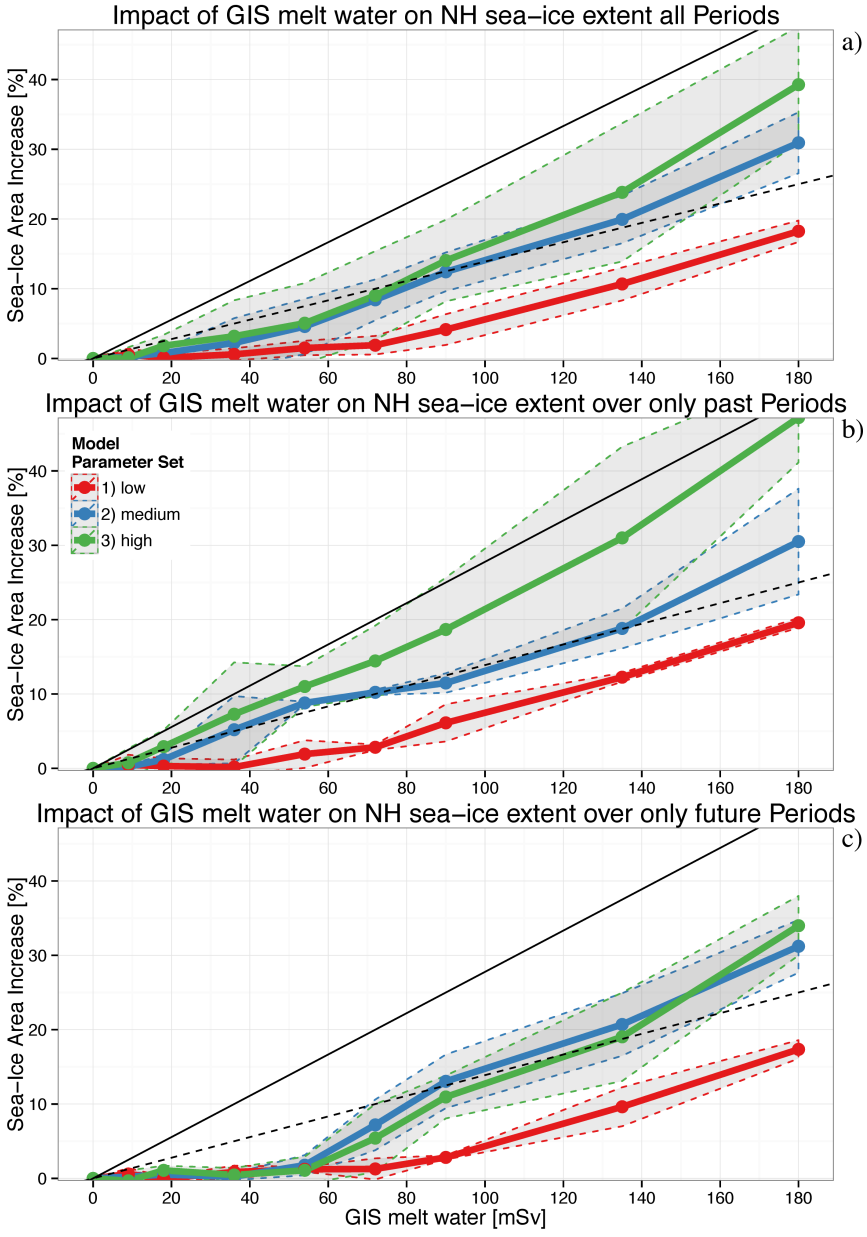

Figure 5.5: Caption on previous Page

5.3.3 Convective activity and sea-ice feedback

Connected by the strong cooling during winter, convection and sea ice formation are seasonal processes that interact with each other and make it hard to distinguish between feedback and forcing. Nevertheless we find in Fig. 5.5 (sea-ice extent anomaly compared to control), a difference that corresponds well with the separation made in Fig. 5.3. Before 54 mSv GIS melt, the future scenarios have hardly any sea-ice feedback (Fig. 5.5c), compared to the past climates (Fig. 5.5b) in the medium and high sensitivity parameter sets. In order to connect better to the convection areas and analyse the different response in the lower and the higher GIS melt range, we take two example GIS melt scenarios, one at 36 mSv (20% GIS mass loss) and one at 135 mSv (75% GIS mass loss), and the corresponding control simulation. Furthermore, we focus only on LIG, PIG and RCP6, because RCP3 and RCP85 show minimal differences in convection depth and sea-ice margin patterns compared to RCP6 and only for the medium model parameter set. The maps show absolute annual sea surface salinities (SSS) for the control simulations (Fig. 5.6,column 1) and anomalies for the freshwater perturbed simulations (columns 2 and 3), as well as winter maximum and summer minimum sea-ice extent and winter maximum convection layer depth as black contours. For the control simulation, results show some differences between different time periods mostly south of Denmark Strait. For example, this area is in the LIG and RCP6 much fresher compared to the PIG most likely related to a more southern sea-ice extent and related melting during summer. Convective activity can be found in the Labrador Sea (LS), Around Iceland (AI), such as in the Irminger Sea, and in the Norwegian Sea (NS). In the control simulations convection is active in all regions (Fig. 5.6, black contours). Once we added 36 mSv of GIS melt water (Fig. 5.6, column 2), the LIG has no convection and an enhanced sea-ice extent in the LS compared to PIG and RCP6. The freshening signal in SSS in LS is much more expressed in the LIG compared to PIG or RCP6 given the same amount of GIS melt.

In the PIG and RCP6, LS convection remains active, though reduced. However, the response and spatial pattern of freshening is quite different between the three periods. In the PIG the centre of freshening is close to the Denmark Strait, reducing convection and expanding sea ice to the tip of Greenland. In the LIG the freshening is centred on the west coast of Greenland in the LS, shutting down convection there and covering the LS with sea ice. In RCP6 the surface freshening is weakest compared to the past periods with a centre close to the tip of Greenland and weaker impacts on convective activity (Fig. 5.3c) and minor changes in sea-ice extent. The sea-ice extent, the amount of freshening and the corresponding location of active convection characterize some of the differences between the past climates and the future cases. Major differences between PIG and LIG are the freshening in the LS and the maximum and minimum sea-ice extent, as the Arctic becomes almost ice-free at the end of summer in the LIG. At this point it seems clear that the LS and the origin of this extended freshening in the LS is key in explaining the different response seen in Fig. 5.3 between past and future climates. We continue with the higher GIS melt simulations before we focus more on convection in the LS.

In our simulations with a higher GIS melt flux (135 mSv; Fig. 5.6, column 3) we find a relatively similar picture for all periods (LIG, PIG, RCP6) in terms of surface freshening of the North Atlantic, but a different one for the past climates (LIG, PIG) and RCP6 in terms of sea-ice extent. Convective activity is reduced in all convection areas and no LS convection is present in any of the presented simulations (cf. Fig. 5.7a). AMOC reductions in Fig. 5.3 indicate that past climates are relatively close together and share almost the same sea-ice extent (Fig. 5.5, Fig. 5.6a-b). While the sea-ice advance in RCP6 is different compared to the PIG, convective activity is comparable except for a slight weakening in NS in RCP6. A detailed analysis of each melt case (cf. Fig. 5.7a and Fig. SI.B.3 on page 193) suggests that LS is the most

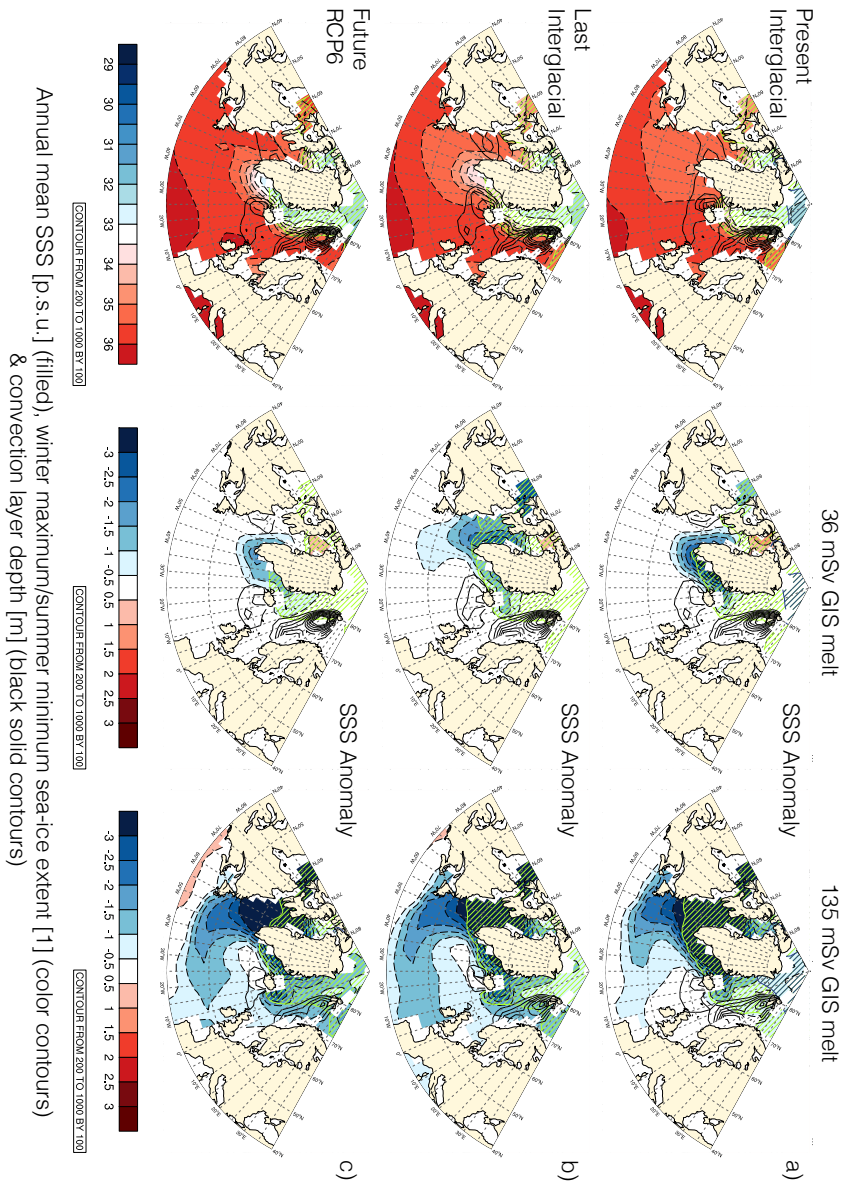

Figure 5.6: Convection areas and sea-ice margin for the control simulations, 36 mSv or 20% and 135 mSv or 75% GIS melt. Maps show annual sea surface salinities (SSS), winter maximum convection depth (m) as well as winter maximum (red striped) and summer minimum (blue striped) sea-ice extent (described by the lead fraction above 15 %) over the last 100 yrs of each simulation considering the medium sensitivity version of our model. a) simulations of the PIG, b) simulations of the LIG, c) simulations of RCP6.

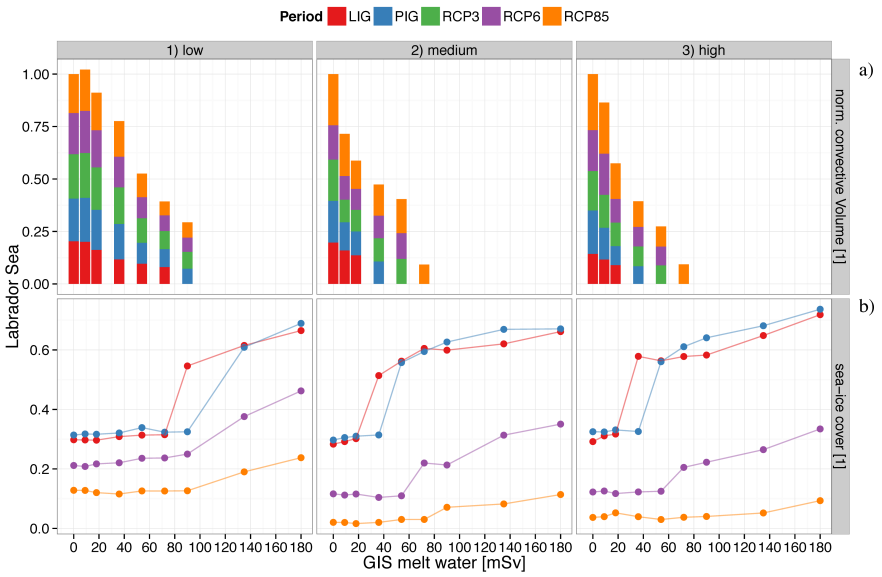

Figure 5.7: Labrador Sea normalized convective volume resembling convection activity and sea-ice cover. a) Normalized convective volume, that is calculated using the convective layer depth (above 200m) multiplied by the area and then normalized using the unperturbed volume (with total volume of all 5 experiments being 1.0). Additional information in Fig. SI.B.3 on page 193. b) Annual mean sea-ice cover. The values are calculated from the last 100 yrs of each simulation in the Labrador Sea (LS, 90-45°W, 50-70°N).

sensitive convection region in terms of freshwater needed to inhibit convection there. Beyond a certain amount of GIS melt, the LS becomes sea ice covered for the past climates and stratified in the future cases (Fig. 5.7b). This result is independent of model realization. Whereas this higher sensitivity exists in the past climates at different GIS melt rates, LIG 36 mSv and PIG 54 mSv, in the future scenarios this seems to be missing. However as we have seen in Fig. 5.6 a major difference between LIG and PIG is the freshening of LS as well as extensive sea-ice cover. At this point it is unclear whether surface freshening or sea-ice cover shielding convective activity in the LS in the LIG is more relevant, as the leading and lagging of the two processes is hard to distinguish.

However, in combination with results seen in Fig. 5.7, we find that in the PIG just a bit more GIS melt water is needed to give a similar response in the LS. This thus suggests, that the amount of freshening in the LS is different between the two climates. Vertical profiles in the Labrador Sea (Fig. 5.8) exhibit more stratification in the LIG compared to any other model simulation and support the idea that indeed surface freshening is more relevant as opposed to sea-ice cover shielding convection. Indicated by the advancing sea-ice cover towards the tip of Greenland in Fig. 5.6a in the PIG, it seems likely that the expansion of sea-ice acts as a freshwater transport to the South and into the LS. This additional freshening causes LS convection to collapse at lower GIS melt rates in the LIG compared to the PIG and RCP6.

The response seen in Fig. 5.3 between the past and future simulations is clearly impacted by the circumstances in the LS, but as well by the activities in the other convection areas. Convective activity around Iceland is rather robust and again relatively independent of the model parameter set. Related to a weakening of convection in LS, the AI strength increases as a result of a shift of convection outside LS and sea-ice related cooling and advection of relatively cooler air. Therefore a slight increase in convective activity in all simulations can be seen in AI. However, the biggest changes can be seen in the NS in terms of model parameter set, time period and GIS melt flux. The NS convection region, the most important convection site in our model, is found just southwest of Svalbard, so relatively close to the sea-ice edge. This makes this region, on one hand, prone to advancing sea ice that can hamper ocean-atmosphere heat exchange, but on the other hand, resistant because of the low temperatures at this extremely northern position. Medium and high model parameter sets show both a considerable decrease of convection depth in NS with high GIS melt rates, in agreement with results from Fig. 5.3. Whereas for lower GIS melt rates all model versions give weak increases in convection layer depth in NS, potentially related to decreases of other convection sites and the overall increase of sea ice and related cooling.

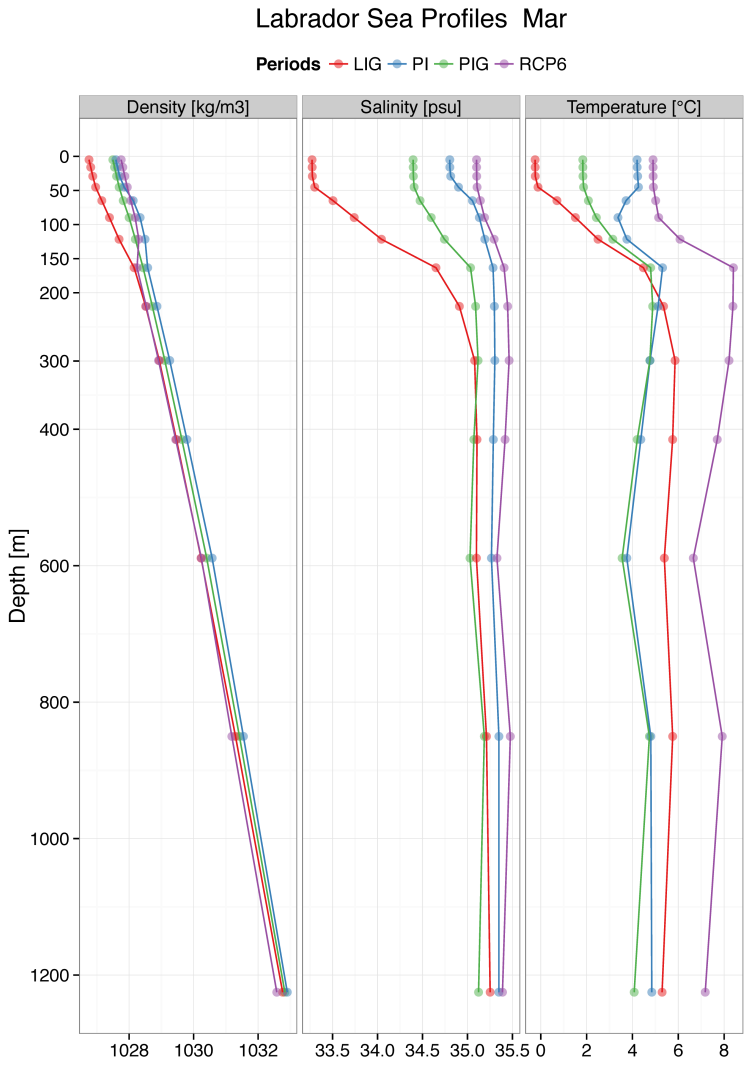

Figure 5.8: March Labrador Sea vertical profiles of density, temperature and salinity. Simulations LIG, PIG and RCP6 include 36 mSv of GIS melt water as seen in Fig.6, simulation PI represents a pre-industrial reference simulation that does not include additional GIS melt water. All model simulation values have been calculated from the last 100 yrs of each simulation in the Labrador Sea (LS, 90-45°W, 50-70°N).

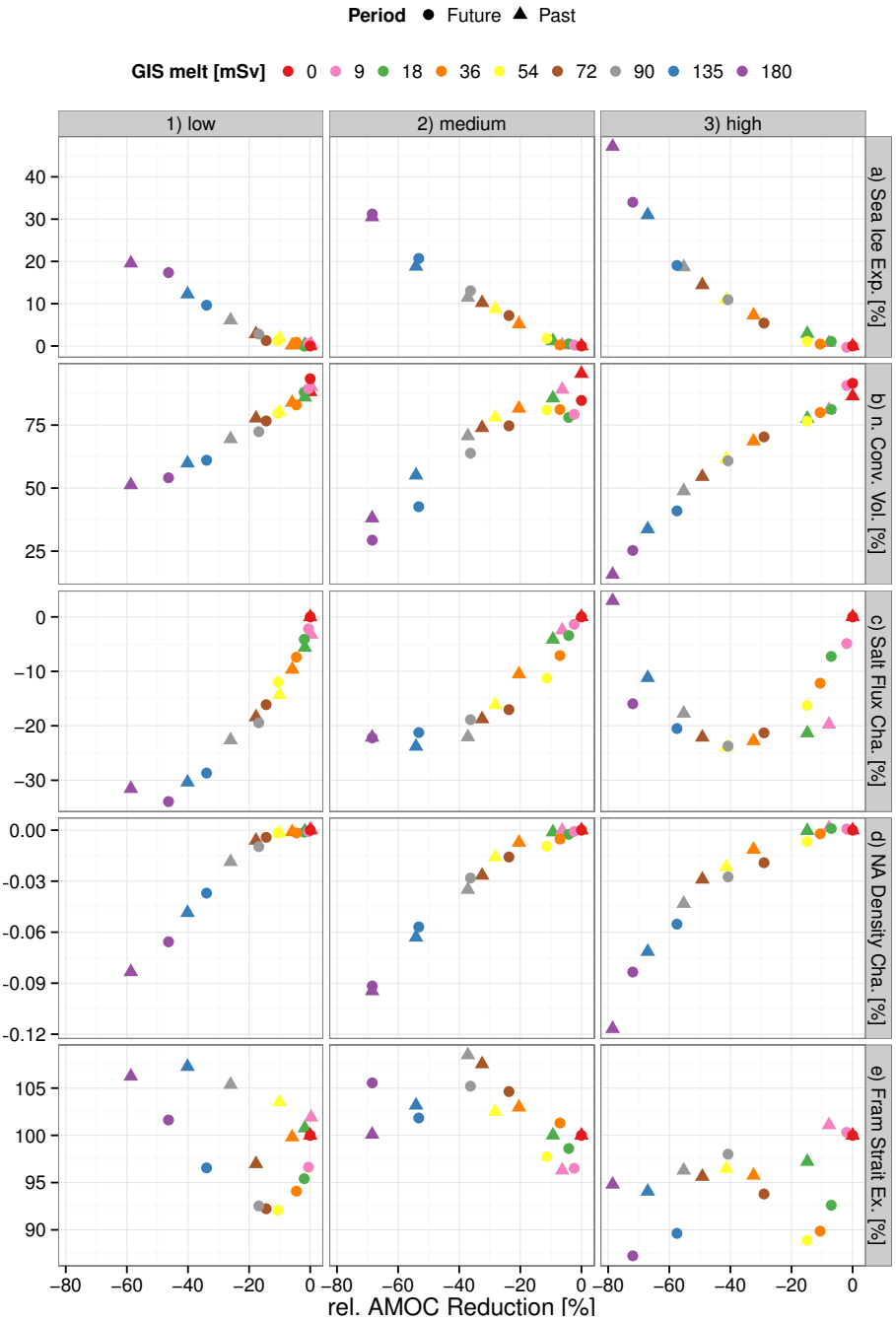

Figure 5.9: Caption on next page

Summarizing, for the past warm periods we find that the different response of the AMOC in the lower GIS melt range relates to the convective activity in the convection areas (as summarized in Fig. 5.7a, the North Atlantic) and the seasonal cycle of sea-ice formation and melt (Fig. 5.7a). The response of the sea-ice expansion due to GIS melting depends on the climatic conditions of the background climate and it is only in such cases when the expansion of sea ice reaches far enough to affect convection in the LS, that a different response in AMOC strength can be found. In the future scenarios, this sea-ice response and transport of freshwater into the LS is only a minor process, most likely because of higher winter temperatures (up to 4.4K in RCP8.5, Section 5.2.3) and subsequent smaller expansion of sea ice (Fig. 5.5c). At higher GIS melt rates the stratification of the ocean surface inhibits or weakens convection at different convection sites, resulting in cooling and sea-ice expansion and reduced AMOC values alike (Fig. 5.3b-c). However, there are still important differences between the periods. For example, in the future scenarios at higher GIS melt rates, the LS is stratified, rather than covered by sea ice as in the LIG or the PIG (Fig. 5.6c), whereas the NS convection site is impacted by both freshening and sea-ice cover in all climates alike.

Other mechanisms that have been suggested to explain differences in the AMOC sensitivity to melt water input are discussed in the next section.

Figure 5.9: Scatterplot of relevant variables compared to AMOC reduction to GIS melt water for past and future simulations and per model parameter set. a) Northern Hemisphere sea-ice area, as anomaly compared to the control simulation, as in Fig. 5.5. b) North Atlantic normalized convective volume, as in Fig. SI.B.3. c) Salt flux at 30°S northward in the North Atlantic, as anomaly compared to the control simulation, as in Fig. 5.2c. d) Sea surface density of the North Atlantic as anomaly compared to the control simulation, as in Fig. 5.2d. e) Fram Strait sea-ice export as anomaly compared to the control simulations.

5.3.4 Discussion and Context

The comparison of past and future AMOC sensitivity can be done on the basis of annual mean insolation, or radiative forcing for future emission scenarios respectively, and yield higher values for climates that have less forcing. We argue that this is related to the fact that cooler climates depend stronger on the heat transport northward, as has been previously shown by Swingedouw et al. (2009). However, our results also show, that future climates can become more sensitive to higher GIS melt (Fig. 5.3c), hence it is more likely that a dynamic feedback interacts with the GIS melt water and the AMOC. We find the sea-ice response in past and future climates to be different just like the response of the AMOC to GIS melting (Fig. 5.5) in the lower GIS melt range. Our results further show that this different response is caused mainly by the sensitivity of the LS convection site to freshwater entering the LS, thus the amount of freshening. The transport of freshwater by the sea-ice expansion into the LS brings convection there closer to a collapse and modifies the overall response to a given GIS melt rate. The expansion of sea ice is most likely driven locally by surface cooling and freshwater stratifying the surface ocean as well as globally by the heat transport and the seasonality of the climate. Not unlikely, but inconclusive is the idea that changes in Fram Strait sea-ice export (autorefcha4:fig.9e) could cause the reported sea-ice expansion and highlight the Arctic Ocean as the source of this different response. Modeling results give weak changes (5-10%) but large inter-annual variability (30%).

Other studies (Rahmstorf, 1996; Latif et al., 2000; Swingedouw et al., 2007) have shown that the salt import into the North Atlantic is crucial for the stability of convection and the AMOC sensitivity to melt water forcing. Our results agree with this interpretation to some extent, as the salt import into the North Atlantic (Fig. 5.7c) relates as well to the AMOC strength. However, SSDs for the unperturbed states (Fig. 5.2d) are lower in the future scenarios and decrease even further with higher

GIS melt rates (Fig. 5.7d). Increased inflow of salty waters in the future scenarios is counteracted by more local sea-ice melting and surface warming, yielding lower SSDs in the convection areas (Fig. SI.B.4 on page 194). Therefore, it is reasonable to argue that this stabilizing effect (Rahmstorf, 1996; Latif et al., 2000; Swingedouw et al., 2007) is not the main mechanism that controls the difference between past (LIG, PIG) and future (RCP3, RCP6, RCP85) AMOC sensitivity in the lower GIS melt ranges. The difference in sea-ice expansion, freshwater transport and its interaction with convection, most prominently in the LS, allows explaining this difference in AMOC response to GIS melting. Ultimately this difference lies in the seasonality of the climate, which determines the amount of sea ice formation and modifies the oceanic response to a land-based ice sheet melting.

To better understand how future climate change compares with changes that occurred in past warm periods, we have investigated the relationship between the background climate state, the AMOC's strength and GIS melt. We have systematically analysed the sensitivity of the AMOC to freshwater forcing from the GIS and found that the model parameter set, which describes mainly the sensitivity of the model to freshwater forcing, plays a major role in determining what consequences can be expected from using past reconstructions in future predictions. If we consider a freshwater-sensitive parameter set, our results suggest that, at lower GIS melt rates (less than 54 mSv), the relation between the AMOC and GIS melt differs considerably between past and future warm periods. However, they are very similar when a parameter set with lower freshwater sensitivity is used. Unfortunately there is little constraint on the sensitivity of the AMOC to freshwater forcing in the real world. Nonetheless, in two out of three cases (medium, high) impacts on past climates are different from future ones in terms of ocean circulation. This could imply that the differences in the seasonal distribution of the radiative forcing make past climates very different from present and future climates in terms of convection depth and sea-ice feedback and

therewith the overall AMOC response.

Climate sensitivity describes the response of global temperatures to changes in global radiation modified by numerous feedbacks from all components of the climate system. Our primary interest is the AMOC as a feedback and whether our climate-related AMOC sensitivity in the lower GIS melt range is impacting global climate sensitivity. An estimation of climate sensitivity (defined as the annual mean global temperature change divided by the radiative forcing) in all our future cases, including all GIS melting scenarios, yields relatively constant values per parameter set (0.39, 0.42, 0.51 K/Wm^{-2} for low, medium and high parameter sets), varying weakly (0.04 K/Wm^{-2}) by emission scenario or GIS melt. This near constancy of the climate sensitivity in the future scenarios is a result of the relatively large simulated global warming of 1 to 4 K compared to an up to 0.6 K decrease due to GIS melting (depending on parameter set). The stronger impacts are found in the weaker warming scenarios and in the medium to high parameter sets. The melting of the GIS weakens the AMOC and therewith the northward transport of heat and causes an expansion of the sea-ice cover, resulting in global cooling. Similar temperature impacts of 0.7 K (LIG) to 0.9 K (PIG) due to GIS melting are found in the past simulations. Due to the relatively small magnitude of the annual mean warming (LIG: 0.5 K, PIG: 0.2 K) it is in the same order of magnitude with the cooling. However, following the methodology of climate sensitivity to compare global annual mean temperatures with global annual mean radiation changes, we find that for our past warm climates the corresponding climate sensitivity varies strongly as a function of GIS melt amount and AMOC strength (-1 to +3 K/Wm^{-2}). Furthermore, we find that the GIS melt related reductions in global temperatures are consistently larger, even though the differences are relatively small, in the past simulations compared to the future scenarios, mainly caused by stronger feedbacks related to the Arctic sea-ice cover in the past climates (e.g., ice-albedo and ice-insulation feedbacks). The application of the climate sensitivity

concept to small annual forcings (LIG, PIG) has to be seen with caution. Firstly, it can be argued that in climates, such as the future, that are strongly forced by changes in greenhouse gases, the feedback from a GIS-melt-reduced AMOC on climate sensitivity can be regarded as of only minor importance within the 500yr of our experiment length. On longer time scales its importance can potentially be much larger. Secondly, our results indicate that it is not straightforward to use reconstructions of past warm climates that are characterised by changes in the seasonal forcing, such as the PIG and LIG, to infer the climate sensitivity of the future warm climate that is dominated by greenhouse-gas forcing.

Because of the seasonality in the orbital forcing, it has been argued (e.g. Zeebe, 2013) that the Paleocene-Eocene Thermal Maximum (PETM) would be more suited to estimate climate sensitivity for future projections, because the PETM was also primarily greenhouse-gas driven. However, the PETM (about 55 million yrs ago) is about 50 million years before glaciation in the Northern Hemisphere occurred, making it unsuitable to study the feedback related to GIS melt. Another period sometimes referred to as a good analogue, in terms of insolation, is Marine Isotope Stage 11 because it had a similar seasonal distribution of insolation (Loutre and Berger, 2003). However, there are some uncertainties concerning whether it was generally warmer (Milker et al., 2013) than present-day climate or not (Loutre and Berger, 2003). Milker et al. (2013) indicate that regional differences are quite large, but on a global scale the surface ocean underwent deglacial warming in pace with CO_2 rise. However, it is unlikely that there was a period that matched "anthropogenic" development exactly, including all boundary conditions, such as ice sheets. Therefore, the problem of a correct analogue for future changes is very challenging and is accompanied by practical concerns about using data from periods so far back in time like data availability, uncertainties in the reconstructions and an overall lack of information about the boundary conditions in those climates.

Besides the discussion whether the early PIG and LIG are appropriate analogues for future changes, Valdes (2011) pointed out that the AMOC in the GCMs used for predictions of future warming, might not be sensitive enough to show abrupt changes such as cold stadial events recorded in the Greenland ice cores. However, according to our model experiments, the future AMOC is in two out of three cases less sensitive to GIS melt water than during the LIG and PIG, particularly because of reduced seasonal differences and winter warming. Our results partly suggest that future predictions are less impacted by freshwater sensitivity than the LIG and PIG, and that the insensitivity suggested by Valdes (2011) is thus possibly of less importance for future predictions. However, in our model this difference in sensitivity is mainly related to sea ice and Stroeve et al. (2007) found an overestimation of IPCC AR4 (2007) models and observed sea-ice cover over the last decades, that suggests, consistent with our results, that GCM's insensitivity is potentially related to sea-ice processes. This argumentation is supported by Goosse et al. (2007), who found that using different model parameter sets allowed a closer match to observed sea-ice extent. Their results suggest (based on a slightly different version of LOVECLIM and partly different parameter sets) that our least sensitive version (low; comparable to their parameter version E1) is likely to be too insensitive in terms of sea-ice response to recent reductions in sea-ice extent. Despite some differences between their parameter sets and ours, their findings suggest that the medium and high parameter sets are likely to result in a better representation of the climate. Therefore, we argue that the AMOC's sensitivity to GIS melt found in the medium and high parameter set is more trustworthy than results of the low version.

The close relation of sea-ice formation and deep convection accounts for a large part for the higher sensitivity of the AMOC to GIS melt in past climates compared to the future. At present we cannot assess how important the low complexity and resolution of our model is in relation

with sea-ice distribution and deep convection and therefore AMOC sensitivity. We thus encourage testing this result with higher complexity models, as the found threshold is model specific and is dependent on the physical approximations within a model. The parameterization of sub-grid processes such as convection or mixing is one example of that dependency, as observed values of these parameters are poorly known for the global ocean (Stone, 2004). Dalan et al. (2005) report for an EMIC that varying the diapycnal mixing, a parameter crucial for the ocean circulation, modifies the freshwater sensitivity of the ocean circulation and changes the threshold for a shutdown of the thermohaline circulation. Therefore, further testing could help us to better understand the parameterization of physical processes in our model that influence the interactions of convection and sea-ice formation, as these interactions appear to be clearly different in past and future climate scenarios.

The future will be in many ways different from the past. Catastrophic cooling events as recorded in the past are unlikely to happen within the next century (Meehl et al., 2007), but the question on how long the warming will continue remains important. The role of slow feedbacks, such as the interaction between the GIS and the AMOC, are critical to long-term changes in the climate system.

5.4 Conclusions

We have systematically analysed the impact of various GIS melt rates on the AMOC strength in two past warm climates and three future warming cases, and with three different model parameter sets that yield different sensitivities of the AMOC to a freshwater perturbation. Results with the two freshwater-sensitive model versions (medium and high) suggest: The AMOC sensitivity to GIS melt can be separated into two GIS melt ranges.

- In the first GIS melt range (<54 mSv), the AMOC's sensitivity differs between past and future climates and thus depends on the background climate.
  - The high/low AMOC sensitivity in the past/future climates corresponds well with larger/smaller seasonal temperature ranges.
  - This difference in AMOC sensitivity between past and future climates is strongly dependent on amount of freshwater being supplied to the Labrador Sea convection site. In climates with a stronger (past climates) or weaker (future climates) sea-ice expansion, more (past) or less (future) freshwater is being transported into the Labrador Sea, bringing the convection site closer to a local shutdown, given the same amount of GIS melting.
  - The increased freshwater transport by sea ice in the past climates compared to the future projections is a result of the enhanced seasonality. Both winter and summer temperatures act on the expansion of sea ice and the release of freshwater during summer.
  - Due to the difference of past and future AMOC sensitivity, it is likely that, for GIS melt fluxes <54 mSv, proxy-based reconstructions of past AMOC sensitivity will overestimate the importance of GIS melting if interpreted for future applications.
- In the second GIS melt range (>54 mSv), the AMOC's sensitivity is similar in all time periods investigated and thus independent of the background climate state.
  - The sea-ice extent varies stronger between model parameter sets (low, medium and high) than between past and future climates.
  - Proxy-based reconstructions of past AMOC sensitivity are likely to be applicable to future cases for GIS melt fluxes >54 mSv.

Results with the freshwater-insensitive version (low) suggest:

- The AMOC's sensitivity to GIS melt water is insensitive to the background climate state and the GIS melt water forcing.

- Proxy-based reconstructions of past AMOC sensitivity are likely to be applicable to future cases regardless of the applied GIS melt flux.

- However, the parameters in the low version are similar to a parameter set that was rejected by Goosse et al. (2007) for being too insensitive to simulate the observed recent decrease in sea-ice extent, rendering its predictions as less reliable for future interpretations.

Overall our results indicate that the AMOC's sensitivity in a model can be altered considerably by tuning its parameterized processes and that results are not independent of these choices. Furthermore, our results suggest that, in contrast to the past warm periods, the feedback from a GIS-melt-reduced AMOC has relatively little impact on future climate sensitivity because of the overwhelming GHG forced warming. However, this can potentially change if the balance between the magnitude of the warming and the climate feedback changes on the long run.

Chapter 6

Synthesis and Perspective

6.1 Synthesis

This thesis deals with climate variability in the Nordic Seas from numerical model simulations compared to proxy-based reconstructions during the Holocene. In the climate system, climate variability can be created by the components of the climate system and their response to forcings. We have shown in the previous chapters examples of the complex interaction between the atmosphere (chapter 3 - shelf flooding), the ocean and melting ice sheets (chapter 2,4,5). Our results show that changes forced to take place in one component of the climate system (e.g. fixed ice sheet melting, land-ocean changes) results in substantial changes in the other components and the overall climate, thus highlighting the strong interactivity between components of the climate system. Our results further indicate that the melting of the Greenland ice sheet and the shelf flooding in the Arctic influence the Nordic Seas climate considerably, thus highlighting this region as a region of climatic importance.

In the following section we give summaries and answers to the questions raised in the introduction before we extend a bit more on the assumptions and implications of our approach and future research challenges.

1st Research Question – *What is the impact of GIS melting on the Holocene Thermal Maximum?*

In one sentence: **In our model the GIS melt water cools the western Nordic Seas, and thus modifies the spatial structure of the HTM in the Nordic Seas, which compares better to proxy-based reconstructions of SSTs in the Nordic Seas.**

In chapter 2, we investigated in LOVECLIM experiments the impact of Greenland ice sheet (GIS) melting on the spatial and temporal expression of the Holocene Thermal Maximum, a period of relatively warm early Holocene climate in response to an orbitally forced summer insolation maximum. Proxy-based reconstructions in the North Atlantic and Nordic Seas region reveal a complex interaction of mechanisms and expression of the HTM. Previous studies have investigated the impact of the Laurentide ice sheet (LIS), as a remnant from the preceding glaciation, altering climate conditions with a continuous supply of melt water to the Labrador Sea and adjacent seas, and with a downwind cooling effect from the remnant LIS. The additional GIS melt water (up to 26 mSv) results in an additional ocean surface cooling of up to 2 K in the western Nordic Seas and a weak temperature reduction (0.5 K) in the eastern Nordic Seas. This thus alters the spatial structure of the HTM in the Nordic Seas considerably, delaying the response to the insolation maximum in western part longer (up to 1000 yrs) than the eastern part and aligning better with proxy-based reconstructions in the area. Our results confirm the regional importance of the GIS for understanding the HTM in the early Holocene.

The second effect the melting of the early Holocene ice sheets had on the climate, was the rising sea level. Melting of land-based ice sheets is directly linked to changes in sea level and the steady increase from low glacial to high interglacial levels, caused present-day shelf areas to be flooded. Hence the question:

2nd Research Question – *What impact does the flooding of an Arctic shelf introduce in the Nordic Seas?*

In one sentence: **In our model the flooding of the Siberian Shelf results in an annual cooling in the Nordic Seas, caused by a reduction of the meridional temperature gradient from land-ocean conversion.**

Glacial terminations are characterised by a strong rise in global sea level related to ice sheet melting. However this sea level rise is not uniform all over the world, because of regional effects (uplift and subsidence of coastal zones) are superimposed on global trends. In the early Holocene the Siberian shelf, Arctic continental shelf area, became flooded by 7.5 kyr BP and the coastline reached the modern-day high stand at about 5 kyr BP. This area is presently considered as one of the major sea-ice production zones in the Arctic Ocean and contributes to the sea-ice export through Fram Strait. In chapter 3, we investigated the flooding of this Siberian shelf and found a complex interplay of ocean-atmosphere interaction, which alters the Nordic Seas climate as a teleconnection transported via the atmosphere. The flooding of the shelf produces more Northern Hemisphere sea-ice (15%) and less Fram Strait sea-ice export (-15%). The changes in land-sea mask alter the atmospheric circulation, in particular the strength of the Polar Vortex, which transports the signal into the Nordic Seas, increasing the meridional component of the atmospheric flow. Hence the winter Greenland High and the Icelandic Low strengthen, yielding stronger winds on both sides of the Nordic Seas. Increased winds along the East Greenland Current support the local production of sea ice and transport southward, resulting in a southward shift of the convection area. A 4% decrease of the AMOC and the heat transport in the Atlantic basin (7%), result in an annual cooling pattern over the Nordic Seas by up to 4 K. Our results suggest that the flooding of Arctic shelf and in particular the Siberian Shelf, result in an negative feedback to orbitally-induced warming and related glacio-eustatic sea level rise.

Following from the investigation in research question #1 and the importance of the AMOC for the Nordic Seas climate as partly shown in the results of research question #2, we investigate further and ask the question:

3rd Research Question – *What was the strength of the AMOC and its subcomponents during the Holocene?*

In one sentence: **The modelled AMOC was lower in the early Holocene and reached modern-day values at about 7 kyr BP, which is partly confirmed by proxy-based reconstructions compared to different subcomponents of the AMOC in our model.**

The climate and the ocean circulation in the North Atlantic region changed over the course of the Holocene, partly because of disintegrating ice sheets and partly because of an orbital induced insolation trend. In the early Holocene, the Laurentide ice sheet cooled large parts of the Northern Hemisphere by melt fluxes into the North Atlantic and by the cooling effect of the remnant ice sheet itself. In the Nordic Seas, this impact was accompanied by a rather small, but significant, amount of Greenland ice sheet melting that reduced local ocean surface temperatures even further. After about 7 ka BP, these ice-sheet impacts vanished, marking the start of a relatively warm period (known as the Holocene Thermal Maximum period) under influence of the orbitally-forced, relatively high summer insolation. This was the warmest period in the Northern Hemisphere in the Holocene before the climate continued to follow the orbital induced cooling trend towards present-day. We have compared our model simulations with proxy-based reconstructions of $\delta^{13}\mathrm{C}$, sortable silt (SS) and magnetic susceptibility (κ) allowing to infer changes of past ocean circulation over the last 9000 years. The various reconstructions exhibit different long-term evolutions suggesting changes of either the overturning in the Atlantic in total or of subcomponents of the ocean circulation, such as the overflow waters across the Greenland-Scotland ridge (GSR). Thus the question rises whether these

reconstructions agree with each other or not? A comparison with model results indicates that $\delta^{13}C$, employed as an indicator of overturning, agrees well with the long-term evolution of the modelled overturning strength in the North Atlantic (AMOC). Regional differences in the reconstructions are most likely originating from influences of ^{13}C depleted water masses, such as Antarctic Bottom Water. The modelled AMOC evolution corresponds well to a $\delta^{13}C$ reconstruction in the Norwegian Sea, but the recorded magnitude is much smaller compared to the model. In a further step to trace Nordic Seas deep water across the GSR, we compared our model results to reconstructions employing SS and κ to infer changes in the Iceland-Scotland Overflow Waters (ISOW). Reconstructions at the Gardar Drift correspond well with modelled Nordic Seas normalized convective volume, representing overflow source waters. However, a direct comparison of modelled flow speed at the location and reconstructed deep-water flow strength from SS do not agree on the long-term evolution from 7 kyr BP towards present. In summary, the model results including early Holocene ice sheet impacts suggest that different long-term trends in subcomponents of the AMOC, such as ISOW, are consistent with proxy-based reconstructions and allow reconciling some of the reconstructions with each other. The modelled and reconstructed (from $\delta^{13}C$) AMOC strength over the past 9000 years, showed an early Holocene weakening and a fast recovery until about 7 kyr BP and a weak increasing trend of 12 mSv/kyr towards present, with relatively low variability on centennial to millennial time scales.

Following up from the results of question #1, showing the relatively large impact of GIS melting on the early Holocene climate (x1, x2, x4 GIS), and question #3, showing the long-term stability of the AMOC over the past 7,000 yrs, and given the likelihood of increased melt from the GIS under future emission scenarios, we ask the final question:

4th Research Question – *What is the impact of GIS melting beyond the Holocene and what can we learn for the future?*

In one sentence: **The modelled AMOC response to GIS melting, below 54 mSv (30% GIS ice volume), is weaker in climates with a weaker seasonal contrast, such as the future, compared to orbitally-forced warm past climates.**

The sensitivity of the climate system to changes in radiative forcing is crucial for our understanding of past and future climates. Especially important are feedbacks related to melting of ice sheets like the Greenland Ice Sheet (GIS) and its potential impact on the Atlantic meridional overturning circulation (AMOC). These effects are likely to delay and dampen predicted long-term warming trends. Estimates of climate sensitivity may be deduced from palaeoclimate-reconstructions, but this raises the question whether past climate sensitivity is applicable to the future. Therefore we have analysed the impact of GIS melt water on the AMOC strength in two past warm climates (Last Interglacial and early Present Interglacial) and three future scenarios with three different model parameter sets. These model parameter sets represent three different model sensitivities to freshwater perturbation: low, moderate and high. In both the moderate and high sensitivity versions, we find for lower GIS melt rates (below 54 mSv) a clear differences between past and future warm climates in the sensitivity of the AMOC to GIS melt. These differences are connected to the sea-ice cover extent. In contrast, for higher GIS melt rates (over 54 mSv) we find similar reductions of the AMOC strength in all cases. Considering the low sensitivity version of our model, we find that for all GIS melt rates the influence of freshwater forcing on the AMOC is independent of the background climate. Our results and implications are thus strongly determined by the parameter set considered in our model. Nonetheless, our results from two out of three model versions suggest that proxy-based reconstructions of past AMOC sensitivity to GIS melt are likely to be misleading if interpreted for future applications.

The thesis has provided detailed results to answer the above-mentioned questions with the help of the intermediate complexity model LOVECLIM. In particular this thesis has dealt with the impact of GIS melting on the early Holocene, the Last Interglacial and future climates, as well as impacts from Arctic shelf flooding.

6.2 Perspective

A fundamental question is to which extent weather and climate can be predicted? The nonlinear and chaotic nature of the climate system imposes natural limits on the extent to which skilful predictions of climate statistics can be done (Kirtman et al., 2013). For example, the predictability of weather is largely determined by uncertainty in a forecasts starting conditions, whilst the predictability of climate variations is also influenced by uncertainty in representing computationally the equations that govern climate (for example, how to represent the effects of convective instabilities in a model that cannot resolve individual cloud systems) and the boundary conditions (Palmer, 2000; Sun and Wang, 2013). Thus as Palmer (2000) writes: "*Chaos theory implies that all such environmental forecasts must be expressed probabilistically; the laws of physics dictate that society cannot expect arbitrarily accurate weather and climate forecasts.*" Estimates of predictability are achieved by running ensemble forecasts, which quantify uncertainty in weather and climate prediction. In practice, the economic value of a reliable probability forecast (produced from an ensemble prediction system) exceeds the value of a single deterministic forecast with uncertain accuracy (Palmer, 2000). While such ensemble simulations can address uncertainties in initial conditions and boundary conditions, uncertainties in model formulation are harder to account for. Multi-model ensembles such as in the 5th Coupled Model Intercomparison Project (CMIP5, Taylor et al., 2012) or the 3rd Palaeoclimate Modelling Intercomparison Project (PMIP3, Braconnot et al., 2012) are a first and necessary step towards better understanding

uncertainties. However, it can be argued that these models do not cover the full range of model uncertainties (Lambert and Boer, 2001; Knutti et al., 2013; Collins et al., 2013), as the different model definitions are not fully independent of each other. A particular problem of past climates and associated uncertainties reside on the initial and boundary conditions. For example, one possibility is to exclude the ice sheets as a dynamic component and make them a forcing, thus a boundary condition problem. Or another possibility is to make ice sheets a dynamical component and deal with the initialization of the ice sheet component, which is sensitive to the boundary conditions. For example, the ice sheet extent at the last glacial maximum is relatively well known (e.g. Dyke et al., 2002), but large uncertainties remain in the ice sheet thickness (Carlson and Clark, 2012). There is not simply one solution that can be reconstructed from geological evidence nor is there just one solution from a coupled dynamical ice sheet model. Obviously the changes in ice sheet topography make a difference in the rest of the climate system, thus indicating how crucial initial or boundary conditions can be for past climates as well. This is not only true for the ice sheet extent and topography, but also for the ice sheet melt water. Related to the volume of the ice sheets on land should be the corresponding sea level lowering and then as the ice starts to melt also the sea level rise and the melt water to the ocean surface. The implications of such sea level rise will be the flooding of shelf areas and most dramatically the opening or closing of the Bering Strait for example. Thus it is quite surprising how few of such features are represented in modeling frameworks, as there are numerous palaeoclimate applications and occurrences of such changes in the past. We can only hope that brilliant minds are at work as you read this to solve the corresponding problems to integrate such dynamical transformation of land and ocean into future modeling frameworks, as this transformation is clearly another climatic feedback in the response of the climate system to a forcing.

Inspired by the results summarized in this thesis and the challenges that

have been overcome to produce these results, I find myself drawn to the following future research directions and model developments:

1. The estimation of uncertainty in results is key in making reliable statements about past and future climate change, as well as variability. In climate modelling a good practice is to use ensembles applying slightly different initial conditions or forcings to address errors in the prescribed forcings and show dependencies in the results. The way these ensembles are created is critical as one would like to address uncertainty in all components of the climate system. This is likely to improve comparisons to proxy-based reconstructions as well.

2. Motivated by the results from chapter 3, on the shelf flooding in the Arctic, the atmospheric circulation and sea-ice production in the Arctic are key processes towards a better understanding of the dynamic floodings of past and future climate change. In particular the atmospheric circulation is relatively coarse in the results presented in this thesis and should be conducted with higher resolution models to validate the presented results. Related to this and to results from chapter 4, on the AMOC over the Holocene, it became clear that the resolution of the ocean model needs to be higher to represent overflow proxy-based reconstructions such as sortable silt. Regardless of localized effects, a higher resolution in the Nordic Seas and the sub-polar North Atlantic could be useful in the comparison to reconstructions and of course in representing ocean dynamics. This might also help to distinguish misleading information from useful.

3. A next step from the results presented in this thesis is to use dynamic ice sheets and their interaction with ocean and atmosphere. More specifically ice sheets should be coupled to ocean and atmosphere in a way that land-sea conversions can be simulated.

4. Although I am not an expert on proxy-based reconstructions or the involved data production techniques, I am a user and from a user

perspective I have to say that timing is everything. It should be considered standard practice to make "ensembles" of proxy-based reconstructions with uncertainties connected to the age model, the reconstructed values and the proxy itself, such as is done in proxy system modelling. This information would allow making better comparisons between model and proxy data.

Supplementary Information A

Holocene North Atlantic Overturning in an atmosphere-ocean-sea-ice model compared to proxy-based reconstructions

Individual records as presented in Fig. 4.9 in the main text.

Figure SI.A.1: Holocene proxy records of δ^{13}C, Magnetic Susceptibility (κ) and Sortable Silt (SS) from 9 different locations shown in Fig. 4.9 and summarized in Fig. 4.10 in the manuscript. The panels give individual core location in absolute values as supplied by the corresponding authors. a) SS from MD95-2024 (Hoogakker et al., 2011), b) SS from MD99-2251 (Hoogakker et al., 2011), c) SS from ODP984C (Praetorius et al., 2008), d) SS from MD08-3182Cq (Kissel et al., 2013), e) SS from Gardar-stack (Thornalley et al., 2013), f) δ^{13}C from MD08-3182Cq (Kissel et al., 2013), g) δ^{13}C from ODP980 (Oppo et al., 2003), h) δ^{13}C from MD95-2042 (Shackleton et al., 2000), i) δ^{13}C from ODP984C (Praetorius et al., 2008), j) δ^{13}C from GIK23258-2 (Sarnthein et al., 2003), k) κ from MD03-2676Cq (Kissel et al., 2013) and l) κ from MD08-3182Cq (Kissel et al., 2013). Thick lines denote smoothed splines (n=9 or n=21) to give longer term trends.

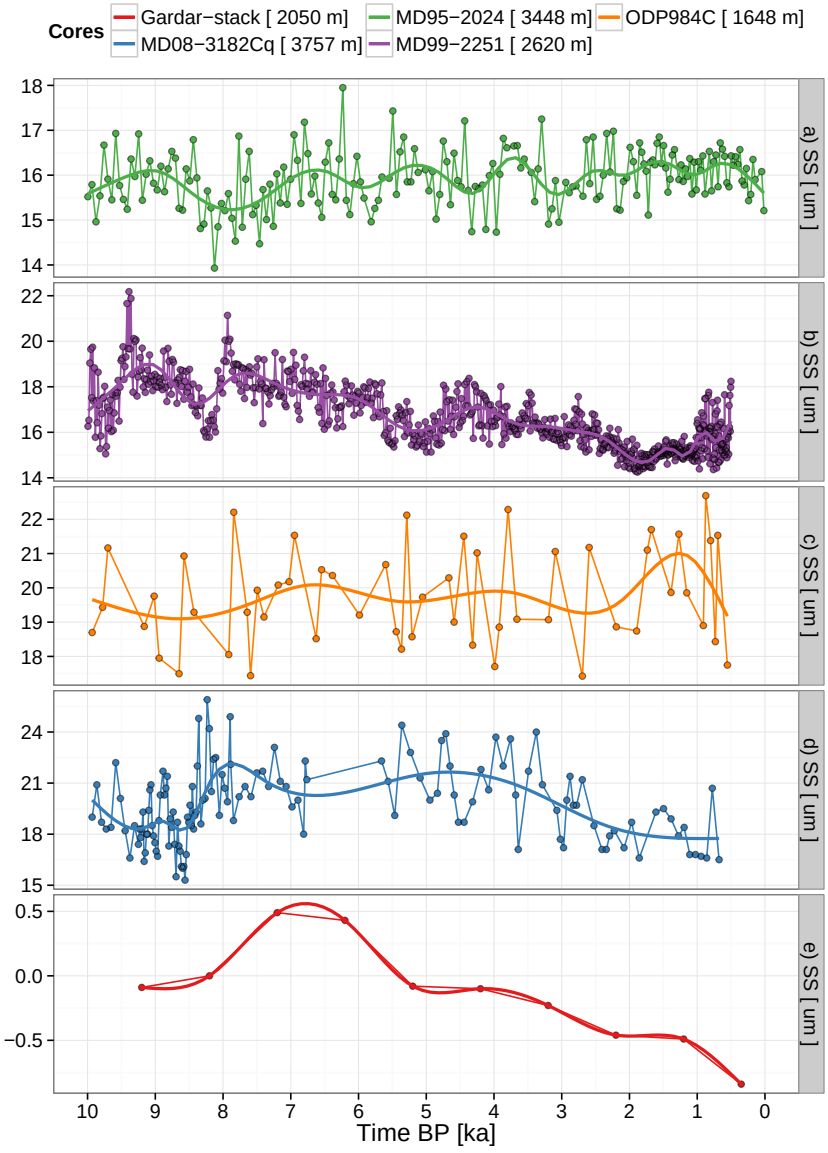

Figure SI.A.1: Sortable Silt Records (Caption on Page 183)

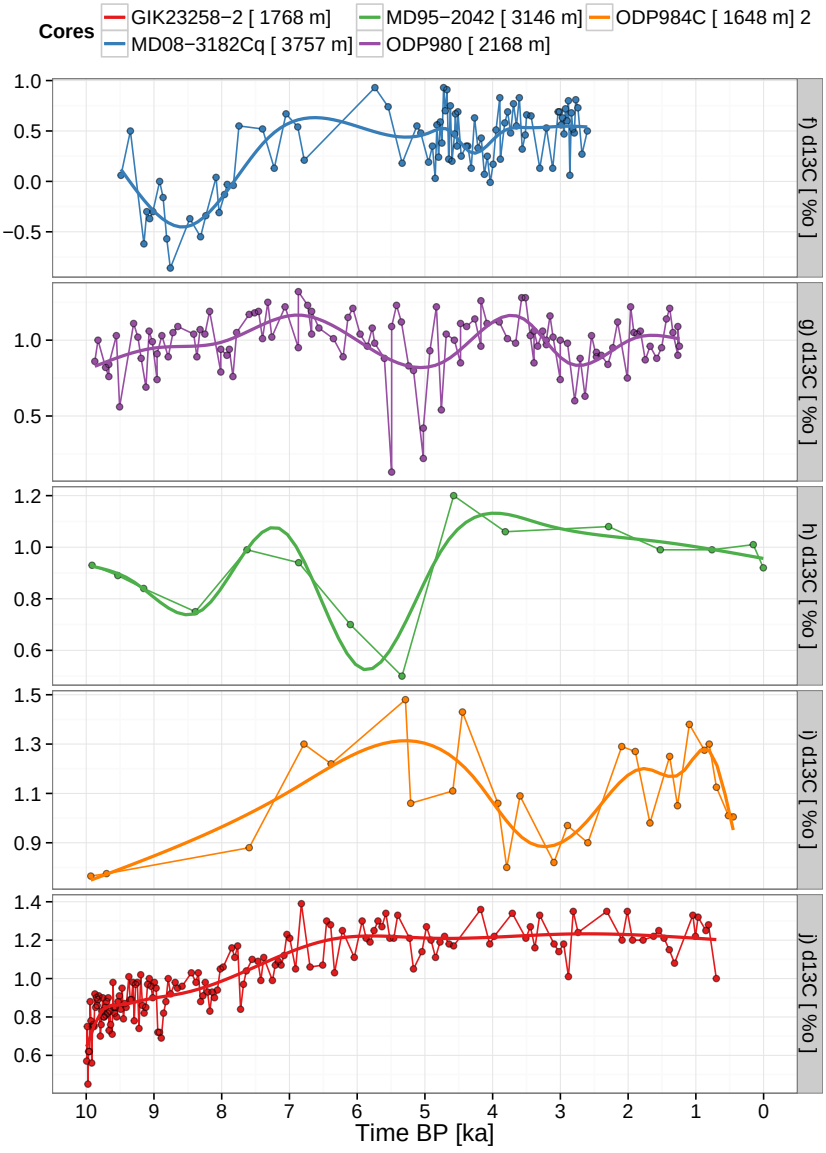

Figure SI.A.1: δ^{13}C Records (Caption on Page 183)

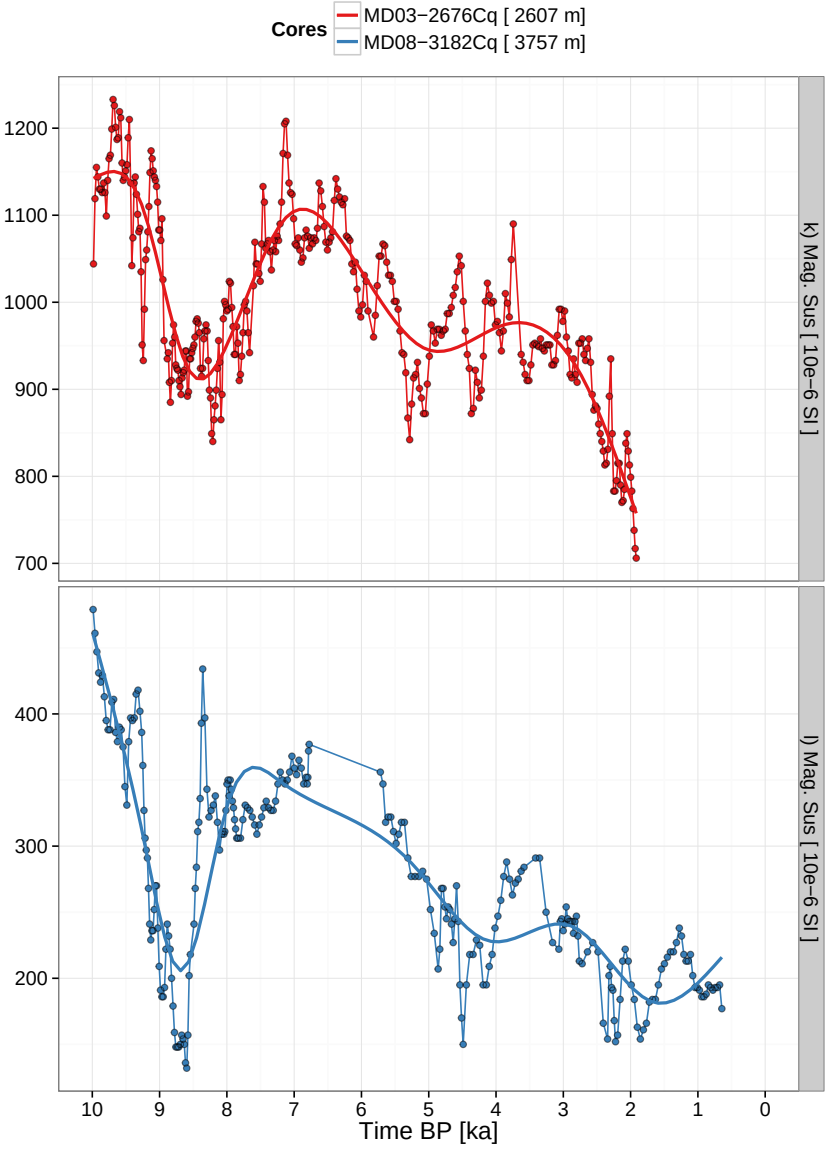

Figure SI.A.1: Magnetic Susceptibility (κ) Records (Caption on Page 183)

Supplementary Information B

The influence of Greenland Ice sheet melting on the Atlantic meridional overturning circulation during past and future warm periods: a model study

Contents:

1. Table of model parameter sets
2. Figure of impacts of some parameters on the model's freshwater and greenhouse-gas sensitivity
3. Figures of impacts of AMOC reductions vs. freshwater forcing from the GIS, as percentage and absolute values for individual simulations, as summarized in Fig. 5.3 in the main text.
4. Figure of changes of norm. convection volume at the different convection sites
5. Figure of sea surface density at the different convection sites

Additional Information for **Section 5.2.1**

The Model

Sensitivity of LOVECLIM to freshwater forcing with three different parameter sets (low, medium, high) and to a doubling of CO_2 concentrations, as defined by Loutre et al. (2011) and Goosse et al. (2010). We summarize the different effects of Tab. SI.B.1 and give indications of contributions to the observed differences. The main difference between the medium and the low version is the vertical diffusivity of the ocean, however other changes such as long-wave radiation are also likely to impact the difference between the two model versions. The main difference between the medium and the high version is the precipitation correction in the North Atlantic.

Table SI.B.1: Summary of model parameter sets and their corresponding names and values (c.f. Description of LOVECLIM in Goosse et al., 2010). A summary of these changes and their most likely impact on the sensitivity of the model is also given in Fig. SI.B.1.

	ModifiedParameter		medium	low	high	Unit
O	Diffusivity	avkb	1.50E-05	1.00E-05	-	$[m^2/s]$
	Albedo of the Ocean	albocef	0.95	1.00	0.90	
A	Exponent in LW Radiation Scheme	expir	0.40	0.33	-	
	Amplification of Moisture Profile in the Tropics affecting IR flux	hproftrop	1.25	1.00	1.20	
C	Precipitation Correction in Atlantic	corAN	-0.085	-	-0.0425	
low and high common	Coefficient of isopycnal diffusion	ai	300	200	200	$[m^2/s]$
	Gent-McWilliams thickness diffusion coefficient	aitd	300	200	200	$[m^2/s]$
	Rossby radii of deformation	$\lambda 2$	0.131	0.125	0.125	
		$\lambda 4$	0.071	0.07	0.07	
	Amplification of LW radiation feedback at 0°N	ampeqir	1.8	1.5	1.5	
	Amplification of Humidity Profile at the Equator	hprofeq	1.02	1.00	1.00	
	Amplification of Humidity Profile North Atlantic	hprofan	0.75	1.00	1.00	
	Albedo of snow	alphd	0.72	0.70	0.70	
	Albedo of bare ice	alphdi	0.62	0.60	0.60	
	Albedo of melting snow	alphs	0.53	0.51	0.51	
	Albedo of melting ice	albice	0.44	0.42	0.42	

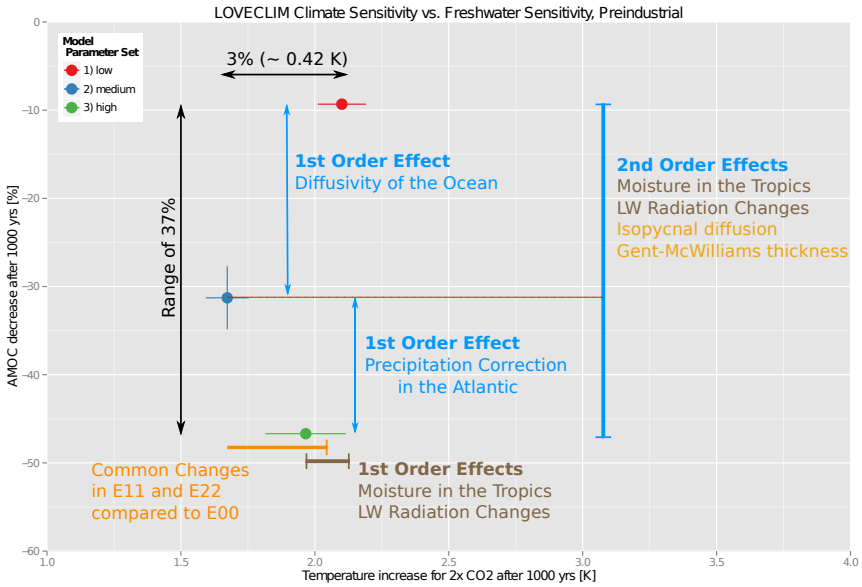

Figure SI.B.1: Schematic summary of impacts of parameter sets on freshwater and greenhouse-gas sensitivity of the model. We summarize the different changes of parameters in Tab. SI.B.1 and give indications of their possible impacts and separate them into differences between low and high (1st Order Effect) and common changes (2nd Order Effects). Unfortunately it is not possible to completely disentangle the impact of changes in each individual parameter. However, the 1st order effects are clear differences and are likely to stand out as a major difference towards the others. The 3% denote the temperature range converted to relative change similar to the values of the AMOC reductions.

Additional Information for **Section 5.3.1** Impact of freshwater forcing on the AMOC strength

We show the individual simulations (LIG, HOL, RCP3 ,RCP6 ,RCP85) per model parameter set as anomalies compared to the control simulations and as absolute values.

Figure SI.B.2: AMOC changes due to GIS freshwater forcing per model realization. In the first sub-figure AMOC reductions are in percentage for individual simulations. In the second sub-figure absolute values of AMOC strength are shown. AMOC strength is at 27°N and the mean value as well as the standard deviation (error bars) are based on the last 100 yrs of each simulation.

Figure SI.B.3: Summary of convection areas and normalized convective volume, that is calculated using the convective layer depth (above 200m) multiplied by the area and then normalized using the unperturbed volume. The advantage of using this potential volume is to get an idea of the importance of convective activity at a certain location and its contribution to the total convective volume production. Therefore have we included a total volume, represented by the red line. We further defined three convection areas, the Around Iceland (AI, 45°W-30°E, 50-64°N) including Irminger Sea convection, the Labrador Sea (LS, 90-45°W, 50-70°N) and the Norwegian Sea (NS, 45°W-30°E, 64-90°N). Shown are normalized values per region and model realization. The data used here is comparable to Fig. 5.4 in the main text and is based on the last 100 yrs of each simulation.

Figure SI.B.4: Summary of convection areas and sea surface density. We define a whole North Atlantic box (90-30°W, 35-90°N) and three convection areas, the Around Iceland (AI, 45°W-30°E, 50-64°N) including Irminger Sea convection, the Labrador Sea (LS, 90-45°W, 50-70°N) and the Norwegian Sea (NS, 45°W-30°E, 64-90°N). Shown are absolute values per region and model realization. The data used here is comparable to Fig. 5.1d in the main text and is based on the last 100 yrs of each simulation.

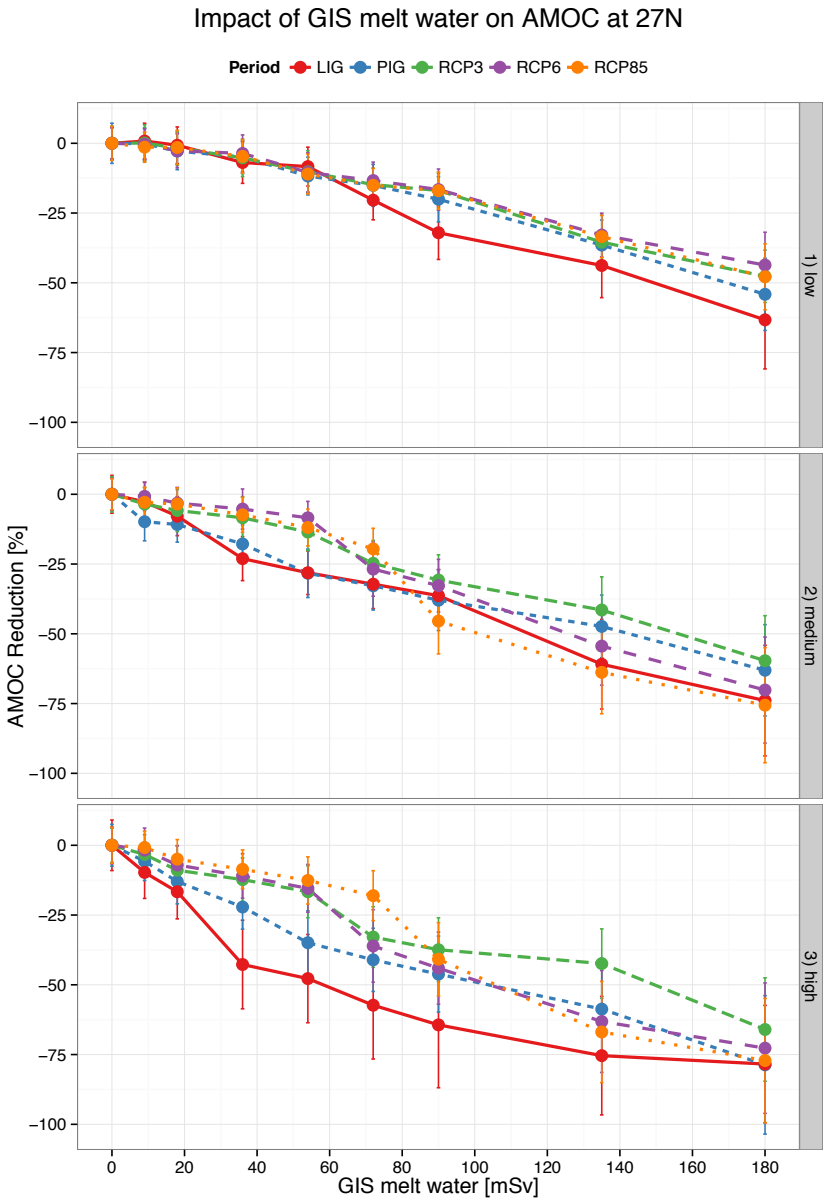

Figure SI.B.2: Relative AMOC Changes vs. GIS freshwater forcing.

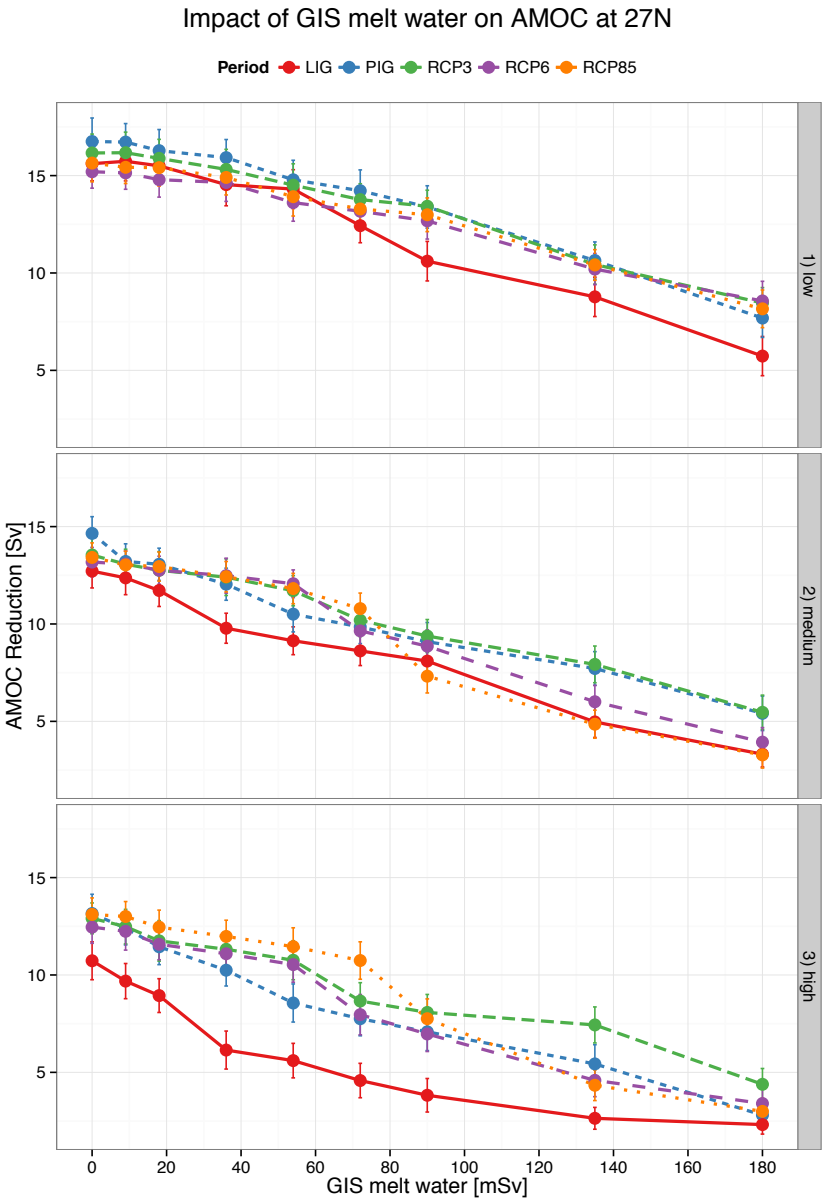

Figure SI.B.2: Absolute AMOC Changes vs. GIS freshwater forcing.

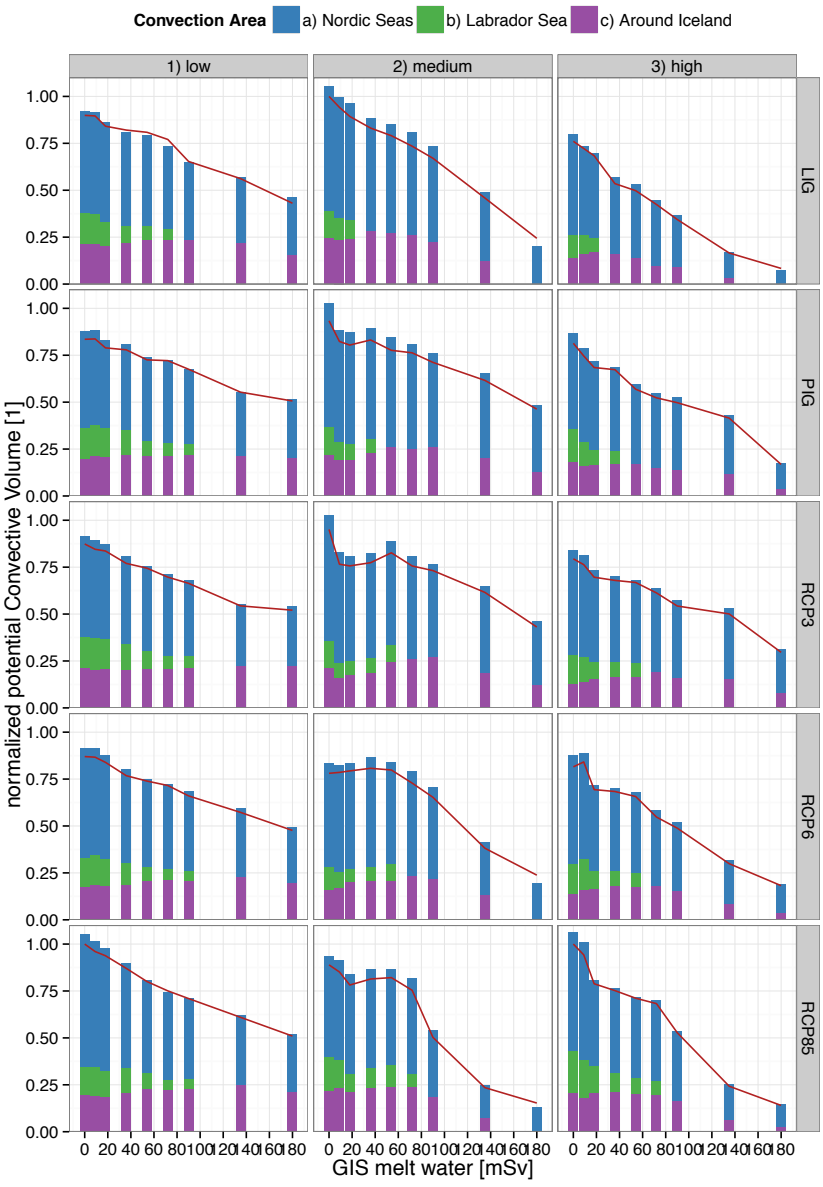

Figure SI.B.3: Summary of convection areas and normalized convective volume.

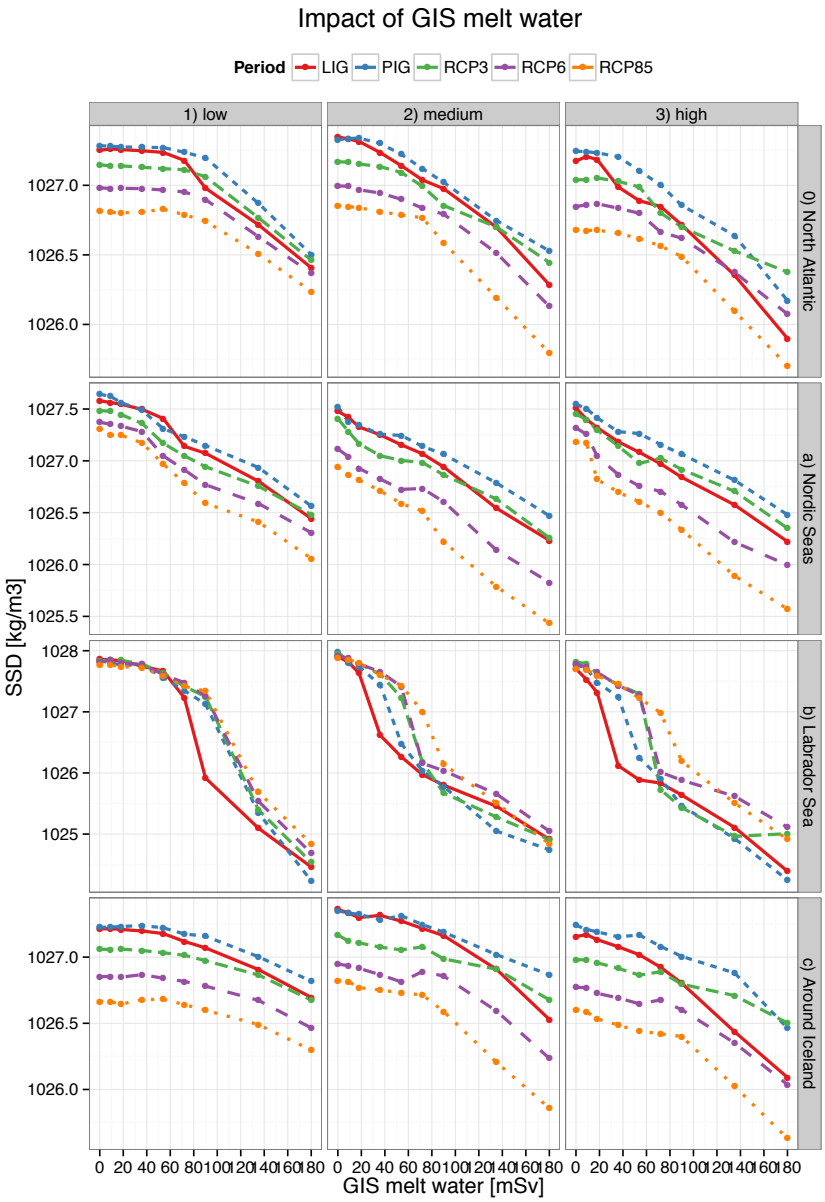

Figure SI.B.4: Summary of convection areas and sea surface density.

Bibliography

Alley, R. B.: Wally Was Right: Predictive Ability of the North Atlantic Conveyor Belt Hypothesis for Abrupt Climate Change, Annual Review of Earth and Planetary Sciences, 35, 241–272, doi: 10.1146/annurev.earth.35.081006.131524, 2007. 135

Alley, R. B. and Ágústsdóttir, A. M.: The 8k event: cause and consequences of a major Holocene abrupt climate change, Quaternary Science Reviews, 24, 1123–1149, doi: 10.1016/j.quascirev.2004.12.004, 2005. 22, 102

Alley, R. B., Mayewski, P. A., Sowers, T., Stuiver, M., Taylor, K. C., and Clark, P. U.: Holocene climatic instability: A prominent, widespread event 8200 yr ago, Geology, 25, 483–486, doi: 10.1130/0091-7613(1997)025⟨0483:HCIAPW⟩2.3.CO;2, 1997. 10, 135

Andersen, C., Koç, N., Jennings, A., and Andrews, J. T.: Nonuniform response of the major surface currents in the Nordic Seas to insolation forcing: Implications for the Holocene climate variability, Paleoceanography, 19, PA2003–, doi: 10.1029/2002PA000873, 2004a. 29, 30, 42, 43, 52, 53, 55

Andersen, C., Koç, N., and Moros, M.: A highly unstable Holocene climate in the subpolar North Atlantic: evidence from diatoms, Quaternary Science Reviews, 23, 2155–2166, doi: 10.1016/j.quascirev.2004.08.004, 2004b. 20

Andersson, C., Pausata, F. S. R., Jansen, E., Risebrobakken, B., and Telford, R. J.: Holocene trends in the foraminifer record from the Norwegian Sea and the North Atlantic Ocean, Climate of the Past, 6, 179–193, doi: 10.5194/cp-6-179-2010, 2010. 30, 45

Andrews, J., Darby, D., Eberle, D., Jennings, A., Moros, M., and Ogilvie, A.: A robust, multisite Holocene history of drift ice off northern Iceland: implications for North Atlantic climate, The Holocene, 19, 71–77, doi: 10.1177/0959683608098953, 2009. 62, 84, 85

Bakker, P., Van Meerbeeck, C. J., and Renssen, H.: Sensitivity of the North Atlantic climate to Greenland Ice Sheet melting during the Last Interglacial, Climate of the Past, 8, 995–1009, doi: 10.5194/cp-8-995-2012, 2012. 36, 140, 151

Bakker, P., Renssen, H., and Van Meerbeeck, C.: Early Last Interglacial Greenland Ice Sheet melting and a sustained period of meridional overturning weakening: a model analysis of the uncertainties, Climate Dynamics, pp. 1–15, doi: 10.1007/s00382-013-1935-1, 2013a. 146

Bakker, P., Stone, E. J., Charbit, S., Gröger, M., Krebs-Kanzow, U., Ritz, S. P., Varma, V., Khon, V., Lunt, D. J., Mikolajewicz, U., Prange, M., Renssen, H., Schneider, B., and Schulz, M.: Last interglacial temperature evolution - a model inter-comparison, Climate of the Past, 9, 605–619, doi: 10.5194/cp-9-605-2013, 2013b. 18, 148

Bamber, J., van den Broeke, M., Ettema, J., Lenaerts, J., and Rignot, E.: Recent large increases in freshwater fluxes from Greenland into the North Atlantic, Geophysical Research Letters, 39, L19 501–, doi: 10.1029/2012GL052552, 2012. 144

Bauch, H., Mueller-Lupp, T., Taldenkova, E., Spielhagen, R., Kassens, H., Grootes, P., Thiede, J., Heinemeier, J., and Petryashov, V.: Chronology of the Holocene transgression at the North Siberian margin, Global and Planetary Change, 31, 125–139, doi: 10.1016/S0921-8181(01)00116-3, 2001. 21, 61, 62, 63, 66, 68, 84

Berger, A. and Loutre, M.: Insolation values for the climate of the last 10 million years, Quaternary Science Reviews, 10, 297–317, doi: 10.1016/0277-3791(91)90033-Q, 1991. 3, 7, 37, 56, 103, 143

Berger, M., Brandefelt, J., and Nilsson, J.: The sensitivity of the Arctic sea ice to orbitally induced insolation changes: a study of the mid-Holocene Paleoclimate Modelling Intercomparison Project 2 and 3 simulations, Climate of the Past, 9, 969–982, doi: 10.5194/cp-9-969-2013, 2013. 19

Bianchi, G. G. and McCave, I. N.: Holocene periodicity in North Atlantic climate and deep-ocean flow south of Iceland, Nature, 397, 515–517, doi: 10.1038/17362, 1999. 22, 95, 135

Blaschek, M. and Renssen, H.: The Holocene thermal maximum in the Nordic Seas: the impact of Greenland Ice Sheet melt and other forcings in a coupled atmosphere–sea-ice–ocean model, Climate of the Past, 9, 1629–1643, doi: 10.5194/cp-9-1629-2013, 2013a. 18, 64, 65, 66, 67, 68, 75, 84, 85, 97, 98, 99, 102, 104, 119, 135, 143

Blaschek, M. and Renssen, H.: The impact of early Holocene Arctic shelf flooding on climate in an atmosphere-ocean-sea-ice model, Climate of the Past, 9, 2651–2667, doi: 10.5194/cp-9-2651-2013, 2013b.

Blaschek, M., Bakker, P., and Renssen, H.: The influence of Greenland ice sheet melting on the Atlantic meridional overturning circulation during past and future warm periods: a model study, Climate Dynamics, pp. 1–21, doi: 10.1007/s00382-014-2279-1, 2014.

Born, A., Nisancioglu, K. H., and Risebrobakken, B.: Late Eemian warming in the Nordic Seas as seen in proxy data and climate models, Paleoceanography, 26, PA2207–, doi: 10.1029/2010PA002027, 2011. 148

Bosch, T., Colijn, F., Ebinghaus, R., Körtzinger, A., Latif, M., Matthiessen, B., Melzner, F., Oschlies, A., Petersen, S., Proelß, A., Quaas, M., Requate, T., Reusch, T. B., Rosenstiel, P., Schrottke,

K., Sichelschmidt, H., Siebert, U., Soltwedel, R., Sommer, U., Stattegger, K., Sterr, H., Sturm, R., Treude, T., Vafeidis, A., van Bernem, C., van Beusekom, J., Visbeck, M., Wahl, M., Wallmann, K. J. G., Weinberger, F., Bollmann, M., Froese, R., Khalilian, S., Reichenbach, J., Schmidt, J., and Voss, R.: World Ocean Review 2010 : Mit den Meeren leben, Mare, Hamburg, URL `http://oceanrep.geomar.de/11936/`, 2010. 3, 4

Braconnot, P., Otto-Bliesner, B., Harrison, S., Joussaume, S., Peterchmitt, J.-Y., Abe-Ouchi, A., Crucifix, M., Driesschaert, E., Fichefet, T., Hewitt, C. D., Kageyama, M., Kitoh, A., Laîné, A., Loutre, M.-F., Marti, O., Merkel, U., Ramstein, G., Valdes, P., Weber, S. L., Yu, Y., and Zhao, Y.: Results of PMIP2 coupled simulations of the Mid-Holocene and Last Glacial Maximum - Part 1: experiments and large-scale features, Climate of the Past, 3, 261–277, doi: 10.5194/cp-3-261-2007, 2007. 18, 19

Braconnot, P., Harrison, S. P., Kageyama, M., Bartlein, P. J., Masson-Delmotte, V., Abe-Ouchi, A., Otto-Bliesner, B., and Zhao, Y.: Evaluation of climate models using palaeoclimatic data, Nature Climate Change, 2, 417–424, doi: 10.1038/nclimate1456, 2012. 19, 179

Broecker, W. S. and Peng, T. H.: Carbon cycle; 1985 glacial to interglacial changes in the operation of the global carbon cycle., Radiocarbon, 28, 309–327, 1986. 121

Brovkin, V., Bendtsen, J., Claussen, M., Ganopolski, A., Kubatzki, C., Petoukhov, V., and Andreev, A.: Carbon cycle, vegetation, and climate dynamics in the Holocene: Experiments with the CLIMBER-2 model, Global Biogeochemical Cycles, 16, 86–1–86–20, doi: 10.1029/2001GB001662, 2002. 16, 33, 66, 101, 137

Calvo, E., Grimalt, J., and Jansen, E.: High resolution U37K sea surface temperature reconstruction in the Norwegian Sea during the Holocene, Quaternary Science Reviews, 21, 1385–1394, doi: 10.1016/S0277-3791(01)00096-8, 2002. 30, 42, 43, 52, 53, 55

Campin, J.-M. and Goosse, H.: Parameterization of density-driven downsloping flow for a coarse-resolution ocean model in z-coordinate, Tellus Series A, 51, 412, doi: 10.1034/j.1600-0870.1999.t01-3-00006.x, 1999. 16, 101

Carlson, A. E. and Clark, P. U.: Ice sheet sources of sea level rise and freshwater discharge during the last deglaciation, Reviews of Geophysics, 50, doi: 10.1029/2011RG000371, 2012. 10, 61, 180

Charbit, S., Ritz, C., Philippon, G., Peyaud, V., and Kageyama, M.: Numerical reconstructions of the Northern Hemisphere ice sheets through the last glacial-interglacial cycle, Climate of the Past, 3, 15–37, 2007. 17

Clark, P. U., Marshall, S. J., Clarke, G. K. C., Hostetler, S. W., Licciardi, J. M., and Teller, J. T.: Freshwater Forcing of Abrupt Climate Change During the Last Glaciation, Science, 293, 283–287, doi: 10.1126/science.1062517, 2001. 10

Claussen, M., Mysak, L. A., Weaver, A. J., Crucifix, M., Fichefet, T., Loutre, M.-F., Weber, S. L., Alcamo, J., Alexeev, V. A., Berger, A., Calov, R., Ganopolski, A., Goosse, H., Lohmann, G., Lunkeit, F., Mokhov, I. I., Petoukhov, V., Stone, P., and Wang, Z.: Earth system models of intermediate complexity: closing the gap in the spectrum of climate system models, Climate Dynamics, 18, 579–586, doi: 10.1007/s00382-001-0200-1, 2002. 14

Collins, M., Knutti, R., Arblaster, J., Dufresne, J.-L., Fichefet, T., Friedlingstein, P., Gao, X., Gutowski, W. J., Johns, T., Krinner, G., Shongwe, M., Tebaldi, C., Weaver, A. J., and Wehner, M.: Long-term Climate Change: Projections, Commitments and Irreversibility, book section 12, pp. 1029–1136, Cambridge University Press, Cambridge, United Kingdom and New York, NY, USA, 2013. 180

Cortese, G., Dolven, J. K., Bjrklund, K. R., and Malmgren, B. A.: Late PleistoceneHolocene radiolarian paleotemperatures in the Norwegian

Sea based on artificial neural networks, Palaeogeography, Palaeoclimatology, Palaeoecology, 224, 311–332, doi: 10.1016/j.palaeo.2005.04.015, 2005. 30

Crucifix, M.: Why could ice ages be unpredictable?, Climate of the Past, 9, 2253–2267, doi: 10.5194/cp-9-2253-2013, 2013. 6

Crucifix, M., Loutre, M.-F., Tulkens, P., Fichefet, T., and Berger, A.: Climate evolution during the Holocene: a study with an Earth system model of intermediate complexity, Climate Dynamics, 19, 43–60, doi: 10.1007/s00382-001-0208-6, 2002. 19

Curry, W. B., Duplessy, J. C., Labeyrie, L. D., and Shackleton, N. J.: Changes in the distribution of 13C of deep water CO2 between the Last Glaciation and the Holocene, Paleoceanography, 3, 317–341, doi: 10.1029/PA003i003p00317, 1988. 97

Dahl-Jensen, D., Albert, M., Aldahan, A., Azuma, N., Balslev-Clausen, D., Baumgartner, M., Berggren, A.-M., Bigler, M., Binder, T., Blunier, T., et al.: Eemian interglacial reconstructed from a Greenland folded ice core, Nature, 493, 489–494, doi: 10.1038/nature11789, 2013. 23, 142

Dalan, F., Stone, P. H., Kamenkovich, I. V., and Scott, J. R.: Sensitivity of the Ocean's Climate to Diapycnal Diffusivity in an EMIC. Part I: Equilibrium State., Journal of Climate, 18, 2460–2481, doi: 10.1175/JCLI3411.1, 2005. 169

Dansgaard, W.: Stable isotopes in precipitation, Tellus, 16, 436–468, 1964. 12

Darby, D. A., Polyak, L., and Bauch, H. A.: Past glacial and interglacial conditions in the Arctic Ocean and marginal seas a review, Progress in Oceanography, 71, 129–144, doi: 10.1016/j.pocean.2006.09.009, 2006. 21

Dethleff, D. and Kuhlmann, G.: Fram Strait sea-ice sediment provinces based on silt and clay compositions identify Siberian Kara and Laptev seas as main source regions, Polar Research, 29, 265–282, doi: 10.1111/j.1751-8369.2010.00149.x, 2010. 21, 63

Dethleff, D., Loewe, P., and Kleine, E.: The Laptev Sea flaw leaddetailed investigation on ice formation and export during 1991/1992 winter season, Cold Regions Science and Technology, 27, 225–243, doi: 10.1016/S0165-232X(98)00005-6, 1998. 62

Dickson, R., Rudels, B., Dye, S., Karcher, M., Meincke, J., and Yashayaev, I.: Current estimates of freshwater flux through Arctic and subarctic seas, Progress In Oceanography, 73, 210–230, doi: 10.1016/j.pocean.2006.12.003, 2007. 23, 31, 144

Dickson, R. R. and Brown, J.: The production of North Atlantic Deep Water: Sources, rates, and pathways, Journal of Geophysical Research: Oceans, 99, 12 319–12 341, doi: 10.1029/94JC00530, 1994. 94

Dmitrenko, I. A., Kirillov, S. A., Tremblay, L. B., Bauch, D., and Willmes, S.: Sea-ice production over the Laptev Sea shelf inferred from historical summer-to-winter hydrographic observations of 1960s-1990s, Geophysical Research Letters, 36, L13 605–, doi: 10.1029/2009GL038775, 2009. 63

Dolven, J. K., Cortese, G., and Bjørklund, K. R.: A high-resolution radiolarian-derived paleotemperature record for the Late Pleistocene-Holocene in the Norwegian Sea, Paleoceanography, 17, 1072–, doi: 10.1029/2002PA000780, 2002. 30

Driesschaert, E., Fichefet, T., Goosse, H., Huybrechts, P., Janssens, I., Mouchet, A., Munhoven, G., Brovkin, V., and Weber, S. L.: Modeling the influence of Greenland ice sheet melting on the Atlantic meridional overturning circulation during the next millennia, Geophysical Research Letters, 34, L10 707–, doi: 10.1029/2007GL029516, 2007. 32

Drijfhout, S. S. and Hazeleger, W.: Changes in MOC and gyre-induced Atlantic Ocean heat transport, Geophysical Research Letters, 33, L07 707, doi: 10.1029/2006GL025807, 2006. 134

Dutton, A. and Lambeck, K.: Ice Volume and Sea Level During the Last Interglacial, Science, 337, 216–, doi: 10.1126/science.1205749, 2012. 142

Dyke, A., Andrews, J., Clark, P., England, J., Miller, G., Shaw, J., and Veillette, J.: The Laurentide and Innuitian ice sheets during the Last Glacial Maximum, Quaternary Science Reviews, 21, 9–31, doi: 10.1016/S0277-3791(01)00095-6, 2002. 180

Elias, S. A., Short, S. K., Nelson, C. H., and Birks, H. H.: Life and times of the Bering land bridge, Nature, 382, 60–63, doi: 10.1038/382060a0, 1996. 67

Elliot, M., Labeyrie, L., and Duplessy, J.-C.: Changes in North Atlantic deep-water formation associated with the DansgaardOeschger temperature oscillations (6010 ka), Quaternary Science Reviews, 21, 1153 – 1165, doi: 10.1016/S0277-3791(01)00137-8, 2002. 135

Emiliani, C.: Pleistocene Temperatures, Journal of Geology, 63, 538–578, doi: 10.1086/626295, 1955. 13

Emiliani, C.: Oxygen Isotopic Analysis of the Size Fraction Between 62 and 250 Micrometers in Caribbean Cores P6304-8 and P6304-9, Science, 198, 1255–1256, doi: 10.1126/science.198.4323.1255, 1977. 12

Emiliani, C.: The cause of the ice ages, Earth and Planetary Science Letters, 37, 349–354, doi: 10.1016/0012-821X(78)90050-X, 1978. 12

Fagel, N. and Mattielli, N.: Holocene evolution of deep circulation in the northern North Atlantic traced by Sm, Nd and Pb isotopes and bulk sediment mineralogy, Paleoceanography, 26, doi: 10.1029/2011PA002168, 2011. 95

Fichefet, T. and Maqueda, M. A. M.: Sensitivity of a global sea ice model to the treatment of ice thermodynamics and dynamics, Journal of Geophysical Research, 102, 12 609–12 646, doi: 10.1029/97JC00480, 1997. 16, 33, 65, 101, 137

Fichefet, T. and Maqueda, M. A. M.: Modelling the influence of snow accumulation and snow-ice formation on the seasonal cycle of the Antarctic sea-ice cover, Climate Dynamics, 15, 251–268, doi: 10.1007/s003820050280, 1999. 16, 33, 65, 101, 137

Fichefet, T., Poncin, C., Goosse, H., Huybrechts, P., Janssens, I., and Le Treut, H.: Implications of changes in freshwater flux from the Greenland ice sheet for the climate of the 21st century, Geophysical Research Letters, 30, 1911–, doi: 10.1029/2003GL017826, 2003. 134

Flato, G., Marotzke, J., Abiodun, B., Braconnot, P., Chou, S., Collins, W., Cox, P., Driouech, F., Emori, S., Eyring, V., Forest, C., Gleckler, P., Guilyardi, E., Jakob, C., Kattsov, V., Reason, C., and Rummukainen, M.: Evaluation of Climate Models, book section 9, pp. 741–866, Cambridge University Press, Cambridge, United Kingdom and New York, NY, USA, 2013. 14, 15

Fleming, K. and Lambeck, K.: Constraints on the Greenland Ice Sheet since the Last Glacial Maximum from sea-level observations and glacial-rebound models, Quaternary Science Reviews, 23, 1053–1077, doi: 10.1016/j.quascirev.2003.11.001, 2004. 143

Fontugne, M. and Duplessy, J. C.: Carbon isotope ratio of marine plankton related to surface water masses, Earth and Planetary Science Letters, 41, 365–371, doi: 10.1016/0012-821X(78)90191-7, 1978. 12

Friedrich, T., Timmermann, A., Menviel, L., Elison Timm, O., Mouchet, A., and Roche, D. M.: The mechanism behind internally generated centennial-to-millennial scale climate variability in an earth system model of intermediate complexity, Geoscientific Model Development, 3, 377–389, doi: 10.5194/gmd-3-377-2010, 2010. 21, 64

Funder, S., Goosse, H., Jepsen, H., Kaas, E., Kjr, K. H., Korsgaard, N. J., Larsen, N. K., Linderson, H., Lys, A., Mller, P., Olsen, J., and Willerslev, E.: A 10,000-Year Record of Arctic Ocean Sea-Ice VariabilityView from the Beach, Science, 333, 747–750, doi: 10.1126/science.1202760, 2011a. 20, 31

Funder, S., Kjeldsen, K. K., Kjr, K. H., and Cofaigh, C.: Chapter 50 - The Greenland Ice Sheet During the Past 300,000 Years: A Review, in: Quaternary Glaciations - Extent and Chronology A Closer Look, edited by Jrgen Ehlers, P. L. G. and Hughes, P. D., vol. Volume 15, pp. 699–713, Elsevier, doi: 10.1016/B978-0-444-53447-7.00050-7, 2011b. 143

Ganachaud, A. and Wunsch, C.: Large-Scale Ocean Heat and Freshwater Transports during the World Ocean Circulation Experiment, Journal of Climate, 16, 696–705, doi: 10.1175/1520-0442(2003)016⟨0696:LSOHAF⟩2.0.CO;2, 2003. 8, 94

Ganopolski, A. and Rahmstorf, S.: Rapid changes of glacial climate simulated in a coupled climate model, Nature, 409, 153–158, doi: 10.1038/35051500, 2001. 7, 133, 135, 145

Gherardi, J.-M., Labeyrie, L., Nave, S., Francois, R., McManus, J. F., and Cortijo, E.: Glacial-interglacial circulation changes inferred from 231Pa/230Th sedimentary record in the North Atlantic region, Paleoceanography, 24, doi: 10.1029/2008PA001696, 2009. 95

Ghil, M.: Natural climate variability, Encyclopedia of global environmental change, 1, 544–549, 2002. 2, 3

Goodess, C., Palutikof, J., and Davies, T.: The nature and causes of climate change : assessing the long-term future, Belhaven [etc.], London [etc.], 1992. 3

Goosse, H. and Fichefet, T.: Importance of ice-ocean interactions for the global ocean circulation: A model study, Journal of Geophysical

Research, 104, 23 337–, doi: 10.1029/1999JC900215, 1999. 16, 33, 65, 101, 137

Goosse, H. and Renssen, H.: A two-phase response of the Southern Ocean to an increase in greenhouse gas concentrations, Geophysical Research Letters, 28, 3469–3472, doi: 10.1029/2001GL013525, 2001. 71, 82

Goosse, H., Selten, F., Haarsma, R., and Opsteegh, J.: Decadal variability in high northern latitudes as simulated by an intermediate-complexity climate model, Annals of Glaciology, 33, 525–532, doi: 10.3189/172756401781818482, 2001. 71

Goosse, H., Selten, F. M., Haarsma, R. J., and Opsteegh, J. D.: Large sea-ice volume anomalies simulated in a coupled climate model, Climate Dynamics, 20, 523–536, doi: 10.1007/s00382-002-0290-4, 2003. 71, 82

Goosse, H., Driesschaert, E., Fichefet, T., and Loutre, M.-F.: Information on the early Holocene climate constrains the summer sea ice projections for the 21st century, Climate of the Past, 3, 683–692, doi: 10.5194/cp-3-683-2007, 2007. 33, 65, 70, 138, 168, 171

Goosse, H., Brovkin, V., Fichefet, T., Haarsma, R., Huybrechts, P., Jongma, J., Mouchet, A., Selten, F., Barriat, P.-Y., Campin, J.-M., Deleersnijder, E., Driesschaert, E., Goelzer, H., Janssens, I., Loutre, M.-F., Morales Maqueda, M. A., Opsteegh, T., Mathieu, P.-P., Munhoven, G., Pettersson, E. J., Renssen, H., Roche, D. M., Schaeffer, M., Tartinville, B., Timmermann, A., and Weber, S. L.: Description of the Earth system model of intermediate complexity LOVECLIM version 1.2, Geoscientific Model Development, 3, 603–633, doi: 10.5194/gmd-3-603-2010, 2010. 15, 16, 17, 18, 32, 33, 34, 48, 64, 65, 66, 100, 101, 137, 138, 188

Gradstein, F. M., Ogg, J. G., and Smith, A. G.: A Geologic Time Scale 2004, 2005. 5

Hansen, B. and Østerhus, S.: North Atlantic - Nordic Seas exchanges, Progress in Oceanography, 45, 109 – 208, doi: 10.1016/S0079-6611(99)00052-X, 2000. 94

Hays, J. D., Imbrie, J., and Shackleton, N. J.: Variations in the Earth's Orbit: Pacemaker of the Ice Ages, Science, 194, 1121–1132, doi: 10.1126/science.194.4270.1121, 1976. 5, 13

Held, I. M. and Suarez, M. J.: A Two-Level Primitive Equation Atmospheric Model Designed for Climatic Sensitivity Experiments., Journal of Atmospheric Sciences, 35, 206–229, doi: 10.1175/1520-0469(1978)035⟨0206:ATLPEA⟩2.0.CO;2, 1978. 15

Helsen, M. M., van de Berg, W. J., van de Wal, R. S. W., van den Broeke, M. R., and Oerlemans, J.: Coupled regional climate–ice-sheet simulation shows limited Greenland ice loss during the Eemian, Climate of the Past, 9, 1773–1788, doi: 10.5194/cp-9-1773-2013, 2013. 142

Hillaire-Marcel, C., de Vernal, A., Bilodeau, G., and Weaver, A. J.: Absence of deep-water formation in the Labrador Sea during the last interglacial period, Nature, 410, 1073–1077, doi: 10.1038/35074059, 2001. 36, 100, 121

Hillaire-Marcel, C., de Vernal, A., and Piper, D. J. W.: Lake Agassiz Final drainage event in the northwest North Atlantic, Geophysical Research Letters, 34, L15 601–, doi: 10.1029/2007GL030396, 2007. 10, 36

Hofmann, M., Rahmstorf, S., and Schellnhuber, H. J.: On the Stability of the Atlantic Meridional Overturning Circulation, Proceedings of the National Academy of Sciences of the United States of America, 106, pp.20 584–20 589, doi: 10.1073/pnas.0909146106, 2009. 134

Hoogakker, B. A. A., Chapman, M. R., McCave, I. N., Hillaire-Marcel, C., Ellison, C. R. W., Hall, I. R., and Telford, R. J.: Dynamics of

North Atlantic Deep Water masses during the Holocene, Paleoceanography, 26, PA4214, doi: 10.1029/2011PA002155, 2011. 95, 114, 115, 117, 118, 119, 121, 183

Hu, A., Meehl, G. A., Han, W., and Yin, J.: Effect of the potential melting of the Greenland Ice Sheet on the Meridional Overturning Circulation and global climate in the future, Deep Sea Research Part II: Topical Studies in Oceanography, 58, 1914 – 1926, doi: 10.1016/j.dsr2.2010.10.069, 2011. 134, 146

Huang, R. X.: Ocean, Energy Flows in, in: Encyclopedia of Energy, edited by Cleveland, C. J., pp. 497 – 509, Elsevier, New York, doi: 10.1016/B0-12-176480-X/00053-X, 2004. 9, 93

Huybers, P.: Early Pleistocene Glacial Cycles and the Integrated Summer Insolation Forcing, Science, 313, 508–511, doi: 10.1126/science.1125249, 2006. 140, 141, 142, 143, 145

Huybers, P. and Wunsch, C.: Paleophysical Oceanography with an Emphasis on Transport Rates, Annual Review of Marine Science, 2, 1–34, doi: 10.1146/annurev-marine-120308-081056, 2010. 13, 18

Huybrechts, P.: Sea-level changes at the LGM from ice-dynamic reconstructions of the Greenland and Antarctic ice sheets during the glacial cycles, Quaternary Science Reviews, 21, 203–231, doi: 10.1016/S0277-3791(01)00082-8, 2002. 16

Huybrechts, P., Goelzer, H., Janssens, I., Driesschaert, E., Fichefet, T., Goosse, H., and Loutre, M.-F.: Response of the Greenland and Antarctic Ice Sheets to Multi-Millennial Greenhouse Warming in the Earth System Model of Intermediate Complexity LOVECLIM, Surveys in Geophysics, 32, 397–416, doi: 10.1007/s10712-011-9131-5, 2011. 16

Imbrie, J., van Donk, J., and Kipp, N. G.: Paleoclimatic investigation of a late Pleistocene Caribbean deep-sea core: Comparison of isotopic

and faunal methods*1, Quaternary Research, 3, 10–38, doi: 10.1016/0033-5894(73)90051-3, 1973. 13

IPCC: Climate Change: The Scientific Basis, chap. 6, pp. 349–416, Cambridge University Press, Cambridge, UK and New York, NY, USA, 2001. 37, 103, 140

IPCC: Climate Change 2013: The Physical Science Basis. Contribution of Working Group I to the Fifth Assessment Report of the Intergovernmental Panel on Climate Change, Cambridge University Press, Cambridge, United Kingdom and New York, NY, USA, 2013. 1, 14

Irval, N., Ninnemann, U. S., Galaasen, E. V., Rosenthal, Y., Kroon, D., Oppo, D. W., Kleiven, H. F., Darling, K. F., and Kissel, C.: Rapid switches in subpolar North Atlantic hydrography and climate during the Last Interglacial (MIS 5e), Paleoceanography, 27, doi: 10.1029/2011PA002244, 2012. 135

Jakobsson, M.: Hypsometry and volume of the Arctic Ocean and its constituent seas, Geochemistry, Geophysics, Geosystems, 3, 1–18, doi: 10.1029/2001GC000302, 2002. 21

Jansen, E., Overpeck, J., Briffa, K., Duplessy, J.-C., Joos, F., Masson-Delmotte, V., Olago, D., Otto-Bliesner, B., Peltier, W., Rahmstorf, S., Ramesh, R., Raynaud, D., Rind, D., Solomina, O., Villalba, R., and Zhang, D.: Palaeoclimate. In: Climate Change 2007: The Physical Science Basis, URL `http://www.ipcc.ch/publications_and_data/ar4/wg1/en/ch6.html`, 2007. 28, 121

Jansen, E., Andersson, C., Moros, M., Nisancioglu, K. H., Nyland, B. F., and Telford, R. J.: The Early to Mid-Holocene Thermal Optimum in the North Atlantic, pp. 123–137, Wiley Blackwell, doi: 10.1002/9781444300932.ch5, 2008. 28, 30

Jennings, A. E., Knudsen, K. L., Hald, M., Hansen, C. V., and Andrews, J. T.: A mid-Holocene shift in Arctic sea-ice variability on the East Greenland Shelf, The Holocene, 12, 49–58, doi: 10.1191/0959683602hl519rp, 2002. 62, 85

Johannessen, O. M., Bengtsson, L., Miles, M. W., Kuzmina, S. I., Semenov, V. A., Alekseev, G. V., Nagurnyi, A. P., Zakharov, V. F., Bobylev, L. P., Pettersson, L. H., Hasselmann, K., and Cattle, H. P.: Arctic climate change: observed and modelled temperature and sea-ice variability, Tellus A, 56, 328–341, doi: 10.1111/j.1600-0870.2004.00060.x, 2004. 11

Johns, W. E., Baringer, M. O., Beal, L. M., Cunningham, S. A., Kanzow, T., Bryden, H. L., Hirschi, J. J. M., Marotzke, J., Meinen, C. S., Shaw, B., and Curry, R.: Continuous, Array-Based Estimates of Atlantic Ocean Heat Transport at 26.5N, Journal of Climate, 24, 2429–2449, doi: 10.1175/2010JCLI3997.1, 2011. 8, 93, 133

Joussaume, S. and Braconnot, P.: Sensitivity of paleoclimate simulation results to season definitions, Journal of Geophysical Research: Atmospheres, 102, 1943–1956, doi: 10.1029/96JD01989, 1997. 146

Jungclaus, J. H., Macrander, A., and Kse, R. H.: Modelling the Overflows Across the Greenland-Scotland Ridge, in: Arctic-Subarctic Ocean Fluxes, edited by Dickson, R., Meincke, J., and Rhines, P., pp. 527–549, Springer Netherlands, doi: 10.1007/978-1-4020-6774-7_23, 2008. 95, 107

Junge, M., Blender, R., Fraedrich, K., Gayler, V., Luksch, U., and Lunkeit, F.: A world without Greenland: impacts on the Northern Hemisphere winter circulation in low- and high-resolution models, Climate Dynamics, 24, 297–307, doi: 10.1007/s00382-004-0501-2, 2005. 137

Kanzow, T., Cunningham, S. A., Johns, W. E., Hirschi, J. J.-M., Marotzke, J., Baringer, M. O., Meinen, C. S., Chidichimo, M. P.,

Atkinson, C., Beal, L. M., Bryden, H. L., and Collins, J.: Seasonal Variability of the Atlantic Meridional Overturning Circulation at 26.5N, Journal of Climate, 23, 5678–5698, doi: 10.1175/2010JCLI3389.1, 2010. 18, 22, 48, 72, 94, 138

Kaplan, M. R. and Wolfe, A. P.: Spatial and temporal variability of Holocene temperature in the North Atlantic region, Quaternary Research, 65, 223–231, doi: 10.1016/j.yqres.2005.08.020, 2006. 29, 100

Kaufman, D., Ager, T., Anderson, N., Anderson, P., Andrews, J., Bartlein, P., Brubaker, L., Coats, L., Cwynar, L., Duvall, M., Dyke, A., Edwards, M., Eisner, W., Gajewski, K., Geirsdttir, A., Hu, F., Jennings, A., Kaplan, M., Kerwin, M., Lozhkin, A., MacDonald, G., Miller, G., Mock, C., Oswald, W., Otto-Bliesner, B., Porinchu, D., Rhland, K., Smol, J., Steig, E., and Wolfe, B.: Holocene thermal maximum in the western Arctic (0180W), Quaternary Science Reviews, 23, 529–560, doi: 10.1016/j.quascirev.2003.09.007, 2004. 20, 29, 30, 53, 55, 100

Kirtman, B., Power, S. B., Adedoyin, J. A., Boer, G. J., Bojariu, R., Camilloni, I., Doblas-Reyes, F., Fiore, A. M., Kimoto, M., Meehl, G. A., Prather, M., Sarr, A., Schär, C., Sutton, R., van Oldenborgh, G., Vecchi, G., and Wang, H. J.: Near-term Climate Change: Projections and Predictability, book section 11, pp. 953–1028, Cambridge University Press, Cambridge, United Kingdom and New York, NY, USA, 2013. 179

Kissel, C., Laj, C., Mulder, T., Wandres, C., and Cremer, M.: The magnetic fraction: A tracer of deep water circulation in the North Atlantic, Earth and Planetary Science Letters, 288, 444 – 454, doi: 10.1016/j.epsl.2009.10.005, 2009. 95, 96, 118

Kissel, C., Toer, A. V., Laj, C., Cortijo, E., and Michel, E.: Variations in the strength of the North Atlantic bottom water during Holocene, Earth and Planetary Science Letters, pp. –, doi: 10.1016/j.epsl.2013.03.042, 2013. 95, 96, 114, 115, 117, 118, 119, 121, 127, 183

Kleinen, T., Osborn, T., and Briffa, K.: Sensitivity of climate response to variations in freshwater hosing location, Ocean Dynamics, 59, 509–521, doi: 10.1007/s10236-009-0189-2, 2009. 50

Kleiven, H. K. F., Kissel, C., Laj, C., Ninnemann, U. S., Richter, T. O., and Cortijo, E.: Reduced North Atlantic Deep Water Coeval with the Glacial Lake Agassiz Freshwater Outburst, Science, 319, 60–64, doi: 10.1126/science.1148924, 2008. 10, 95

Knutti, R., Masson, D., and Gettelman, A.: Climate model genealogy: Generation CMIP5 and how we got there, Geophysical Research Letters, 40, 1194–1199, doi: 10.1002/grl.50256, 2013. 180

Koç, N., Jansen, E., and Haflidason, H.: Paleoceanographic reconstructions of surface ocean conditions in the Greenland, Iceland and Norwegian seas through the last 14 ka based on diatoms, Quaternary Science Reviews, 12, 115–140, doi: 10.1016/0277-3791(93)90012-B, 1993. 30

Köhler, P., Fischer, H., Munhoven, G., and Zeebe, R. E.: Quantitative interpretation of atmospheric carbon records over the last glacial termination, Global Biogeochemical Cycles, 19, GB4020, doi: 10.1029/2004GB002345, 2005. 121

Köhler, P., Bintanja, R., Fischer, H., Joos, F., Knutti, R., Lohmann, G., and Masson-Delmotte, V.: What caused Earth's temperature variations during the last 800,000 years? Data-based evidence on radiative forcing and constraints on climate sensitivity, Quaternary Science Reviews, 29, 129 – 145, doi: 10.1016/j.quascirev.2009.09.026, 2010. 132

Kopp, R. E., Simons, F. J., Mitrovica, J. X., Maloof, A. C., and Oppenheimer, M.: Probabilistic assessment of sea level during the last interglacial stage, Nature, 462, 863–867, doi: 10.1038/nature08686, 2009. 142

Kuhlbrodt, T., Griesel, A., Montoya, M., Levermann, A., Hofmann, M., and Rahmstorf, S.: On the driving processes of the Atlantic

meridional overturning circulation, Reviews of Geophysics, 45, doi: 10.1029/2004RG000166, 2007. 9, 22, 93, 94, 107, 133

Kukla, G. and Gavin, J.: Milankovitch climate reinforcements, Global and Planetary Change, 40, 27–48, doi: 10.1016/S0921-8181(03) 00096-1, 2004. 6

Kwok, R., Cunningham, G. F., and Pang, S. S.: Fram Strait sea ice outflow, Journal of Geophysical Research: Oceans, 109, doi: 10.1029/ 2003JC001785, 2004. 72

Lambeck, K. and Chappell, J.: Sea Level Change Through the Last Glacial Cycle, Science, 292, 679–686, doi: 10.1126/science.1059549, 2001. 61

Lambert, S. J. and Boer, G. J.: CMIP1 evaluation and intercomparison of coupled climate models, Climate Dynamics, 17, 83–106, doi: 10. 1007/PL00013736, 2001. 180

Lang, B., Bedford, A., Brooks, S. J., Jones, R. T., Richardson, N., Birks, H. J. B., and Marshall, J. D.: Early-Holocene temperature variability inferred from chironomid assemblages at Hawes Water, northwest England, The Holocene, 20, 943–954, doi: 10.1177/0959683610366157, 2010. 135

Latif, M., Roeckner, E., Mikolajewicz, U., and Voss, R.: Tropical stabilization of the thermohaline circulation in a greenhouse warming simulation., Journal of Climate, 13, doi: 10.1175/1520-0442(2000) 013⟨1809:L⟩2.0.CO;2, 2000. 164, 165

LeBel, D. A., Jr., W. M. S., Rhein, M., Kieke, D., Fine, R. A., Bullister, J. L., Min, D.-H., Roether, W., Weiss, R. F., Andri, C., Smythe-Wright, D., and Jones, E. P.: The formation rate of North Atlantic Deep Water and Eighteen Degree Water calculated from CFC-11 inventories observed during {WOCE}, Deep Sea Research Part I: Oceanographic Research Papers, 55, 891 – 910, doi: 10.1016/j.dsr.2008.03.009, 2008. 94, 118

Licciardi, J. M., Teller, J. T., and Clark, P. U.: Freshwater routing by the Laurentide Ice Sheet during the last deglaciation, AGU Geophysical Monograph, 112, 177–201, URL http://www.unh.edu/esci/people/pdf/licciardi_et-al-1999-agu.pdf, 1999. 35, 37, 102

Lisiecki, L. E. and Raymo, M. E.: A Pliocene-Pleistocene stack of 57 globally distributed benthic δ^{18}O records, Paleoceanography, 20, PA1003, doi: 10.1029/2004PA001071, 2005. 5, 13

Liu, Z., Otto-Bliesner, B. L., He, F., Brady, E. C., Tomas, R., Clark, P. U., Carlson, A. E., Lynch-Stieglitz, J., Curry, W., Brook, E., Erickson, D., Jacob, R., Kutzbach, J., and Cheng, J.: Transient Simulation of Last Deglaciation with a New Mechanism for Blling-Allerd Warming, Science, 325, 310–314, doi: 10.1126/science.1171041, 2009. 7

Lorenz, E. N.: Dimension of weather and climate attractors, Nature, 353, 241–244, doi: 10.1038/353241a0, 1991. 3

Lorenz, E. N.: Climate is what you expect, Prepared for publication by NCAR, pp. 1–33, 1995. 2

Lorenz, S. J., Kim, J.-H., Rimbu, N., Schneider, R. R., and Lohmann, G.: Orbitally driven insolation forcing on Holocene climate trends: Evidence from alkenone data and climate modeling, Paleoceanography, 21, PA1002, doi: 10.1029/2005PA001152, 2006. 100

Loutre, M. and Berger, A.: Marine Isotope Stage 11 as an analogue for the present interglacial, Global and Planetary Change, 36, 209–217, doi: 10.1016/S0921-8181(02)00186-8, 2003. 167

Loutre, M. F., Mouchet, A., Fichefet, T., Goosse, H., Goelzer, H., and Huybrechts, P.: Evaluating climate model performance with various parameter sets using observations over the recent past, Climate of the Past, 7, 511–526, doi: 10.5194/cp-7-511-2011, 2011. 138, 139, 188

Lozier, M. S.: Overturning in the North Atlantic, Annual Review of Marine Science, 4, 291–315, doi: 10.1146/annurev-marine-120710-100740, 2012. 94, 95

Lunt, D. J., Noblet-Ducoudr, N., and Charbit, S.: Effects of a melted greenland ice sheet on climate, vegetation, and the cryosphere, Climate Dynamics, 23, 679–694, doi: 10.1007/s00382-004-0463-4, 2004. 137

Lunt, D. J., Williamson, M. S., Valdes, P. J., Lenton, T. M., and Marsh, R.: Comparing transient, accelerated, and equilibrium simulations of the last 30 000 years with the GENIE-1 model, Climate of the Past, 2, 221–235, doi: 10.5194/cp-2-221-2006, 2006. 98

Lunt, D. J., Haywood, A. M., Schmidt, G. A., Salzmann, U., Valdes, P. J., and Dowsett, H. J.: Earth system sensitivity inferred from Pliocene modelling and data, Nature Geosci, 3, 60–64, doi: 10.1038/ngeo706, 2010. 132

Macrander, A., Send, U., Valdimarsson, H., Jónsson, S., and Käse, R. H.: Interannual changes in the overflow from the Nordic Seas into the Atlantic Ocean through Denmark Strait, Geophysical Research Letters, 32, L06606, doi: 10.1029/2004GL021463, 2005. 94

Manley, G.: Central England temperatures: monthly means 1659 to 1973, Quarterly Journal of the Royal Meteorological Society, 100, 389–405, 1974. 12

MARGO Project Members, Waelbroeck, C., Paul, A., Kucera, M., Rosell-Melé, A., Weinelt, M., Schneider, R., Mix, A. C., Abelmann, A., Armand, L., Bard, E., Barker, S., Barrows, T. T., Benway, H., Cacho, I., Chen, M.-T., Cortijo, E., Crosta, X., de Vernal, A., Dokken, T., Duprat, J., Elderfield, H., Eynaud, F., Gersonde, R., Hayes, A., Henry, M., Hillaire-Marcel, C., Huang, C.-C., Jansen, E., Juggins, S., Kallel, N., Kiefer, T., Kienast, M., Labeyrie, L., Leclaire, H., Londeix, L., Mangin, S., Matthiessen, J., Marret, F., Meland, M., Morey, A. E., Mulitza, S., Pflaumann, U., Pisias, N. G., Radi, T., Rochon, A., Rohling, E. J., Sbaffi, L., Schäfer-Neth, C., Solignac, S., Spero, H., Tachikawa, K., and Turon, J.-L.: Constraints on the magnitude

and patterns of ocean cooling at the Last Glacial Maximum, Nature Geoscience, 2, 127–132, doi: 10.1038/ngeo411, 2009. 45

Marshall, J. and Schott, F.: Open-ocean convection: Observations, theory, and models, Reviews of Geophysics, 37, 1–64, doi: 10.1029/98RG02739, 1999. 9, 133

Masson-Delmotte, V., Schulz, M., Abe-Ouchi, A., Beer, J., Ganopolski, A., Rouco, J. G., Jansen, E., Lambeck, K., Luterbacher, J., Naish, T., Osborn, T., Otto-Bliesner, B., Quinn, T., Ramesh, R., Rojas, M., Shao, X., and Timmermann, A.: Information from Paleoclimate Archives, book section 5, pp. 383–464, Cambridge University Press, Cambridge, United Kingdom and New York, NY, USA, 2013. 23

McBean, G., Alekseev, G., Chen, D., Foerland, E., Fyfe, J., Groisman, P. Y., King, R., Melling, H., Vose, R., and Whitfield, P. H.: Chapter 2: Arctic Climate: past and present, Arctic Climate Impact Assessment.[np]., 2005. 11

McCartney, M. S.: Recirculating components to the deep boundary current of the northern North Atlantic, Progress in Oceanography, 29, 283–383, doi: 10.1016/0079-6611(92)90006-L, 1992. 118

McCave, I. N. and Hall, I. R.: Size sorting in marine muds: Processes, pitfalls, and prospects for paleoflow-speed proxies, Geochemistry, Geophysics, Geosystems, 7, Q10N05, doi: 10.1029/2006GC001284, 2006. 96

McCave, I. N., Manighetti, B., and Robinson, S. G.: Sortable silt and fine sediment size/composition slicing: Parameters for palaeocurrent speed and palaeoceanography, Paleoceanography, 10, 593–610, doi: 10.1029/94PA03039, 1995. 96

McCave, I. N., Hall, I. R., and Bianchi, G. G.: Laser vs. settling velocity differences in silt grainsize measurements: estimation of palaeocurrent vigour, Sedimentology, 53, 919–928, doi: 10.1111/j.1365-3091.2006.00783.x, 2006. 96

McManus, J. F., Francois, R., Gherardi, J.-M., Keigwin, L. D., and Brown-Leger, S.: Collapse and rapid resumption of Atlantic meridional circulation linked to deglacial climate changes, Nature, 428, 834–837, doi: 10.1038/nature02494, 2004. 22, 95, 98

Meehl, G., Stocker, T., Collins, W., Friedlingstein, P., Gaye, A., Gregory, J., Kitoh, A., Knutti, R., Murphy, J., Noda, A., Raper, S., Watterson, I., Weaver, A., and Zhao, Z.-C.: Global Climate Projections. In: Climate Change 2007: The Physical Science Basis, URL `http://www.ipcc.ch/pdf/assessment-report/ar4/wg1/ar4-wg1-chapter10.pdf`, 2007. 101, 133, 134, 135, 138, 144, 169

Meinshausen, M., Smith, S., Calvin, K., Daniel, J., Kainuma, M., Lamarque, J.-F., Matsumoto, K., Montzka, S., Raper, S., Riahi, K., Thomson, A., Velders, G., and van Vuuren, D.: The RCP greenhouse gas concentrations and their extensions from 1765 to 2300, Climatic Change, 109, 213–241, doi: 10.1007/s10584-011-0156-z, 2011. 57, 69, 139, 143, 144

Members, C.: Last Interglacial Arctic warmth confirms polar amplification of climate change, Quaternary Science Reviews, 25, 1383 – 1400, doi: 10.1016/j.quascirev.2006.01.033, 2006. 142

Milankovitch, M.: Théorie mathématique des phénomènes thermiques produits par la radiation solaire, vol. 339, Paris, 1920. 5

Milankovitch, M.: Kanon der Erdebestrahlung und seine anwendung auf das eiszeitenproblem, Königlich Serbische Akademie, 1941. 3

Milker, Y., Rachmayani, R., Weinkauf, M. F. G., Prange, M., Raitzsch, M., Schulz, M., and Kučera, M.: Global and regional sea surface temperature trends during Marine Isotope Stage 11, Climate of the Past, 9, 2231–2252, doi: 10.5194/cp-9-2231-2013, 2013. 167

Mitchell, J. M.: An overview of climatic variability and its causal mechanisms, Quaternary Research, 6, 481–493, doi: 10.1016/0033-5894(76)90021-1, 1976. 2, 4

Müller, J., Masse, G., Stein, R., and Belt, S. T.: Variability of sea-ice conditions in the Fram Strait over the past 30,000 years, Nature Geosci, 2, 772–776, doi: 10.1038/ngeo665, 2009. 62, 85

National Geophysical Data Center, NESDIS, N. U. D. o. C.: NGDC, ETOPO2 Global 2' Elevations, URL `http://rda.ucar.edu/datasets/ds759.3`, 2001. 62

Oppo, D. W., McManus, J. F., and Cullen, J. L.: Palaeo-oceanography: Deepwater variability in the Holocene epoch, Nature, 422, 277–277, doi: 10.1038/422277b, 2003. 95, 115, 116, 119, 121, 126

Opsteegh, J. D., Haarsma, R. J., Selten, F. M., and Kattenberg, A.: ECBILT: a dynamic alternative to mixed boundary conditions in ocean models, Tellus A, 50, 348–367, doi: 10.1034/j.1600-0870.1998.t01-1-00007.x, 1998. 15, 33, 66, 101, 137

Overpeck, J. T., Otto-Bliesner, B. L., Miller, G. H., Muhs, D. R., Alley, R. B., and Kiehl, J. T.: Paleoclimatic Evidence for Future Ice-Sheet Instability and Rapid Sea-Level Rise, Science, 311, 1747–1750, doi: 10.1126/science.1115159, 2006. 142

Palaeosens Project Members, Rohling, E. J., Rohling, E. J., Sluijs, A., Dijkstra, H. A., Köhler, P., van de Wal, R. S. W., von der Heydt, A. S., Beerling, D. J., Berger, A., Bijl, P. K., Crucifix, M., Deconto, R., Drijfhout, S. S., Fedorov, A., Foster, G. L., Ganopolski, A., Hansen, J., Hönisch, B., Hooghiemstra, H., Huber, M., Huybers, P., Knutti, R., Lea, D. W., Lourens, L. J., Lunt, D., Masson-Demotte, V., Medina-Elizalde, M., Otto-Bliesner, B., Pagani, M., Pälike, H., Renssen, H., Royer, D. L., Siddall, M., Valdes, P., Zachos, J. C., and Zeebe, R. E.: Making sense of palaeoclimate sensitivity, Nature, 491, 683–691, doi: 10.1038/nature11574, 2012. 132

Palmer, K. and Stoffer, D.: Chaos in almost periodic systems, Zeitschrift Angewandte Mathematik und Physik, 40, 592–602, doi: 10.1007/BF00944809, 1989. 3

Palmer, T. N.: Predicting uncertainty in forecasts of weather and climate, Reports on Progress in Physics, 63, 71–116, doi: 10.1088/0034-4885/63/2/201, 2000. 179

Peltier, W.: Global Glacial Isostasy And The Surface Of The Ice-age Earth: The ICE-5G (VM2) Model And Grace, Annual Review of Earth and Planetary Sciences, 32, 111–149, doi: 10.1146/annurev.earth.32.082503.144359, 2004. 8, 17, 31, 32, 35, 36, 37, 38, 62, 66, 68, 98, 103, 104, 135, 143

Peltier, W. R.: Ice Age Paleotopography, Science, 265, 195–201, doi: 10.1126/science.265.5169.195, 1994. 98

Pickart, R. S., Spall, M. A., Ribergaard, M. H., Moore, G. W. K., and Milliff, R. F.: Deep convection in the Irminger Sea forced by the Greenland tip jet, Nature, 424, 152–156, doi: 10.1038/nature01729, 2003. 9, 133

Polyak, L., Alley, R. B., Andrews, J. T., Brigham-Grette, J., Cronin, T. M., Darby, D. A., Dyke, A. S., Fitzpatrick, J. J., Funder, S., Holland, M., Jennings, A. E., Miller, G. H., O'Regan, M., Savelle, J., Serreze, M., St. John, K., White, J. W., and Wolff, E.: History of sea ice in the Arctic, Quaternary Science Reviews, 29, 1757–1778, doi: 10.1016/j.quascirev.2010.02.010, 2010. 63

Praetorius, S. K., McManus, J. F., Oppo, D. W., and Curry, W. B.: Episodic reductions in bottom-water currents since the last ice age, Nature Geosci, 1, 449–452, doi: 10.1038/ngeo227, 2008. 96, 115, 117, 118, 119, 121, 126, 183

Rahmstorf, S.: On the freshwater forcing and transport of the Atlantic thermohaline circulation, Climate Dynamics, 12, 799–811, doi: 10.1007/s003820050144, 1996. 22, 164, 165

Rahmstorf, S.: Ocean circulation and climate during the past 120,000 years, Nature, 419, 207–214, doi: 10.1038/nature01090, 2002. 135

Rahmstorf, S. and Ganopolski, A.: Long-Term Global Warming Scenarios Computed with an Efficient Coupled Climate Model, Climatic Change, 43, 353–367, doi: 10.1023/A:1005474526406, 1999. 8, 93

Rayner, N. A., Parker, D. E., Horton, E. B., Folland, C. K., Alexander, L. V., Rowell, D. P., Kent, E. C., and Kaplan, A.: Global analyses of sea surface temperature, sea ice, and night marine air temperature since the late nineteenth century, Journal of Geophysical Research: Atmospheres, 108, doi: 10.1029/2002JD002670, 2003. 72

Renssen, H., Goosse, H., and Fichefet, T.: Contrasting trends in North Atlantic deep-water formation in the Labrador Sea and Nordic Seas during the Holocene, Geophysical Research Letters, 32, L08 711–, doi: 10.1029/2005GL022462, 2005a. 98

Renssen, H., Goosse, H., Fichefet, T., Brovkin, V., Driesschaert, E., and Wolk, F.: Simulating the Holocene climate evolution at northern high latitudes using a coupled atmosphere-sea ice-ocean-vegetation model, Climate Dynamics, 24, 23–43, doi: 10.1007/s00382-004-0485-y, 2005b. 19, 48

Renssen, H., Goosse, H., Muscheler, R., et al.: Coupled climate model simulation of Holocene cooling events: oceanic feedback amplifies solar forcing, Climate of the Past, 2, 79–90, doi: 10.5194/cp-2-79-2006, 2006. 34, 139

Renssen, H., Seppa, H., Heiri, O., Roche, D. M., Goosse, H., and Fichefet, T.: The spatial and temporal complexity of the Holocene thermal maximum, Nature Geosci, 2, 411–414, doi: 10.1038/ngeo513, 2009. vii, xiv, 18, 20, 22, 28, 29, 31, 32, 34, 36, 48, 49, 64, 66, 68, 84, 102, 105, 106, 143

Renssen, H., Goosse, H., Crosta, X., and Roche, D. M.: Early Holocene Laurentide Ice Sheet deglaciation causes cooling in the high-latitude Southern Hemisphere through oceanic teleconnection, Paleoceanography, 25, PA3204–, doi: 10.1029/2009PA001854, 2010. 42, 66, 102

Renssen, H., Sepp, H., Crosta, X., Goosse, H., and Roche, D.: Global characterization of the Holocene Thermal Maximum, Quaternary Science Reviews, 48, 7–19, doi: 10.1016/j.quascirev.2012.05.022, 2012. 66, 102

Rhein, M., Kieke, D., Hüttl-Kabus, S., Roessler, A., Mertens, C., Meissner, R., Klein, B., Böning, C. W., and Yashayaev, I.: Deep water formation, the subpolar gyre, and the meridional overturning circulation in the subpolar North Atlantic, Deep Sea Research Part II: Topical Studies in Oceanography, 58, 1819–1832, doi: 10.1016/j.dsr2.2010.10.061, 2011. 94

Rial, J., Pielke, RogerA., S., Beniston, M., Claussen, M., Canadell, J., Cox, P., Held, H., de Noblet-Ducoudr, N., Prinn, R., Reynolds, J., and Salas, J.: Nonlinearities, Feedbacks and Critical Thresholds within the Earth's Climate System, Climatic Change, 65, 11–38, doi: 10.1023/B:CLIM.0000037493.89489.3f, 2004. 3, 4

Ridley, J. K., Huybrechts, P., Gregory, J. M., and Lowe, J. A.: Elimination of the Greenland Ice Sheet in a High CO2 Climate, Journal of Climate, 18, 3409–3427, doi: 10.1175/JCLI3482.1, 2005. 16, 134, 144

Rignot, E., Velicogna, I., van den Broeke, M. R., Monaghan, A., and Lenaerts, J.: Acceleration of the contribution of the Greenland and Antarctic ice sheets to sea level rise, Geophysical Research Letters, 38, L05 503–, doi: 10.1029/2011GL046583, 2011. 11, 23, 32, 57, 144

Rigor, I. and Colony, R.: Sea-ice production and transport of pollutants in the Laptev Sea, 19791993, Science of the Total Environment, 202, 89–110, doi: 10.1016/S0048-9697(97)00107-1, 1997. 63

Risebrobakken, B., Jansen, E., Andersson, C., Mjelde, E., and Hevry, K.: A high-resolution study of Holocene paleoclimatic and paleoceanographic changes in the Nordic Seas, Paleoceanography, 18, 1017–, doi: 10.1029/2002PA000764, 2003. 30

Risebrobakken, B., Dokken, T., Smedsrud, L. H., Andersson, C., Jansen, E., Moros, M., and Ivanova, E. V.: Early Holocene temperature variability in the Nordic Seas: The role of oceanic heat advection versus changes in orbital forcing, Paleoceanography, 26, PA4206–, doi: 10.1029/2011PA002117, 2011. 30, 45, 49

Ritz, S. P., Stocker, T. F., Grimalt, J. O., Menviel, L., and Timmermann, A.: Estimated strength of the Atlantic overturning circulation during the last deglaciation, Nature Geosci, 6, 208–212, doi: 10.1038/ngeo1723, 2013. 98

Robinson, A., Calov, R., and Ganopolski, A.: Greenland ice sheet model parameters constrained using simulations of the Eemian Interglacial, Climate of the Past, 7, 381–396, doi: 10.5194/cp-7-381-2011, 2011. 142

Roche, D. M.: δ^{18}O water isotope in the iLOVECLIM model (version 1.0) Part 1: Implementation and verification, Geosci. Model Dev., 6, 1481–1491, doi: 10.5194/gmd-6-1481-2013, 2013. 17

Roche, D. M., Dokken, T. M., Goosse, H., Renssen, H., and Weber, S. L.: Climate of the Last Glacial Maximum: sensitivity studies and model-data comparison with the LOVECLIM coupled model, Climate of the Past, 3, 205–224, doi: 10.5194/cp-3-205-2007, 2007. 17, 21, 64

Roche, D. M., Renssen, H., and Paillard, D.: A Spatial View on Temperature Change and Variability During the Last Deglaciation: A Model Analysis, in: Climate Change, edited by Berger, A., Mesinger, F., and Sijacki, D., pp. 79–91, Springer Vienna, doi: 10.1007/978-3-7091-0973-1_6, 2012. 7, 21, 64

Roe, G.: Feedbacks, Timescales, and Seeing Red, Annual Review of Earth and Planetary Sciences, 37, 93–115, doi: 10.1146/annurev.earth.061008.134734, 2009. 132

Rossow, W. B.: International Satellite Cloud Climatology Project (ISCCP): documentation of new cloud datasets, NASA Goddard Space Flight Center, 1996. 16, 101, 137

Sandström, J. W.: Dynamische versuche mit meerwasser, Ann. Hydrogr. Mar. Meteorol, 36, 6–23, 1908. 93

Sarnthein, M., Van Kreveld, S., Erlenkeuser, H., Grootes, P. M., Kucera, M., Pflaumann, U., and Schulz, M.: Centennial-to-millennial-scale periodicities of Holocene climate and sediment injections off the western Barents shelf, 75N, Boreas, 32, 447–461, doi: 10.1111/j.1502-3885.2003.tb01227.x, 2003. 97, 115, 119, 121, 183

Schmittner, A., Latif, M., and Schneider, B.: Model projections of the North Atlantic thermohaline circulation for the 21st century assessed by observations, Geophysical Research Letters, 32, L23 710–, doi: 10.1029/2005GL024368, 2005. 33, 134, 138

Schneider, B., Latif, M., and Schmittner, A.: Evaluation of Different Methods to Assess Model Projections of the Future Evolution of the Atlantic Meridional Overturning Circulation, Journal of Climate, 20, 2121, doi: 10.1175/JCLI4128.1, 2007. 133

Schrama, E. J. O. and Wouters, B.: Revisiting Greenland ice sheet mass loss observed by GRACE, Journal of Geophysical Research, 116, B02 407–, doi: 10.1029/2009JB006847, 2011. 32

Shackleton, N.: Oxygen Isotope Analyses and Pleistocene Temperatures Re-assessed, Nature, 215, 15–17, doi: 10.1038/215015a0, 1967. 13

Shackleton, N. J.: The Oxygen Isotope Stratigraphic Record of the Late Pleistocene, Royal Society of London Philosophical Transactions Series B, 280, 169–179, doi: 10.1098/rstb.1977.0104, 1977. 12

Shackleton, N. J., Hall, M. A., and Vincent, E.: Phase relationships between millennial-scale events 64,00024,000 years ago, Paleoceanography, 15, 565–569, doi: 10.1029/2000PA000513, 2000. 115, 119, 121, 183

Shakun, J. D. and Carlson, A. E.: A global perspective on Last Glacial Maximum to Holocene climate change, Quaternary Science Reviews, 29, 1801–1816, doi: 10.1016/j.quascirev.2010.03.016, 2010. 153

Siddall, M., Rohling, E. J., Almogi-Labin, A., Hemleben, C., Meischner, D., Schmelzer, I., and Smeed, D. A.: Sea-level fluctuations during the last glacial cycle, Nature, 423, 853–858, doi: 10.1038/nature01690, 2003. 8, 21, 35, 60

Simpson, M. J., Milne, G. A., Huybrechts, P., and Long, A. J.: Calibrating a glaciological model of the Greenland ice sheet from the Last Glacial Maximum to present-day using field observations of relative sea level and ice extent, Quaternary Science Reviews, 28, 1631–1657, doi: 10.1016/j.quascirev.2009.03.004, 2009. 16, 31, 143

Singarayer, J. S. and Valdes, P. J.: High-latitude climate sensitivity to ice-sheet forcing over the last 120 kyr, Quaternary Science Reviews, 29, 43–55, doi: 10.1016/j.quascirev.2009.10.011, 2010. 64

Smethie, W. M., Lebel, D. A., Fine, R. A., Rhein, M., and Kieke, D.: Strength and Variability of the Deep Limb of the North Atlantic Meridional Overturning Circulation from Chlorofluorocarbon Inventories, pp. 119–130, American Geophysical Union, doi: 10.1029/173GM09, 2013. 94, 112, 127, 129

Smith, R. and Gregory, J.: The last glacial cycle: transient simulations with an AOGCM, Climate Dynamics, 38, 1545–1559, doi: 10.1007/s00382-011-1283-y, 2012. 98, 99, 105

Smith, T. M., Reynolds, R. W., Peterson, T. C., and Lawrimore, J.: Improvements to NOAAs Historical Merged Land-Ocean Surface Temperature Analysis (1880-2006), Journal of Climate, 21, 2283–2296, doi: 10.1175/2007JCLI2100.1, 2008. 43

Spreen, G., Kern, S., Stammer, D., and Hansen, E.: Fram Strait sea ice volume export estimated between 2003 and 2008 from satellite data,

Geophysical Research Letters, 36, doi: 10.1029/2009GL039591, 2009. 70, 72

Srokosz, M., Baringer, M., Bryden, H., Cunningham, S., Delworth, T., Lozier, S., Marotzke, J., and Sutton, R.: Past, Present, and Future Changes in the Atlantic Meridional Overturning Circulation, Bulletin of the American Meteorological Society, 93, 1663–1676, doi: 10.1175/BAMS-D-11-00151.1, 2012. 22, 134, 135

Stone, E. and Lunt, D.: The role of vegetation feedbacks on Greenland glaciation, Climate Dynamics, 40, 2671–2686, doi: 10.1007/s00382-012-1390-4, 2013. 137, 142

Stone, P. H.: Climate prediction: The limits of ocean models, Washington DC American Geophysical Union Geophysical Monograph Series, 150, 259–267, doi: 10.1029/150GM20, 2004. 101, 169

Stouffer, R. J., Yin, J., Gregory, J. M., Dixon, K. W., Spelman, M. J., Hurlin, W., Weaver, A. J., Eby, M., Flato, G. M., Hasumi, H., Hu, A., Jungclaus, J. H., Kamenkovich, I. V., Levermann, A., Montoya, M., Murakami, S., Nawrath, S., Oka, A., Peltier, W. R., Robitaille, D. Y., Sokolov, A., Vettoretti, G., and Weber, S. L.: Investigating the Causes of the Response of the Thermohaline Circulation to Past and Future Climate Changes, Journal of Climate, 19, 1365–1387, doi: 10.1175/JCLI3689.1, 2006. 50, 134

Straneo, F.: On the Connection between Dense Water Formation, Overturning, and Poleward Heat Transport in a Convective Basin*, Journal of Physical Oceanography, 36, 1822, doi: 10.1175/JPO2932.1, 2006. 94

Stroeve, J., Holland, M. M., Meier, W., Scambos, T., and Serreze, M.: Arctic sea ice decline: Faster than forecast, Geophysical Research Letters, 34, doi: 10.1029/2007GL029703, 2007. 168

Sun, B. and Wang, H.: Larger variability, better predictability?, International Journal of Climatology, 33, 2341–2351, doi: 10.1002/joc.3582, 2013. 179

Svendsen, J. I., Alexanderson, H., Astakhov, V. I., Demidov, I., Dowdeswell, J. A., Funder, S., Gataullin, V., Henriksen, M., Hjort, C., Houmark-Nielsen, M., Hubberten, H. W., Inglfsson, O., Jakobsson, M., Kjr, K. H., Larsen, E., Lokrantz, H., Lunkka, J. P., Lys, A., Mangerud, J., Matiouchkov, A., Murray, A., Mller, P., Niessen, F., Nikolskaya, O., Polyak, L., Saarnisto, M., Siegert, C., Siegert, M. J., Spielhagen, R. F., and Stein, R.: Late Quaternary ice sheet history of northern Eurasia, Quaternary Science Reviews, 23, 1229–1271, doi: 10.1016/j.quascirev.2003.12.008, 2004. 21, 68

Swingedouw, D., Braconnot, P., and Marti, O.: Sensitivity of the Atlantic Meridional Overturning Circulation to the melting from northern glaciers in climate change experiments, Geophysical Research Letters, 33, L07 711, doi: 10.1029/2006GL025765, 2006. 133

Swingedouw, D., Braconnot, P., Delecluse, P., Guilyardi, E., and Marti, O.: Quantifying the AMOC feedbacks during a 2CO2 stabilization experiment with land-ice melting, Climate Dynamics, 29, 521–534, doi: 10.1007/s00382-007-0250-0, 2007. 133, 134, 164, 165

Swingedouw, D., Mignot, J., Braconnot, P., Mosquet, E., Kageyama, M., and Alkama, R.: Impact of Freshwater Release in the North Atlantic under Different Climate Conditions in an OAGCM, Journal of Climate, 22, 6377–6403, doi: 10.1175/2009JCLI3028.1, 2009. 134, 152, 153, 164

Swingedouw, D., Rodehacke, C., Behrens, E., Menary, M., Olsen, S., Gao, Y., Mikolajewicz, U., Mignot, J., and Biastoch, A.: Decadal fingerprints of freshwater discharge around Greenland in a multi-model ensemble, Climate Dynamics, pp. 1–26, doi: 10.1007/s00382-012-1479-9, 2012. 49

Taldenkova, E., Bauch, H. A., Gottschalk, J., Nikolaev, S., Rostovtseva, Y., Pogodina, I., Ovsepyan, Y., and Kandiano, E.: History of ice-rafting and water mass evolution at the northern Siberian continental margin (Laptev Sea) during Late Glacial and Holocene times, Quaternary Science Reviews, 29, 3919–3935, doi: 10.1016/j.quascirev.2010.09.013, 2010. 21, 61, 84

Tamura, T. and Ohshima, K. I.: Mapping of sea ice production in the Arctic coastal polynyas, Journal of Geophysical Research, 116, C07 030–, doi: 10.1029/2010JC006586, 2011. 61, 72, 73

Tarasov, L. and Peltier, W. R.: Greenland glacial history, borehole constraints, and Eemian extent, Journal of Geophysical Research: Solid Earth, 108, 2143, doi: 10.1029/2001JB001731, 2003. 142

Taylor, K. E., Stouffer, R. J., and Meehl, G. A.: An Overview of CMIP5 and the Experiment Design, Bulletin of the American Meteorological Society, 93, 485–498, doi: 10.1175/BAMS-D-11-00094.1, 2012. 179

Telford, R. J., Heegaard, E., and Birks, H. J. B.: All age-depth models are wrong: but how badly?, Quaternary Science Reviews, 23, 1–5, doi: 10.1016/j.quascirev.2003.11.003, 2004. 13

Thornalley, D. J. R., Elderfield, H., and McCave, I. N.: Holocene oscillations in temperature and salinity of the surface subpolar North Atlantic, Nature, 457, 711–714, doi: 10.1038/nature07717, 2009. 10

Thornalley, D. J. R., Blaschek, M., Davies, F. J., Praetorius, S., Oppo, D. W., McManus, J. F., Hall, I. R., Kleiven, H., Renssen, H., and McCave, I. N.: Long-term variations in Iceland-Scotland overflow strength during the Holocene, Climate of the Past Discussions, 9, 1627–1656, doi: 10.5194/cpd-9-1627-2013, 2013. 22, 95, 96, 97, 102, 108, 114, 115, 118, 119, 121, 123, 126, 127, 129, 183

Trenberth, K. E. and Caron, J. M.: Estimates of Meridional Atmosphere and Ocean Heat Transports, Journal of Climate, 14, 3433–3443, doi: 10.1175/1520-0442(2001)014⟨3433:EOMAAO⟩2.0.CO;2, 2001. 8

Urey, H. C.: Oxygen Isotopes in Nature and in the Laboratory, Science, 108, 489–496, doi: 10.1126/science.108.2810.489, 1948. 12

Valdes, P.: Built for stability, Nature Geosci, 4, 414–416, doi: 10.1038/ngeo1200, 2011. 135, 168

van de Berg, W. J., van den Broeke, M., Ettema, J., van Meijgaard, E., and Kaspar, F.: Significant contribution of insolation to Eemian melting of the Greenland ice sheet, Nature Geosci, 4, 679–683, doi: 10.1038/ngeo1245, 2011. 135, 142, 144

Vellinga, M. and Wood, R.: Global Climatic Impacts of a Collapse of the Atlantic Thermohaline Circulation, Climatic Change, 54, 251–267, doi: 10.1023/A:1016168827653, 2002. 8

Vinther, B. M., Buchardt, S. L., Clausen, H. B., Dahl-Jensen, D., Johnsen, S. J., Fisher, D. A., Koerner, R. M., Raynaud, D., Lipenkov, V., Andersen, K. K., Blunier, T., Rasmussen, S. O., Steffensen, J. P., and Svensson, A. M.: Holocene thinning of the Greenland ice sheet, Nature, 461, 385–388, doi: 10.1038/nature08355, 2009. 31

Weaver, A. J., Sedlek, J., Eby, M., Alexander, K., Crespin, E., Fichefet, T., Philippon-Berthier, G., Joos, F., Kawamiya, M., Matsumoto, K., Steinacher, M., Tachiiri, K., Tokos, K., Yoshimori, M., and Zickfeld, K.: Stability of the Atlantic meridional overturning circulation: A model intercomparison, Geophysical Research Letters, 39, doi: 10.1029/2012GL053763, 2012. 18, 66, 128, 134

Werner, K., Spielhagen, R. F., Bauch, D., Hass, H. C., and Kandiano, E.: Atlantic Water advection versus sea-ice advances in the eastern Fram Strait during the last 9 ka: Multiproxy evidence for a two-phase Holocene, Paleoceanography, doi: 10.1002/palo.20028, 2013. 63

Wiersma, A. and Renssen, H.: Modeldata comparison for the 8.2 ka BP event: confirmation of a forcing mechanism by catastrophic drainage of Laurentide Lakes, Quaternary Science Reviews, 25, 63–88, doi: 10.1016/j.quascirev.2005.07.009, 2006. 18, 34, 66, 102

Williams, D. F. and Johnson, W. C.: Diversity of recent planktonic foraminifera in the southern Indian Ocean and Late Pleistocene paleotemperatures, Quaternary Research, 5, 237–250, doi: 10.1016/0033-5894(75)90026-5, 1975. 12

Willmes, S., Adams, S., Schrder, D., and Heinemann, G.: Spatio-temporal variability of polynya dynamics and ice production in the Laptev Sea between the winters of 1979/80 and 2007/08, Polar Research, 30, URL http://www.polarresearch.net/index.php/polar/article/view/5971, 2011. 62

Wunsch, C.: Quantitative estimate of the Milankovitch-forced contribution to observed Quaternary climate change, Quaternary Science Reviews, 23, 1001 – 1012, doi: 10.1016/j.quascirev.2004.02.014, 2004. 6

Wunsch, C.: Towards understanding the Paleocean, Quaternary Science Reviews, 29, 1960–1967, doi: 10.1016/j.quascirev.2010.05.020, 2010. 14

Zakharov, V.: The role of flaw leads off the edge of fast ice in the hydrological and ice regime of the Laptev Sea, Oceanology, 6, 815–821, 1966. 63

Zeebe, R. E.: Time-dependent climate sensitivity and the legacy of anthropogenic greenhouse gas emissions, Proceedings of the National Academy of Sciences, doi: 10.1073/pnas.1222843110, 2013. 132, 134, 167

Zhang, J. and Rothrock, D. A.: Modeling Global Sea Ice with a Thickness and Enthalpy Distribution Model in Generalized Curvilinear Coordinates, Monthly Weather Review, 131, 845–861, doi: 10.1175/1520-0493(2003)131\%3C0845:MGSIWA\%3E2.0.CO;2, 2003. 69, 70, 72

Zweck, C. and Huybrechts, P.: Modeling of the northern hemisphere ice sheets during the last glacial cycle and glaciological sensitivity,

Journal of Geophysical Research (Atmospheres), 110, D07103, doi: 10.1029/2004JD005489, 2005. 17, 98